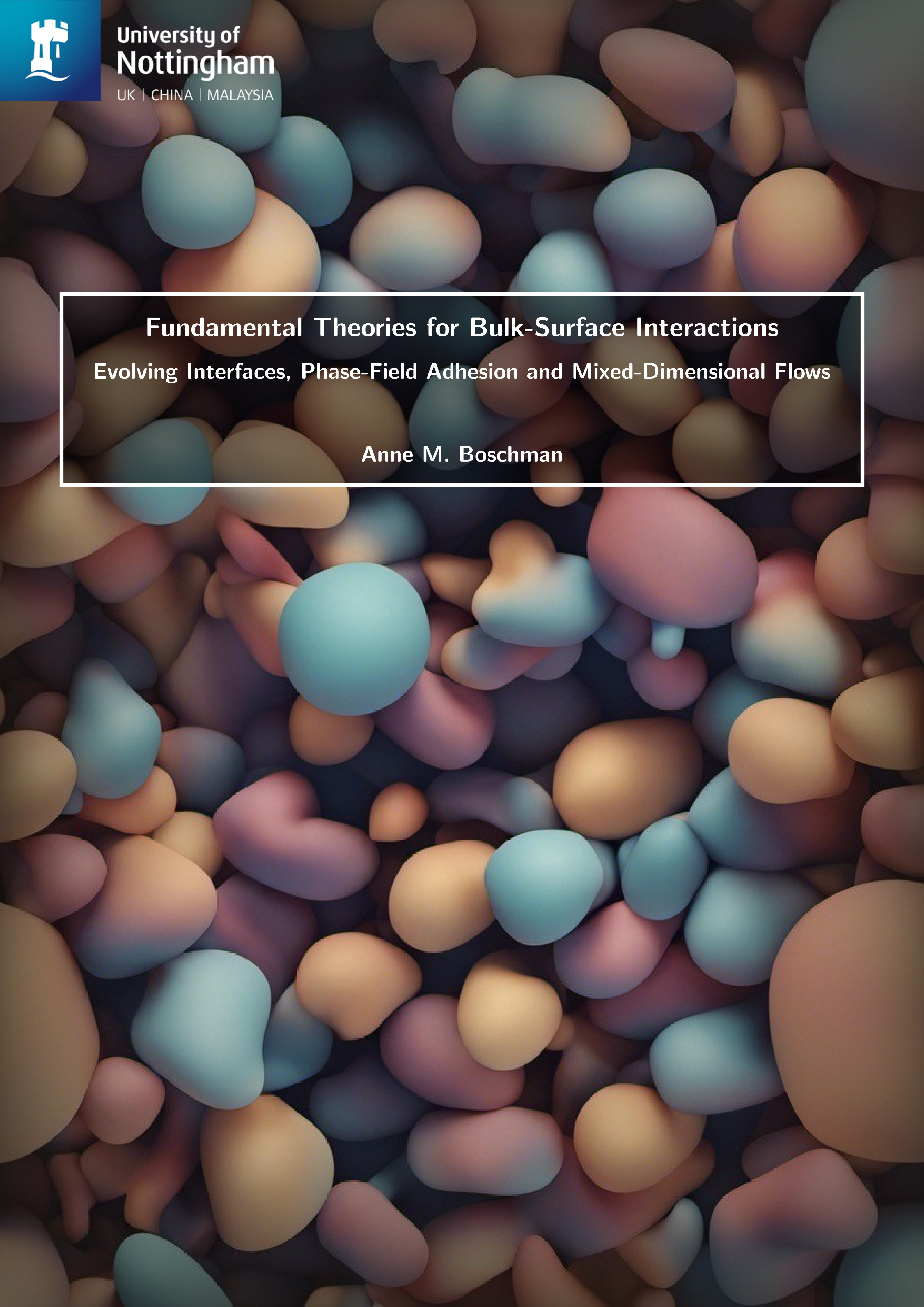

University of Nottingham
UK | CHINA | MALAYSIA

Fundamental Theories for Bulk-Surface Interactions

Evolving Interfaces, Phase-Field Adhesion and Mixed-Dimensional Flows

Anne M. Boschman

Fundamental Theories for Bulk-Surface Interactions

Evolving Interfaces, Phase-Field Adhesion and Mixed-Dimensional Flows

Anne M. Boschman

Thesis submitted to the University of Nottingham for the degree of
Doctor of Philosophy, September 2023.

Supervised by:
K. G. van der Zee
School of Mathematical Sciences
University of Nottingham

M. Icardi
School of Mathematical Sciences
University of Nottingham

B. S. Brook
School of Mathematical Sciences
University of Nottingham

L. Espath
School of Mathematical Sciences
University of Nottingham

Assessed by:
M. E. Hubbard
School of Mathematical Sciences
University of Nottingham

H. Gomez
School of Mechanical Engineering
Purdue University

Abstract

In a wide range of engineering and biological applications, processes at a stationary or moving surface affect the dynamics in the bulk material. Examples of these processes include cellular migration caused by protein interactions at cell membranes, or the decrease in surface tension due to the presence of surface active compounds in cleaning products. Computational models are essential to gain insight into these bulk-surface interactions and to make accurate predictions about the behaviour of these complex systems. From a mathematical perspective, models proposed for the study of these phenomena are based on either a sharp or diffuse interpretation of the surface. Yet, the exact coupling of the bulk and surface dynamics is challenging due to its non-linear character, and many of the current bulk-surface models lack a comprehensive continuum theory as a foundation.

This thesis aims to arrive at fundamental theories for bulk-surface interactions. To this end, it first outlines several frameworks used for the construction of models for moving surfaces. Although each framework offers distinct insights and motivation for the system's dynamics, it is demonstrated that for particular modelling choices the same models can be established.

Secondly, a framework is proposed to describe adhesive interactions between surfaces. This framework is based on a diffuse description of the moving surfaces. The form of the system's underlying energy is key to establishing the adhesive interaction, more specifically, it includes terms that only play a role in the diffuse region representing the surface. In a novel way, equilibrium states of the adhesion model are characterized, which connect the proposed diffuse framework with a sharp theory for adhesion. Numerical experiments provide further geometrical insights into the proposed adhesion model.

As a third contribution, a continuum theory based on a sharp description of the surface is presented for bulk-surface fluids. In particular, a bulk fluid coupled to a surface fluid is considered, which both deform in an incompressible way. This framework also accounts for additional mechanics, such as phase separation and species transport in the bulk-surface material. Here, the framework is founded on a so-called bulk-surface principle of virtual power, which reflects the energetic structure of the coupled system. Another energy-based argument provides the dynamic coupling conditions between the bulk and surface fluid, thereby complementing the framework in a consistent manner.

Finally, the frameworks developed within this thesis can be tailored to diverse bulk-surface applications. In combination with efficient computational tools, these frameworks are capable of improving our understanding of the interplay between bulk and surface within complex materials.

Acknowledgements

This thesis was not written in a single day, and most importantly, it would not have come together without the support, guidance and encouragement of certain individuals. Here, I would like to express my gratitude to those who have played significant roles in my PhD journey.

First and foremost, I would like to thank my principal supervisor, Kris van der Zee, for all his support and guidance. Working with you has been a genuine pleasure, and I appreciate the wealth of knowledge and enthusiasm for science you have shared with me over the years.

I would also like to express my gratitude to Luis Espath for his unwavering support. I have sincerely enjoyed the numerous meaningful discussions we have shared. Thank you for your patience and assistance in further developing these research ideas.

I wish to extend my appreciation to Matteo Icardi for his invaluable mentorship. I am grateful for the opportunities you have provided me over the years, allowing me to grow on both personal and academic fronts.

A heartfelt thank you to Bindi Brook for her support and guidance. I appreciate the pleasant meetings we have shared, which breathed life into this research project and helped shape the results presented in this work.

Then, thank you to those who have made my time in Nottingham so pleasant. I have enjoyed all work and non-work related chats (in and outside room A14), the numerous pub visits, the (bi)weekly Finite Element Method coffee hours, the SIAM activities and meetings, as well as the visits to the bouldering hall and bicycle rides in and around Nottingham. I would also like to extend my gratitude to my family and friends in the Netherlands, who have kept me emotionally grounded and provided the much appreciated (online) support and entertainment.

My thanks extend massively to my parents, who listened to all highs and lows and made me feel loved and supported. Thank you for being there for me as I navigate life, even when my decisions lead to moving abroad (a second time)!

Finally, Rik, thank you for being my home and sharing all that matters and all that is trivial with me. I am very much looking forward to our upcoming adventures in Australia, and happy to have you next to me on this journey.

Contents

Part III A Bulk-Surface Continuum Theory for Fluid Flows and Phase Separation

Chapter 1

Introduction

Coupled bulk-surface partial differential equations arise in systems involving an *active* interface, such as cellular dynamics in biological applications or surfactant transport in two-phase fluid flows. Yet, the exact coupling of the bulk and surface dynamics is far from trivial, both in its thermodynamical foundation and its numerical treatment. However, if we approach these coupled moving boundary problems from the right mathematical perspective, we are able to formalise fundamental insights in these bulk-surface interactions and their thermodynamics. In combination with appropriate numerical techniques, these mathematical frameworks can provide valuable insights in biological and engineering applications in which active interfaces are key.

1.1 Background

From a mathematical perspective, bulk-surface interactions are challenging problems due to their multiscale and multiphysics nature. Moreover, oftentimes these problems are also characterized as free-boundary problems, as in many applications the surface evolves due to the bulk-surface interplay. Various classes of models and numerical techniques have been developed to address the challenges associated with these problems. Here, we distinguish between *sharp-interface* approaches and *diffuse-interface* methods, which we further introduce in the following subsections, before arriving at a comprehensive overview of the current state of bulk-surface models in literature.

1.1.1 Moving boundary problems

A wide variety of computational mechanics problems involve moving interfaces, e.g. free surfaces[1] or internal material boundaries. Well-studied examples of these *moving-boundary problems* are the Stefan problem (phase transformation driven by heat diffusion) [145, 109], fluid-structure interaction [11] and crack propagation in solids [99, 124]. Mathematically, this class of problems is typically formulated as a set of partial differential equations on a moving domain. The moving boundary is described as a *sharp interface* with zero thickness, thereby allowing for discontinuities in quantities across the interface (e.g. stresses and energies). The key characteristic of a moving boundary problem is that the evolution of the boundary is not known a priori and is driven by the coupling of the interface dynamics to the dynamics of the material, oftentimes in the form of dynamic boundary conditions [109].

The complex nature of moving-boundary problems makes its analysis challenging, as it encompasses multiple time and length scales, as well as geometric non-linear terms

[1] In physics, a free surface is subject to zero shear stress, e.g. the interface between two immiscible fluids or the interface between gas and liquid.

resulting from the moving domain. Analytical solutions can only be found for a few special cases. The natural alternative is numerical methods, which also poses difficulties, especially in case of topologically complex three-dimensional interfaces that are subject to interactions resulting in branching, merging or pinching-off of the interface [138].

On the basis of the mathematical description of the moving boundary, we can distinguish between two classes of numerical techniques to solve moving boundary problems: *interface-tracking* and *non-interface tracking* techniques. Interface-tracking methods employ an explicit parametrization of the interface, leading most naturally to computations being performed on a moving grid, such as the Arbitrary Lagrangian-Eulerian (ALE) method [41] and Lagrangian methods. Also, the Front Tracking (FT) method [166] and the immersed boundary approach [134] are examples of interface-tracking techniques. The second class of numerical techniques, consisting of the non-interface tracking methods, can be further subdivided into two subclasses (i) *volume tracking* methods, which are based on a characteristic function defining the volume of the materials from which the interface can be reconstructed, e.g. the Volume of Fluid (VOF) methods [92], Simple Line Interface Calculation (SLIC) [128] and Piecewise Linear Interface Construction (PLIC) [143], and (ii) *interface-capturing* approaches, which employ a function to capture the interface and require additional information to describe its temporal evolution, e.g. the level-set method [132].

1.1.2 Computational phase-field modelling

The *phase-field method* [51, 138, 157] can be used as an alternative approach to the sharp-interface theory and overcomes some of the limitations associated with sharp-interface methods. In the phase-field formulation, an additional time-dependent variable, viz. the so-called phase field, is introduced, which acts as the positional marker of the different phases[2]. The phase field is designed in such a way that it takes on a distinct value in each phase, e.g. for a problem involving two phases $\varphi = -1$ in one phase and $\varphi = +1$ in the other. Since it is smoothly defined on the domain of interest, it gives rise to internal transition layers, thereby substituting the sharp interface of the original moving-boundary problem for an interface with a small yet finite width. This *diffuse interface*[3] is the key difference between phase-field theories and moving-boundary problems, and is hence the reason that phase-field methods are also called diffuse-interface models, whereas moving-boundary problems are referred to as sharp-interface theories (see Figure 1.1). By smoothing the interface and its properties phase-field modelling avoids the complex interfacial conditions used in sharp-interface theories. Instead, evolution of the diffuse interface becomes part of the solution of the phase-field equations, thereby circumventing the explicit tracking of the interface as is required for many sharp-interface methods.

In particular cases, it can be proven by means of the theory of *matched asymptotic expansions* that a phase-field model converges to a sharp-interface model, see for instance [25, 22, 49, 51, 138]. This sharp-interface counterpart is also referred to as the sharp-interface limit of the phase-field model, as the limiting case is achieved by letting the

[2]Although the phase-field theory was originally developed for phase separation problems [27, 28, 26], here phase should be interpreted broadly. It may for instance refer to one of the types of fluids present in a multi-phase fluid flow, but it may also indicate the position of a fracture in a solid or of a tumour in soft tissue. In summary, it should be understood as a compositional marker, which can be used to locate regions rich or low in the constituent of interest, and be thought of as a mass fraction, volume fraction, concentration or order parameter.

[3]The concept of a diffuse interface can be traced back to van der Waals's thermodynamic considerations (1979) [167] on the change in density between a liquid and its vapour.

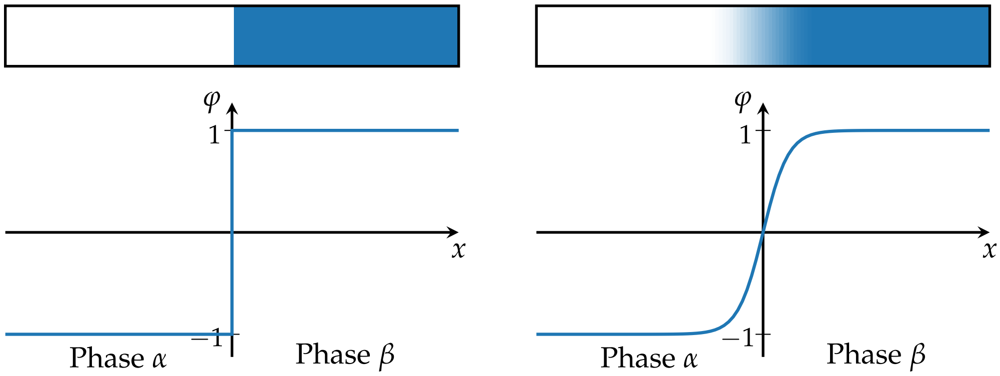

(a) Sharp-interface approach. **(b)** Diffuse-interface approach.

Figure 1.1: Schematic of a (a) sharp and (b) diffuse interface: the phase-field variable ϕ is a function of the spatial coordinate x and marks the interface.

parameter controlling the interface width go to zero. Apart from validating the phase-field model, this method of asymptotic analysis can serve to gain insight in restrictions on the phase-field model's parameters [51]. Conversely, a phase-field model may be derived from a moving-boundary problem by means of *diffusification*[4], i.e. regularization of the moving-boundary problem by smoothing out its sharp interface into a thin interfacial layer with finite thickness.

Notwithstanding their correspondence to sharp-interface models, phase-field methods are more than a mere computational trick to overcome certain numerical difficulties. It should be understood that phase-field models do not per se require a regularized moving-boundary problem as origin. Phase-field equations may be derived using the variational principles from the theory of thermodynamics [86, 78]. A phenomenological phase-field description starts by defining a free-energy functional as function of the phase field and other continuum fields (e.g. temperature, concentration, strain measures). It is supplemented with fundamental balance equations, as well as constitutive laws reflecting the materials' behaviour. The phase-field model's equations are then derived by restricting constitutive choices in such a way that the model's energy structure is consistent with the second law of thermodynamics. This framework justifies the use of phase-field formulations thermodynamically, and additionally can be used to obtain phase-field models of phenomena for which no sharp-interface theory is (yet) available.

Over the last several decades, phase-field modelling has proven to be a powerful theoretical and computational approach. Using the phase-field approach, significant progress has been made in the modelling and prediction of interfacial phenomena in numerous fields of research, e.g. in fracture mechanics [1, 2, 17, 15, 119], (fluid-mechanical instabilities such as) viscous [68] or gravitational fingering [75], multiphase flow [76, 156], cellular migration [127, 149], vesicle dynamics [13, 88], tumour growth [89, 170, 112, 131, 175] and image inpainting [12].

[4]The term diffusification has only recently been introduced by Gomez & van der Zee (2017) [78] and does not occur in phase-field literature before 2017. For an example of the diffusification procedure, viz. for a generalized Stefan problem describing the solidification of pure materials, the reader is referred to [78]. It should be noted that the diffusification procedure does not per se yield a thermomechanically-consistent phase-field model.

1.1.3 Bulk-surface modelling

Systems involving mixed-dimensional dynamics, such as bulk-surface dynamics, have been studied extensively due to their numerous applications in engineering, chemistry and biology. Yet, no uniform definition exists for a bulk-surface model. Different classes of bulk-surface models can be identified based on the used description for the (moving) boundary, that is, whether the interface has a diffuse or sharp nature.

In sharp-interface approaches, short-range interactions between the bulk and surface dynamics can be established through *dynamic boundary conditions* at the surface. Early work on these coupling conditions considers phase separation in a bulk material where one component is favoured by an impenetrable surface [14]. This way the dynamics in the bulk is enriched through its interaction with an interface. In the context of mixed-dimensional phase-field equations, that is, a set of phase-field equations living on the bulk and surface, the boundary conditions coupling the phase-field variables in the bulk and surface are also known as transmission conditions, see for instance [36, 111, 96] and references therein. Depending on the application many other types of coupling conditions have been proposed, although these have been predominantly presented for reaction-diffusion type of processes [117, 116, 115, 67]. Further applications are found for instance in bulk-surface systems involving adsorption-desorption of surfactants at the sharp interface [79], asymmetric stem cell division [58, 57], crystal growth [100], electro-reaction-diffusion systems [74], receptor-ligand interactions in cell signalling dynamics [69, 8], and multi-phase flows [73]. The main difficulties encountered within this class of bulk-surface problems arise from the presence of the non-linear coupling through the boundary conditions, especially within the context of moving domains. Many works address these difficulties and focus on numerical treatment of the bulk-surface equations. However, the presented mathematical models often include ad-hoc terms, and lack a rigorous continuum framework through which the coupling terms are formulated.

In the diffuse-interface community, bulk-surface models typically include a regularization term constricting the sharp-interface dynamics to a diffuse interface, a method in literature focussing on surface partial differential equations known as the *diffuse-interface approach*. Essentially, the surface equation of interest is approximated by a bulk equation with coefficients which rapidly tend to zero outside the diffuse-interface region. This way a coupled bulk-surface system with a sharp interface can be written as a single bulk-system with an additional bulk equation accounting for the (moving) diffuse interface. This diffuse-interface approach has been used to solve surface partial differential equations on stationary surfaces [140], as well as moving interfaces [141, 47, 113, 50]. Alternatively, when particular bulk dynamics are restricted to subregions in the domain using a suitable regularizing function, we speak of the *diffuse-domain approach*. Such an approach is in particular useful for complex stationary [98, 107, 59] and evolving domains [108, 146, 81]. For both type of regularizations, it has been demonstrated that the reformulated partial differential equations asymptotically converge to the sharp-interface system as the interfacial thickness goes to zero, see for instance [108, 105, 137, 178]. Using these regularization approaches bulk-surface models have been developed with applications in cellular migration [125, 127], multi-phase flows [142], signalling networks [139], surfactant flow [161], transport processes including the adsorption and desorption of species [160], and inextensible vesicles in flows [5]. Here, the use of the diffuse method is mainly motivated by its ease in numerical implementation: standard numerical methods can be used to include the complex (moving) geometries on which the quantities of interest live. The mathematical models presented in literature oftentimes take a sharp-interface model as a starting point, which is then *diffusified* and rewritten using appropriate regularizing functions. Such approaches are then made rigorous by asymptotic arguments. Yet, knowing that phase-field theories can be derived in a consistent manner without the need for a sharp-interface counterpart, a fundamental framework for bulk-surface interactions would benefit from taking a diffuse-interface interpretation as a point of departure. Such a framework may pave the way for novel types of bulk-surface interactions, that could not have been established using a diffusification procedure.

1.2 Aims and main contributions

The aim of this thesis is to develop general bulk-surface frameworks, and subsequently propose and study novel bulk-surface models within these frameworks. In particular, we define three main objectives

- To investigate the main characteristics of the different frameworks available for the modelling of evolving interfaces;
- To construct a thermomechanically-consistent phase-field model for adhesion, and to propose an asymptotics framework to characterize its steady states;
- To develop a general continuum framework starting from a comprehensive virtual power principle for mixed-dimensional multi-phase fluid flows, and to propose new models within this framework in which microscopic variations in the surface fluid's thickness are allowed.

As a first contribution, we provide an overview of four different frameworks that form the foundation of many models encountered in the study of interfacial phenomena. In the overview of these perspectives, we focus on the description of the interface, the underlying (energy) functional and the postulated dissipative mechanism, which together establish the evolution equations for the interface. Oftentimes proposed models are derived and studied within one of these frameworks. Yet, by making the connection to another one of these perspectives, new interpretations of the model and valuable insights in its governing mechanics can be obtained. The objective here is to present the machinery and theoretical background of these perspectives, which will be employed and expanded on in the remainder of this work.

Secondly, using a thermodynamically-consistent approach to phase-field modelling, we develop phase-field models that describe adhesive interactions between interfaces. These models are based on a class of energy functionals which include terms that are restricted to the diffuse interface, yielding bulk-surface type of interactions. Through formal asymptotic analysis we characterize the model's steady states, thereby exploiting the connection between the sharp-interface and diffuse-interface approaches. Using the finite element method and an energy-stable time-discretization scheme known as the scalar auxiliary variable approach, we arrive at numerical results reflecting the geometrical insights obtained through the asymptotic analysis. Such characterization of the adhesion model is key, before it can be further extended to describe more complex dynamics, such as dynamic surface species transport governing the adhesive strength or its coupling to fluid flow.

As a third contribution, we present a continuum theory for bulk-surface materials undergoing deformation and phase separation. In this mixed-dimensional setting, we consider an immiscible bulk fluid enclosed by a thin immiscible binary fluid film. We detail the implications of the dependency of the apparent surface density on the surface thickness. The governing equations are derived by means of a coupled bulk-surface postulate for the virtual power balance. Aside from this systematical treatment based on the virtual power principle, we consider free-energy imbalances for bulk-surface theories to arrive at classes of consistent constitutive response functions. Additionally, we complement the framework by detailing the boundary conditions, including a set of mixed dissipative coupling conditions on the dynamic surface. This complete continuum framework can be used and further extended to model bulk-surface applications.

1.3 Thesis overview

This thesis is divided into three Parts, with each Part dedicated to addressing one of the three objectives outlined in the previous Section. An overview per Chapter is detailed below. We wish to emphasize that the theory presented in Part I is based on existing literature, whereas Part II and III feature novel results that either have been accepted [16] or are in preparation for publication.

Part I (*Four Perspectives on the Modelling of Evolving Interfaces*) contains an introduction to the fundamental theories for moving interfaces and their dynamics. It details four perspectives, each with their own characteristics, yet which for particular modelling choices may produce evolution equations describing the same dynamics.

Chapter 2 (*Geometric Flows*) presents a geometrical description of moving interfaces and demonstrates how shape functionals can be used to establish geometric gradient-descent flows of sharp interfaces.

Chapter 3 (*Phase-Field Gradient Flows*) presents gradient flows using a phase-field description for the interface, and details how these are based on a choice of energy functional and an operator reflecting a dissipative mechanism.

Chapter 4 (*Variational Framework for Phase-Field Models*) details how phase-field equations can be derived in a thermomechanically-consistent manner by postulating a free-energy functional as function of the phase field and other continuum fields. This energy is supplemented with balance laws, as well as constitutive response functions that describe the materials' behaviour. The evolution equations are then derived by restricting the constitutive choices such that its energy structure is consistent with the second law of thermodynamics.

Chapter 5 (*Microkinetic Framework*) details how phase-field equations can be derived using an additional balance law, i.e. the balance of microforces. Together with constitutive response functions consistent with the second law of thermodynamics for the microkinetic quantities, such as the microstress and microforces, generalized evolution equations for the transition layers in a material can be established.

Part I is closed in Chapter 6 (*Summary of Perspectives*) in which the previously discussed perspectives on the modelling of evolving interfaces are summarized.

In **Part II (*Phase-Field Modelling of Adhesive Interfaces*)**, we apply the variational framework for thermomechanically-consistent phase-field models presented in Chapter 4 to study adhesive interactions between steady and moving interfaces.

Chapter 7 (*Introduction and Background*) motivates the development of a phase-field adhesion model. Furthermore, we present related literature for the asymptotic study into the model's equilibrium states.

In Chapter 8 (*Phase-field Models for Adhesion*), we propose a phase-field based approach to study adhesive interactions between moving interfaces. Following the variational principles presented in Chapter 4, we demonstrate that these phase-field adhesion models are thermodynamically consistent.

Chapter 9 (*Sharp-Interface Limit of the Cahn-Hilliard Energy*) focusses on the characterization of equilibrium solutions of the well-known Cahn-Hilliard phase-field model through formal asymptotics. The methods presented in this Chapter are extendable to other phase-field problems. Moreover, they provide the foundation for the convergence study of the adhesion energy in Chapter 10.

Chapter 10 (*Sharp-Interface Limit of the Adhesion Energy*) aims to characterize equilibrium solutions of the phase-field model for adhesion. By employing asymptotic expansions in the adhesion energy functional, we arrive at a sharp-interface energy counterpart. Minimizers of the sharp-interface energy connect the phase-field adhesion problem to an equivalent geometrical problem, in which curvature and contact angle characterize the shape of the equilibrium solutions.

In Chapter 11 (*Numerical Results*), the scalar auxiliary variable approach is applied to the adhesion theory to produce energy-stable numerical results of the phase-field adhesion equations. In various numerical examples, we investigate the adhesive interactions between steady and moving interfaces. In particular, the effect of curvature, adhesion strength and interfacial thickness on the equilibrium shapes are studied.

Chapter 12 (*Concluding Remarks*) summarizes the main contributions in Part II, and presents some ideas for future research involving the adhesion theory.

In **Part III (*A Bulk-Surface Continuum Theory for Fluid Flows and Phase Separation*)**, we propose a mathematical framework to study the mechanical interplay of bulk-surface materials undergoing deformation and phase separation.

Chapter 13 (*Introduction and Preliminaries*) motivates the development of such a bulk-surface continuum theory. Furthermore, we present the preliminary definitions required to establish this framework.

In Chapter 14 (*Isochoric Motion and Mass Balance*), we detail the assumption that the bulk material and enclosing thin layer of fluid are only allowed to undergo isochoric motions, that is, we consider that both flows are incompressible. Based on this hypothesis, we derive the balance of mass for the bulk and surface material. Additionally, we derive the balances accounting for the mass transport of the two species present in the bulk-surface system.

In Chapter 15 (*Principle of Virtual Power*), we provide readers new to the principle of virtual power with an introduction to this formalism, after which we postulate a virtual power balance to arrive at the field equations for the bulk-surface material. In addition, we show the consequences of frame indifference and derive relevant partwise balance laws.

Chapter 16 (*Free-Energy Imbalance and Constitutive Response Functions*) presents the free-energy imbalance for the coupled bulk-surface material. Its implications in terms of the constitutive response functions are discussed and general thermodynamically-consistent classes of response functions are detailed.

In Chapter 17 (*Boundary Conditions and Dissipation Inequalities*), we supplement the system with appropriate boundary conditions, including a set of mixed boundary conditions that allow for slip between the surface and the bulk material, which are dissipative in nature. These boundary conditions are employed to arrive at the Lyapunov decay relation for the coupled bulk-surface material, which characterizes the dissipative nature of the bulk-surface system and its interaction with the environment.

Lastly, Chapter 18 (*Concluding Remarks and Future Directions*) summarizes the main results of Part III and provides some directions for future research involving this continuum theory.

Finally, Chapter 19 (*Final Reflections*) closes this thesis. Here, we reflect on the main achievements and future research.

Part I

Four Perspectives on the Modelling of Evolving Interfaces

Chapter 2

Geometric Flows

As illustrated in Chapter 1, bulk-surface phenomena arise in a wide variety of applications. An elementary way of modelling these moving boundary problems takes a geometric description of the interface as a starting point. By prescribing the movement of the individual points that constitute the sharp interface, evolution of the interface is established. The corresponding transformation is referred to as the *flow* of the prescribed velocity field. In Section 2.1, we introduce the reader to these geometric flows and discuss two well-known examples: *mean curvature flow* and *surface diffusion*. In Section 2.2, we study *shape functionals*, which provide some quantitative measure of geometric properties, and in Section 2.3 we define their *shape derivatives*. These shape derivatives offer insight into the sensitivity of shape functionals to shape variations. In Section 2.4, we employ these shape functionals and their derivatives to establish *geometric gradient-descent flows* and discuss their dissipative nature. We conclude this Chapter by demonstrating that the earlier presented mean curvature flow and surface diffusion are both geometric gradient-descent flows.

2.1 Geometric evolution of interfaces

We consider a sufficiently smooth compact hypersurface $\Gamma(t) \subset D \subseteq \mathbb{R}^{n_{\mathrm{dim}}}$ oriented by the normal vector field $\boldsymbol{n}$. The initial configuration is given by $\Gamma_0 := \Gamma(0)$. A straightforward way to evolve the interface Γ is by directly prescribing its velocity, that is for each each time $t \in (0, T]$

$$\boldsymbol{v}(\boldsymbol{x}) = \hat{\boldsymbol{v}}_t(\boldsymbol{x}), \qquad \forall \boldsymbol{x} \in \Gamma(t), \tag{2.1}$$

where $\hat{\boldsymbol{v}}_t(\boldsymbol{x}) : \Gamma(t) \to \mathbb{R}^{n_{\mathrm{dim}}}$ is a given function, see Figure 2.1. Moreover, the solution of

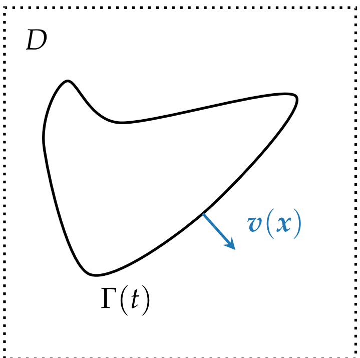

Figure 2.1: Geometric evolution of an interface $\Gamma(t)$.

the differential equation

$$\frac{\partial \boldsymbol{x}}{\partial t}(\boldsymbol{x}_0, t) = \boldsymbol{v}(\boldsymbol{x}(\boldsymbol{x}_0, t)), \qquad \forall t \in (0, T], \tag{2.2}$$

$$x(\boldsymbol{x}_0, 0) = \boldsymbol{x}_0, \tag{2.3}$$

captures the interfacial motion.

Alternatively, we can introduce a transformation $\boldsymbol{T}_t$, a diffeomorphism for each $t \in [0, T]$, describing the interfacial motion. Then, let $\boldsymbol{T}_t : \Gamma_0 \to \Gamma(t)$ be the transformation corresponding to the flow of $\boldsymbol{v}$, that is $\boldsymbol{T}_t(\boldsymbol{x}_0) = \boldsymbol{x}(\boldsymbol{x}_0, t)$, so that

$$\boldsymbol{v}(\boldsymbol{x}) := \left(\frac{\partial \boldsymbol{T}_t}{\partial t}\right) \circ \boldsymbol{T}_t^{-1}(\boldsymbol{x}), \qquad \forall \boldsymbol{x} \in \Gamma(t), \tag{2.4}$$

where $\boldsymbol{T}_0 = \mathbf{1}$. In other words, starting in $\boldsymbol{x}_0$, each point $\boldsymbol{x}(\boldsymbol{x}_0, t) = \boldsymbol{T}_t(\boldsymbol{x}_0)$ moves along the trajectory $t \mapsto \boldsymbol{x}(\boldsymbol{x}_0, t)$ with velocity $\boldsymbol{v}(\boldsymbol{x}(\boldsymbol{x}_0, t))$.

Well-studied examples of geometric evolution of $\Gamma(t)$ include motion by mean curvature and surface diffusion. These geometric flows are both based on a particular choice for the velocity $\boldsymbol{v} = V\boldsymbol{n}$, with V the magnitude of the normal velocity, see Figure 2.2. Additionally, for both flows the prescribed velocity is dependent on the curvature $K_{\mathrm{a}} := \nabla_\Gamma \cdot \boldsymbol{n}$, see Remark 2.1.

In *mean curvature flow*, a closed interface moves proportionally to its curvature, thereby decreasing the interfacial area (resp. curve length), until the interface (resp. curve) reaches a point of extinction in finite time. For this reason, two-dimensional mean curvature flow is also called curve-shortening flow.

Surface diffusion is a flow in which the surface area (resp. curve length) is minimized while the enclosed volume (resp. area) remains constant. In this process, the velocity of the interface is proportional to the surface Laplacian of the mean curvature. This choice of velocity leads to the redistribution of material on the surface, resulting in a gradual evolution towards a shape with minimized surface area (resp. curve length).

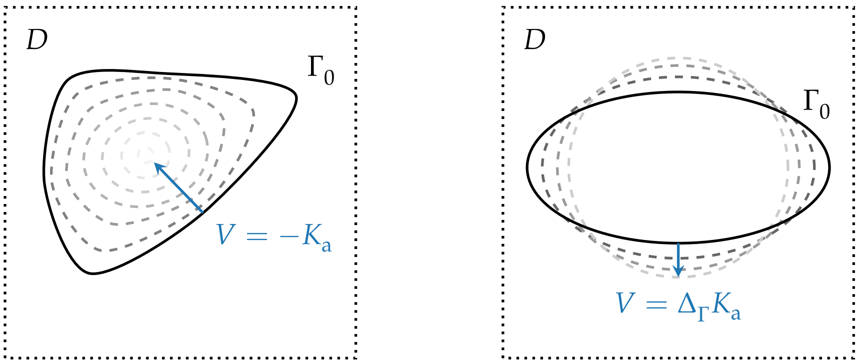

(a) Mean curvature flow. **(b)** Surface diffusion.

Figure 2.2: Examples of geometric flows.

Remark 2.1 (Mean and additative curvatures) Although, the flow depicted in Figure 2.2a is referred to as the *mean* curvature flow in literature, oftentimes the sum of the $n_{\mathrm{dim}} - 1$ principal curvatures is used instead of its average value. Thus, it is more correct to speak of an *additive* curvature $K_{\mathrm{a}} := \nabla_\Gamma \cdot \boldsymbol{n}$, instead of the mean curvature $K := (n_{\mathrm{dim}} - 1)^{-1} \nabla_\Gamma \cdot \boldsymbol{n}$. □

2.2 Shape functionals

Shape functionals are functionals that quantify geometric properties of shapes, such as interfaces or (sub)domains. To define these functionals in a more precise manner, we consider a *hold-all* domain or *universe* $D \subseteq \mathbb{R}^{n_{\text{dim}}}$. Furthermore, let $\mathcal{F}$ denote an admissible family of domains in D.

Definition 2.2 (Shape functional) A *shape functional* is a map $\mathcal{J} : \mathcal{F} \to \mathbb{R}$ from an admissible family $\mathcal{F}$ of domains into $\mathbb{R}$. □

In Definition 2.2, we establish that for a given domain $\Omega \in \mathcal{F}$, a shape functional $\mathcal{J}(\cdot)$ returns the value $\mathcal{J}(\Omega) \in \mathbb{R}$, which typically measures a specific geometric feature of the given domain. Elementary examples of shape functionals are the domain measure

$$\mathcal{J}_{\text{dom}}(\Omega) := |\Omega| = \int_{\Omega} \mathrm{d}\Omega, \tag{2.5}$$

and its boundary measure

$$\mathcal{J}_{\text{bnd}}(\Omega) := |\Gamma| = \int_{\Gamma} \mathrm{d}\Gamma, \tag{2.6}$$

where $\Gamma := \partial\Omega$. For $n_{\text{dim}} = 3$, $\mathcal{J}_{\text{dom}}(\Omega)$ measures the volume of the domain Ω and $\mathcal{J}_{\text{bnd}}(\Omega)$ the interfacial area Γ, whilst for $n_{\text{dim}} = 2$ these correspond to the domain area and its perimeter, respectively.

To define the derivatives of shape functionals in Section 2.3, we first need to consider changes or perturbations in the domain itself. In Definition 2.2, the shape functional is defined on a shape space $\mathcal{F}$, which represents the admissible family of domains or subsets in the hold-all domain D. The construction of these shape spaces can be achieved through various methods. In this Chapter, we use the *velocity method* [155, 40], also known as the *speed method* or *artificial velocity method*, to construct the admissible family of domains $\mathcal{F}$. In particular, we consider an autonomous velocity field $\boldsymbol{v} : \overline{D} \to \mathbb{R}^{n_{\text{dim}}}$ that we can use to define *one-parameter families of transformations* of a fixed domain, provided that the changes in the domain do not alter the domain's topology. Essentially, this method should be thought of as an extension of the theory presented in Section 2.1 here accounting for a deforming domain instead of a moving interface.

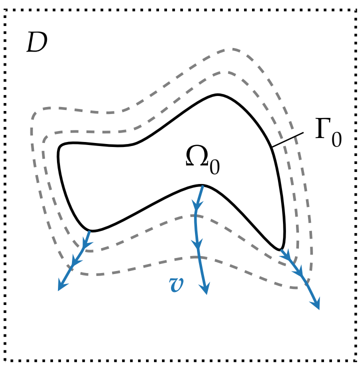

Figure 2.3: A one-parameter family of domains $\{\Omega_t\}$ constructed using the velocity method, where $\Omega_t \subset D$. The parameterized outer boundary is given by $\Gamma_t := \partial\Omega_t$.

We proceed by considering the transformation map induced by an admissible velocity field $\boldsymbol{v} : \overline{D} \to \mathbb{R}^{n_{\text{dim}}}$. For each $t \in [0, T]$, the associated transformation $\boldsymbol{T}_t$ is a diffeomorphism that maps a point $\boldsymbol{x}_0 \in \Omega_0$ onto $\boldsymbol{x}(\boldsymbol{x}_0, t) = \boldsymbol{T}_t(\boldsymbol{x}_0) \in \Omega_t$, where t is the (artificial) time parameter governing the domain transformation. Similar to (2.2), the evolution of the domain is given by the solution $\boldsymbol{x}(\boldsymbol{x}_0, t)$ to the initial value problem

$$\frac{\partial \boldsymbol{x}}{\partial t}(\boldsymbol{x}_0, t) = \boldsymbol{v}(\boldsymbol{x}(\boldsymbol{x}_0, t)), \qquad \forall t \in (0, T], \tag{2.7}$$

$$\boldsymbol{x}(\boldsymbol{x}_0, 0) = \boldsymbol{x}_0. \tag{2.8}$$

Starting in its reference position $\boldsymbol{x}_0 \in \Omega_0$, each point $\boldsymbol{x}(\boldsymbol{x}_0, t) = \boldsymbol{T}_t(\boldsymbol{x}_0) \in \Omega_t$ moves along the trajectory $t \mapsto \boldsymbol{x}(\boldsymbol{x}_0, t)$ with current velocity $\boldsymbol{v}(\boldsymbol{x}(\boldsymbol{x}_0, t))$, thereby capturing the flow of $\boldsymbol{v}$. Thus, the family of $\{\boldsymbol{T}_t\}$ generates the family of domains $\{\Omega_t\}$, where

$$\Omega_t = \boldsymbol{T}_t(\Omega) := \{\boldsymbol{x} \in \mathbb{R}^{n_{\text{dim}}} : \boldsymbol{x} = \boldsymbol{T}_t(\boldsymbol{x}_0),\ \forall \boldsymbol{x}_0 \in \Omega_0\}. \tag{2.9}$$

with $\boldsymbol{T}_t$ mapping interior (resp. boundary) points of Ω_0 onto interior (resp. boundary) points on Ω_t, see Figure 2.3. This continuous perturbation of the initial domain is the main characteristic of the velocity method.

2.3 Shape derivatives

To define shape derivatives of shape functionals, we consider the velocity field $\boldsymbol{v} : \overline{D} \to \mathbb{R}^{n_{\text{dim}}}$ and associated transformation $\boldsymbol{T}_t$ defined in Section 2.2, generating the perturbed domain $\Omega_t = \boldsymbol{T}_t(\Omega)$. Formally, shape differentiability should be understood as in Definitions 2.3 and 2.4.

Definition 2.3 (Eulerian semiderivative of a shape functional) The Eulerian semiderivative of the shape functional $\mathcal{J}(\cdot)$ at Ω in the direction of $\boldsymbol{v}$ is defined as the one-sided limit

$$\mathcal{J}'(\Omega; \boldsymbol{v}) = \lim_{t \searrow 0} \frac{\mathcal{J}(\Omega_t) - \mathcal{J}(\Omega)}{t}, \tag{2.10}$$

if the limit exists in $\mathbb{R}$. □

Definition 2.4 (Shape differentiability) The functional $\mathcal{J} : \mathcal{F} \to \mathbb{R}$ is *shape differentiable* at $\Omega \in \mathcal{F}$ if (i) the Eulerian semiderivative $\mathcal{J}'(\Omega; \boldsymbol{v})$ exists for all admissible directions $\boldsymbol{v}$ and (ii) the mapping $\boldsymbol{v} \to \mathcal{J}'(\Omega; \boldsymbol{v})$ is linear and continuous. □

Theorem 2.A (Hadamard[5] formula) *If the shape functional $\mathcal{J}(\cdot)$ is shape differentiable at Ω, then its shape gradient $\mathcal{J}'(\Omega; \cdot)$ is supported on Γ. Moreover, if Γ is sufficiently smooth, we can write*

$$\mathcal{J}'(\Omega; \boldsymbol{v}) = \int_\Gamma g(\Gamma) \boldsymbol{v} \cdot \boldsymbol{n} \, \mathrm{d}\Gamma, \tag{2.11}$$

for some $g(\Gamma) \in L^1(\Gamma)$. We call $g(\Gamma)$ the Hadamard shape-gradient. □

Proof. See [40] (page 479) for the unconstrained case ($D = \mathbb{R}^{n_{\text{dim}}}$) and [38] for the constrained case ($D \subset \mathbb{R}^{n_{\text{dim}}}$). ■

The first part in Theorem 2.A states that the shape derivative $\mathcal{J}'(\Omega; \cdot)$ is supported on Γ (as a distribution), which implies that $\mathcal{J}'(\Omega; \boldsymbol{v}) = 0$ if $\boldsymbol{v}|_\Gamma = \mathbf{0}$. Thus, changes in the

[5] The origin of this theorem can be attributed to Hadamard [87], who studied in 1907 displacements along the normal of the boundary of a C^∞-domain to compute the eigenvalues of a clamped plate. The structure theorem in (2.A) for the Eulerian shape derivative of smooth domains was first given by Zolesio [183], and later generalized to nonsmooth domains by Delfour & Zolesio [38].

shape functional are primarily influenced by variations in the velocity at the boundary, i.e. non-zero $\boldsymbol{v}|_\Gamma$. This validates our choice for an autonomous velocity, as for a nonautonomous velocity $\boldsymbol{v}(\boldsymbol{x}, t)$ only its value at $t = 0$ would be relevant.

Next to the contribution from the $(\boldsymbol{v} \cdot \boldsymbol{n})|_\Gamma$ term, we also learn that Hadamard's shape gradient $g(\Gamma)|_\Gamma$ contributes to the shape derivative $\mathcal{J}'(\Omega; \boldsymbol{v})$. The choice of shape functional $J(\cdot)$ determines the form of the Hadamard shape-gradient $g(\Gamma)|_\Gamma$.

In the remainder of this section, we consider the shape derivatives of two fundamental shape functionals: domain integrals (Subsection 2.3.1) and boundary integrals (2.3.2). We employ Hadamard's formula (Theorem (2.A)) and derive the Hadamard shape-gradient for each type of shape integral.

2.3.1 Shape derivative of domain integrals

In the following, we consider the open bounded Lipschitz domain Ω in $\mathbb{R}^{n_{\text{dim}}}$ and let the domain integral of a global function $\phi : \mathbb{R}^{n_{\text{dim}}} \to \mathbb{R}$ be given by

$$\mathcal{J}_\phi(\Omega) := \int_\Omega \phi \, \mathrm{d}\Omega. \tag{2.12}$$

Furthermore, let $\boldsymbol{v} : \overline{D} \to \mathbb{R}^{n_{\text{dim}}}$ be an admissible velocity field. The associated transformation $\boldsymbol{T}_t$ maps $\Omega := \Omega_0$ onto $\Omega_t := \boldsymbol{T}_t(\Omega)$ with $\Gamma_t = \partial\Omega_t$, so that the family of domains $\{\Omega_t\}$ consists of bounded open Lipschitz domains in D, which all have a piecewise smooth boundary. In Theorem 2.B, the shape derivative of $\mathcal{J}_\phi(\Omega)$ in (2.12) is derived by differentiating $t \mapsto \mathcal{J}_\phi(\Omega_t)$ at $t = 0$.

Theorem 2.B (Shape derivative of domain integral) *For $\phi \in W^{1,1}(\mathbb{R}^{n_{\text{dim}}})$, the shape derivative of the domain integral in* (2.12) *is given by*

$$\mathcal{J}_\phi{}'(\Omega; \boldsymbol{v}) = \int_\Omega \nabla \cdot (\phi \boldsymbol{v}) \, \mathrm{d}\Omega = \int_\Gamma \phi \boldsymbol{v} \cdot \boldsymbol{n} \, \mathrm{d}\Gamma. \tag{2.13}$$

for sufficiently smooth Γ. □

Proof. Using a change of variables, we write

$$\mathcal{J}_\phi(\Omega_t) = \int_{\Omega_t} \phi \, \mathrm{d}\Omega_t = \int_\Omega \phi \circ \boldsymbol{T}_t J_t \, \mathrm{d}\Omega, \tag{2.14}$$

where $J_t := |\mathrm{D}\boldsymbol{T}_t| > 0$ denotes the Jacobian of $\boldsymbol{T}_t$, with $|\mathrm{D}\boldsymbol{T}_t|$ the determinant of the Jacobian matrix. Next, we obtain the shape derivative as follows

$$\begin{aligned}
\mathcal{J}_\phi{}'(\Omega; \boldsymbol{v}) &= \frac{\mathrm{d}}{\mathrm{d}t} \mathcal{J}_\phi(\Omega_t) \bigg|_{t=0} \\
&= \int_\Omega \frac{\partial}{\partial t} (\phi \circ \boldsymbol{T}_t J_t) \bigg|_{t=0} \mathrm{d}\Omega \\
&= \int_\Omega \left(\left(\nabla\phi(\boldsymbol{T}_t(\boldsymbol{x}_0)) \cdot \frac{\partial}{\partial t} \boldsymbol{T}_t(\boldsymbol{x}_0) \right) J_t + (\phi \circ \boldsymbol{T}_t) \frac{\partial}{\partial t} J_t \right) \bigg|_{t=0} \mathrm{d}\Omega \\
&= \int_\Omega (\nabla\phi \cdot \boldsymbol{v} + \phi \nabla \cdot \boldsymbol{v}) \, \mathrm{d}\Omega,
\end{aligned} \tag{2.15}$$

where we have used that

$$\begin{aligned}
\frac{\partial}{\partial t} (\phi \circ \boldsymbol{T}_t)|_{t=0} &= \left(\nabla\phi(\boldsymbol{T}_t(\boldsymbol{x}_0)) \cdot \frac{\partial}{\partial t} \boldsymbol{T}_t(\boldsymbol{x}_0) \right) \bigg|_{t=0} \\
&= \nabla\phi(\boldsymbol{x}_0) \cdot \boldsymbol{v}(\boldsymbol{x}_0),
\end{aligned} \tag{2.16}$$

as well as

$$\frac{\partial}{\partial t} J_t|_{t=0} = J_t \mathrm{tr}(\nabla \boldsymbol{v})|_{t=0} = \nabla \cdot \boldsymbol{v}, \tag{2.17}$$

with $J_t|_{t=0} = 1$. Application of the divergence problem finishes the proof. For further details, the reader is referred to [40] (Theorem 4.1 on page 482) and [168] (Section 4.3.3 starting on page 67). ■

In view of Theorem 2.B, we confirm that the shape derivative of $\mathcal{J}_\phi(\Omega)$ given in (2.13) is supported on Γ and scales with $\phi|_\Gamma$. Thus, for domain shape functionals of the form (2.12), we find $g_\phi(\Gamma) := \phi|_\Gamma$ as the associated Hadamard shape-gradient.

2.3.2 Shape derivative of boundary integrals

Consider the global function $\psi : \mathbb{R}^{n_{\mathrm{dim}}} \to \mathbb{R}$ and its corresponding boundary shape functional

$$\mathcal{J}_\psi(\Omega) = \int_\Gamma \psi \,\mathrm{d}\Gamma. \tag{2.18}$$

Similar to Section 2.3.1, we let $\boldsymbol{v} : \overline{D} \to \mathbb{R}^{n_{\mathrm{dim}}}$ denote an admissible velocity field, which is sufficiently smooth, and let $\boldsymbol{T}_t$ denote the associated transformation generating the domain $\Omega_t = \boldsymbol{T}_t(\Omega)$ with boundary $\Gamma(t) = \partial\Omega_t$. The shape derivative of the boundary shape functional (2.18) for a sufficiently smooth and closed Γ is given in Theorem 2.C.

Theorem 2.C (Shape derivative of boundary integral) *For $\psi \in W^{2,1}(\mathbb{R}^{n_{\mathrm{dim}}})$, the shape derivative of the boundary integral in* (2.18) *is given by*

$$\mathcal{J}_\psi{}'(\Omega; \boldsymbol{v}) = \int_\Gamma \left(\frac{\partial \psi}{\partial n} + K_{\mathrm{a}} \psi \right) \boldsymbol{v} \cdot \boldsymbol{n} \,\mathrm{d}\Gamma, \tag{2.19}$$

for sufficiently smooth and closed Γ. □

Proof. Using a change of variables, we write

$$\mathcal{J}_\psi(\Omega_t) = \int_{\Gamma_t} \psi \,\mathrm{d}\Gamma_t = \int_\Gamma \psi \circ \boldsymbol{T}_t j_t \,\mathrm{d}\Gamma, \tag{2.20}$$

where $j_t := J_t |\mathrm{D}\boldsymbol{T}_t^{-\top} \boldsymbol{n}| > 0$ denotes the areal Jacobian. In view of

$$\frac{\partial}{\partial t} (\psi \circ \boldsymbol{T}_t)|_{t=0} = \left(\nabla_\Gamma \psi + \frac{\partial \psi}{\partial n} \boldsymbol{n} \right) \cdot \boldsymbol{v}, \qquad \text{on } \Gamma, \tag{2.21}$$

and

$$\frac{\partial}{\partial t} j_t|_{t=0} = \nabla_\Gamma \cdot \boldsymbol{v}, \tag{2.22}$$

we write shape derivative of $\mathcal{J}_\psi$ as

$$\begin{aligned} \mathcal{J}_\psi{}'(\Omega; \boldsymbol{v}) &= \frac{\mathrm{d}}{\mathrm{d}t} \mathcal{J}_\psi(\Omega_t) \Big|_{t=0} \\ &= \int_\Gamma \frac{\partial}{\partial t} (\psi \circ \boldsymbol{T}_t j_t) \Big|_{t=0} \mathrm{d}\Gamma \\ &= \int_\Gamma \left(\nabla_\Gamma \psi \cdot \boldsymbol{v} + \frac{\partial \psi}{\partial n} \boldsymbol{v} \cdot \boldsymbol{n} + \psi \nabla_\Gamma \cdot \boldsymbol{v} \right) \mathrm{d}\Gamma. \end{aligned} \tag{2.23}$$

For sufficiently smooth and closed Γ, we may use the tangential identity

$$\psi \nabla_\Gamma \cdot \boldsymbol{v} + \nabla_\Gamma \psi \cdot \boldsymbol{v} = K_{\mathrm{a}} \psi \boldsymbol{v} \cdot \boldsymbol{n}, \qquad \text{on } \Gamma, \tag{2.24}$$

to arrive at

$$\mathcal{J}_\psi{}'(\Omega; \boldsymbol{v}) = \int_\Gamma \left(\frac{\partial \psi}{\partial n} + K_\mathrm{a}\psi \right) \boldsymbol{v} \cdot \boldsymbol{n} \, \mathrm{d}\Gamma, \tag{2.25}$$

with $K_\mathrm{a} = \nabla_\Gamma \cdot \boldsymbol{n}$ the additive curvature. See [39] (Theorem 4.3 on page 486) and [168] (Section 4.3.4 on page 70) for further details. ∎

In view of Theorem 2.C, the Hadamard shape-gradient for $\mathcal{J}_\psi$ reads

$$g_\psi(\Gamma) = \left(\frac{\partial \psi}{\partial n} + K_\mathrm{a}\psi \right) |_\Gamma, \tag{2.26}$$

where the first term reflects the changes in ψ normal to the boundary Γ and the second implies that changes in the length (or area) of the boundary are proportional to the boundary's curvature.

2.4 Geometric gradient flows

A geometric gradient(-descent) flow is an evolving interface which minimizes a shape functional $\mathcal{J}(\Omega)$ according to

$$V(\boldsymbol{x}) = \mathcal{G}g(\Gamma(t))(\boldsymbol{x}) \qquad \forall \boldsymbol{x} \in \Gamma(t), \tag{2.27}$$

where $g(\Gamma)$ is the Hadamard shape-gradient introduced in Theorem 2.A, and V denotes the normal velocity, i.e. $V := \boldsymbol{v} \cdot \boldsymbol{n}|_\Gamma$. The non-positive operator $\mathcal{G}$ reflects the mechanism driving the minimization process. In Proposition 2.5, we demonstrate how the geometric evolution equation in (2.27) establishes minimization (dissipation) of the shape functional.

Proposition 2.5 (Dissipation in geometric gradient flows) *A geometric gradient flow is dissipative in nature, i.e.*

$$\begin{aligned} \frac{\mathrm{d}\mathcal{J}(\Omega(t))}{\mathrm{d}t} &= \int_{\Gamma(t)} g(\Gamma(t))\mathcal{G}g(\Gamma(t)) \, \mathrm{d}\Gamma \\ &\leq 0, \end{aligned} \tag{2.28}$$

for all geometric evolution laws given by

$$V(\boldsymbol{x}, t) = \mathcal{G}g(\Gamma(t))(\boldsymbol{x}), \qquad \forall \boldsymbol{x} \in \Gamma(t), \tag{2.29}$$

where $\mathcal{G}$ is a non-positive operator. □

Proof. By combining Theorem (2.A) with the geometric evolution equation in (2.27), we derive

$$\begin{aligned} \frac{\mathrm{d}\mathcal{J}(\Omega(t))}{\mathrm{d}t} &= \mathcal{J}'(\Omega(t); \boldsymbol{v}) \\ &= \int_{\Gamma(t)} g(\Gamma(t))\boldsymbol{v} \cdot \boldsymbol{n} \, \mathrm{d}\Gamma \\ &= \int_{\Gamma(t)} g(\Gamma(t))\mathcal{G}g(\Gamma(t)) \, \mathrm{d}\Gamma \\ &\leq 0, \end{aligned} \tag{2.30}$$

where $\mathcal{G}$ is a non-positive operator, which completes our proof. ∎

2.4.1 Mean curvature flow

Under mean curvature flow, a closed hypersurface $\Gamma(t) \subset D \subseteq \mathbb{R}^{n_{\mathrm{dim}}}$ moves according to

$$V(\boldsymbol{x}, t) = -K_{\mathrm{a}}(\Gamma(t))(\boldsymbol{x}), \qquad \forall \boldsymbol{x} \in \Gamma(t), \tag{2.31}$$

where $K_{\mathrm{a}} = \nabla_{\Gamma} \cdot \boldsymbol{n}$ denotes the curvature. This equation states that $\Gamma(t)$ evolves in time by moving in the direction opposite to the curvature K_{a} at each point $\boldsymbol{x} \in \Gamma(t)$, with a velocity proportional to K_{a}. This flow causes the hypersurface to contract, ultimately leading to its extinction within a finite time, see Figure 2.2a. Motion by mean curvature has been extensively investigated and finds applications in material science and image processing. Noteworthy are the studies into the singularities that can occur under the flow, and the topological changes these singularities may induce, see [34] and references therein.

In the following, we demonstrate that the geometric equation for mean curvature flow (2.31), is a geometric gradient flow for the area shape functional $\mathcal{J}_{\mathrm{bnd}}(\Omega)$ in (2.6) and non-positive operator $\mathcal{G} = -\mathbf{1}$. Noting that $\mathcal{J}_{\mathrm{bnd}}(\Omega)$ corresponds to $\mathcal{J}_{\psi=1}(\Omega)$ in (2.18), and by employing Theorem (2.C) we obtain the following dissipation associated with the mean curvature flow (2.31)

$$\begin{aligned} \frac{\mathrm{d}\mathcal{J}_{\mathrm{bnd}}(\Omega(t))}{\mathrm{d}t} &= \mathcal{J}_{\mathrm{bnd}}{}'(\Omega(t); \boldsymbol{v}) \\ &= \int_{\Gamma(t)} K_{\mathrm{a}}(\Gamma(t)) \boldsymbol{v} \cdot \boldsymbol{n} \, \mathrm{d}\Gamma \\ &= -\int_{\Gamma(t)} K_{\mathrm{a}}(\Gamma(t))^2 \, \mathrm{d}\Gamma \\ &\leq 0, \end{aligned} \tag{2.32}$$

as the Hadamard shape derivative is given by $g_{\psi=1} = K_{\mathrm{a}}(\Gamma(t))$. Thus, in line with Proposition 2.5, we may call (2.31) a geometric gradient descent flow for $\mathcal{J}_{\mathrm{bnd}}(\Omega)$ and operator $\mathcal{G} = -\mathbf{1}$. Minimizers are called shrinkers or extinction points.

2.4.2 Surface diffusion

Surface diffusion, similar to mean curvature flow, also minimizes the interfacial area $\mathcal{J}_{\mathrm{bnd}}(\Omega)$ of a closed hypersurface $\Gamma(t) \subset D \subseteq \mathbb{R}^{n_{\mathrm{dim}}}$. However, a different mechanism is governing the dissipation, viz. the operator $\mathcal{G} = \Delta_{\Gamma}$, which is the surface Laplacian. Thus, the geometric evolution law for surface diffusion is

$$V(\boldsymbol{x}, t) = \Delta_{\Gamma} \left(K_{\mathrm{a}}(\Gamma(t))(\boldsymbol{x}) \right), \qquad \forall \boldsymbol{x} \in \Gamma(t), \tag{2.33}$$

where we have used the associated Hadamard shape derivative $g_{\psi=1} = K_{\mathrm{a}}(\Gamma(t))$. The dissipation structure of this flow is given by

$$
\begin{aligned}
\frac{\mathrm{d}\mathcal{J}_{\mathrm{bnd}}(\Omega(t))}{\mathrm{d}t} &= \mathcal{J}_{\mathrm{bnd}}{}'(\Omega(t);\boldsymbol{v}) \\
&= \int_{\Gamma(t)} K_{\mathrm{a}}(\Gamma(t))\boldsymbol{v}\cdot\boldsymbol{n}\,\mathrm{d}\Gamma, \\
&= \int_{\Gamma(t)} K_{\mathrm{a}}(\Gamma(t))\Delta_{\Gamma}K_{\mathrm{a}}(\Gamma(t))\,\mathrm{d}\Gamma \\
&= -\int_{\Gamma(t)} |\nabla_{\Gamma}\left(K_{\mathrm{a}}(\Gamma(t))\right)|^2\,\mathrm{d}\Gamma + \int_{\Gamma(t)} \nabla_{\Gamma}\cdot\left(K_{\mathrm{a}}(\Gamma(t))\nabla_{\Gamma}K_{\mathrm{a}}(\Gamma(t))\right)\,\mathrm{d}\Gamma \\
&\leq 0,
\end{aligned}
\tag{2.34}
$$

where we note that $\int_{\Gamma(t)} \nabla_{\Gamma}\cdot\left(K_{\mathrm{a}}(\Gamma(t))\nabla_{\Gamma}K_{\mathrm{a}}(\Gamma(t))\right)\,\mathrm{d}\Gamma = 0$.

As graphically represented in Figure 2.2b, surface diffusion preserves the volume of the domain Ω enclosed by the interface $\Gamma := \partial\Omega_t$, whilst minimizing the surface area, thereby forcing the interface to form a spherical shape with constant curvature.

Chapter 3

Phase-Field Gradient Flows

In this Chapter, we consider *phase-field gradient flows* which govern the evolution of one or more *phase-field variables*. These phase-field variables capture the diffuse transition layers in the system of interest, representing its ordering or physical structure. Phase-field gradient flows have a similar form to the geometric gradient-descent flows presented in Chapter 2. Instead of a choice for a shape functional, they involve a choice for a functional that depends on the phase-field variable(s). Again, providing the system with a suitable operator is key to achieving dissipation.

This Chapter is organized as follows: In Section 3.1, the general gradient flow structure for phase-field models is presented. Section 3.2 demonstrates how two classical phase-field equations, that is the Allen-Cahn and Cahn-Hilliard equations, can be derived within the gradient flow framework. Originally, both equations were not derived using a gradient flow approach, but via physical arguments, which we detail in Chapter 4.

3.1 Gradient flow structure for phase-field models

Generally, a gradient flow is defined as an evolution process in which a functional decreases along its gradient until a local minimum is found. In the following, we demonstrate that this process is determined by specifying both (i) the functional of interest and (ii) the dissipation mechanism.

For phase-field gradient flows defined on a bounded domain $\Omega \subset \mathbb{R}^{n_{\mathrm{dim}}}$, the governing functional depends on the phase-field variable $\varphi : \Omega \to \mathbb{R}$, and can be denoted as $\mathcal{F} : \mathcal{V} \to \mathbb{R}$

$$\mathcal{F}(\varphi) := \int_{\Omega} \psi(\varphi(\boldsymbol{x}), \nabla\varphi(\boldsymbol{x}))\,\mathrm{d}x, \tag{3.1}$$

for a choice of the function[6] $\psi : \mathbb{R} \times \mathbb{R}^{n_{\mathrm{dim}}} \to \mathbb{R}$. Here, $\mathcal{V}$ is an appropriate Sobolev space and ψ is chosen such that $\mathcal{F}$ is bounded. The Sobolev space is equipped with norm $\|\cdot\|_{\mathcal{V}}$. In physical applications, the functional $\mathcal{F}$ is often referred to as the free-energy functional, and choices for ψ may include a smooth function $W(\varphi) : \mathbb{R} \to \mathbb{R}$ that is non-negative and has equal minima at $\varphi = \varphi_-$ and $\varphi = \varphi_+ = -\varphi_-$.

To establish a gradient flow for the time-dependent $\varphi(\cdot, t) \in \mathcal{V}$ we need to define the derivative of the functional $\mathcal{F}$ in the direction $\delta\varphi$. For this purpose, we introduce the *Gâteaux derivative* of $\mathcal{F} : \mathcal{V} \to \mathbb{R}$ as

$$\mathcal{F}'(\varphi; \delta\varphi) = \lim_{s\to 0} \left(\frac{\mathcal{F}(\varphi + s\delta\varphi) - \mathcal{F}(\varphi)}{s} \right), \qquad \forall \delta\varphi \in \mathcal{X} \subseteq \mathcal{V}, \tag{3.2}$$

[6] A broader class of functions for ψ may be considered. Here, we focus on the general class given by $\psi : \mathbb{R} \times \mathbb{R}^{n_{\mathrm{dim}}} \to \mathbb{R}$.

if the limit exists for the considered $\varphi(\cdot,t) \in \mathcal{V}$ and all $\delta\varphi \in \mathcal{X}$. Here, the constrained space $\mathcal{X}$ may be used to limit the directions $\delta\varphi$, which can for instance be used to account for certain boundary conditions.

Next, suppose that $\mathcal{F}$ is Gâteaux differentiable at φ. In addition, let $\mathcal{W}$ be an inner product space such that $\mathcal{V} \subseteq \mathcal{W}$, and let $(\cdot,\cdot)_{\mathcal{W}}$ to denote the inner product. Following [37], suppose that there exists a unique $D\mathcal{F}(\varphi) \in \mathcal{W}$ such that

$$\mathcal{F}'(\varphi;\delta\varphi) = \Big(D\mathcal{F}(\varphi), \delta\varphi\Big)_{\mathcal{W}}, \qquad \forall \delta\varphi \in \mathcal{X} \subseteq \mathcal{V} \subseteq \mathcal{W}, \tag{3.3}$$

where $D\mathcal{F}(\varphi)$ is called the Riesz representative of the map $\mathcal{F}'(\varphi,\cdot)$ or the *Gâteaux gradient*.

Then, the evolution of the phase field $\varphi(\boldsymbol{x},t)$ is driven by the energy functional $\mathcal{F}$ in the direction opposite to its gradient, that is

$$\frac{\partial\varphi}{\partial t} = -mD\mathcal{F}(\varphi), \tag{3.4}$$

with $m \geq 0$. The form of the phase-field gradient flow (3.4) guarantees free-energy-dissipation in time. Specifically, we find that

$$\frac{\mathrm{d}}{\mathrm{d}t}\mathcal{F}(\varphi) = \mathcal{F}'\Big(\varphi;\frac{\partial\varphi}{\partial t}\Big) = \Big(D\mathcal{F}(\varphi),\frac{\partial\varphi}{\partial t}\Big)_{\mathcal{W}} = -m\|D\mathcal{F}(\varphi)\|^2_{\mathcal{W}} \leq 0. \tag{3.5}$$

Thus, the dissipation mechanism in the system depends on the choice of $m \geq 0$ and the considered inner product space $\mathcal{W}$. We shall see in Section 3.2 how the choice of a physically relevant space is affects this dissipation structure.

In this Chapter, we restrict ourselves to functionals that only depend on the phase-field variable. Nevertheless, this framework can be expanded to depend on more state variables, allowing for further generalizations and extensions to other applications. Examples of these involve elasticity [147], flow through (deformable) porous media [29, 159], and reaction-diffusion systems [120]. A further introduction to gradient flows can for instance be found in [172, 133].

3.2 Examples of phase-field gradient flows

This Section aims to demonstrate how the classical phase-field equations, that is, the Allen-Cahn and Cahn-Hilliard equations, can be derived within the gradient flow framework for phase-field models.

For both systems, the governing functional is the so-called free-energy functional $\mathcal{F} : \mathcal{V} \to \mathbb{R}$, that is

$$\mathcal{F}(\varphi) := \int_\Omega \Big(W(\varphi) + \frac{\varepsilon^2}{2}|\nabla\varphi|^2\Big)\,\mathrm{d}x, \tag{3.6}$$

where $\varepsilon > 0$ is a small parameter and $W(\varphi)$ the smooth double-well function introduced in Section 3.1. Depending on the exact growth rate of $W(\varphi)$, $\mathcal{V} = H^1(\Omega)$ could be sufficient. Throughout this Section, we consider suitable homogeneous boundary conditions, and therefore let $\mathcal{X} := C_0^\infty \subseteq \mathcal{W}$. Thus, the Gâteaux derivative (3.2) becomes

$$\begin{aligned}\mathcal{F}'(\varphi;\delta\varphi) &= \lim_{s\to 0}\left(\frac{\mathcal{F}(\varphi+s\delta\varphi)-\mathcal{F}(\varphi)}{s}\right)\\ &= \int_\Omega (\partial_\varphi\psi\,\delta\varphi + \partial_{\nabla\varphi}\psi\cdot\nabla(\delta\varphi))\,\mathrm{d}x\\ &= \int_\Omega (\partial_\varphi\psi - \nabla\cdot(\partial_{\nabla\varphi}\psi))\delta\varphi\,\mathrm{d}x\\ &= \int_\Omega (W'(\varphi)-\varepsilon^2\Delta\varphi)\delta\varphi\,\mathrm{d}x, \end{aligned}\tag{3.7}$$

which holds for all $\delta\varphi \in C_0^\infty$.

3.2.1 Allen-Cahn equation

In the following, we derive the L^2-gradient flow of the functional (3.6). This gradient flow is also known as the Allen-Cahn equation, which physical background we further detail in Section 4.2. Using $\mathcal{W} := L^2$ in expression (3.3), we find

$$\mathcal{F}'(\varphi;\delta\varphi) = \Big(D\mathcal{F}(\varphi),\delta\varphi\Big)_{L^2(\Omega)} = \int_\Omega D\mathcal{F}(\varphi)\delta\varphi\,\mathrm{d}x. \tag{3.8}$$

Then, in view of (3.7), we arrive at the expression for the Gâteaux gradient

$$D\mathcal{F}(\varphi) = W'(\varphi) - \varepsilon^2\Delta\varphi. \tag{3.9}$$

By substitution of the expression (3.9) in the general form of the evolution law (3.4), we arrive at the L^2-gradient flow

$$\frac{\partial\varphi}{\partial t} = -m(W'(\varphi)-\varepsilon^2\Delta\varphi), \tag{3.10}$$

which is the Allen-Cahn equation [7]. The corresponding dissipation structure is given by

$$\frac{\mathrm{d}}{\mathrm{d}t}\mathcal{F}(\varphi) = \Big(D\mathcal{F}(\varphi),\frac{\partial\varphi}{\partial t}\Big)_{L^2(\Omega)} = -m\|D\mathcal{F}(\varphi)\|^2_{L^2(\Omega)} \leq 0, \tag{3.11}$$

where we have used that $m \geq 0$.

3.2.2 Cahn-Hilliard equation

The Cahn-Hilliard equation is defined as the H^{-1}-gradient flow. Using $\mathcal{W} := H^{-1}$ in the expression for the Gâteaux gradient (3.3), we derive

$$\mathcal{F}'(\varphi;\delta\varphi) = \Big(D\mathcal{F}(\varphi),\delta\varphi\Big)_{H^{-1}(\Omega)} = \int_\Omega \nabla(\Delta^{-1}D\mathcal{F}(\varphi))\cdot\nabla(\Delta^{-1}\delta\varphi)\,\mathrm{d}x. \tag{3.12}$$

Here, the inverse Laplacian operator $-\Delta^{-1} : H^{-1} \to H_0^1$ is defined through the equivalent problems

$$\Delta^{-1}f = v \qquad \Longleftrightarrow \qquad (\nabla v,\nabla\eta)_{L^2(\Omega)} = < f,\eta >_{H^{-1},H_0^1}, \quad \forall\eta\in H_0^1, \tag{3.13}$$

where the pairing $< f,\eta >_{H^{-1},H_0^1}$ can be written as the linear form

$$< f,\eta >_{H^{-1},H_0^1} = f(\eta) := \int_\Omega f\eta\,\mathrm{d}x, \tag{3.14}$$

if f is smooth enough. Thus, using $v := \Delta^{-1}\delta\varphi$ and $\eta := \Delta^{-1}D\mathcal{F}(\varphi)$, we arrive at

$$\mathcal{F}'(\varphi;\delta\varphi) = -\int_\Omega \Delta^{-1}(D\mathcal{F}(\varphi))\delta\varphi\,\mathrm{d}x. \tag{3.15}$$

Combining (3.7) and (3.15), we arrive at

$$\mathcal{F}'(\varphi;\delta\varphi) = \int_\Omega \Delta^{-1}(D\mathcal{F}(\varphi))\delta\varphi\,\mathrm{d}x = \int_\Omega (W'(\varphi) - \varepsilon^2\Delta\varphi)\delta\varphi\,\mathrm{d}x, \tag{3.16}$$

and hence in weak sense

$$D\mathcal{F}(\varphi) = -\Delta(W'(\varphi) - \varepsilon^2\Delta\varphi). \tag{3.17}$$

Thus, the evolution equation reads

$$\frac{\partial\varphi}{\partial t} = -m\Delta(W'(\varphi) - \varepsilon^2\Delta\varphi), \tag{3.18}$$

which is the Cahn-Hilliard equation [27], subject to suitable homogeneous boundary conditions. The corresponding dissipation structure reads

$$\frac{\mathrm{d}}{\mathrm{d}t}\mathcal{F}(\varphi) = \left(D\mathcal{F}(\varphi), \frac{\partial\varphi}{\partial t}\right)_{H^{-1}(\Omega)} = -m\|D\mathcal{F}(\varphi)\|^2_{H^{-1}(\Omega)} \leq 0, \tag{3.19}$$

where we have used that $m \geq 0$.

Finally, by integrating the H^{-1}-gradient flow (3.18) over the domain Ω, we obtain

$$\begin{aligned}\frac{\mathrm{d}}{\mathrm{d}t}\int_\Omega \varphi\,\mathrm{d}x &= \int_\Omega \frac{\partial\varphi}{\partial t}\,\mathrm{d}x \\ &= -m\int_\Omega \Delta(W'(\varphi) - \varepsilon^2\Delta\varphi)\,\mathrm{d}x \\ &= -m\int_{\partial\Omega} \nabla(W'(\varphi) - \varepsilon^2\Delta\varphi)\cdot\boldsymbol{n}\,\mathrm{d}a.\end{aligned} \tag{3.20}$$

This implies that the phase-field variable is conserved during its gradient flow. For further (technical) details, please see [60, 37, 104].

Chapter 4

Variational Framework for Phase-Field Models

This Chapter details how thermodynamically-consistent phase-field models can be derived using a variational approach. In Section 4.1, we outline the general framework following Gomez & van der Zee [78]. Section 4.2 shows how the classical phase-field equations, that is, the Allen-Cahn and Cahn-Hilliard equations, can be derived using this variational framework. In addition, we reflect on the physical interpretation of these equations.

4.1 General framework

The foundation of the variational framework for phase-field models presented in this Chapter rests upon the rational approach to thermodynamics by Truesdell and Noll [165]. In this rational approach, a strict distinction between balance laws and constitutive equations is made. Balance laws are the fundamental physical laws that govern the conservation of quantities in systems, i.e. the conservation of mass, linear momentum, angular momentum, energy, electric charge and magnetic flux, whereas constitutive equations specify the material behaviour of the system of interest.

Following Gomez & van der Zee [78], the central idea of this thermomechanical framework is that the postulate for the free-energy density ψ depends on the phase-field variable and gradients thereof. This free-energy density is also known as the Helmholtz free energy and describes the state of a system. The canonical class for the Helmholtz free energy may thus be defined as

$$\psi = \hat{\psi}(\varphi, \nabla\varphi), \tag{4.1}$$

and the corresponding energy functional $\mathcal{E} : \mathcal{V} \to \mathbb{R}$ reads

$$\mathcal{E} = \int_\Omega \hat{\psi}(\varphi, \nabla\varphi)\, \mathrm{d}x, \tag{4.2}$$

defining the total free energy in the domain $\Omega \subset \mathbb{R}^{n_\mathrm{dim}}$ occupied by the material of interest. Here, the vector space $\mathcal{V}$ is an appropriate Sobolev space on Ω for the choice of the free energy ψ.

The second principle of the framework states that constitutive response functions are allowed to depend on the variational derivative of the total free energy with respect to the phase-field variable, as well as gradients of these variational derivatives. In the style of Landau [102], we define the chemical potential as the variational derivative of the total free energy. In particular, for the class of free energy densities given in (4.1) the chemical potential reads

$$\mu := \frac{\delta \mathcal{E}}{\delta \varphi} = \partial_\varphi \psi - \nabla \cdot (\partial_{\nabla\varphi} \psi), \tag{4.3}$$

where the variational derivative is defined through the Gâteaux derivative, see Remark 4.1.

Remark 4.1 (The variational derivative as the Gâteaux gradient) The variational derivative of a functional can be found via the Gâteaux derivative, and is also known as the Gâteaux gradient. Given the energy functional defined (4.2), the corresponding Gâteaux derivative reads

$$\begin{aligned}
\mathcal{E}'(\varphi; v) &= \lim_{s\to 0}\left(\frac{\mathcal{E}(\varphi + sv) - \mathcal{E}(\varphi)}{s}\right) \\
&= \int_\Omega (\partial_\varphi \psi v + \partial_{\nabla\varphi}\psi \cdot \nabla v)\,\mathrm{d}x, \\
&= \int_\Omega (\partial_\varphi \psi - \nabla \cdot (\partial_{\nabla\varphi}\psi))v\,\mathrm{d}x,
\end{aligned} \tag{4.4}$$

which holds for all $v \in C_0^\infty$. The Gâteaux gradient is then defined as

$$\frac{\delta \mathcal{E}}{\delta \varphi} := \partial_\varphi \psi - \nabla \cdot (\partial_{\nabla\varphi}\psi). \tag{4.5}$$

□

Lastly, to ensure that the phase-field theory is *thermomechanically-consistent*, all constitutive equations are restricted in a manner that yields an *energy-dissipative* (or *entropy-productive*) phase-field model, that is, a model that is consistent with the second law of thermodynamics.

To illustrate this, we consider an arbitrary part $\mathcal{P} \subset \Omega$ in the domain occupied by the material This part $\mathcal{P}$ is fixed in time, as we do not consider any deformation of the material here. In general, the energy-dissipation property has the form

$$\frac{\mathrm{d}}{\mathrm{d}t}\mathcal{E}(\mathcal{P}) = \mathcal{W}(\mathcal{P}) - \mathcal{D}(\mathcal{P}), \tag{4.6}$$

where $\mathcal{E}(\mathcal{P})$ denotes the total energy of the system in $\mathcal{P}$, $\mathcal{D}(\mathcal{P}) \geq 0$ the dissipation and $\mathcal{W}(\mathcal{P})$ the work from external forces or energy supplies across the boundary of $\mathcal{P}$ on the material. Given the class of free energy functions in (4.1), energy-dissipation property can be written as

$$\begin{aligned}
\frac{\mathrm{d}}{\mathrm{d}t}\int_\mathcal{P} \hat{\psi}(\varphi, \nabla\varphi)\,\mathrm{d}x &= \int_\mathcal{P}\Big(\partial_t\varphi(\partial_\varphi\hat{\psi} - \nabla\cdot(\partial_{\nabla\varphi}\hat{\psi})) + \nabla\cdot(\partial_t\varphi\,\partial_{\nabla\varphi}\hat{\psi})\Big)\,\mathrm{d}x \\
&= \int_\mathcal{P} \mu\partial_t\varphi\,\mathrm{d}x + \int_{\partial\mathcal{P}} \partial_{\nabla\varphi}\hat{\psi}\cdot\boldsymbol{\nu}\partial_t\varphi\,\mathrm{d}a,
\end{aligned} \tag{4.7}$$

where $\boldsymbol{\nu}$ denotes the outward normal to the boundary $\partial\mathcal{P}$ of the part $\mathcal{P}$.

Finally, the energy-dissipation property (4.7) should be supplemented with the balance laws governing the problem of interest. Specifically, expression (4.7) requires a balance law stating how the phase-field variable should evolve in time. After substitution of such a balance law, the external work $\mathcal{W}(\mathcal{P})$ and dissipation $\mathcal{D}(\mathcal{P})$ in the system can be identified. Subsequently, following a Coleman-Noll type of procedure [35], any constitutive relations present in the inequality should be restricted such that $\mathcal{D}(\mathcal{P}) \geq 0$. Furthermore, in case no external work is performed onto the system, i.e. $\mathcal{W}(\mathcal{P}) = 0$, the framework demands that the total free energy of the system in (4.7) decreases over time.

By extending this framework, a description for various classes of physical phenomena involving a diffuse moving interface can be found. More specifically, these theories can be established by (i) introducing new dependencies in the constitutive class for the free energy, e.g. strain measures, and (ii) subsequently supplying the conservation postulates relevant to the problem of interest. Again, (iii) constitutive relations should be restricted by demanding that a non-negative dissipation term $\mathcal{D}$ can be identified. The reader is referred to Gomez & van der Zee (2017) [78] for further examples and derivations of such extensions, which includes models for immiscible two-fluid flow, brittle fracture in solids, tumour growth and liquid-vapour phase transformations.

4.2 Classical thermodynamically-consistent equations

Two classic phase-field theories are the Allen-Cahn and the Cahn-Hilliard equation. Both phase-field equations are used in material science to describe the evolution of microstructure over time. The Cahn-Hilliard equation was originally derived as a model for phase separation of immiscible fluids [27, 28], while the Allen-Cahn equation[7] was proposed as a model for antiphase domain coarsening in Fe-Al alloys [7]. Both phase-field theories are based on the same choice for the free-energy density function, which physical background we detail in Subsection 4.2.1. The principal difference between the two theories is that the Cahn-Hilliard equation accounts for conserved phase-field dynamics, whereas the phase-field variable is not conserved in the Allen-Cahn equation. Using the variational framework in Section 4.1, we demonstrate that different postulates for the mass balance are required to arrive at the Allen-Cahn (Section 4.2.2) and Cahn-Hilliard (Section 4.2.2) equations.

4.2.1 Physical background

Let $\mathcal{B}$ be a body occupying a region of Euclidean point space $\mathscr{E}$. More specifically, we consider a material body $\mathcal{B}$ that is composed of two constituents, $\mathcal{B}_\alpha$ and $\mathcal{B}_\beta$, which comprise the entire region of $\mathcal{B}$. In what follows, we assume that the body does not undergo any deformation. Furthermore, we let $\varrho(\boldsymbol{x}, t)$ denote the local mass density of the mixture. Then, the total mass in an arbitrary part $\mathcal{P}$ of the material is given by

$$M := \int_{\mathcal{P}} \varrho \,\mathrm{d}x = \int_{\mathcal{P}} (\varrho_\alpha + \varrho_\beta) \,\mathrm{d}x = M_\alpha + M_\beta, \tag{4.8}$$

where ϱ_i denotes the mass of each species per unit volume of the mixture, and M_i the total mass of each species in the part, with $i = \alpha, \beta$. The local mass fraction of each component is then defined as

$$w_i := \frac{\varrho_i}{\varrho}, \qquad i = \alpha, \beta. \tag{4.9}$$

We postulate that the following balance law holds for each species in the material

$$\frac{\mathrm{d}}{\mathrm{d}t} \int_{\mathcal{P}} \varrho w_i \,\mathrm{d}x = - \int_{\partial\mathcal{P}} \boldsymbol{\jmath}_i \cdot \boldsymbol{\nu} \,\mathrm{d}a + \int_{\mathcal{P}} R_i \,\mathrm{d}x, \qquad i = \alpha, \beta, \tag{4.10}$$

with $\boldsymbol{\jmath}_i$ denoting the species mass flux and R_i the kinetic rate supplying species mass due to internal interactions with the other constituent. For the sake of simplicity, we assume

[7] In literature, the Allen-Cahn equation is also referred to the Ginzburg-Landau equation, which is also attributed to Landau and Ginzburg, and was proposed as a phenomenological model of superconductivity [102].

that the local density is constant, more specifically, let $\varrho = 1$, so that the pointwise mass balance is given by

$$\frac{\partial w_i}{\partial t} + \nabla \cdot \jmath_i = R_i, \qquad i = \alpha, \beta, \tag{4.11}$$

as $\mathcal{P}$ is independent of time. Bearing in mind that $w_\alpha + w_\beta = 1$, we can write the pointwise mass balances (4.11) as a single mass balance. For this purpose, we let the phase-field variable be defined as $\varphi := w_\alpha - w_\beta$, which yields

$$\frac{\partial \varphi}{\partial t} + \nabla \cdot \jmath = R, \tag{4.12}$$

with $\jmath := \jmath_\alpha - \jmath_\beta$ and $R := R_\alpha - R_\beta$. Furthermore, mixture theory arguments provide us with $R_\alpha + R_\beta = 1$, as well as $\jmath_\alpha + \jmath_\beta = 1$ [89]. Thus, the phase-field variable φ here denotes the local difference in mass fraction of the two species, and we have that

$$\varphi(\boldsymbol{x}, t) := \begin{cases} \varphi_\alpha, & \text{in phase } \alpha, \\ \varphi_\beta, & \text{in phase } \beta, \\ \in (\varphi_\alpha, \varphi_\beta), & \text{in the interfacial region,} \end{cases} \tag{4.13}$$

where φ_α and φ_β are the constant values the phase-field variable takes on in the pure phases.

A classical choice for the free-energy density dates back to Cahn & Hilliard (1958) [27] and is of the form

$$\psi = G(\varphi) + \frac{\varepsilon^2}{2} |\nabla \varphi|^2, \tag{4.14}$$

for some function $G(\varphi)$ and parameter ε. This classical function for the Helmholtz free energy belongs to the class (4.1) and the corresponding energy functional reads

$$\mathcal{E} = \int_{\mathcal{P}} \Big(G(\varphi) + \frac{\varepsilon^2}{2} |\nabla \varphi|^2 \Big) \, \mathrm{d}x, \tag{4.15}$$

which is oftentimes referred to as the Ginzburg-Landau functional. The first term in Equation (4.15) accounts for the homogeneous energy of the system, and is also known as the free energy of mixing. The second term is also referred to as the interfacial energy. It depends on the gradient of the phase-field variable and is scaled by the non-negative parameter ε, which is a measure of the interfacial thickness. Following its definition (4.3), the chemical potential corresponding to the canonical free-energy functional (4.15) is given by

$$\mu = G'(\varphi) - \varepsilon^2 \Delta \varphi, \tag{4.16}$$

where $\Delta(\cdot)$ denotes the Laplace operator, i.e. $\Delta(\cdot) = \nabla^2(\cdot) = \nabla \cdot \nabla(\cdot)$.

In view of the classical energy functional (4.15), minimization of the system's energy can be achieved in two ways, namely (i) by reducing the contribution of homogeneous energy term, meaning that the mixture's composition shifts towards the equilibrium mass fractions, a process also known as phase separation [176], and (ii) by minimizing the interfacial energy via a coarsening process, thereby diminishing interfaces.

Various forms have been adapted for the homogeneous free-energy function $G(\varphi)$ governing the phase separation process, each with its own smoothness properties. For a two-phase system, oftentimes a non-convex double-well potential $W(\varphi)$ is used. A general form for such a double-well potential [77] reads

$$W(\varphi) = \frac{\alpha}{4} \Big(\varphi^2 - \frac{\beta}{\alpha} \Big)^2, \tag{4.17}$$

for positive constants α and β, which local minima are located at

$$\varphi_\alpha = -\sqrt{\frac{\beta}{\alpha}}, \qquad \text{and} \qquad \varphi_\beta = \sqrt{\frac{\beta}{\alpha}}, \tag{4.18}$$

see Figure 4.1. Typically, one finds $\varphi_\alpha = -1$ and $\varphi_\beta = 1$ as the chosen equilibrium mass fraction values in literature.

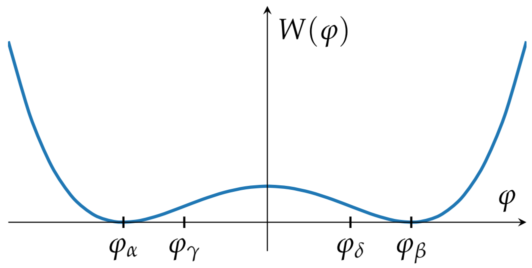

Figure 4.1: Classical double-well potential governing phase separation. The equilibrium mass fractions are denoted by φ_α and φ_β. They are also known as the binodal points and mark the boundaries of the miscibility gap (φ_α, φ_β), that is, the region in which the mixture is unstable. Only in the spinodal region $\varphi \in (\varphi_\gamma, \varphi_\delta)$, in which holds that $\partial^2 W/\partial\varphi^2 < 0$, small perturbations will lead to decomposition into the two equilibrium mass fractions, a process known as phase separation driven by spinodal decomposition [21]. The double-well potential is oftentimes a function of the temperature [138], which is not depicted here as we only consider isothermal processes in this work.

4.2.2 Allen-Cahn equation

The Allen-Cahn equation accounts for non-conserved phase-field dynamics. Therefore, we postulate that the following mass balance holds

$$\frac{\partial\varphi}{\partial t} = R, \tag{4.19}$$

with R being the mass supply. Notice, that we have obtained the above balance by choosing $\boldsymbol{\jmath} = \mathbf{0}$ in the general mass balance (4.12). Furthermore, by restricting the kinetic rate R to the following constitutive class

$$R = \hat{R}(\varphi, \nabla\varphi, \mu). \tag{4.20}$$

we aim to establish a thermodynamically-consistent phase-field model. Next, substitution of the mass-balance postulate (4.19) in the energy-dissipation law (4.7) yields

$$\frac{\mathrm{d}}{\mathrm{d}t}\int_{\mathcal{P}} \psi \,\mathrm{d}x = \int_{\mathcal{P}} \mu R \,\mathrm{d}x + \int_{\partial\mathcal{P}} \partial_{\nabla\varphi}\psi \cdot \boldsymbol{\nu}\partial_t\varphi \,\mathrm{d}a. \tag{4.21}$$

In the above expression (4.21), we identify the following terms

$$\mathcal{D}(\mathcal{P}) := -\int_{\mathcal{P}} \mu R \,\mathrm{d}x, \qquad \text{and} \qquad \mathcal{W}(\mathcal{P}) := \int_{\partial\mathcal{P}} \partial_{\nabla\varphi}\psi \cdot \boldsymbol{\nu}\partial_t\varphi \,\mathrm{d}a, \tag{4.22}$$

as dissipation and external work, respectively. To ensure that $\mathcal{D}(\mathcal{P}) \geq 0$, and thus that the model is thermomechanically consistent, we further restrict the reaction term to the following choice

$$R = -m(\varphi)\mu, \tag{4.23}$$

with $m(\varphi) \geq 0$ the so-called mobility[8]. Thus, for the constitutive choices $\jmath = \mathbf{0}$ and $R = -m(\varphi)\mu$, the mass balance (4.12) is given by

$$\frac{\partial \varphi}{\partial t} = -m(\varphi)\mu. \tag{4.24}$$

Then, in view of the chemical potential (4.16), we arrive at the Allen-Cahn equation

$$\frac{\partial \varphi}{\partial t} = -m(\varphi)\left(G'(\varphi) - \varepsilon^2 \Delta\varphi\right), \tag{4.25}$$

which is a reaction-diffusion type of partial differential equation [78]. The underlying dissipation structure of the Allen-Cahn equation becomes clear for $\mathcal{W}(\Omega) = 0$, that is, the total energy in the system decreases over time in case no external work is performed on the system. Thus, when the system is subject to natural or periodic boundary conditions for φ and μ, we find $\mathcal{D}(\Omega) \geq 0$, see Theorem 4.A.

Theorem 4.A (Energy dissipation structure of the Allen-Cahn equation) *Let $\nabla\varphi \cdot \boldsymbol{\nu} = \nabla\mu \cdot \boldsymbol{\nu} = 0$ be on $\partial\Omega$, or assume periodic boundary conditions for φ and μ on $\partial\Omega$. Furthermore, let $m(\varphi) \geq 0$. Then, the Allen-Cahn equation* (4.25) *ensures that its total energy* (4.15) *decreases over time. In particular, the dissipation is given by*

$$\mathcal{D}(\Omega) = \int_\Omega m(\varphi)|\mu|^2 \,\mathrm{d}x. \tag{4.26}$$

□

Proof. Take $\mathcal{P} = \Omega$. In view of the boundary conditions, the energy-dissipation law (4.21) reads

$$\begin{aligned} \frac{\mathrm{d}}{\mathrm{d}t}\mathcal{E} &= -\int_\Omega m(\varphi)|\mu|^2 \,\mathrm{d}x + \int_{\partial\Omega} \varepsilon^2 (\nabla\varphi \cdot \boldsymbol{\nu})\partial_t \varphi \,\mathrm{d}a \\ &= -\int_\Omega m(\varphi)|\mu|^2 \,\mathrm{d}x \leq 0, \end{aligned} \tag{4.27}$$

with $\mathcal{E}$ (4.15) the Ginzburg-Landau energy functional and $R = -m(\varphi)\mu$ the kinetic rate. ■

4.2.3 Cahn-Hilliard equation

For the derivation of the Cahn-Hilliard equation, we assume that mass is conserved, implying that

$$\frac{\partial \varphi}{\partial t} + \nabla \cdot \jmath = 0, \tag{4.28}$$

which corresponds to setting $R = 0$ in (4.12). Let the constitutive class for the species mass flux $\jmath$ be given by

$$\jmath = \hat{\jmath}(\varphi, \nabla\varphi, \mu, \nabla\mu). \tag{4.29}$$

Using the mass-balance postulate (4.28) in the energy-dissipation law (4.7) yields

$$\frac{\mathrm{d}}{\mathrm{d}t}\int_\mathcal{P} \psi \,\mathrm{d}x = -\int_\mathcal{P} \mu\nabla\cdot\jmath \,\mathrm{d}x + \int_{\partial\mathcal{P}} \partial_{\nabla\varphi}\psi \cdot \boldsymbol{\nu}\partial_t\varphi \,\mathrm{d}a, \tag{4.30}$$

[8]The mobility is often assumed to be constant, although the degenerate mobility defined by $m(\varphi) = \frac{1}{4}\left(1 - \varphi^2\right)$ agrees better to experimental results, especially in case of Ostwald ripening, viz. a process where particles smaller than a characteristic length scale vanish, so that larger particles can grow. The underlying idea is that in the pure phases (here $\varphi_\alpha = -1$ and $\varphi_\beta = 1$), the mobility vanishes and transport is thus restricted to the interfacial region.

which can be rewritten as

$$\frac{\mathrm{d}}{\mathrm{d}t}\int_{\mathcal{P}} \psi \,\mathrm{d}x = \int_{\mathcal{P}} \jmath \cdot \nabla \mu \,\mathrm{d}x + \int_{\partial\mathcal{P}} (\partial_{\nabla\varphi}\psi \cdot \boldsymbol{\nu}\partial_t\varphi - \mu\jmath \cdot \boldsymbol{\nu})\,\mathrm{d}a. \tag{4.31}$$

The following terms can then be identified as the dissipation and work from external forces, respectively,

$$\mathcal{D}(\mathcal{P}) = -\int_{\mathcal{P}} \jmath \cdot \nabla\mu \,\mathrm{d}x, \qquad \text{and} \qquad \mathcal{W}(\mathcal{P}) = \int_{\partial\mathcal{P}} (\partial_{\nabla\varphi}\psi \cdot \boldsymbol{\nu}\partial_t\varphi - \mu\jmath \cdot \boldsymbol{\nu})\,\mathrm{d}a, \tag{4.32}$$

where the last term in the integrand of $(4.32)_2$ can be interpreted as the free-energy flux. The following constitutive choice for the species mass flux $\jmath$ guarantees free-energy dissipation

$$\jmath = \hat{\jmath}(\varphi, \nabla\mu) = -m(\varphi)\nabla\mu, \tag{4.33}$$

with $m(\varphi) \geq 0$ being the mobility. Thus, the mass-balance postulate (4.28) for the Cahn-Hilliard phase-field theory reads

$$\frac{\partial\varphi}{\partial t} = \nabla \cdot (m(\varphi)\nabla\mu). \tag{4.34}$$

The Cahn-Hilliard equation is then given by

$$\frac{\partial\varphi}{\partial t} = \nabla \cdot (m(\varphi)\nabla(G'(\varphi) - \varepsilon^2\Delta\varphi)), \tag{4.35}$$

which is a fourth-order, non-linear partial differential equation describing so-called *up-hill* or *backwards* diffusion, i.e. diffusion against the phase-field gradient, while conserving the system's mass [78]. The underlying energy dissipation structure becomes clear in absence of any external work on the system, that is, when natural or periodic boundary conditions are used for φ and μ, see Theorem 4.B.

Theorem 4.B (Energy dissipation structure of the Cahn-Hilliard equation) *Let* $\nabla\varphi \cdot \boldsymbol{\nu} = \nabla\mu \cdot \boldsymbol{\nu} = 0$ *be on* $\partial\Omega$*, or assume periodic boundary conditions for* φ *and* μ *on* $\partial\Omega$*. Furthermore, let* $m(\varphi) \geq 0$*. Then, the Cahn-Hilliard equation* (4.35) *ensures that its total energy* (4.15) *decreases over time. In particular, the dissipation is given by*

$$\mathcal{D}(\Omega) = \int_{\Omega} m(\varphi)|\nabla\mu|^2 \,\mathrm{d}x. \tag{4.36}$$

□

Proof. Consider $\mathcal{P} = \Omega$. For the natural (or periodic) boundary conditions, the energy-dissipation law in Equation (4.31) can be written as

$$\begin{aligned}\frac{\mathrm{d}}{\mathrm{d}t}\mathcal{E} &= -\int_{\Omega} m(\varphi)\nabla\mu \cdot \nabla\mu \,\mathrm{d}x + \int_{\partial\Omega} (\varepsilon^2\nabla\varphi \cdot \boldsymbol{\nu}\partial_t\varphi + m(\varphi)\mu\nabla\mu \cdot \boldsymbol{\nu})\,\mathrm{d}a \\ &= -\int_{\Omega} m(\varphi)|\nabla\mu|^2 \,\mathrm{d}x \leq 0,\end{aligned} \tag{4.37}$$

with $\mathcal{E}$ (4.15) the Ginzburg-Landau energy functional and $\jmath = -m(\varphi)\nabla\mu$ the species mass flux. ■

Chapter 5

Microkinetic Framework

In this Chapter, we present the microkinetic framework for phase-field theories. This framework was developed by Fried & Gurtin [64, 63], and further generalized by Gurtin (1996) [84]. In Section 5.1, a general introduction to the framework is given. In Section 5.2, we demonstrate how the classical phase-field equations can be derived within this framework, that is the generalized Allen-Cahn and Cahn-Hilliard equations.

5.1 General microkinetic framework

Following Gurtin (1996) [84], we here present the microkinetic framework for phase-field models. Central to this framework are that (i) balance laws are distinguished from constitutive equations; and that (ii) the governing equations are based on a balance law for microforces. The motivation for this microforce balance is based on the idea that energy-based physical laws should account for the expenditure of power (work), associated with the kinematical processes. For phase-field theories, these kinematical processes are given by temporal changes in the phase-field variable, which represents the ordering of the system of interest, or its so-called microstructure.

Fried & Gurtin postulated that changes in the microstructure, e.g. the rearrangement of molecules of densities, can be accredited to so-called *microforces*. These microforces, that is the internal microforce π and external microforce γ, are scalar quantities, which are related to a vector quantity $\boldsymbol{\xi}$, also known as the microstress. Together, these physical quantities form the *balance of microforces*, which reads

$$\int_{\mathcal{P}} (\pi + \gamma)\, \mathrm{d}x = -\int_{\partial\mathcal{P}} \boldsymbol{\xi} \cdot \boldsymbol{\nu}\, \mathrm{d}a, \tag{5.1}$$

for each part $\mathcal{P}$ in a material body $\mathcal{B}$. Here, $\boldsymbol{\nu}$ denotes the outward normal to the boundary $\partial\mathcal{P}$ of $\mathcal{P}$. Using the divergence theorem, followed by the localization argument, we find that the pointwise balance of microforces is given by

$$\nabla \cdot \boldsymbol{\xi} + \pi + \gamma = 0. \tag{5.2}$$

Then, the second law of thermodynamics states that the rate in free energy can not exceed the external work, and thus that the following dissipation inequality should hold

$$\mathcal{D}(\mathcal{P}) = \mathcal{W}_{\text{ext}}(\mathcal{P}) - \frac{\mathrm{d}}{\mathrm{d}t} \int_{\mathcal{P}} \psi\, \mathrm{d}x \geq 0, \tag{5.3}$$

with $\mathcal{D}$ the non-negative dissipation term and ψ the free-energy density. Here, the external work $\mathcal{W}_{\text{ext}}(\mathcal{P})$ is given by

$$\mathcal{W}_{\text{ext}}(\mathcal{P}) = \int_{\mathcal{P}} \gamma \partial_t \varphi\, \mathrm{d}x + \int_{\partial\mathcal{P}} (\boldsymbol{\xi} \cdot \boldsymbol{\nu}) \partial_t \varphi\, \mathrm{d}a. \tag{5.4}$$

where the first term represents the power expended on the atoms within $\mathcal{P}$ by sources external to the body, whereas the second term reflects the power expended across the boundary $\partial\mathcal{P}$ by configurations exterior to $\mathcal{P}$, yet neighbouring its boundary $\partial\mathcal{P}$.

Following a similar procedure to the one outlined in Chapter 4, constitutive classes chosen for physical quantities need to be restricted so that they are compatible with the dissipation inequality (5.3). Using this approach, thermodynamically-consistent phase-field theories can be derived.

The framework outlined above has been extended by Espath & Calo (2021) [55] and also by Espath (2023) [54]. In these works, phase-field gradient theories for enriched continua are proposed, based on Fosdick's approach [62, 61]. In addition to the microstress and external microforce, these theories account for a surface-couple microtraction, a boundary-edge and a internal-edge microtractions emerging from internal surface interactions. Again, the balance equations are first derived in a general manner independent of constitutive laws. Then, thermodynamical considerations constrain the constitutive choices, thereby providing foundation for second-grade phase field equations such as the Swift-Hohenberg equation and the phase-field crystal equation [55].

5.2 Classical phase-field equations

Similar to the variational framework discussed in Chapter 4, we start by considering the free energy in the system of interest, which defined on an arbitrary part $\mathcal{P}$ in the material body takes the following form

$$\mathcal{E} = \int_{\mathcal{P}} \psi(\varphi, \nabla\varphi)\,\mathrm{d}x. \tag{5.5}$$

In the following Subsections, we will use this total free-energy to establish the generalized Allen-Cahn equation and Cahn-Hilliard equation.

5.2.1 Generalized Allen-Cahn equation

To derive the Allen-Cahn equation, we postulate that the following dependencies are allowed

$$\boldsymbol{\xi} = \hat{\boldsymbol{\xi}}(\varphi, \nabla\varphi), \qquad \text{and} \qquad \pi = \hat{\pi}(\varphi, \nabla\varphi, \partial_t\varphi). \tag{5.6}$$

Then, in view of (5.5), the pointwise dissipation inequality can be written as

$$-(\pi + \partial_\varphi\psi)\partial_t\varphi + (\boldsymbol{\xi} - \partial_{\nabla\varphi}\psi)\cdot\partial_t(\nabla\varphi) \geq 0, \tag{5.7}$$

from which follows that

$$\boldsymbol{\xi} := \partial_{\nabla\varphi}\psi. \tag{5.8}$$

Additionally, we conclude from inequality (5.7) that

$$\pi := -\partial_\varphi\psi + \pi_{\mathrm{dis}}, \tag{5.9}$$

with $\pi_{\mathrm{dis}} \leq 0$ a dissipative internal microforce, which can be of the class

$$\pi_{\mathrm{dis}} = -\beta(\varphi, \nabla\varphi, \partial_t\varphi)\partial_t\varphi, \tag{5.10}$$

provided that the constitutive modulus $\beta(\varphi, \nabla\varphi, \partial_t\varphi) \geq 0$. Finally, using the quantities (5.8) and (5.9) in the microforce balance (5.2), we arrive at the generalized Allen-Cahn equation

$$\beta(\varphi, \nabla\varphi, \partial_t\varphi)\frac{\partial\varphi}{\partial t} = \nabla\cdot(\partial_{\nabla\varphi}\psi) - \partial_\varphi\psi + \gamma. \tag{5.11}$$

5.2.2 Generalized Cahn-Hilliard equation

Using a procedure similar to the one used to derive the generalized Allen-Cahn equation in Section 5.2.1, we here establish a generalized form of the Cahn-Hilliard equation. In addition to the balance of microforces, we also require a species mass balance, which is given by

$$\frac{\partial \varphi}{\partial t} + \nabla \cdot \boldsymbol{\jmath} = R. \tag{5.12}$$

Now, apart from the external work (5.4), the following contributions arise in the dissipation inequality due to the species transport

$$\mathcal{T}(\mathcal{P}) = \int_{\mathcal{P}} \mu R \,\mathrm{d}x - \int_{\partial\mathcal{P}} \mu \boldsymbol{\jmath} \cdot \boldsymbol{\nu} \,\mathrm{d}a, \tag{5.13}$$

where μ denotes the chemical potential. Next, let the constitutive classes be given by

$$\boldsymbol{\xi} = \hat{\boldsymbol{\xi}}(\varphi, \nabla\varphi, \mu, \nabla\mu), \tag{5.14}$$

$$\pi = \hat{\pi}(\varphi, \nabla\varphi, \mu, \nabla\mu), \tag{5.15}$$

$$\boldsymbol{\jmath} = \hat{\boldsymbol{\jmath}}(\varphi, \nabla\varphi, \mu, \nabla\mu). \tag{5.16}$$

Taking into account the energy transfer due to species transport (5.13), the pointwise dissipation inequality reads

$$(\mu - \pi - \partial_\varphi \psi)\partial_t \varphi + (\boldsymbol{\xi} - \partial_{\nabla\varphi}\psi) \cdot \partial_t(\nabla\varphi) - \boldsymbol{\jmath} \cdot \nabla\mu \geq 0. \tag{5.17}$$

From this inequality follows that

$$\boldsymbol{\xi} := \partial_{\nabla\varphi}\psi, \qquad \text{and} \qquad \pi := \mu - \partial_\varphi \psi. \tag{5.18}$$

Furthermore, let

$$\boldsymbol{\jmath} := -\mathbf{A}(\varphi, \nabla\varphi, \mu, \nabla\mu)\nabla\mu, \tag{5.19}$$

with $\mathbf{A}(\varphi, \nabla\varphi, \mu, \nabla\mu)$ the mobility tensor consistent with the inequality

$$\nabla\mu \cdot \mathbf{A}(\varphi, \nabla\varphi, \mu, \nabla\mu)\nabla\mu \geq 0. \tag{5.20}$$

Thus, in view of expressions (5.2), (5.12), (5.18) and (5.19), the generalized Cahn-Hilliard equation reads

$$\frac{\partial \varphi}{\partial t} = \nabla \cdot \mathbf{A}\nabla \left(\partial_\varphi \psi - \nabla \cdot (\partial_{\nabla\varphi}\psi) - \gamma\right) + R. \tag{5.21}$$

Chapter 6

Summary of Perspectives

In this Chapter, we provide a summary of the various frameworks for the modelling of moving interfaces detailed in Chapters 2 - 5.

Geometric gradient-descent flows A geometric gradient-descent flow consists of a choice for a shape functional $\mathcal{J}(\Omega(t))$ and a non-positive operator $\mathcal{G}$. Together these establish a geometric gradient-descent flow, in which an interface $\Gamma(t) = \partial\Omega_t$ evolves with the normal velocity

$$V(\boldsymbol{x},t) = \mathcal{G}g(\Gamma(t))(\boldsymbol{x}), \qquad \forall \boldsymbol{x} \in \Gamma(t), \tag{6.1}$$

where the Hadamard shape gradient $g(\Gamma(t))$ follows from the choice for $\mathcal{J}(\Omega)$. This motion ensures minimization of the shape functional, that is

$$\frac{\mathrm{d}\mathcal{J}(\Omega(t))}{\mathrm{d}t} = -\int_{\Gamma(t)} g(\Gamma(t))\mathcal{G}g(\Gamma(t))\,\mathrm{d}\Gamma \le 0. \tag{6.2}$$

Phase-field models as gradient flows A phase-field gradient flow is a process in which the steepest descent of a phase-field dependent functional $\mathcal{F} : \mathcal{V} \to \mathbb{R}$ is followed. Here, the dissipation mechanism is characterised by the gradient $D\mathcal{F}(\varphi) \in \mathcal{V} \subseteq \mathcal{W}$, which may be subject to constraints arising from boundary conditions. Thus, to develop a phase-field model within this gradient flow framework suitable choices should be made for the (i) functional $\mathcal{F}(\varphi)$ and (ii) the dissipation mechanism characterized by the norm $\|D\mathcal{F}(\varphi)\|^2_{\mathcal{W}}$. The phase-field variable evolves in the direction opposite to its gradient $D\mathcal{F}(\varphi)$, that is

$$\frac{\partial\varphi}{\partial t} = -mD\mathcal{F}(\varphi), \tag{6.3}$$

with $m > 0$. The associated dissipation structure reads

$$\frac{\mathrm{d}}{\mathrm{d}t}\mathcal{F}(\varphi) = \Big(D\mathcal{F}(\varphi), \frac{\partial\varphi}{\partial t}\Big)_{\mathcal{W}} = -m(\varphi)\|D\mathcal{F}(\varphi)\|^2_{\mathcal{W}} \le 0. \tag{6.4}$$

Variational framework for phase-field models Derivation of a phase-field theory within this framework requires (i) a choice for the energy functional $\mathcal{E}(\varphi)$ through the energy density function $\psi = \hat{\psi}(\varphi, \nabla\varphi, \cdot)$, which defines (ii) a chemical potential i.e. $\mu := \delta\mathcal{E}/\delta\varphi$, and (iii) a postulate for the (mass) balance law, in which thermodynamically-consistent choices for the response functions are made, e.g. for the flux $\jmath = \hat{\jmath}(\varphi, \nabla\varphi, \mu, \nabla\mu, \cdot)$ and kinetic rate $R = \hat{R}(\varphi, \nabla\varphi, \mu, \nabla\mu, \cdot)$. Here, the mass balance postulate forms the foundation of the evolution equation for the phase-field variable, which reads

$$\frac{\partial\varphi}{\partial t} + \nabla\cdot\hat{\jmath} = \hat{R}, \tag{6.5}$$

and can be supplemented with balance laws for other state variables $(\cdot)$. The choice for ψ determines the form of the work $\mathcal{W}(\mathcal{P})$ and dissipation $\mathcal{D}(\mathcal{P})$ terms appearing in the second energy law, which is given by

$$\frac{\mathrm{d}}{\mathrm{d}t}\left(\int_{\mathcal{P}} \hat{\psi}\,\mathrm{d}\boldsymbol{x}\right) = \mathcal{W}(\mathcal{P}) - \mathcal{D}(\mathcal{P}), \qquad \forall\mathcal{P} \in \Omega. \tag{6.6}$$

Then, a Coleman-Noll type of procedure restricts the classes of the constitutive response functions $(\jmath, R, \cdot)$, so that a non-negative dissipation term, i.e. $\mathcal{D}(\mathcal{P}) \geq 0$, can be identified for all conceivable processes.

Microkinetic framework Central to phase-field theories derived within the microforce framework is a postulate for the balance of microforces, which reads

$$\nabla \cdot \boldsymbol{\xi} + \pi + \gamma = 0, \tag{6.7}$$

in addition to a free-energy density function ψ, that defines the free-energy in a part $\mathcal{P}$ as

$$\mathcal{E} = \int_{\mathcal{P}} \psi\,\mathrm{d}x. \tag{6.8}$$

By accounting for the power expenditures in the system as a result of the temporal changes in the phase-field variable, the partwise free-energy imbalance or dissipation-inequality reads

$$\mathcal{D}(\mathcal{P}) = \mathcal{W}_{\text{ext}}(\mathcal{P}) - \frac{\mathrm{d}}{\mathrm{d}t}\int_{\mathcal{P}} \psi\,\mathrm{d}x \geq 0, \tag{6.9}$$

where $\mathcal{W}_{\text{ext}}(\mathcal{P})$ accounts for the external work by the microforces. This dissipation-inequality is used to restrict the constitutive response functions in a suitable way. Substitution of these restrictive classes into the considered balance laws produces a phase-field theory. Note that this framework can be further extended by supplementing it with additional balance laws and by accounting for the related power expenditures in the free-energy imbalance.

Part II

Phase-Field Modelling of Adhesive Interfaces

The Chapters in this Part form the basis of a paper in preparation: A. BOSCHMAN, B. BROOK, M. ICARDI, AND K. VAN DER ZEE, *Phase-field Modelling of Adhesive Interfaces*, (2024).

Chapter 7

Introduction and Background

This second Part of this thesis focusses on phase-field models describing adhesion between moving interfaces. Motivation for the theoretical and computational study into adhesive interactions is presented in Section 7.1. Related literature on sharp-interface limits and equilibrium states is detailed in Section 7.2. In Section 7.3, we summarize the main aims and provide an outline of the contents in this Part.

7.1 Adhesion and its application in cell biology

Material behaviour is determined by its molecular arrangement and interactions. These intermolecular interactions are governed by electromagnetic forces, which may be weak or strong in nature depending on the type of molecules interacting. When these forces result in an attractive and binding effect between two distinct materials, we refer to it as adhesion. This adhesive interaction is often dependent on the local surface properties, such as its roughness or specific intermolecular forces, which may play a role in the contact between the interfaces [94]. Understanding and control of these adhesive properties is important in material design, manufacturing, and development of new technologies in various disciplines.

An application of adhesion that we wish to highlight here, as it involves an active interface, can be found within the field of cell biology, namely the interaction between two cell membranes. Such adhesive interactions can also be present between a cell membrane and the extracellular matrix (ECM) or substrate material, respectively. Proteins expressed at the cell membrane establish bonds, thereby effectively adhering the two interfaces. At the inside of the cell these transmembrane proteins are connected to the cytoskeleton, a network of filaments responsible for the cell's spatial organisation and structure. On the outside of the cell, the proteins are either connected to proteins expressed at another membrane or to the extracellular matrix material, which contains a network of fibers and macromolecules providing the ECM its structure and elasticity. This way these transmembrane proteins play a primary role in the transfer of mechanical forces and the regulation of cell attachment and movement [6].

A cell's adhesion onto a substrate material or another cell membrane can be described in three stages: (i) sedimentation (a process of initial attachment which is usually driven by electrostatic interactions); (ii) flattening of the cell onto the substrate material regulated by membrane protein bonding; and (iii) subsequent spreading of the cell and internal reorganization of the cell's cytoskeleton, see Figure 7.1. In this last stage, the formation of so-called focal adhesions, i.e. transmembrane proteins linked to both the ECM and the cytoskeleton, is key to establishing stable bonds. In general, the transmembrane proteins mediate the adhesion strength, in particular during the last two stages of adhesion, as their interactions with the exterior substrate or cell triggers cellular responses such as cytoskeleton rearrangements and production, as well as the expression of more transmembrane proteins [93, 95].

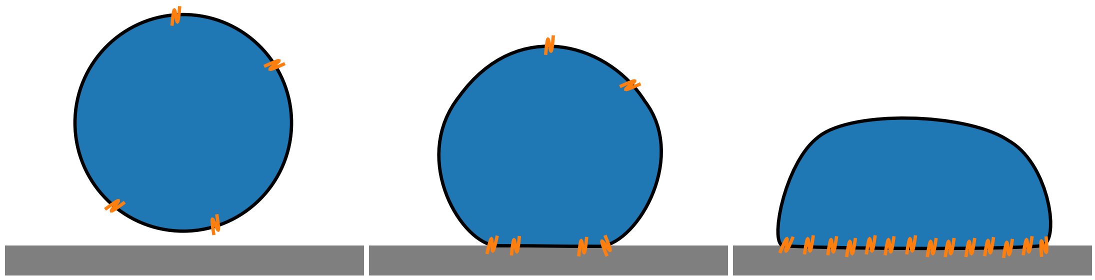

(a) Sedimentation. **(b)** Cell attachment. **(c)** Stable adhesion.

Figure 7.1: Schematic representation of three different stages of cellular adhesion: (a) sedimentation, (b) cell attachment and (c) cell spreading and stable adhesion. The transmembrane proteins regulate the adhesive interaction with the substrate material. This Figure is based on [93, 95].

Over the recent years, phase-field modelling has been used intensively for the study of biological problems, for instance in tumour modelling [112, 89] and angiogenesis (the formation of new blood vessels) [170, 171, 154]. On cell level, phase-field variables have been introduced to describe cellular movement, including adhesive dynamics and cell polarization [130, 182, 180, 42, 181, 126], as well as cell morphodynamics (shape change) [150]. Apart from certain computational benefits, a main advantage of using phase-field modelling is that extension to multiple phases is often straightforward, so that for instance the study of multi-cellular migration and multicellular interactions [127, 130] are within reach.

7.2 Sharp-interface limit and equilibrium states

Phase-field solutions are transition layers marking the diffuse interface. Through the small, yet finite, parameter ε controlling the thickness of the diffuse interface, phase-field models are intrinsically connected to geometric problems. While for some phase-field models it is known what steady states look like geometrically, e.g. for the Cahn-Hilliard equation steady states are perimeter (resp. area in 3-D) minimizers such as circles in 2-D (resp. spheres in 3-D), for complex phase-field models these equilibrium states may be much more nontrivial, and are generally not known a priori.

Standard approaches for proving the convergence of phase-field models are based on the theory of *matched asymptotic expansions*, see for instance [24, 91, 103]. The main focus of this type of analysis is on the partial differential equations, that is, to relate the equations evolving the diffuse-interface on a fixed domain to a set of partial differential equations communicating via boundary conditions at a moving sharp interface. In these standard approaches, however, the behaviour in the sharp limit of the diffuse-interface energy functional, on which basis the phase-field equations are derived, is often not considered.

Equilibrium configurations of a fluid within the Van der Waals-Cahn-Hilliard theory of phase-transitions, and the corresponding sharp-interface limit have been studied extensively [123, 114, 56, 23, 32]. The connection of the governing diffuse-interface energy, i.e. the Ginzburg-Landau functional $\mathcal{E}^{\varepsilon}_{\mathrm{GL}}(\varphi)$, to the interfacial area and surface tension in the sharp limit is well established. Moreover, it is known that geometrically, the variation of interfacial area is related to the mean curvature of the surface. These convergence results can be summarized in the following diagram

$$\begin{array}{ccc}
\mathcal{E}^{\varepsilon}_{\mathrm{GL}}(\varphi) = \displaystyle\int_{\Omega} \left(\frac{1}{4\varepsilon}(\varphi^2-1)^2 + \frac{\varepsilon}{2}|\nabla\varphi|^2 \right) \mathrm{d}x & \xrightarrow[\varepsilon\to 0]{} & \mathcal{E}_{\mathrm{GL}}(\Gamma) = \displaystyle\int_{\Gamma} \mathrm{d}a \\
\text{variation of } \varphi \Big\downarrow & & \Big\downarrow \text{variation of } \Gamma \\
\dfrac{\delta \mathcal{E}^{\varepsilon}_{\mathrm{GL}}(\varphi)}{\delta\varphi} = \dfrac{1}{\varepsilon}\varphi(\varphi^2-1) - \varepsilon\Delta\varphi & \xrightarrow[\varepsilon\to 0]{\text{at } \{\varphi=0\}\to\Gamma} & \dfrac{\delta \mathcal{E}_{\mathrm{GL}}(\Gamma)}{\delta\Gamma} \cdot \boldsymbol{n} = K
\end{array}$$

where φ denotes the phase-field variable, K the mean curvature, Γ the sharp interface and $\boldsymbol{n}$ the unit normal.

More recently, similar approaches have been applied to a newer class of phase-field models, in which the diffuse interfaces are governed by curvature-dependent energies. Such models and their asymptotic analysis are relevant in the study of vesicle dynamics and their equilibrium configurations [43]. In the sharp-interface limit, the phase-field formulation is found to be connected to the Willmore problem, with the diffuse-interface energy converging to the bending energy and the variational derivative of the phase-field based energy to the Willmore stress, respectively. The following diagram shows these connections

$$\begin{array}{ccc}
\mathcal{E}^{\varepsilon}_{\mathrm{B}}(\varphi) = \dfrac{\varepsilon}{2} \displaystyle\int_{\Omega} \left(\Delta\varphi - \frac{1}{\varepsilon^2}(\varphi^2-1)\varphi \right)^2 \mathrm{d}x & \xrightarrow[\varepsilon\to 0]{} & \mathcal{E}_{\mathrm{B}}(\Gamma) = \displaystyle\int_{\Gamma} K^2 \,\mathrm{d}a \\
\text{variation of } \varphi \Big\downarrow & & \Big\downarrow \text{variation of } \Gamma \\
\dfrac{\delta \mathcal{E}^{\varepsilon}_{\mathrm{B}}(\varphi)}{\delta\varphi} = \varepsilon\Delta f - \dfrac{1}{\varepsilon}(3\varphi^2-1)f & \xrightarrow[\varepsilon\to 0]{\text{at } \{\varphi=0\}\to\Gamma} & \dfrac{\delta \mathcal{E}_{\mathrm{B}}(\Gamma)}{\delta\Gamma} \cdot \boldsymbol{n} = -\Delta_{\Gamma}K - 2K(K^2-G)
\end{array}$$

thereby summarizing the analysis in [44, 144, 174]. Here G denotes the Gaussian curvature, and $f(\varphi) := \Delta\varphi - \frac{1}{\varepsilon^2}(\varphi^2-1)\varphi$.

7.3 Aims and outline

The objective of this second Part is to develop a phase-field theory for adhesive interactions and to further characterize the proposed adhesion model through asymptotic methods and numerical studies.

To this end, we consider the variational framework presented in Chapter 3 to ensure thermodynamical-consistency of the models for adhesion. The phase-field adhesion framework is based on a postulate for the energy functional, which includes a term representing the adhesive interaction between one diffuse interface and another. This framework is detailed in Chapter 8, in which we present two type of adhesion models: the first describing the interaction of a moving phase-field with a steady substrate field, and the second describing these adhesive interactions between multiple moving phase fields.

To characterize the steady states of the proposed adhesion phase-field problem, we first consider a simpler problem, i.e. the Cahn-Hilliard phase-field model. In Chapter 9, we develop an asymptotics framework for the characterization of its equilibrium solutions. For this purpose, we exploit the connection between the diffuse-interface and sharp-interface energy functional, as illustrated in the first diagram in Section 7.2, to finally arrive at a description of the sharp-interface steady states of the Cahn-Hilliard problem.

The formal asymptotics detailed in Chapter 9 form the foundation of the convergence study for the adhesion problem presented in Chapter 10. In Chapter 10, we demonstrate that the adhesion model's diffuse-interface energy converges to a sharp-interface energy in the sharp-interface limit. We conclude the Chapter by characterizing the minimizers of this sharp-interface energy, which provides a geometrical interpretation of the phase-field adhesion problem and insight into the role of the parameters.

In Chapter 11, we study the adhesive interactions between steady and moving interfaces numerically. To this end, we employ an energy-stable time-discretization scheme exploiting the gradient flow structure of the phase-field adhesion models. The presented results demonstrate the effect of curvature, adhesion strength and interfacial thickness on the equilibrium shapes.

Chapter 12 concludes this second Part by summarizing the main contributions, and discusses future directions for the phase-field adhesion theory.

Chapter 8

Phase-Field Models for Adhesion

In this Chapter, we present a novel phase-field based approach to study adhesive interactions between moving interfaces. The models presented here are developed within the variational framework discussed in Chapter 4, thereby making these models thermodynamically consistent. In Section 8.1, we present the phase-field equations of adhesive interactions between a moving phase-field and a steady substrate, which we refer to as the *single-phase adhesion model*. Section 8.2 presents a *multi-phase adhesion model*, in which multiple phase-fields can undergo adhesive interactions with each other. In both Sections, the model's energetic structure and underlying mechanics are detailed.

8.1 Single-phase adhesion

Following the variational framework for phase-field models detailed in Section 4.1, we postulate a free-energy density function, which describes the state of the system. Here, we consider a phase-field $\varphi(\boldsymbol{x}, t)$ that can interact with a steady substrate field $\varphi_{\mathrm{s}}(\boldsymbol{x})$ in the domain Ω. In Figure 8.1 the configuration of this adhesion problem is depicted.

Then, given a sufficiently smooth $\varphi_{\mathrm{s}}(\boldsymbol{x})$ marking the diffuse interface of the adhesive substrate, the single-phase adhesion energy density reads

$$\psi_{\text{single}}(\varphi, \nabla\varphi) := \frac{1}{\varepsilon}W(\varphi) + \frac{\varepsilon}{2}|\nabla\varphi|^2 + \varepsilon\sigma B(\varphi)B(\varphi_{\mathrm{s}})\nabla\varphi \cdot \nabla\varphi_{\mathrm{s}}, \tag{8.1}$$

where $\varepsilon > 0$ denotes a small parameter governing the thickness of the diffuse interface. Here, we consider a double-well potential $W(\varphi)$ of the class in (4.17), with equilibrium phase $\varphi_- = -1$ and $\varphi_+ = 1$. Furthermore, σ is a non-negative constant controlling the adhesive interaction. In the single-phase adhesion free-energy density (8.1), the function $B(\varphi)$ is any function subject to

$$\lim_{|\xi|\to\infty} B(\xi)\xi = 0, \qquad \text{and} \qquad B(\varphi) \in L^\infty(\mathbb{R}),^{9} \tag{8.2}$$

such that $B(\varphi)$ vanishes outside the diffuse interface of the respective field. Thus, the terms $B(\varphi)$ and $B(\varphi_{\mathrm{s}})$ ensure that the adhesive interaction is regularized to the shared diffuse interface of the phase-field φ and the substrate field φ_{s}. Such regularizing functions have been used before to solve partial differential equations on stationary [140], as well as moving interfaces [141, 47, 113, 50].

Then, the energy functional defined on the domain Ω corresponding to the free-energy density reads

$$\mathcal{E}^{\varepsilon}_{\text{single}}(\varphi) := \int_\Omega \left(\frac{1}{\varepsilon}W(\varphi) + \frac{\varepsilon}{2}|\nabla\varphi|^2 + \varepsilon\sigma B(\varphi)B(\varphi_{\mathrm{s}})\nabla\varphi \cdot \nabla\varphi_{\mathrm{s}}\right) \mathrm{d}x, \tag{8.3}$$

[9] Alternatively, we may use $B \in L^\infty([\varphi_-, \varphi_+])$ such that $B(\varphi)$ has a truncated extension to $L^\infty(\mathbb{R})$.

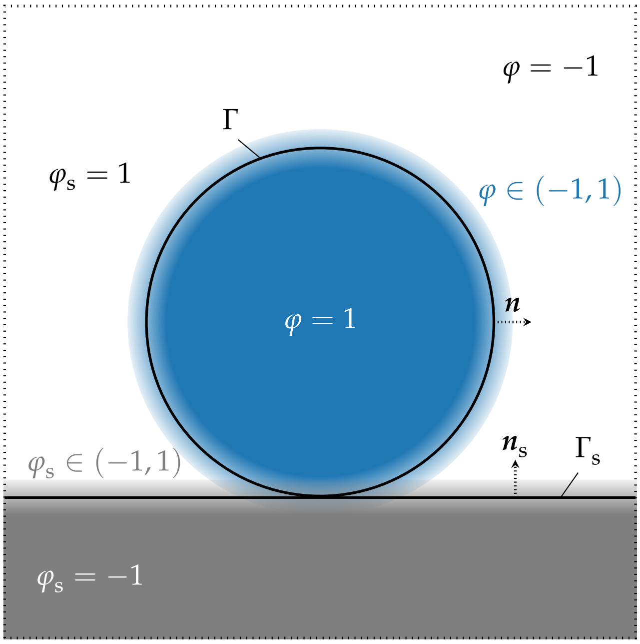

Figure 8.1: Configuration of the single-phase adhesion problem. The material of interest is defined through the phase-field variable $\varphi(\boldsymbol{x}, t)$, and the adhesive substrate is represented by a steady field $\varphi_s(\boldsymbol{x})$. In the sharp-interface representation of this problem the material's interface is denoted by Γ, whereas the substrate's interface is denoted by Γ_s. Here, we have used $\varphi_- = -1$ and $\varphi_+ = 1$ to illustrate the fully separated phases.

To distinguish between the different contributions in the total energy functional (8.3), we introduce the following functionals

$$\mathcal{E}_{\text{hom}}(\varphi) := \int_\Omega \frac{1}{\varepsilon} W(\varphi)\, \mathrm{d}x, \tag{8.4}$$

$$\mathcal{E}_{\text{int}}(\varphi) := \int_\Omega \frac{\varepsilon}{2} |\nabla \varphi|^2\, \mathrm{d}x, \tag{8.5}$$

$$\mathcal{E}_{\text{adh}}(\varphi) := \int_\Omega \varepsilon\sigma B(\varphi) B(\varphi_s) \nabla\varphi \cdot \nabla\varphi_s\, \mathrm{d}x. \tag{8.6}$$

The homogeneous energy $\mathcal{E}_{\text{hom}}$ and the interfacial energy $\mathcal{E}_{\text{int}}$ form the classical Ginzburg-Landau energy functional (4.15). These contributions ensure that stable configurations consist of fully-separated phases, which are separated by the least amount of interface. The interface is diffuse in nature and its thickness scales with ε. The postulated adhesion energy $\mathcal{E}_{\text{adh}}$ implies that the system favours states in which the diffuse interfaces of the phase-field and the substrate field overlap. From a sharp-interface viewpoint, one could say that the lowest contributions from the adhesion energy correspond to configurations in which the normal fields orienting the interfaces Γ and Γ_s are aligned in opposite direction, that is $\boldsymbol{n}_s \cdot \boldsymbol{n} = -1$, see also Figure 8.1. Relating this sharp-interface interpretation to the diffuse-interface approach, we find that these normal fields scale with gradient of the respective phase-fields, that is $\boldsymbol{n}_s \sim \nabla\varphi_s$ and $\boldsymbol{n} \sim \nabla\varphi$. Lastly, the regularizing terms $B(\varphi)$ and $B(\varphi_s)$ restrict this adhesive interaction to the region in close proximity of both interfaces. Following the procedure discussed in Chapter 4, we define the chemical potential for this system as

$$
\begin{aligned}
\mu := \frac{\delta \mathcal{E}^{\varepsilon}_{\text{single}}}{\delta \varphi} &= \partial_{\varphi} \psi_{\text{single}} - \nabla \cdot (\partial_{\nabla \varphi} \psi_{\text{single}}) \\
&= \frac{1}{\varepsilon} W'(\varphi) - \varepsilon \Delta \varphi - \varepsilon \sigma B(\varphi) \nabla \cdot (B(\varphi_{\text{s}}) \nabla \varphi_{\text{s}}) \\
&= \frac{1}{\varepsilon} W'(\varphi) - \varepsilon \Delta \varphi - \varepsilon \sigma B(\varphi)(B(\varphi_{\text{s}}) \Delta \varphi_{\text{s}} + B'(\varphi_{\text{s}}) |\nabla \varphi_{\text{s}}|^2),
\end{aligned} \tag{8.7}
$$

Next, we supply the energy functional with postulate for the constituent mass balance. Similar to the Cahn-Hilliard model presented in Section 4.2.3, we assume that the phase-field variable is conserved. This implies that no new material is locally produced in the system of interest, and thus the pointwise mass balance reads

$$
\frac{\partial \varphi}{\partial t} = -\nabla \cdot \jmath. \tag{8.8}
$$

Furthermore, we employ the following constitutive choice for the species mass flux

$$
\jmath = \hat{\jmath}(\mu) = -\nabla \mu. \tag{8.9}
$$

Substituting the constitutive choice for the species mass flux (8.9) into the pointwise mass balance (8.8) yields the phase-field equations for the single-phase adhesion model. In their mixed formulation, these read

$$
\begin{cases}
\dfrac{\partial \varphi}{\partial t} = \Delta \mu, \\
\mu = \dfrac{1}{\varepsilon} W'(\varphi) - \varepsilon \Delta \varphi - \varepsilon \sigma B(\varphi)(B(\varphi_{\text{s}}) \Delta \varphi_{\text{s}} + B'(\varphi_{\text{s}}) |\nabla \varphi_{\text{s}}|^2),
\end{cases} \tag{8.10}
$$

which are subject to appropriate initial and boundary conditions, and require a suitable function for the adhesive substrate φ_{s}.

This model is a thermodynamically-consistent phase-field model, as the constitutive choice (8.9) ensures energy dissipation, i.e. we can identify a dissipation term $\mathcal{D} \geq 0$ in absence of any external work, see Theorem 8.A.

Theorem 8.A (Energy dissipation structure of the single-phase adhesion model) *Let $\nabla \varphi \cdot \boldsymbol{\nu} = \nabla \varphi_{\text{s}} \cdot \boldsymbol{\nu} = \nabla \mu \cdot \boldsymbol{\nu} = 0$ on $\partial \Omega$, or assume periodic boundary conditions for φ, φ_{s} and μ on $\partial \Omega$. Then, the single-phase adhesion equations* (8.10) *ensure that its total energy* (8.3) *decreases over time. In particular, the dissipation is given by*

$$
\mathcal{D}(\Omega) = \int_{\Omega} |\nabla \mu|^2 \, \mathrm{d}x, \tag{8.11}
$$

for the chemical potential specified in (8.7). □

Proof. For the single-phase adhesion energy functional $\mathcal{E}^{\varepsilon}_{\text{single}}$ (8.3), the energy-dissipation law (4.31) becomes

$$
\begin{aligned}
\frac{\mathrm{d}}{\mathrm{d}t} \mathcal{E}^{\varepsilon}_{\text{single}} &= \int_{\Omega} \mu \Delta \mu \, \mathrm{d}x + \int_{\partial \Omega} \varepsilon (\nabla \varphi \cdot \boldsymbol{\nu} + \varepsilon \sigma B(\varphi) B(\varphi_{\text{s}}) \nabla \varphi_{\text{s}} \cdot \boldsymbol{\nu}) \Delta \mu \, \mathrm{d}a \\
&= - \int_{\Omega} |\nabla \mu|^2 \, \mathrm{d}x \leq 0,
\end{aligned} \tag{8.12}
$$

where we have used that $\jmath = -\nabla \mu$ and that $\nabla \varphi \cdot \boldsymbol{\nu}$, $\nabla \varphi_{\text{s}} \cdot \boldsymbol{\nu}$ and $\nabla \mu \cdot \boldsymbol{\nu}$ vanish on $\partial \Omega$. ■

8.2 Multi-phase adhesion

In this Subsection, we introduce a model for adhesion between multiple phase-field variables, i.e. $\varphi_1(\boldsymbol{x},t),\ldots,\varphi_k(\boldsymbol{x},t)$, with k being the number of constituents in the domain Ω. We arrive at this model by extending the theory presented in Section 8.1 to multiple phase-field variables. Thus, in view of the single-phase energy density function (8.1), the multi-phase adhesion energy density function reads

$$\begin{aligned}\psi_{\text{multi}}(\varphi_1,\ldots,\varphi_k,\nabla\varphi_1,\ldots,\nabla\varphi_k) := \sum_{i=1}^{k}\left(\frac{1}{\varepsilon}W(\varphi_i)+\frac{\varepsilon}{2}|\nabla\varphi_i|^2\right)\\ +\sum_{i=1}^{k}\sum_{j\neq i}^{k}\frac{\varepsilon\sigma_{ij}}{2}B(\varphi_i)B(\varphi_j)\nabla\varphi_i\cdot\nabla\varphi_j,\end{aligned} \tag{8.13}$$

where, for the sake of simplicity, we have assumed that the thickness of the diffuse interface of each phase-field variable scales with the same $\varepsilon > 0$. Again, we consider a double-well potential $W(\varphi)$ of the class in (4.17), with equilibrium phase $\varphi_- = -1$ and $\varphi_+ = 1$ for each constituent. Furthermore, the adhesion strength of each adhesive interaction is governed by $\sigma_{ij} > 0$, where we have assumed that the adhesive interaction is symmetric, that is, constituent i interacts as strongly with j as constituent j with i, and hence $\sigma_{ij} = \sigma_{ji}$. Lastly, the regularization functions $B(\varphi)$ are again defined as in expressions (8.2).

The multi-phase adhesion energy functional corresponding to this free-energy density function is given by

$$\begin{aligned}\mathcal{E}^{\varepsilon}_{\text{multi}}(\varphi_1,\ldots,\varphi_k) := \int_\Omega\Bigg(\sum_{i=1}^{k}\left(\frac{1}{\varepsilon}W(\varphi_i)+\frac{\varepsilon}{2}|\nabla\varphi_i|^2\right)\\ +\sum_{i=1}^{k}\sum_{j\neq i}^{k}\frac{\varepsilon\sigma_{ij}}{2}B(\varphi_i)B(\varphi_j)\nabla\varphi_i\cdot\nabla\varphi_j\Bigg)\,\mathrm{d}x,\end{aligned} \tag{8.14}$$

which contains the following contributions

$$\mathcal{E}_{\text{hom}}(\varphi_i) := \int_\Omega \frac{1}{\varepsilon}W(\varphi_i)\,\mathrm{d}x, \tag{8.15}$$

$$\mathcal{E}_{\text{int}}(\varphi_i) := \int_\Omega \frac{\varepsilon}{2}|\nabla\varphi_i|^2\,\mathrm{d}x, \tag{8.16}$$

$$\mathcal{E}_{\text{adh}}(\varphi_i) := \int_\Omega \sum_{j\neq i}^{k}\frac{\varepsilon\sigma_{ij}}{2}B(\varphi_i)B(\varphi_j)\nabla\varphi_i\cdot\nabla\varphi_j\,\mathrm{d}x. \tag{8.17}$$

for each constituent i. Then, the chemical potential associated with each φ_i is defined as

$$\begin{aligned}\mu_i &:= \frac{\delta\mathcal{E}^{\varepsilon}_{\text{multi}}}{\delta\varphi_i} = \partial_{\varphi_i}\psi_{\text{multi}} - \nabla\cdot(\partial_{\nabla\varphi_i}\psi_{\text{multi}}),\\ &= \frac{1}{\varepsilon}W'(\varphi_i) - \varepsilon\Delta\varphi_i - \sum_{j\neq i}^{k}\varepsilon\sigma_{ij}B(\varphi_i)\nabla\cdot(B(\varphi_j)\nabla\varphi_j),\\ &= \frac{1}{\varepsilon}W'(\varphi_i) - \varepsilon\Delta\varphi_i - \sum_{j\neq i}^{k}\varepsilon\sigma_{ij}B(\varphi_i)(B(\varphi_j)\Delta\varphi_j + B'(\varphi_j)|\nabla\varphi_j|^2), \quad \forall i = 1,\ldots,k.\end{aligned} \tag{8.18}$$

Following the single-phase adhesion model's derivation, we use the pointwise mass balances

$$\frac{\partial \varphi_i}{\partial t} = -\nabla \cdot \jmath_i, \qquad \forall i = 1, \ldots, k. \tag{8.19}$$

Furthermore, we employ the following constitutive choice for the species mass flux

$$\jmath_i = \hat{\jmath}_i(\mu_i) = -\nabla \mu_i. \tag{8.20}$$

Finally, by substituting the constitutive choice for the species mass flux (8.20) into the pointwise mass balances (8.19), we obtain the phase-field equations for the multi-phase adhesion model. In their mixed formulation, these are given by

$$\begin{cases} \dfrac{\partial \varphi_i}{\partial t} = \Delta \mu_i, & \forall i = 1, \ldots, k, \\ \mu_i = \dfrac{1}{\varepsilon} W'(\varphi_i) - \varepsilon \Delta \varphi_i & \\ \qquad - \displaystyle\sum_{j \neq i}^{k} \varepsilon \sigma_{ij} B(\varphi_i)(B(\varphi_j)\Delta \varphi_j + B'(\varphi_j)|\nabla \varphi_j|^2), & \forall i = 1, \ldots, k, \end{cases} \tag{8.21}$$

which are subject to suitable initial and boundary conditions. This model can also be classified as a thermodynamically-consistent model, see Theorem 8.B.

Theorem 8.B (Energy dissipation structure of the multi-phase adhesion model) *Let $\nabla \varphi_i \cdot \boldsymbol{\nu} = \nabla \mu_i \cdot \boldsymbol{\nu} = 0$ on $\partial\Omega$, or assume periodic boundary conditions for φ_i and μ_i on $\partial\Omega$. Then, the multi-phase adhesion equations* (8.21) *ensure that the energy functional* (8.14) *decreases over time. In particular, the dissipation is given by*

$$\mathcal{D}(\Omega) = \int_\Omega \sum_{i=1}^{k} |\nabla \mu_i|^2 \, \mathrm{d}x, \tag{8.22}$$

for the chemical potentials specified in (8.18). □

Proof. The energy-dissipation law for the multi-phase adhesion energy functional $\mathcal{E}^\varepsilon_{\text{multi}}$ (8.14) can be written as

$$\begin{aligned} \frac{\mathrm{d}}{\mathrm{d}t} \mathcal{E}^\varepsilon_{\text{multi}} &= \int_\Omega \sum_{i=1}^{k} \Big((\partial_{\varphi_i} \psi_{\text{multi}} - \nabla \cdot (\partial_{\nabla \varphi_i} \psi_{\text{multi}})) \partial_t \varphi_i + \nabla \cdot (\partial_t \varphi_i \partial_{\nabla \varphi_i} \psi_{\text{multi}}) \Big) \, \mathrm{d}x \\ &= \int_\Omega \sum_{i=1}^{k} \mu_i \Delta \mu_i \, \mathrm{d}x + \int_{\partial\Omega} \sum_{i=1}^{k} \Big(\varepsilon \nabla \varphi_i \cdot \boldsymbol{\nu} + \sum_{j \neq i}^{k} \frac{\varepsilon \sigma_{ij}}{2} B(\varphi_i) B(\varphi_j) \nabla \varphi_j \cdot \boldsymbol{\nu} \Big) \Delta \mu_i \, \mathrm{d}a \\ &= -\int_\Omega \sum_{i=1}^{k} |\nabla \mu_i|^2 \, \mathrm{d}x \leq 0, \end{aligned} \tag{8.23}$$

where we have used the phase-field equations (8.21) and that the terms involving $\nabla \varphi_i \cdot \boldsymbol{\nu}$ and $\nabla \mu_i \cdot \boldsymbol{\nu}$ vanish on $\partial\Omega$, for all $i = 1, \ldots, k$. ∎

Chapter 9

Sharp-Interface Limit of the Cahn-Hilliard Energy

This Chapter investigates the shapes of steady states of the Cahn-Hilliard equation. For this purpose, we study the sharp-interface limit of the Ginzburg-Landau energy functional under evolution of the Cahn-Hilliard dynamics. In particular, we exploit the connection between the minimizers of both energies. In Section 9.1, we further introduce the problem and outline the approaches used. Section 9.2, focusses on the diffuse-interface energy minimization, while Section 9.3 introduces the *Lagrange multiplier* to enforce the mass constraint associated with the Cahn-Hilliard problem. Next, Section 9.4 details the key assumptions and machinery for the convergence study. Then, through *asymptotic expansions* in Section 9.5, we recover insights in the structure of the diffuse-interface minimizers. These insights are used in Section 9.6 to recover the sharp-interface limit of the diffuse-interface energy functional associated with the Cahn-Hilliard problem. Using the sharp-interface energy functional, we find its sharp-interface minimizers in Section 9.7, which provide insight in the geometrical properties of the equilibrium states of the Cahn-Hilliard problem.

Lastly, we emphasize that the main results presented in this Chapter focus on the characterization of minimizers through formal asymptotics. In related work by Modica (& Luckhaus) [123, 114] and Sternberg [158], the existence of these minimizers using Γ-convergence is shown, in addition to further characterization of the sharp-interface energy. Moreover, the methods presented in this Chapter also form the foundation for the convergence study of the diffuse-interface adhesion energy, which results are presented in Chapter 10.

9.1 Problem statement

Central in this Chapter is the Ginzburg-Landau free-energy functional

$$\mathcal{E}^{\varepsilon}_{\mathrm{GL}}(\varphi) := \int_{\Omega} \left(\frac{1}{\varepsilon} W(\varphi) + \frac{\varepsilon}{2} |\nabla \varphi|^2 \right) \mathrm{d}x, \tag{9.1}$$

which governs the Cahn-Hilliard equation (4.35) and is here defined on a smooth and bounded domain $\Omega \subseteq \mathbb{R}^{n_{\mathrm{dim}}}$ (with $n_{\mathrm{dim}} = 2, 3$). Let $\boldsymbol{\nu}$ denote the outer unit normal vector to the Lipschitz continuous boundary $\partial\Omega$. Here, $W(\varphi)$ denotes a double-well potential, which we define as $W(\varphi) = (1/4)(1 - \varphi^2)^2$. Furthermore, $\varepsilon > 0$ is a small parameter controlling the thickness of the interface separating the two phases. The roots of $W(\varphi)$ are $\varphi_+ = 1$ and $\varphi_- = -1$ for our choice of double-well potential, and correspond to the fully separated phases. The zero-level set, that is $\{\varphi(\boldsymbol{x}) = 0\}$, defines the diffuse interface between these two equilibrium phase values.

As illustrated in the first diagram in Section 7.2, the aim of this Chapter is to relate the diffuse-interface energy functional (9.1) to the following sharp-interface energy

$$\mathcal{E}_{\text{CH}}(\Gamma) := C_W \int_\Gamma \mathrm{d}a, \tag{9.2}$$

as the interfacial thickness goes to zero, i.e. $\varepsilon \to 0$. In the above definition, C_W is a coefficient oftentimes referred to as the surface tension, which is given by

$$C_W = \int_{\varphi_-}^{\varphi_+} \sqrt{2W(s)}\,\mathrm{d}s. \tag{9.3}$$

For our choice of double well potential, namely $W(\varphi) = (1/4)(1-\varphi^2)^2$, we demonstrate in this Chapter that the surface-energy coefficient C_W corresponds to $\frac{2\sqrt{2}}{3}$. Here, the sharp interface $\Gamma \subset \Omega$ is a sufficiently smooth hypersurface that separates the domain Ω into two subdomains, such that $\Omega = \Omega_+ \cup \Omega_-$. These subdomains are described by the characteristic function

$$\chi_\Omega(\boldsymbol{x}) = \begin{cases} \varphi_+, & \text{on } \Omega_+, \\ \varphi_-, & \text{on } \Omega_-. \end{cases} \tag{9.4}$$

Next, we consider a system in which the phase-field variable, for instance representing the species mass per domain volume, is conserved for all time $t \in (0, T]$, i.e.

$$M(\varphi) := \frac{1}{|\Omega|} \int_\Omega \varphi \,\mathrm{d}x = M_0, \tag{9.5}$$

where $|\Omega|$ denotes the domain size. This consideration is consistent with the Cahn-Hilliard dynamics, see Section 4.2.3. Here, the mean-field of the phase-field variable $M(\varphi)$ is specified through its initial condition, i.e. $M_0 = M(\varphi_0(\boldsymbol{x})) = M(\varphi(\boldsymbol{x}, 0)) \in \mathbb{R}$. For M_0 to have a meaningful interpretation, we require that $M_0 \in (\varphi_-, \varphi_+)$. In other words, the initial data $\varphi_0(\boldsymbol{x})$ should ensure that M_0 takes on a realistic value. We will discuss this requirement in more detail in Remark 9.6 in Section 9.3.

In this Chapter, we employ the following approach to relate the diffuse-interface energy (9.1) to the sharp-interface energy (9.2):

(i) First, we define the diffuse-interface energy minimization problem (Section 9.2). Through the Lagrange multiplier method we characterize the saddle points, which correspond to the constrained minimizers (Section 9.3).

(ii) Next, through asymptotic expansions (Section 9.4), we determine the leading order solution to the diffuse-interface minimization problem, and thereby obtain the form of the global minimizers (Section 9.5);

(iii) Third, the leading order solution is substituted into the expanded diffuse-interface energy. We employ the *co-area formula* to arrive at the sharp-interface energy (Section 9.6).

(iv) Lastly, we find the minimizers of the sharp-interface energy, which provide us with a geometrical interpretation of the equilibrium states of the Cahn-Hilliard model (Section 9.7).

In summary, we wish to verify, through asymptotic expansions, that the zero-level set of minimizers of $\mathcal{E}^\varepsilon_{\text{GL}}(\varphi^*)$, which we denote as $\{\varphi^* = 0\}$, converges to the critical surface Γ^* as $\varepsilon \to 0$, with Γ^* denoting the minimizer of the sharp-interface energy $\mathcal{E}_{\text{GL}}(\Gamma^*)$.

9.2 Diffuse-interface energy minimization

In Problem 9.1 we present the minimization problem for the diffuse-interface energy, which has as objective to find minimizers φ^* of the diffuse-interface energy $\mathcal{E}^{\varepsilon}_{\mathrm{GL}}$ (9.1). To arrive at Problem 9.1, we restrict φ^* to a sensible class, which includes the mean-field constraint in Equation (9.5).

Problem 9.1 (Diffuse-interface energy minimization problem) *For an arbitrary, yet fixed $\varepsilon > 0$, find $\varphi^* \in \mathcal{L}_M$ such that*

$$\mathcal{E}^{\varepsilon}_{\mathrm{GL}}(\varphi^*) = \inf_{\varphi \in \mathcal{L}_M} \mathcal{E}^{\varepsilon}_{\mathrm{GL}}(\varphi), \tag{9.6}$$

over the admissible class $\mathcal{L}_M := \{\varphi \in H^1(\Omega) \mid M(\varphi) = M_0,\ \varphi = \varphi_- \text{ at } \partial\Omega,\ \nabla\varphi \cdot \boldsymbol{\nu} = 0 \text{ at } \partial\Omega\}$. □

Remark 9.2 (Analogous minimizers to the Cahn-Hilliard problem) The minimizers in Problem 9.1 are analogous to the steady-state solutions of the Cahn-Hilliard equation, as well as the equilibrium solutions of the conserved Allen-Cahn equation. In literature, one can also find the stable configurations of a fluid within the Van der Waals-Cahn-Hilliard theory of phase-transitions, see for instance [123, 114], which are also analogous to the minimizers of 9.1. Because the minimizers correspond to the steady states of the system, we can neglect the system's dynamics: only the governing free-energy functional and its variation with respect to the phase-field variable are relevant. □

9.3 Lagrange-multiplier method and saddle points

Problem 9.1 is a constrained minimization problem, as we are looking for minimizers within a specific class $\mathcal{L}_M$, that is, minimizers that satisfy the mass constraint (9.5). We can remove this constraint from $\mathcal{L}_M$ using the *Lagrange-multiplier* technique. The principal idea is that we introduce a scalar variable $\lambda \in \mathbb{R}$, which is called the *Lagrange multiplier*. In addition, we define the *Lagrangian* $\mathscr{L}(\cdot,\cdot)$, which for Problem 9.1 reads

$$\mathscr{L}(\varphi,\lambda) = \mathcal{E}^{\varepsilon}_{\mathrm{GL}}(\varphi) + \lambda(M(\varphi) - M_0), \tag{9.7}$$

bearing in mind that

$$M(\varphi) = \frac{1}{|\Omega|}\int_{\Omega} \varphi \,\mathrm{d}x. \tag{9.8}$$

Here, the main idea is that for a given φ the Lagrangian satisfies

$$\sup_{\lambda\in\mathbb{R}} \mathscr{L}(\varphi,\lambda) = \begin{cases} \mathcal{E}^{\varepsilon}_{\mathrm{GL}}(\varphi), & \text{if } M(\varphi) = M_0, \quad \forall \lambda \in \mathbb{R}, \\ \infty, & \text{otherwise.} \end{cases} \tag{9.9}$$

This leads us to the *saddle-point problem* in Problem 9.3, which is equivalent to the constrained minimization problem in Problem 9.1.

Problem 9.3 (Diffuse-interface saddle-point problem) *For an arbitrary, yet fixed $\varepsilon > 0$, find $(\varphi^*, \lambda^*) \in \mathcal{L} \times \mathbb{R}$ such that*

$$\mathscr{L}(\varphi^*,\lambda^*) = \inf_{\varphi\in\mathcal{L}} \sup_{\lambda\in\mathbb{R}} \mathscr{L}(\varphi,\lambda), \tag{9.10}$$

with the admissible class $\mathcal{L} := \{\varphi \in H^1(\Omega) \mid \varphi = \varphi_- \text{ at } \partial\Omega,\ \nabla\varphi\cdot\boldsymbol{\nu} = 0 \text{ at } \partial\Omega\}$. □

Solutions to Problem 9.3 are called *saddle points* and require that the directional derivatives vanish at (φ^*, λ^*), that is

$$\begin{cases} 0 = \mathscr{L}'(\varphi^*, \lambda^*; \delta\lambda), & \forall \delta\lambda \in \mathbb{R}, \\ 0 = \mathscr{L}'(\varphi^*, \lambda^*; \delta\varphi), & \forall \delta\varphi \in \mathcal{L}. \end{cases} \tag{9.11}$$

In view of the Lagrangian (9.7), we can write (9.11) as

$$\begin{cases} 0 = M(\varphi^*) - M_0, \\ 0 = \dfrac{\delta \mathcal{E}^\varepsilon_{\mathrm{GL}}(\varphi^*)}{\delta\varphi^*} + \lambda^* \dfrac{\delta M(\varphi^*)}{\delta\varphi^*} = \dfrac{1}{\varepsilon} W'(\varphi^*) - \varepsilon\Delta\varphi^* + \lambda^*. \end{cases} \tag{9.12}$$

Integration of $(9.12)_2$ over the domain Ω, yields the following expression for the Lagrange multiplier

$$\lambda^* = -\frac{1}{\varepsilon|\Omega|} \int_\Omega W'(\varphi^*)\, \mathrm{d}x, \tag{9.13}$$

where we have used that $\nabla\varphi^* \cdot \boldsymbol{\nu} = 0$ at $\partial\Omega$.

9.4 Minimizers of the diffuse-interface energy

Let $\varphi^* = \varphi^\varepsilon$ solve the constrained minimization problem in Problem 9.1 for an arbitrary but fixed ε. Furthermore, let $\{\varphi^\varepsilon\}_{\varepsilon \geq 0}$ denote the one-parameter family of functions in the admissible solution space $\mathcal{L}_M$, which approach a singular limit denoted by φ^0. Suppose the following assumptions on φ^ε hold:

(A.1) There exists a family of smooth and compact hypersurfaces embedded in Ω, which we denote by $\{\Gamma^\varepsilon\}_{\varepsilon \geq 0}$. These hypersurfaces converge uniformly to Γ^0 as $\varepsilon \to 0$. For each $\varepsilon > 0$, the signed distance function $d^\varepsilon(\boldsymbol{x}) : \Omega \to \mathbb{R}$ measures the distance of a point $\boldsymbol{x}$ to the interface Γ^ε. The function $d^\varepsilon(\boldsymbol{x})$ takes on positive values in the interior subdomain Ω^ε_+ and negative values in the exterior subdomain Ω^ε_-. Note that the interface is defined through the distance function by $\Gamma^\varepsilon := \{d^\varepsilon(\boldsymbol{x}) = 0\}$;

(A.2) The solution φ^* to Problem 9.1 takes on the form

$$\varphi^*(\boldsymbol{x}) = \varphi^\varepsilon(\boldsymbol{x}) = \psi\left(\frac{d^\varepsilon(\boldsymbol{x})}{\varepsilon}\right) + \varepsilon h(\boldsymbol{x}) + g(\boldsymbol{x}), \tag{9.14}$$

where $\psi : \mathbb{R} \to \mathbb{R}$ and $h : \Omega \to \mathbb{R}$ are sufficiently smooth functions, independent of ε. Furthermore, we assume that $\|\nabla^k g\|_{L^\infty} = o(\varepsilon)$ for sufficiently many k;

(A.3) Let the leading order term $\psi(\xi)$ in the asymptotic expansion (9.14) with $\xi := d^\varepsilon(\boldsymbol{x})/\varepsilon$ solve the following problem:

$$\psi''(\xi) = W'(\psi(\xi)), \qquad \forall \xi \in \mathbb{R}, \tag{9.15}$$

subject to $\psi(-\infty) = \varphi_-$, $\psi(0) = 0$ and $\psi(\infty) = \varphi_+$.

The asymptotic expansion in (A.2) implies that φ^* is a perturbed transition layer marking the free interface. In Section 9.5, we will see that the problem in Assumption (A.3) is in fact the leading order problem of the expanded and unconstrained Euler-Lagrange equation of the diffuse-interface energy functional $\mathcal{E}^\varepsilon_{\mathrm{GL}}$. Furthermore, Assumption (A.1) leads to an important lemma involving functions of d^ε on the ε-scale, which is known as the *co-area formula* [56], see Lemma 9.4. In this Lemma we demonstrate that a certain class of integrable functions, namely functions of $\xi := d^\varepsilon(\boldsymbol{x})/\varepsilon$ that are smoothly decaying for $|\xi| \to \infty$, can be viewed as a δ-sequence of the limiting surface Γ^0. In other words, by introducing a change of coordinates in the small neighbourhood of the interface we can split a domain integral of a function weighted by a suitably decaying function into (i) a line integral in direction normal to the interface; and (ii) a surface integral over the limiting surface Γ^0, provided that Assumption (A.1) holds. Furthermore, in Section 9.5 and 9.6, we need a bound on the order of convergence for odd functions within the class of functions for which the co-area formula is valid. We show in Lemma 9.5 that this particular class of integrals belongs to $\mathcal{O}(\varepsilon^2)$. Lastly, in Remark 9.6, we reflect on the consistency of Assumption (A.1) with the class of admissible solutions $\mathcal{L}_M$ defined in Problem 9.1.

Lemma 9.4 (Co-area formula) *Let Γ^ε and d^ε be given as in (A.1). Furthermore, given are the functions $f \in C^0(\Omega)$ and $p \in L^1(\mathbb{R})$, that satisfy*

$$\max_{|t|>s} |p(t)t| \leq \frac{C}{s^m}, \qquad m > 1. \tag{9.16}$$

with $C > 0$. Then, we have that

$$\lim_{\varepsilon \to 0} \frac{1}{\varepsilon} \int_\Omega p\left(\frac{d^\varepsilon(\boldsymbol{x})}{\varepsilon}\right) f(\boldsymbol{x})\, \mathrm{d}x = \int_{-\infty}^{\infty} p(t)\mathrm{d}t \int_{\Gamma^0} f\, \mathrm{d}a. \tag{9.17}$$

□

Proof. The following proof is based on [44] and [91]. Let the hypersurface Γ^ε be parameterized by a function α^ε. For this hypersurface, there exists an open set W of $\mathbb{R}^{(n_{\text{dim}}-1)}$ such that the mapping α^ε from $\overline{W}$ onto Γ^ε is smooth and the inverse mapping $(\alpha^\varepsilon)^{-1}$ is continuous from Γ^ε onto $\overline{W}$. For $n_{\text{dim}} = 2$, the mapping α^ε is written as

$$\alpha^\varepsilon(z) = (\alpha_1^\varepsilon(z), \alpha_2^\varepsilon(z)), \qquad \forall z \in \overline{W}, \tag{9.18}$$

whereas for $n_{\text{dim}} = 3$ we have

$$\alpha^\varepsilon(z_1, z_2) = (\alpha_1^\varepsilon(z_1, z_2), \alpha_2^\varepsilon(z_1, z_2), \alpha_3^\varepsilon(z_1, z_2)), \qquad \forall (z_1, z_2) \in \overline{W}. \tag{9.19}$$

For the sake of simplicity, we will consider $n_{\text{dim}} = 2$ in what follows. Therefore, we will continue writing $\alpha^\varepsilon(z)$, but it should be understood that extension to the three-dimensional case ($n_{\text{dim}} = 3$) is straightforward, see [91] for more details.

Let O^ε be the neighbourhood of Γ^ε in which ∇d^ε is Lipschitz continuous. Let $\delta > 0$ be a small parameter and let $\eta^\varepsilon(z, \tau) : \overline{W} \times [-\delta, \delta] \to \mathbb{R}^{n_{\text{dim}}}$ denote the integral curves of ∇d^ε, which satisfy

$$\begin{cases} \dfrac{\partial \eta^\varepsilon(z, \tau)}{\partial \tau} = \nabla d^\varepsilon(\eta^\varepsilon(z, \tau)), \\ \eta^\varepsilon(z, 0) = \alpha^\varepsilon(z). \end{cases} \tag{9.20}$$

Bearing in mind that we consider $n_{\text{dim}} = 2$ here, we write $\eta^\varepsilon(z, \tau) = (\eta_1^\varepsilon(z, \tau), \eta_2^\varepsilon(z, \tau))$ with $\eta_i^\varepsilon : \overline{W} \times [-\delta, \delta] \to \mathbb{R}$. We define $U^\varepsilon := \eta^\varepsilon(\{\overline{W} \times [-\delta, \delta]\})$ and choose δ small enough so that $U^\varepsilon \subset O^\varepsilon$. In view of (9.20), we have that

$$\frac{\mathrm{d}}{\mathrm{d}\tau} d^\varepsilon(\eta^\varepsilon(z, \tau)) = \nabla d^\varepsilon(\eta^\varepsilon(z, \tau)) \frac{\partial \eta^\varepsilon(z, \tau)}{\partial \tau} = |\nabla d^\varepsilon(\eta^\varepsilon(z, \tau))|^2 = 1, \tag{9.21}$$

and

$$d^\varepsilon(\eta^\varepsilon(z, 0)) = d^\varepsilon(\alpha^\varepsilon(z)) = 0. \tag{9.22}$$

Therefore, by integrating over τ we recover

$$d^\varepsilon(\eta^\varepsilon(z, \tau)) = \tau, \qquad \forall\, z \in \overline{W}. \tag{9.23}$$

Furthermore, let $J^\varepsilon(z,\tau)$ denote the determinant of the Jacobian matrix of η^ε at (z,τ), i.e.

$$J^\varepsilon(z,\tau) := |\nabla_{z,\tau}\eta^\varepsilon(z,\tau)|. \tag{9.24}$$

Then, bearing in mind that

$$\begin{aligned}\frac{\partial\eta^\varepsilon(z,\tau)}{\partial z} &= \left(\frac{\partial\eta_1^\varepsilon(z,\tau)}{\partial z}, \frac{\partial\eta_2^\varepsilon(z,\tau)}{\partial z}\right),\\ \frac{\partial\eta^\varepsilon(z,\tau)}{\partial \tau} &= \left(\frac{\partial\eta_1^\varepsilon(z,\tau)}{\partial \tau}, \frac{\partial\eta_2^\varepsilon(z,\tau)}{\partial \tau}\right),\end{aligned} \tag{9.25}$$

we find at $z \in \overline{W}$ that

$$\begin{aligned}\boldsymbol{\tau}^\varepsilon &:= \frac{\partial\eta^\varepsilon(z,0)}{\partial z} = \left(\frac{\partial\eta_1^\varepsilon(z,0)}{\partial z}, \frac{\partial\eta_2^\varepsilon(z,0)}{\partial z}\right),\\ \boldsymbol{n}^\varepsilon &:= \frac{\partial\eta^\varepsilon(z,0)}{\partial \tau} = \left(\frac{\partial\eta_1^\varepsilon(z,0)}{\partial \tau}, \frac{\partial\eta_2^\varepsilon(z,0)}{\partial \tau}\right),\end{aligned} \tag{9.26}$$

with $\boldsymbol{n}^\varepsilon$ the outward normal vector to Γ^ε and $\boldsymbol{\tau}^\varepsilon$ the vector spanning the tangent space, both defined at a point $\eta^\varepsilon(z,0) = \alpha^\varepsilon(z)$. Thus, the determinant of the Jacobian (9.24) satisfies

$$J^\varepsilon(z,0) := |\nabla_{z,\tau}\eta^\varepsilon(z,0)| = 1, \tag{9.27}$$

as $\boldsymbol{n}^\varepsilon$ and $\boldsymbol{\tau}^\varepsilon$ form an orthonormal basis.

Recalling that $U^\varepsilon := \eta^\varepsilon(\{\overline{W}\times[-\delta,\delta]\}) \subset O^\varepsilon$, we perform the change of coordinates $\boldsymbol{x} = \eta^\varepsilon(z,\tau)$ on the following integral and write

$$\begin{aligned}\int_{U^\varepsilon} p\left(\frac{d^\varepsilon(\boldsymbol{x})}{\varepsilon}\right) f(\boldsymbol{x})\,\mathrm{d}x &= \int_{-\delta}^{\delta}\int_W p\left(\frac{d^\varepsilon(\eta^\varepsilon(z,\tau))}{\varepsilon}\right) f(\eta^\varepsilon(z,\tau))J^\varepsilon(z,\tau)\,\mathrm{d}z\mathrm{d}\tau\\ &= \int_{-\delta}^{\delta} p\left(\frac{\tau}{\varepsilon}\right)\int_W f(\eta^\varepsilon(z,\tau))J(z,\tau)\,\mathrm{d}z\mathrm{d}\tau.\end{aligned} \tag{9.28}$$

Next, from application of the change of coordinate $\tau = \varepsilon t$ follows

$$\int_{U^\varepsilon} p\left(\frac{d^\varepsilon(\boldsymbol{x})}{\varepsilon}\right) f(\boldsymbol{x})\,\mathrm{d}x = \varepsilon\int_{-\delta/\varepsilon}^{\delta/\varepsilon} p\,(t)\int_W f(\eta^\varepsilon(z,\varepsilon t))J^\varepsilon(z,\varepsilon t)\,\mathrm{d}z\mathrm{d}t. \tag{9.29}$$

By continuity and convergence of Γ^ε to Γ^0, see Assumption (A.1), we arrive at

$$\begin{aligned}\lim_{\varepsilon\to 0}\frac{1}{\varepsilon}\int_{U^\varepsilon} p\left(\frac{d^\varepsilon(\boldsymbol{x})}{\varepsilon}\right) f(\boldsymbol{x})\,\mathrm{d}x &= \lim_{\varepsilon\to 0}\int_{-\delta/\varepsilon}^{\delta/\varepsilon} p\,(t)\int_W f(\eta^\varepsilon(z,\varepsilon t))J^\varepsilon(z,\varepsilon t)\,\mathrm{d}z\mathrm{d}t\\ &= \int_{-\infty}^{\infty} p\,(t)\int_W f(\eta^0(z,0))J^0(z,0)\,\mathrm{d}z\mathrm{d}t\\ &= \int_{-\infty}^{\infty} p\,(t)\,\mathrm{d}t\int_{\Gamma^0} f\,\mathrm{d}a.\end{aligned} \tag{9.30}$$

Outside the neighbourhood U^ε, i.e. $(U^\varepsilon)^c = \{d^\varepsilon(\boldsymbol{x}) > \delta\}$, we find

$$\begin{aligned}\lim_{\varepsilon\to 0}\frac{1}{\varepsilon}\int_{(U^\varepsilon)^c} p\left(\frac{d^\varepsilon(\boldsymbol{x})}{\varepsilon}\right) f(\boldsymbol{x})\,\mathrm{d}x &\le \lim_{\varepsilon\to 0}\frac{1}{\varepsilon}\left\|p\left(\frac{d^\varepsilon(\boldsymbol{x})}{\varepsilon}\right)\right\|_{L^\infty((U^\varepsilon)^c)}\|f(\boldsymbol{x})\|_{L^1(\Omega)}\\ &= \lim_{\varepsilon\to 0}\max_{|d^\varepsilon|>\delta}\left|\frac{1}{\varepsilon}p\left(\frac{d^\varepsilon(\boldsymbol{x})}{\varepsilon}\right)\right|\int_\Omega |f(\boldsymbol{x})|\,\mathrm{d}x,\end{aligned} \tag{9.31}$$

where we have used Hölder's inequality. Introducing $t = d^\varepsilon(\boldsymbol{x})/\varepsilon$ yields

$$\begin{aligned}\lim_{\varepsilon\to 0}\max_{|d^\varepsilon|>\delta}\left|\frac{1}{\varepsilon}p\left(\frac{d^\varepsilon(\boldsymbol{x})}{\varepsilon}\right)\right|\int_\Omega |f(\boldsymbol{x})|\,\mathrm{d}x &= \lim_{\varepsilon\to 0}\max_{|t|>(\delta/\varepsilon)}\left|\frac{1}{\varepsilon t}p(t)t\right|\int_\Omega |f(\boldsymbol{x})|\,\mathrm{d}x\\ &\leq \lim_{\varepsilon\to 0}\max_{|t|>(\delta/\varepsilon)}\frac{1}{\delta}|p(t)t|\int_\Omega |f(\boldsymbol{x})|\,\mathrm{d}x\\ &\leq \lim_{\varepsilon\to 0}\frac{1}{\delta}\frac{C\varepsilon^m}{\delta^m}\int_\Omega |f(\boldsymbol{x})|\,\mathrm{d}x = 0, \end{aligned} \tag{9.32}$$

as p is a suitably decaying function, see expression (9.16). Combining the integrals (9.30) and (9.32) completes our proof. ■

Lemma 9.5 (Co-area formula for odd functions) *In addition to Lemma 9.4, assume that $f \in C^1(\Omega)$ and $d^\varepsilon \in C^2(U^\varepsilon)$. If p is odd, then*

$$\lim_{\varepsilon\to 0}\frac{1}{\varepsilon^2}\int_\Omega p\left(\frac{d^\varepsilon(\boldsymbol{x})}{\varepsilon}\right) f(\boldsymbol{x})\,\mathrm{d}x < \infty. \tag{9.33}$$

□

Proof. The following proof is based on Lemma 2.2 in [44]. First, recall that $U^\varepsilon := \eta^\varepsilon(\{\overline{W}\times[-\delta,\delta]\}) \subset O^\varepsilon$. Performing the change of coordinates $\boldsymbol{x} = \eta^\varepsilon(z,\tau)$ on the following integral, we obtain

$$\begin{aligned}\int_{U^\varepsilon} p\left(\frac{d^\varepsilon(\boldsymbol{x})}{\varepsilon}\right) f(\boldsymbol{x})\,\mathrm{d}x &= \int_{-\delta}^{\delta}\int_W p\left(\frac{d^\varepsilon(\eta^\varepsilon(z,\tau))}{\varepsilon}\right) f(\eta^\varepsilon(z,\tau))J^\varepsilon(z,\tau)\,\mathrm{d}z\mathrm{d}\tau\\ &= \int_{-\delta}^{\delta} p\left(\frac{\tau}{\varepsilon}\right)\int_W f(\eta^\varepsilon(z,\tau))J(z,\tau)\,\mathrm{d}z\mathrm{d}\tau\\ &= \int_{-\delta}^{\delta} p\left(\frac{\tau}{\varepsilon}\right) F^\varepsilon(\tau)\mathrm{d}\tau. \end{aligned} \tag{9.34}$$

where F^ε is defined as follows

$$F^\varepsilon(\tau) := \int_W f(\eta^\varepsilon(z,\tau))J^\varepsilon(z,\tau)\,\mathrm{d}z. \tag{9.35}$$

In addition, $F^\varepsilon(\tau)$ is continuous in ε and continuously differentiable for $\tau \in (-\delta,\delta)$. Given that p is odd, we may write

$$\int_{U^\varepsilon} p\left(\frac{d^\varepsilon(\boldsymbol{x})}{\varepsilon}\right) f(\boldsymbol{x})\,\mathrm{d}x = \int_{-\delta}^{\delta} p\left(\frac{\tau}{\varepsilon}\right) F^\varepsilon(\tau)\mathrm{d}\tau - \int_{-\delta}^{\delta} p\left(\frac{\tau}{\varepsilon}\right) F^\varepsilon(0)\mathrm{d}\tau, \tag{9.36}$$

with $F^\varepsilon(0)$ constant. Then, let $G^\varepsilon(\tau) = (F^\varepsilon(\tau) - F^\varepsilon(0))/\tau$, so that the above can be written as

$$\int_{U^\varepsilon} p\left(\frac{d^\varepsilon(\boldsymbol{x})}{\varepsilon}\right) f(\boldsymbol{x})\,\mathrm{d}x = \int_{-\delta}^{\delta} p\left(\frac{\tau}{\varepsilon}\right) G^\varepsilon(\tau)\tau\mathrm{d}\tau. \tag{9.37}$$

Next, Hölder's inequality learns us that

$$\begin{aligned}\left|\int_{U^\varepsilon} p\left(\frac{d^\varepsilon(\boldsymbol{x})}{\varepsilon}\right) f(\boldsymbol{x})\,\mathrm{d}x\right| &\leq \max_{\tau\in(-\delta,\delta)}|G^\varepsilon(\tau)|\int_{-\delta}^{\delta}\left|p\left(\frac{\tau}{\varepsilon}\right)\tau\right|\mathrm{d}\tau,\\ &= \varepsilon\max_{\tau\in(-\delta,\delta)}|G^\varepsilon(\tau)|\int_{-\delta}^{\delta}\left|p\left(\frac{\tau}{\varepsilon}\right)\frac{\tau}{\varepsilon}\right|\mathrm{d}\tau, \end{aligned} \tag{9.38}$$

Performing the change of coordinates $\tau = \varepsilon t$ on the last integral, we find

$$\begin{aligned}\left| \int_{U^\varepsilon} p\left(\frac{d^\varepsilon(\boldsymbol{x})}{\varepsilon}\right) f(\boldsymbol{x})\,\mathrm{d}x \right| &\leq \varepsilon^2 \max_{\tau\in(-\delta,\delta)} |G^\varepsilon(\tau)| \int_{-\delta/\varepsilon}^{\delta/\varepsilon} |p(t)t|\,\mathrm{d}t \\ &\leq \varepsilon^2 \max_{\tau\in(-\delta,\delta)} |G^\varepsilon(\tau)| \int_{-\infty}^{\infty} |p(t)t|\,\mathrm{d}t. \end{aligned} \tag{9.39}$$

In expression (9.39) the term involving G^ε is finite, as F^ε is continuous in ε and continuously differentiable for $\tau \in (-\delta, \delta)$. Furthermore, the integral involving $p(t)$ is finite as well, given that $p \in L^1(\Omega)$ and for $|\tau| > (\delta/\varepsilon)$ we have that p is a suitably decaying function, see (9.16). Thus, we arrive at

$$\lim_{\varepsilon\to 0} \frac{1}{\varepsilon^2} \left| \int_\Omega p\left(\frac{d^\varepsilon(\boldsymbol{x})}{\varepsilon}\right) f(\boldsymbol{x})\,\mathrm{d}x \right| < \infty, \tag{9.40}$$

which concludes our proof. ∎

Remark 9.6 (Consistency of Assumption (A.1) with class $\mathcal{L}_M$) Assumption (A.1) is consistent with the class of admissible solutions $\mathcal{L}_M$ used in Problem 9.1. The existence of an embedded hypersurface in Ω ensures that the mean-value of φ is written as $M(\varphi) \in (\varphi_-, \varphi_+)$, and can not be equal to one of the binodal values, that is φ_+ or φ_-. Furthermore, the embedding of the interface in Ω implies that any solution to Problem 9.1 should equal the binodal value φ_- at the domain boundary $\partial\Omega$. Alternatively, one could opt to prescribe the other binodal value φ_+ (where $\varphi_+ > \varphi_-$) at $\partial\Omega$. Note that such a choice would result in a sign change in the definition of the signed distance function $d^\varepsilon(\boldsymbol{x})$, as well as reformulation of the characteristic function χ_Ω (9.4). □

9.5 Asymptotic expansion and leading order problem

In the following, we employ the asymptotic expansion ansatz in Assumption (A.2), namely $\varphi^* = \varphi^\varepsilon$, to further characterize the structure of the diffuse-interface minimizers of Problem 9.1. This implies that $(9.11)_2$ becomes

$$0 = \frac{1}{\varepsilon} W'(\varphi^\varepsilon) - \varepsilon\Delta\varphi^\varepsilon - \frac{1}{\varepsilon|\Omega|} \int_\Omega W'(\varphi^\varepsilon)\,\mathrm{d}x, \tag{9.41}$$

for a given ε. Here, we have used the expression for the Lagrange multiplier (9.13). Next, using Assumption (A.2), we compute the following identity

$$\nabla\varphi^\varepsilon(\boldsymbol{x}) = \frac{1}{\varepsilon}\psi'\left(\frac{d^\varepsilon(\boldsymbol{x})}{\varepsilon}\right)\nabla d^\varepsilon(\boldsymbol{x}) + \varepsilon\nabla h(\boldsymbol{x}) + \nabla g(\boldsymbol{x}). \tag{9.42}$$

Then, bearing in mind that $\|\nabla^k g\|_{L^\infty(\Omega)} = o(\varepsilon)$ and omitting the dependencies for the sake of brevity, we derive the following identities

$$\begin{aligned}
|\nabla \varphi^\varepsilon|^2 &= \frac{1}{\varepsilon^2}(\psi')^2 + 2\psi' \nabla d^\varepsilon \cdot \nabla h + \frac{2}{\varepsilon}\psi' \nabla d^\varepsilon \cdot \nabla g \\
&\quad + \varepsilon^2 |\nabla h|^2 + 2\varepsilon \nabla h \cdot \nabla g + |\nabla g|^2, \qquad (9.43)\\
\Delta \varphi^\varepsilon &= \frac{1}{\varepsilon^2}\psi'' - \frac{2}{\varepsilon} K \psi' + \varepsilon \Delta h + \Delta g, \qquad (9.44)\\
W(\varphi^\varepsilon) &= W(\psi) + \varepsilon W'(\psi)\left(h + \frac{1}{\varepsilon} g\right) \\
&\quad + \frac{\varepsilon^2}{2} W''(\psi)\left(h + \frac{1}{\varepsilon} g\right)^2 + \frac{\varepsilon^3}{6} W'''(\psi)\left(h + \frac{1}{\varepsilon} g\right)^3 + \mathcal{O}(\varepsilon^4) \\
&= W(\psi) + \varepsilon W'(\psi) h + W'(\psi) g + \frac{\varepsilon^2}{2} W''(\psi) h^2 + \varepsilon W''(\psi) h g + \frac{1}{2} W''(\psi) g^2 \\
&\quad + \frac{\varepsilon^3}{6} W'''(\psi) h^3 + \frac{\varepsilon^2}{2} W'''(\psi) h^2 g + \frac{\varepsilon}{2} W'''(\psi) h g^2 + \frac{1}{6} W'''(\psi) g^3 + \mathcal{O}(\varepsilon^4), \qquad (9.45)\\
W'(\varphi^\varepsilon) &= W'(\psi) + \varepsilon W''(\psi) h + W''(\psi) g \\
&\quad + \frac{\varepsilon^2}{2} W'''(\psi) h^2 + \varepsilon W'''(\psi) h g + \frac{1}{2} W'''(\psi) g^2 + \mathcal{O}(\varepsilon^3), \qquad (9.46)\\
\lambda^\varepsilon &= -\frac{1}{\varepsilon|\Omega|}\int_\Omega W'(\psi)\,\mathrm{d}x - \frac{1}{|\Omega|}\int_\Omega W''(\psi) h + \frac{1}{\varepsilon} W''(\psi) g \,\mathrm{d}x \\
&\quad - \frac{1}{|\Omega|}\int_\Omega \frac{\varepsilon}{2} W'''(\psi) h^2 + W'''(\psi) h g + \frac{1}{2\varepsilon} W'''(\psi) g^2 \,\mathrm{d}x + \mathcal{O}(\varepsilon^2), \qquad (9.47)
\end{aligned}$$

where we have used that $|\nabla d^\varepsilon|^2 = 1$. In addition, we have that $\Delta d^\varepsilon(\boldsymbol{x}) = -2K(\boldsymbol{x})$, with K the mean curvature for any $\boldsymbol{x} \in \Gamma^\varepsilon$ [174]. Thus, using the above identities, we write expression (9.41) as

$$\begin{aligned}
&\frac{1}{\varepsilon}\Big(W'(\psi) + \varepsilon W''(\psi) h + W''(\psi) g + \frac{\varepsilon^2}{2} W'''(\psi) h^2 + \varepsilon W'''(\psi) h g + \frac{1}{2} W'''(\psi) g^2 + \mathcal{O}(\varepsilon^3)\Big) \\
&\quad - \varepsilon\left(\frac{1}{\varepsilon^2}\psi'' + \frac{1}{\varepsilon}\psi' \Delta d^\varepsilon + \varepsilon \Delta h + \Delta g\right) + \lambda^\varepsilon = 0. \qquad (9.48)
\end{aligned}$$

Then, substituting the expansion for λ^ε (9.47) and collecting terms of the same order, we obtain

$$\begin{aligned}
0 &= \frac{1}{\varepsilon}\left(W'(\psi) - \psi'' - \frac{1}{|\Omega|}\int_\Omega W'(\psi)\,\mathrm{d}x\right) \\
&\quad + \left(W''(\psi) h - \psi' \Delta d^\varepsilon - \frac{1}{|\Omega|}\int_\Omega W''(\psi) h \,\mathrm{d}x\right) + \mathcal{O}(\varepsilon). \qquad (9.49)
\end{aligned}$$

Following Assumption (A.3), we consider the leading order problem in Problem 9.7. This problem is based on the leading order term in (9.49) except that we omit the contribution from the Lagrange multiplier expansion. In Theorem 9.A, we demonstrate that the solution to this problem is given by $\psi(\xi) = \tanh\left(\frac{\xi}{\sqrt{2}}\right)$. Lastly, in Remark 9.8 we use Lemma 9.5 to demonstrate why Assumption (A.3), and thus the omission of the Lagrange multiplier contribution in the leading terms, leads to consistent results for the leading order solution.

Problem 9.7 (Leading order problem) *Let ψ solve the differential equation*

$$\psi''(\xi) = W'(\psi(\xi)), \qquad \forall \xi \in \mathbb{R}, \tag{9.50}$$

subject to the conditions $\psi(-\infty) = \varphi_-$, $\psi(\infty) = \varphi_+$ and $\psi(0) = 0$. □

Theorem 9.A (Leading order solution) *Suppose that φ^ε solves Problem 9.1 and satisfies Assumptions (A.1) - (A.3), then $\psi(\xi) = \tanh\left(\frac{\xi}{\sqrt{2}}\right)$.* □

Proof. To obtain the leading order solution, we have to solve Problem 9.7, i.e.

$$\psi''(\xi) = W'(\psi(\xi)), \quad \forall \xi \in \mathbb{R}, \tag{9.51}$$

bearing in mind that $W'(\psi) = -\psi(1-\psi^2)$, because of our choice of double-well potential in Section 9.1. Through multiplication with $4\psi'$, followed by integration, we obtain

$$2(\psi')^2 = \psi^4 - 2\psi^2 + C, \tag{9.52}$$

where C denotes the constant of integration. From the boundary conditions follows that ψ is non-decreasing. Also, for $\xi \to \pm|\infty|$ the leading order solution converges to one of the binodal values, i.e. the constants $\varphi_- = -1$ and $\varphi_+ = 1$, implying that $\psi'(-\infty) = \psi'(\infty) = 0$, and thus $C = 1$. Therefore, we can write

$$\psi' = \frac{1}{\sqrt{2}}(1-\psi^2). \tag{9.53}$$

This is a separable ordinary differential equation with solution $\psi(\xi) = \tanh\left(\frac{\xi}{\sqrt{2}}\right)$, see also [56, 20, 44].

Remark 9.8 (Consistency of Assumption (A.3) with the Lagrange multiplier) The contribution from the Lagrange multiplier λ^ε in the leading order term of expression (9.49) is given by

$$-\frac{1}{\varepsilon|\Omega|}\int_\Omega W'(\psi(\xi))\,\mathrm{d}x, \tag{9.54}$$

where $W'(\psi)$ is an odd function. In view of Lemma 9.5, we may conclude that

$$-\frac{1}{|\Omega|}\int_\Omega W'(\psi(\xi))\,\mathrm{d}x = \mathcal{O}(\varepsilon^2). \tag{9.55}$$

Thus, no contributions from the Lagrange multiplier expansion appear in the leading order Problem 9.7. □

9.6 Convergence to the sharp-interface energy

Expansion of Ginzbug-Landau energy functional using the expansion φ^ε for the minimizer formulated in Assumption (A.2) gives

$$\begin{aligned}
\mathcal{E}^\varepsilon_{\mathrm{GL}}(\varphi^\varepsilon) &= \int_\Omega \left(\frac{1}{\varepsilon}W(\varphi^\varepsilon) + \frac{\varepsilon}{2}|\nabla\varphi^\varepsilon|^2\right)\,\mathrm{d}x,\\
&= \frac{1}{\varepsilon}\int_\Omega \left(W(\psi) + \varepsilon W'(\psi)\left(h + \frac{1}{\varepsilon}g\right) + \frac{\varepsilon^2}{2}W''(\psi)\left(h+\frac{1}{\varepsilon}g\right)^2\right)\,\mathrm{d}x\\
&+ \frac{1}{\varepsilon}\int_\Omega \left(\frac{\varepsilon^3}{6}W'''(\psi)\left(h+\frac{1}{\varepsilon}g\right)^3 + \mathcal{O}(\varepsilon^4)\right)\,\mathrm{d}x\\
&+ \frac{\varepsilon}{2}\int_\Omega \left(\frac{1}{\varepsilon^2}\left(\psi'\right)^2 + 2\psi'\nabla d^\varepsilon\cdot\nabla h + \frac{2}{\varepsilon}\psi'\nabla d^\varepsilon\cdot\nabla g\right)\,\mathrm{d}x\\
&+ \frac{\varepsilon}{2}\int_\Omega \left(\varepsilon^2|\nabla h|^2 + 2\varepsilon\nabla h\cdot\nabla g + |\nabla g|^2\right)\,\mathrm{d}x\\
&= \frac{1}{\varepsilon}\int_\Omega \left(W(\psi) + \frac{1}{2}(\psi')^2\right)\,\mathrm{d}x + \int_\Omega W'(\psi)h\,\mathrm{d}x + \mathcal{O}(\varepsilon),
\end{aligned} \tag{9.56}$$

Next, we provide two types of convergence results for the diffuse-energy functional $\mathcal{E}^\varepsilon_{\mathrm{GL}}(\varphi^*)$ to its sharp-interface counterpart $\mathcal{E}_{\mathrm{GL}}(\Gamma^*)$. The first is presented in Theorem 9.B and makes use of the leading order solution for the diffuse-interface minimizer. The second approach, detailed in Theorem 9.C, does not require an explicit form for the leading order solution of the diffuse-interface minimizer. Instead it makes use of an equivalent differential equation, which is presented in Lemma 9.9. The result, the sharp-interface energy functional $\mathcal{E}_{\mathrm{GL}}$, consists of a surface integral weighted by a constant C_W. Here, C_W is also known as the surface tension coefficient, and its value depends on the choice of double-well potential. For our choice of double-well potential, it is equal to $\frac{2\sqrt{2}}{3}$.

Theorem 9.B (Convergence to sharp-interface energy $\mathcal{E}_{\mathrm{GL}}$: approach I) *If φ^* solves Problem 9.1 and satisfies (A.1) - (A.3), then,*

$$\mathcal{E}^0_{\mathrm{GL}}(\Gamma^0) := \lim_{\varepsilon\to 0}\mathcal{E}^\varepsilon_{\mathrm{GL}}(\varphi^\varepsilon) = C_W\int_{\Gamma^0}\mathrm{d}a, \tag{9.57}$$

with $C_W := \frac{2\sqrt{2}}{3}$. □

Proof. From Theorem 9.A follows that the leading order solution is given by $\psi(\xi) = \tanh(d^\varepsilon(\boldsymbol{x})/\sqrt{2}\varepsilon)$. Then, in view of the expansion (9.56) and by Lemma 9.4, we find

$$\begin{aligned}
\lim_{\varepsilon\to 0}\mathcal{E}^\varepsilon_{\mathrm{GL}}(\varphi^\varepsilon) &= \lim_{\varepsilon\to 0}\left(\frac{1}{\varepsilon}\int_\Omega\left(W(\psi) + \frac{1}{2}\left(\psi'\right)^2\right)\,\mathrm{d}x + \int_\Omega W'(\psi)h\,\mathrm{d}x + \mathcal{O}(\varepsilon)\right)\\
&= \frac{1}{2}\int_{-\infty}^{\infty}\mathrm{sech}^4\left(\frac{\xi}{\sqrt{2}}\right)\,\mathrm{d}\xi\int_{\Gamma^0}\mathrm{d}a\\
&\quad + \int_{-\infty}^{\infty}\tanh\left(\frac{\xi}{\sqrt{2}}\right)\left(1-\tanh^2\left(\frac{\xi}{\sqrt{2}}\right)\right)\,\mathrm{d}\xi\int_{\Gamma^0}h\,\mathrm{d}a\\
&= C_W\int_{\Gamma^0}\mathrm{d}a,
\end{aligned} \tag{9.58}$$

where we have used that $W(\varphi) = \frac{1}{4}(\varphi^2-1)^2$ and $\xi = d^\varepsilon(\boldsymbol{x})/\varepsilon$. In addition, the surface-energy coefficient C_W corresponds to $\frac{2\sqrt{2}}{3}$. ■

Lemma 9.9 *The solution to Problem 9.7 also satisfies the differential equation*

$$\psi'(\xi) = \sqrt{2W(\psi)}. \tag{9.59}$$

As a result, we can write

$$\int_{-\infty}^{\infty} (\psi'(\xi))^2 \,\mathrm{d}\xi = \sqrt{2} \int_{\varphi_-}^{\varphi_+} \sqrt{W(\psi)} \,\mathrm{d}\psi. \tag{9.60}$$

□

Proof. We follow the proof in [91], and start by multiplying the differential equation in Problem 9.7 by $\psi'(\xi)$, which gives

$$\psi''(\xi)\psi'(\xi) = W'(\psi(\xi))\psi'(\xi), \tag{9.61}$$

The latter equation can be rewritten into

$$\left(\frac{(\psi'(\xi))^2}{2}\right)' = W'(\psi(\xi))\psi'(\xi) = (W(\psi(\xi)))'. \tag{9.62}$$

Integrating the above equation gives

$$\frac{(\psi'(\xi))^2}{2} = W(\psi(\xi)), \tag{9.63}$$

where we have used that $W(\varphi(\xi))$ and $\psi'(\xi)$ vanish for $\xi \to \pm|\infty|$. From the boundary conditions in Problem 9.7, we deduce that $\psi(\xi)$ is non-decreasing, hence

$$\psi'(\xi) = \sqrt{2W(\psi(\xi))}. \tag{9.64}$$

We complete the proof by writing

$$\int_{-\infty}^{\infty} (\psi'(\xi))^2 \,\mathrm{d}\xi = \int_{-\infty}^{\infty} \psi'(\xi)\sqrt{2W(\psi(\xi))} \,\mathrm{d}\xi = \int_{\varphi_-}^{\varphi_+} \sqrt{2W(\psi)} \,\mathrm{d}\psi. \tag{9.65}$$

■

Theorem 9.C (Convergence to sharp-interface energy $\mathcal{E}_{\mathrm{GL}}$: approach II) *If φ^* solves Problem 9.1 and satisfies (A.1) - (A.3), then,*

$$\mathcal{E}^0_{\mathrm{GL}}(\Gamma^0) := \lim_{\varepsilon\to 0} \mathcal{E}^\varepsilon_{\mathrm{GL}}(\varphi^\varepsilon) = C_W \int_{\Gamma^0} \mathrm{d}a, \tag{9.66}$$

with $C_W := 2\sqrt{2}\int_{\varphi_-}^{\varphi_+} \sqrt{W(\psi)} \,\mathrm{d}\psi$. □

Proof. Using Lemma 9.4 and 9.9, we write

$$\begin{aligned}
\lim_{\varepsilon\to 0} \mathcal{E}^\varepsilon_{\mathrm{GL}}(\varphi^\varepsilon) &= \lim_{\varepsilon\to 0}\left(\frac{1}{\varepsilon}\int_\Omega \left(W(\psi) + \frac{1}{2}(\psi')^2\right) \mathrm{d}x + \int_\Omega W'(\psi)h \,\mathrm{d}x + \mathcal{O}(\varepsilon)\right) \\
&= \lim_{\varepsilon\to 0}\left(\frac{1}{\varepsilon}\int_\Omega (\psi')^2 \,\mathrm{d}x + \mathcal{O}(\varepsilon)\right) \\
&= \int_{-\infty}^{\infty} (\psi'(\xi))^2 \,\mathrm{d}\xi \int_{\Gamma^0} \mathrm{d}a \\
&= \sqrt{2}\int_{\varphi_-}^{\varphi_+} \sqrt{W(\psi)} \,\mathrm{d}\psi \int_{\Gamma^0} \mathrm{d}a.
\end{aligned} \tag{9.67}$$

Additionally, we have used that $W'(\psi)$ is an odd function, and applied Lemma 9.5. Note that for $W(\varphi) = \frac{1}{4}(1-\varphi^2)^2$, the constant C_W corresponds to the one computed in Theorem 9.B, as $\sqrt{2}\int_{\varphi_-}^{\varphi_+} \sqrt{W(\psi)} \,\mathrm{d}\psi = \frac{\sqrt{2}}{2}\int_{-1}^{1}(1-\psi^2) \,\mathrm{d}\psi = \frac{2\sqrt{2}}{3}$. ■

9.7 Minimizers of the sharp-interface energy

Using the sharp-interface energy functional derived in Theorems 9.B and 9.C for the Cahn-Hilliard problem, we formulate the associated constrained minimization Problem 10.7. In this problem, the size of the domain enclosed by the sharp interface is fixed by the initial configuration of the system.

Problem 9.10 (Sharp-interface adhesion minimization problem) *Find* Γ^* *such that*

$$\mathcal{E}_{\text{single}}(\Gamma^*) = \inf_{\Gamma} \mathcal{E}_{\text{GL}}(\Gamma), \tag{9.68}$$

subject to $|\Omega_+| := \int_{\Omega_+} \mathrm{d}x = M_{+,0}$, *with* $M_{+,0} := \int_{\Omega_+(t=0)} \mathrm{d}x$ *and* $\partial\Omega_+ := \Gamma$. □

Next, we define an equivalent saddle-point problem, which Lagrangian reads

$$\mathscr{L}(\Gamma, \lambda) = C_W \int_{\Gamma} \mathrm{d}a + \lambda(|\Omega_+| - M_{+,0}). \tag{9.69}$$

For a given Γ, the Lagrangian satisfies

$$\sup_{\lambda\in\mathbb{R}} \mathscr{L}(\Gamma, \lambda) = \begin{cases} \mathcal{E}_{\text{GL}}(\Gamma), & \text{if } |\Omega_+| = M_{+,0}, \quad \forall\lambda \in \mathbb{R}, \\ \infty, & \text{otherwise}, \end{cases} \tag{9.70}$$

which leads us the saddle-point Problem 9.11.

Problem 9.11 (Sharp-interface saddle-point problem) *Find* (Γ^*, λ^*) *such that*

$$\mathscr{L}(\Gamma^*, \lambda^*) = \inf_{\varphi\in\mathcal{L}} \sup_{\lambda\in\mathbb{R}} \mathscr{L}(\Gamma, \lambda). \tag{9.71}$$

□

Saddle points (Γ^*, λ^*), and therefore minimizers Γ^*, should then satisfy the following expressions

$$\begin{cases} 0 = \mathscr{L}'(\Gamma^*, \lambda^*; \delta\lambda), & \forall\delta\lambda \in \mathbb{R}, \\ 0 = \mathscr{L}'(\Gamma^*, \lambda^*; \boldsymbol{v}), & \forall\boldsymbol{v} \in \mathcal{L}_{\boldsymbol{v}}. \end{cases} \tag{9.72}$$

where we have used the velocity method introduced in Chapter 2 to take the directional derivative. Here, $\mathcal{L}_{\boldsymbol{v}}$ denotes the admissible class of velocity perturbations, which are Lipschitz continuous. By employing the shape derivatives of domain and boundary integrals defined in Theorem 2.B and Theorem 2.C, respectively, we arrive at

$$\begin{cases} 0 = |\Omega_+| - M_{+,0}, \\ 0 = \displaystyle\int_{\Gamma^*} (C_W K + \lambda^*)(\boldsymbol{v} \cdot \boldsymbol{n})\, \mathrm{d}a. \end{cases} \tag{9.73}$$

The velocity field $\boldsymbol{v} \neq \boldsymbol{0}$, so that $\boldsymbol{v} \cdot \boldsymbol{n} \neq 0$, is an admissible choice, and hence we find

$$K = -\frac{\lambda^*}{C_W}, \qquad \forall\boldsymbol{x} \in \Gamma^*. \tag{9.74}$$

This implies that the minimizer Γ^* is a hypersurface with a constant curvature, which exact value is determined by the domain-size constraint. Thus, steady states of the Cahn-Hilliard problem are respectively, spherical phase-field shapes in three dimensions, and circular shapes in two dimensions.

Lastly, an appropriate mechanism to decrease the sharp-interface energy functional whilst maintaining constant domain size enclosed by the surface would be to consider the normal velocity

$$V := \boldsymbol{v} \cdot \boldsymbol{n} = \Delta_\Gamma K, \qquad \forall\boldsymbol{x} \in \Gamma(t), \tag{9.75}$$

with K the mean curvature of Γ. This choice would establish surface diffusion, which is a geometric gradient flow discussed in more detail in Section 2.4.2.

Chapter 10

Sharp-Interface Limit of the Adhesion Energy

This Chapter focusses on the convergence of the adhesion energy functional presented in Chapter 8 to a sharp interface energy. For this purpose, similar approaches to those used in Chapter 9 are employed. The recovered sharp-interface energy functional provides meaningful insights in the equilibrium states of the adhesion problem. Moreover, minimizers of this energy characterize the geometric behaviour of the adhesion model.

This Chapter is organized as follows: Section 10.1 details the adhesion problem that is considered for this convergence study. In Section 10.2, the diffuse-interface energy minimization problem is stated, while Section 10.3 introduces the equivalent saddle-point problem. Next, Section 10.4 details the principal assumptions and machinery for the convergence study. Then, through *asymptotic expansions* in Section 10.5, we characterize the structure of the diffuse-interface minimizers. These results are subsequently employed in Section 10.6 to recover the sharp-interface limit of the diffuse-interface adhesion energy functional. In Section 10.6, we close this Chapter by studying sharp-interface minimizers of the sharp-interface energy, which helps us to understand the phase-field adhesion model geometrically.

10.1 Problem statement

In this Chapter, we aim to define a sharp-interface corresponding to the diffuse-interface energies and the phase-field adhesion problem detailed in Chapter 9. For this purpose, we consider the single-phase adhesion energy functional (8.3) presented in Section 8.1, which reads

$$\mathcal{E}^{\varepsilon}_{\text{single}}(\varphi) := \int_{\Omega} \left(\frac{1}{\varepsilon} W(\varphi) + \frac{\varepsilon}{2} |\nabla \varphi|^2 + \varepsilon \sigma B(\varphi) B(\varphi_{\text{s}}) \nabla \varphi \cdot \nabla \varphi_{\text{s}} \right) \mathrm{d}x, \tag{10.1}$$

for a given external field φ_{s} representing the adhesive substrate. Here, σ is a non-negative constant controlling the adhesive strength, while the small parameter $\varepsilon > 0$ governs the interfacial thickness. Furthermore, we consider the following truncated double-well potential

$$W(\varphi) := \begin{cases} \frac{1}{4}(1-\varphi^2)^2, & \varphi \in [\varphi_-, \varphi_+], \\ 0, & \text{otherwise}, \end{cases} \tag{10.2}$$

with $\varphi_- = -1$ and $\varphi_+ = 1$ as its equilibrium values. Next, let $B(\varphi)$ denote the regularizing function, which throughout this Chapter is defined as

$$B(\varphi) := \begin{cases} \sqrt{W(\varphi)} = \frac{1}{2}(1-\varphi^2), & \varphi \in [\varphi_-, \varphi_+], \\ 0, & \text{otherwise}, \end{cases} \tag{10.3}$$

such that $B(\varphi) \geq 0$ everywhere. Similar to previous Chapter, we consider a system that is subject to the mean phase-field constraint in Equation (9.5) for all time $t \in (0, T]$, that is

$$M(\varphi) := \frac{1}{|\Omega|} \int_\Omega \varphi \, \mathrm{d}x = M_0, \tag{10.4}$$

as the adhesion model (8.10) conserves the phase-field variable. Again, $|\Omega|$ denotes the domain size and $M_0 \in (\varphi_-, \varphi_+)$ the initial mean-field phase field.

Following a similar approach to the one presented in Chapter 9, we relate the diffuse-interface energy functional (10.1) to a sharp-interface energy:

(i) First, we define the diffuse-interface energy minimization problem (Section 10.2). Using the Lagrange multiplier method the structure of the saddle points is characterized. These saddle points correspond to the constrained minimizers in the diffuse-interface minimization problem (Section 10.3).

(ii) Next, we detail some additional assumptions on the adhesive field ϕ_s, which allow us to define the *co-area formula for shared interfaces* (Section 10.4). Via the method of asymptotic expansions, the leading order solution to the minimization problem is determined. Although no analytical solution can be obtained for this problem, an equivalent integral identity can be derived, which provides information about the properties of the global minimizers (Section 10.5);

(iii) Third, the leading order solution is substituted into the expanded diffuse-interface energy. Application of the co-area formulas yields the sharp-interface energy (Section 10.6).

(iv) Finally, we find the minimizers of the sharp-interface energy, which provide us with geometrical insights in the equilibrium states of the adhesion model (Section 10.7).

In conclusion, using asymptotic expansions, we aim to verify that the zero-level set of minimizers of $\mathcal{E}^{\varepsilon}_{\text{single}}(\varphi^*)$, that is $\{\varphi^* = 0\}$, converges to the critical surface Γ^* as $\varepsilon \to 0$, where Γ^* denotes the minimizer of the sharp-interface energy $\mathcal{E}_{\text{single}}(\Gamma^*)$. Furthermore, it should be understood that the approaches applied in this Chapter for the single-phase adhesion energy functional $\mathcal{E}^{\varepsilon}_{\text{single}}$ can be extended to multi-phase energy functional (8.14).

10.2 Diffuse-interface energy minimization

Let φ^* denote the minimizers of the single-phase adhesion energy functional (10.1), which satisfy the mass-conservation constraint (10.4). The corresponding constrained minimization problem is defined in Problem 10.1.

Problem 10.1 (Single-phase adhesion energy minimization problem) *Given are an arbitrary, yet fixed $\varepsilon > 0$ and an admissible adhesive phase-field $\phi_s \in \mathcal{L}_s$, with $\mathcal{L}_s := \{\varphi_s \in H^1(\Omega) \mid \varphi_s = \varphi_- \text{ at } \partial\Omega,\ \nabla\varphi_s \cdot \boldsymbol{\nu} = 0 \text{ at } \partial\Omega\}$. Then, find $\varphi^* \in \mathcal{L}_M$ such that*

$$\mathcal{E}^{\varepsilon}_{\text{single}}(\varphi^*) = \inf_{\varphi \in \mathcal{L}_M} \mathcal{E}^{\varepsilon}_{\text{single}}(\varphi), \tag{10.5}$$

over the admissible class $\mathcal{L}_M := \{\varphi \in H^1(\Omega) \mid M(\varphi) = M_0,\ \varphi = \varphi_- \text{ at } \partial\Omega,\ \nabla\varphi \cdot \boldsymbol{\nu} = 0 \text{ at } \partial\Omega\}$. □

10.3 Lagrange-multiplier method and saddle points

In this Section, an equivalent minimization Problem to the constrained minimization Problem 10.1 is presented in which the mass constraint (10.4) is removed from the restricted class $\mathcal{L}_M$. For this purpose, let $\lambda \in \mathbb{R}$ be the *Lagrange multiplier* and let the *Lagrangian* $\mathscr{L}(\cdot,\cdot)$ be defined as follows

$$\mathscr{L}(\varphi, \lambda) = \mathcal{E}^{\varepsilon}_{\text{single}}(\varphi) + \lambda(M(\varphi) - M_0), \tag{10.6}$$

Now, for a given φ the Lagrangian satisfies

$$\sup_{\lambda \in \mathbb{R}} \mathscr{L}(\varphi, \lambda) = \begin{cases} \mathcal{E}^{\varepsilon}_{\text{single}}(\varphi), & \text{if } M(\varphi) = M_0, \quad \forall \lambda \in \mathbb{R}, \\ \infty, & \text{otherwise}, \end{cases} \tag{10.7}$$

which leads us the *saddle-point* Problem 9.3

Problem 10.2 (Diffuse-interface saddle-point problem) *For an arbitrary, yet fixed $\varepsilon > 0$ and a given admissible adhesive phase-field ϕ_s, find $(\varphi^*, \lambda^*) \in \mathcal{L} \times \mathbb{R}$ such that*

$$\mathscr{L}(\varphi^*, \lambda^*) = \inf_{\varphi \in \mathcal{L}} \sup_{\lambda \in \mathbb{R}} \mathscr{L}(\varphi, \lambda), \tag{10.8}$$

with the admissible class $\mathcal{L} := \{\varphi \in H^1(\Omega) \mid \varphi = \varphi_- \text{ at } \partial\Omega,\ \nabla\varphi \cdot \boldsymbol{\nu} = 0 \text{ at } \partial\Omega\}$. □

Solutions of the Problem 10.2 are called *saddle points* and require that the directional derivatives vanish at (φ^*, λ^*), that is

$$\begin{cases} 0 = \mathscr{L}'(\varphi^*, \lambda^*; \delta\lambda), & \forall \delta\lambda \in \mathbb{R}, \\ 0 = \mathscr{L}'(\varphi^*, \lambda^*; \delta\varphi), & \forall \delta\varphi \in \mathcal{L}. \end{cases} \tag{10.9}$$

Using the expression for the Lagrangian (10.6), we can now write

$$\begin{cases} 0 = M(\varphi^*) - M_0, \\ 0 = \dfrac{\delta \mathcal{E}^{\varepsilon}_{\text{single}}(\varphi^*)}{\delta\varphi^*} + \lambda^* \dfrac{\delta M(\varphi^*)}{\delta\varphi^*} \\ \quad = \dfrac{1}{\varepsilon} W'(\varphi^*) - \varepsilon\Delta\varphi^* - \varepsilon\sigma B(\varphi^*)(\nabla \cdot (B(\varphi_s)\nabla\varphi_s)) + \lambda^*. \end{cases} \tag{10.10}$$

Integration of $(10.10)_2$ over the domain Ω, yields the following expression for the Lagrange multiplier

$$\lambda^* = -\frac{1}{\varepsilon|\Omega|} \int_{\Omega} (W'(\varphi^*) + \sigma\varepsilon^2 B(\varphi_s) B'(\varphi^*) \nabla\varphi^* \cdot \nabla\varphi_s) \,\mathrm{d}x, \tag{10.11}$$

where we have used that $\nabla\varphi^* \cdot \boldsymbol{\nu} = \nabla\varphi_s \cdot \boldsymbol{\nu} = 0$ at $\partial\Omega$.

10.4 Minimizers of the diffuse-interface energy

For an arbitrary yet fixed ε, let $\varphi^* = \varphi^\varepsilon$ be the constrained minimizer of Problem 10.1, or equivalently, let $(\varphi^\varepsilon, \lambda^*)$ be the solution to the saddle-point Problem 10.2. Again, $\{\varphi^\varepsilon\}_{\varepsilon\geq 0}$ denotes the one-parameter family of functions in the admissible solution space $\mathcal{L}_M$, which approach a singular limit denoted by φ^0. In addition to Assumption (A.1) and (A.2) presented in Section 9.4, suppose that the following assumptions on φ^ε and φ_s hold:

(A.4) There exists a sufficiently smooth and differentiable hypersurface Γ_s, which is here taken independent of time, as we are interested in steady state solutions. It separates the domain Ω into two subdomains, such that $\Omega = \Omega_{\mathrm{s},+} \cup \Omega_{\mathrm{s},-}$. Thus, there exists a characteristic function

$$\chi_\mathrm{s}(\boldsymbol{x}) := \begin{cases} \varphi_+, & \text{on } \Omega_{\mathrm{s},+}, \\ \varphi_-, & \text{on } \Omega_{\mathrm{s},-}. \end{cases} \tag{10.12}$$

In addition, we require that $\Omega_{\mathrm{s},+} \subset \Omega_-$, which has implications on the choice for the initial condition $\varphi_0(\boldsymbol{x})$. Next, we introduce the signed distance function $d_\mathrm{s}(\boldsymbol{x}) : \Omega \to \mathbb{R}$, which determines the geometrical properties of Γ_s. Furthermore, let the function $\varphi_\mathrm{s}(\boldsymbol{x}) := \varphi_\mathrm{s}^\varepsilon(\xi_S)$ be the diffuse interpretation of the interface Γ_s, with $\xi_S = d_\mathrm{s}(\boldsymbol{x})/\varepsilon$. We obtain $\varphi_\mathrm{s}^\varepsilon(\xi_S)$ by smearing the limiting function φ_s^0 out in the direction normal to Γ_s. In the limit of $\varepsilon \to 0$, we have

$$\lim_{\varepsilon\to 0} \varphi_\mathrm{s}^\varepsilon \left(\frac{d_\mathrm{s}(\boldsymbol{x})}{\varepsilon}\right) = \varphi_\mathrm{s}^0, \tag{10.13}$$

in addition to

$$\lim_{\varepsilon\to 0} \varphi_\mathrm{s}^\varepsilon \left(\frac{d_\mathrm{s}(\boldsymbol{x})}{\varepsilon}\right) = \begin{cases} \varphi_+, & \text{if } d_\mathrm{s}(\boldsymbol{x}) > 0, \\ \varphi_-, & \text{if } d_\mathrm{s}(\boldsymbol{x}) < 0, \end{cases} \tag{10.14}$$

and $\lim_{\varepsilon\to 0} \varphi_\mathrm{s}^{\varepsilon\prime}(\xi_S) = 0$ for $\xi \to \pm|\infty|$. For completeness, we state that $\Gamma_\mathrm{s} := \{d_\mathrm{s}(\boldsymbol{x}) = 0\} = \{\varphi_\mathrm{s}^\varepsilon(\boldsymbol{x}) = 0\}$;

(A.5) Let $U_\mathrm{s} = \{d_\mathrm{s} \leq \delta\}$ denote the neighbourhood of Γ_s, and let the neighbourhood $U^\varepsilon \subset O^\varepsilon$ of Γ^ε be defined using the integral curves η^ε, see Lemma 9.4 for details. If for a particular δ the neighbourhoods U_s and U^ε overlap, we assume that there exists a shared limiting interface $\Gamma_\mathrm{adh} := \Gamma^0 \cap \Gamma_\mathrm{s}$, which is sufficiently smooth. As a consequence, we have $\Gamma^0 = \Gamma_\mathrm{adh} \cup \Gamma_\mathrm{adh}^c$, where the non-adhered part of the limiting interface is defined as $\Gamma_\mathrm{adh}^c := (\Gamma^0 \backslash \Gamma_\mathrm{adh})$. Furthermore, we assume that Γ_adh has a neighbourhood $U_\mathrm{adh}^\varepsilon$ in which we can employ a single coordinate system, through which we redefine ξ_S as $-\xi$, by setting $d_\mathrm{s}(\boldsymbol{x}) = -d^\varepsilon(\boldsymbol{x})$. In addition, we assume that $\varphi_\mathrm{s}^\varepsilon$ behaves as the leading order term ψ in $U_\mathrm{adh}^\varepsilon$, and therefore $\varphi_\mathrm{s}^\varepsilon(\xi_S) = \psi_\mathrm{s}(\xi_S) = \psi_\mathrm{s}(-\xi) = -\psi(\xi)$. Lastly, we assume that for Problem 10.4 a shared limiting interface exists, that is $\Gamma_\mathrm{adh} \neq \emptyset$.

(A.6) Let the leading order term $\psi(\xi)$ in the asymptotic expansion (9.14) with $\xi = d^\varepsilon(\boldsymbol{x})/\varepsilon$ solve the following problem:

$$\psi'' = W'(\psi) - \sigma B(\psi)(B'(\varphi_\mathrm{s})(\varphi_\mathrm{s}')^2 + B(\varphi_\mathrm{s})\varphi_\mathrm{s}''), \qquad \forall \xi \in \mathbb{R}, \tag{10.15}$$

subject to $\psi(-\infty) = \varphi_-$, $\psi(0) = 0$ and $\psi(\infty) = \varphi_+$.

In the above, Assumption (A.4) states that the diffuse-interface $\varphi_{\mathrm{s}}^{\varepsilon}$ marks the sharp-interface Γ_{s}. Similar to Assumption (A.3), Assumption (A.6) implies that the leading order solution solves an unconstrained problem associated with the minimizers of $\mathcal{E}^{\varepsilon}_{\mathrm{single}}$. This Problem is further detailed in Problem 10.4 in Section 10.5. Lastly, Assumption (A.5) allows us to define the *co-area formula for shared interfaces* in Lemma 10.3.

Lemma 10.3 (Co-area formula for shared interfaces) *Let Γ_{s}, Γ^{ε}, d_{s} and d^{ε} be given as in (A.1), (A.2), (A.4) and (A.5). Suppose that $f \in C^0(\Omega)$ and let $p_i(t) \in L^{\infty}(\Omega)$ $(i = 1, 2)$ satisfy*

$$\max_{|t|>s} |p_i(t)t| \leq \frac{C}{s^m}, \qquad m > 1, \tag{10.16}$$

with $C > 0$. Then

$$\lim_{\varepsilon\to 0} \frac{1}{\varepsilon} \int_{\Omega} p_1\left(\frac{d^{\varepsilon}(\boldsymbol{x})}{\varepsilon}\right) p_2\left(\frac{d_{\mathrm{s}}(\boldsymbol{x})}{\varepsilon}\right) f(\boldsymbol{x})\,\mathrm{d}x = \int_{-\infty}^{\infty} p_1(t)p_2(-t)\,\mathrm{d}t \int_{\Gamma_{\mathrm{adh}}} f\,\mathrm{d}a, \tag{10.17}$$

with $\Gamma_{\mathrm{adh}} := \Gamma_{\mathrm{s}} \cap \Gamma^0$. □

Proof. Following the proof of Lemma 9.4 closely, we write

$$\begin{aligned}\lim_{\varepsilon\to 0} \frac{1}{\varepsilon} \int_{U^{\varepsilon}_{\mathrm{adh}}} p_1\left(\frac{d^{\varepsilon}(\boldsymbol{x})}{\varepsilon}\right) p_2\left(\frac{d_{\mathrm{s}}(\boldsymbol{x})}{\varepsilon}\right) f(\boldsymbol{x})\,\mathrm{d}x &= \int_{-\infty}^{\infty} p_1(t)p_2(-t) \int_{W} f(\eta^0(z,0))J(z,0)\mathrm{d}z\mathrm{d}t \\ &= \int_{-\infty}^{\infty} p_1(t)p_2(-t)\,\mathrm{d}t \int_{\Gamma_{\mathrm{adh}}} f\mathrm{d}a. \end{aligned}\tag{10.18}$$

where we have used the coordinate change $\varepsilon t = \tau = d_{\mathrm{s}}(\eta(z,\tau)) = -d^{\varepsilon}(\eta(z,\tau))$.

Let the outside of the neighbourhood $U^{\varepsilon}_{\mathrm{adh}}$ be denoted by $\left(U^{\varepsilon}_{\mathrm{adh}}\right)^c = \{\boldsymbol{x} \in \Omega \mid d^{\varepsilon}(\boldsymbol{x}) > \delta \text{ or } d_{\mathrm{s}}(\boldsymbol{x}) > \delta\}$. First, we consider

$$\begin{aligned}&\lim_{\varepsilon\to 0} \frac{1}{\varepsilon} \int_{U^c_{\mathrm{s}}} p_1\left(\frac{d^{\varepsilon}(\boldsymbol{x})}{\varepsilon}\right) p_2\left(\frac{d_{\mathrm{s}}(\boldsymbol{x})}{\varepsilon}\right) f(\boldsymbol{x})\,\mathrm{d}x \\ &\qquad \leq \lim_{\varepsilon\to 0} \frac{1}{\varepsilon} \left\| p_1\left(\frac{d^{\varepsilon}(\boldsymbol{x})}{\varepsilon}\right) p_2\left(\frac{d_{\mathrm{s}}(\boldsymbol{x})}{\varepsilon}\right)\right\|_{L^{\infty}(U^c_{\mathrm{s}})} \int_{\Omega} |f(\boldsymbol{x})|\,\mathrm{d}x \\ &\qquad \leq \lim_{\varepsilon\to 0} \max_{|d_{\mathrm{s}}|>\delta} \left| \frac{1}{\varepsilon} p_2\left(\frac{d_{\mathrm{s}}(\boldsymbol{x})}{\varepsilon}\right)\right| \left\| p_1\left(\frac{d^{\varepsilon}(\boldsymbol{x})}{\varepsilon}\right)\right\|_{L^{\infty}(\Omega)} \int_{\Omega} |f(\boldsymbol{x})|\,\mathrm{d}x \\ &\qquad = \lim_{\varepsilon\to 0} \max_{|t_{\mathrm{s}}|>(\delta/\varepsilon)} \left| \frac{1}{\varepsilon t_{\mathrm{s}}} p_2\left(t_{\mathrm{s}}\right) t_{\mathrm{s}}\right| \left\| p_1\left(\frac{d^{\varepsilon}(\boldsymbol{x})}{\varepsilon}\right)\right\|_{L^{\infty}(\Omega)} \int_{\Omega} |f(\boldsymbol{x})|\,\mathrm{d}x \\ &\qquad \leq \lim_{\varepsilon\to 0} \max_{|t_{\mathrm{s}}|>(\delta/\varepsilon)} \frac{1}{\delta} \left| p_2\left(t_{\mathrm{s}}\right) t_{\mathrm{s}}\right| \left\| p_1\left(\frac{d^{\varepsilon}(\boldsymbol{x})}{\varepsilon}\right)\right\|_{L^{\infty}(\Omega)} \int_{\Omega} |f(\boldsymbol{x})|\,\mathrm{d}x \\ &\qquad \leq \lim_{\varepsilon\to 0} \frac{1}{\delta} \frac{C\varepsilon^m}{\delta^m} \left\| p_1\left(\frac{d^{\varepsilon}(\boldsymbol{x})}{\varepsilon}\right)\right\|_{L^{\infty}(\Omega)} \int_{\Omega} |f(\boldsymbol{x})|\,\mathrm{d}x = 0,\end{aligned}\tag{10.19}$$

with $U^c_{\mathrm{s}} = \{d_{\mathrm{s}}(\boldsymbol{x}) > \delta\}$. Similarly, for $(U^{\varepsilon})^c = \{d^{\varepsilon}(\boldsymbol{x}) > \delta\}$, we find

$$\lim_{\varepsilon\to 0} \frac{1}{\varepsilon} \int_{(U^{\varepsilon})^c} p_1\left(\frac{d^{\varepsilon}(\boldsymbol{x})}{\varepsilon}\right) p_2\left(\frac{d_{\mathrm{s}}(\boldsymbol{x})}{\varepsilon}\right) f(\boldsymbol{x})\,\mathrm{d}x = 0. \tag{10.20}$$

Thus, we arrive at

$$\lim_{\varepsilon\to 0} \frac{1}{\varepsilon} \int_{\left(U^{\varepsilon}_{\mathrm{adh}}\right)^c} p_1\left(\frac{d^{\varepsilon}(\boldsymbol{x})}{\varepsilon}\right) p_2\left(\frac{d_{\mathrm{s}}(\boldsymbol{x})}{\varepsilon}\right) f(\boldsymbol{x})\,\mathrm{d}x = 0, \tag{10.21}$$

which together with (10.18) completes our proof.

10.5 Asymptotic expansion and leading order problem

In view of the asymptotic expansion ansatz in Assumption (A.2), we characterize the structure of the diffuse-interface minimizers of Problem 10.1. Substitution of the ansatz, namely $\varphi^* = \varphi^\varepsilon$, and the diffuse-interface interpretation for $\varphi_s = \varphi_s^\varepsilon$ into $(10.10)_2$, yields

$$
\begin{aligned}
0 &= \frac{1}{\varepsilon}W'(\varphi^\varepsilon) - \varepsilon\Delta\varphi^\varepsilon - \varepsilon\sigma B(\varphi^\varepsilon)\left(\nabla\cdot(B(\varphi_s^\varepsilon)\nabla\varphi_s^\varepsilon)\right) + \lambda^\varepsilon \\
&= \frac{1}{\varepsilon}W'(\varphi^\varepsilon) - \varepsilon\Delta\varphi^\varepsilon - \varepsilon\sigma B(\varphi^\varepsilon)\left(B'(\varphi_s^\varepsilon)|\nabla\varphi_s^\varepsilon|^2 + B(\varphi_s^\varepsilon)\Delta\varphi_s^\varepsilon\right) + \lambda^\varepsilon,
\end{aligned}
\tag{10.22}
$$

for a given ε. Then, using the identities (9.42) - (9.46), we obtain

$$
\begin{aligned}
0 = {}& \frac{1}{\varepsilon}W'(\psi) + W''(\psi)\left(h + \frac{1}{\varepsilon}g\right) - \frac{1}{\varepsilon}\psi'' + 2K\psi' \\
& - \frac{1}{\varepsilon}\sigma B(\psi)(B'(\varphi_s^\varepsilon)(\varphi_s^{\varepsilon\prime})^2 + B(\varphi_s^\varepsilon)\varphi_s^{\varepsilon\prime\prime} - 2\varepsilon K_s B(\varphi_s^\varepsilon)\varphi_s^{\varepsilon\prime}) \\
& - \sigma B'(\psi)\left(h + \frac{1}{\varepsilon}g\right)(B'(\varphi_s^\varepsilon)(\varphi_s^{\varepsilon\prime})^2 + B(\varphi_s^\varepsilon)\varphi_s^{\varepsilon\prime\prime} - 2\varepsilon K_s B(\varphi_s^\varepsilon)\varphi_s^{\varepsilon\prime}) \\
& + \lambda^\varepsilon + \mathcal{O}(\varepsilon),
\end{aligned}
\tag{10.23}
$$

bearing in mind that $\psi(\xi) := \psi\left(\frac{d^\varepsilon(x)}{\varepsilon}\right)$ and $\varphi_s^\varepsilon(\xi_S) := \varphi_s^\varepsilon\left(\frac{d_s(x)}{\varepsilon}\right)$. Furthermore, at the sharp-interface Γ_s we have $\Delta d_s(\boldsymbol{x}) = -2K_s(\boldsymbol{x})$ with K_s the mean curvature [174]. In addition, λ^ε represents the expanded form of (10.11), which reads

$$
\lambda^\varepsilon = \frac{1}{\varepsilon|\Omega|}\int_\Omega (\sigma B(\varphi_s^\varepsilon)B'(\psi)\varphi_s^{\varepsilon\prime}\psi'\nabla d^\varepsilon\cdot\nabla d_s - W'(\psi))\,\mathrm{d}x + \mathcal{O}(1).
\tag{10.24}
$$

For brevity, we keep writing λ^ε in what follows. Thus, collecting terms of the same order, we arrive at

$$
\begin{aligned}
0 = {}& \frac{1}{\varepsilon}(W'(\psi) - \psi'' - \sigma B(\psi)(B'(\varphi_s^\varepsilon)(\varphi_s^{\varepsilon\prime})^2 + B(\varphi_s^\varepsilon)\varphi_s^{\varepsilon\prime\prime})) \\
& + W''(\psi)h - 2K\psi' - \sigma B'(\psi)h\left(B'(\varphi_s^\varepsilon)(\varphi_s^{\varepsilon\prime})^2 + B(\varphi_s^\varepsilon)\varphi_s^{\varepsilon\prime\prime}\right) + 2\sigma K_s B(\varphi_s^\varepsilon)\varphi_s^{\varepsilon\prime} \\
& + \lambda^\varepsilon + \mathcal{O}(\varepsilon).
\end{aligned}
\tag{10.25}
$$

The unconstrained leading order term in the above expression defines Problem 10.4. In Lemma 10.5, we demonstrate that an equivalent differential equation exists for this problem, when $\varphi_s^\varepsilon(\xi_S) = -\psi(\xi)$ is considered. Furthermore, in Remark 10.6 we show that the results in Lemma 10.5, which are based on the omission of the Lagrange multiplier contribution in the leading order, establish that the leading order term of the Lagrange multiplier becomes zero. This implies that its omission in Problem 10.4 is consistent.

Problem 10.4 (Leading order problem) *Bearing in mind that* $\psi(\xi) := \psi\left(\frac{d^\varepsilon(x)}{\varepsilon}\right)$ *and also that* $\varphi_s^\varepsilon(\xi_S) := \varphi_s^\varepsilon\left(\frac{d_s(x)}{\varepsilon}\right)$*, let* ψ *solve the differential equation*

$$
W'(\psi) - \psi'' = \sigma B(\psi)(B'(\varphi_s)(\varphi_s^{\varepsilon\prime})^2 + B(\varphi_s^\varepsilon)\varphi_s^{\varepsilon\prime\prime}), \qquad \forall\psi(\xi)\in\mathbb{R},
\tag{10.26}
$$

subject to the conditions $\psi(-\infty) = \varphi_-$, $\psi(\infty) = \varphi_+$ *and* $\psi(0) = 0$. □

Lemma 10.5 *Suppose that* $\xi_{\mathcal{S}} = -\xi$, *so that* $\varphi_{\mathrm{s}}^{\varepsilon}(\xi_{\mathcal{S}}) = -\psi(\xi)$, $\varphi_{\mathrm{s}}^{\varepsilon}{}'(\xi_{\mathcal{S}}) = \psi'(\xi)$ *and* $\varphi_{\mathrm{s}}^{\varepsilon}{}''(\xi_{\mathcal{S}}) = -\psi''(\xi)$. *Furthermore, consider* $0 \leq \sigma < 4$. *Then, the solution to Problem 10.4 also fulfills the differential equation*

$$\psi'(\xi) = \sqrt{2f_\sigma(\psi(\xi))}, \tag{10.27}$$

with

$$f_\sigma(\psi) := \begin{cases} \dfrac{(1-\psi^2)^2}{4-\sigma(1-\psi^2)^2}, & \psi \in [\varphi_-, \varphi_+], \\ 0, & \text{otherwise.} \end{cases} \tag{10.28}$$

Consequently, we can write

$$\int_{-\infty}^{\infty} |\psi'(\xi)|^2 \,\mathrm{d}\xi = \int_{\varphi_-}^{\varphi_+} \sqrt{2f_\sigma(\psi)}\,\mathrm{d}\psi. \tag{10.29}$$

□

Proof. Substituting $\varphi_{\mathrm{s}}^{\varepsilon}(\xi_{\mathcal{S}}) = -\psi(\xi)$, $\varphi_{\mathrm{s}}^{\varepsilon}{}'(\xi_{\mathcal{S}}) = \psi'(\xi)$ and $\varphi_{\mathrm{s}}^{\varepsilon}{}''(\xi_{\mathcal{S}}) = -\psi''(\xi)$ into the differential equation (10.26), multiplying the result by ψ', followed by integration over $\xi \in \mathbb{R}$, yields

$$\begin{aligned}\int_{-\infty}^{\infty} (W'(\psi)\psi' - \psi''\psi')\,\mathrm{d}\xi &= -\sigma \int_{-\infty}^{\infty} B(\psi)\psi' \left(B'(\psi)(\psi')^2 + B(\psi)\psi''\right)\,\mathrm{d}\xi \\ &= -\sigma \int_{-\infty}^{\infty} B(\psi)\psi'(B(\psi)\psi')'\,\mathrm{d}\xi. \end{aligned}\tag{10.30}$$

Here, we have used the definition of the regularizing function (10.3) to write $B(\psi) = B(-\psi)$ and $B'(\psi) = -B'(\psi)$. Next, we write

$$\int_{-\infty}^{\infty} (W(\psi))'\,\mathrm{d}\xi - \int_{-\infty}^{\infty} \frac{1}{2}((\psi')^2)'\,\mathrm{d}\xi = -\frac{\sigma}{2}\int_{-\infty}^{\infty} ((B(\psi)\psi')^2)'\,\mathrm{d}\xi, \tag{10.31}$$

and, recalling that $W(\psi) = (B(\psi))^2$, obtain

$$W(\psi) - \frac{1}{2}(\psi')^2 = -\frac{\sigma}{2}W(\psi)(\psi')^2. \tag{10.32}$$

where the constant of integration is zero, as $W(\varphi(\xi))$ and $\psi'(\xi)$ vanish for $\xi \to \pm|\infty|$. From the above follows that

$$(\psi'(\xi))^2 = 2\left(1 - \sigma W(\psi(\xi))\right)^{-1} W(\psi(\xi)) = 2f_\sigma\left(\psi(\xi)\right), \tag{10.33}$$

and using the choice of $W(\psi)$ in (10.2) we recover definition (10.28) for $f_\sigma(\psi)$. Notice that f_σ is a truncated double-well function for $0 \leq \sigma < 4$. Furthermore, we have that $f_\sigma(\varphi_-) = f_\sigma(\varphi_+) = 0$ and $f_\sigma(0) = \frac{1}{4-\sigma}$. Since $\psi(\xi)$ is non-decreasing, we deduce that

$$\psi'(\xi) = \sqrt{2f_\sigma(\psi(\xi))}. \tag{10.34}$$

As a result, we can now write

$$\int_{-\infty}^{\infty} |\psi'(\xi)|^2\,\mathrm{d}\xi = \int_{-\infty}^{\infty} \sqrt{2f_\sigma(\psi(\xi))}\psi'(\xi)\,\mathrm{d}\xi = \int_{\varphi_-}^{\varphi_+} \sqrt{2f_\sigma(\psi)}\,\mathrm{d}\psi, \tag{10.35}$$

which completes our proof. ■

Remark 10.6 (Consistency of Assumption (A.6) with the Lagrange multiplier) Suppose that we are in the neighbourhood $U^\varepsilon_{\mathrm{adh}}$, with $d^\varepsilon = -d_{\mathrm{s}}$ and $\xi_S = -\xi$, so that $\varphi^\varepsilon_{\mathrm{s}}(\xi_S) = -\psi(\xi)$, $\varphi^{\varepsilon\prime}_{\mathrm{s}}(\xi_S) = \psi'(\xi)$ and $\varphi^{\varepsilon\prime\prime}_{\mathrm{s}}(\xi_S) = -\psi''(\xi)$. Then, the leading order of the expanded Lagrange multiplier (10.24) can be written as

$$\frac{1}{\varepsilon|\Omega|}\int_\Omega (\sigma B(\varphi^\varepsilon_{\mathrm{s}})B'(\psi)\varphi^{\varepsilon\prime}_{\mathrm{s}}\psi'\nabla d^\varepsilon\cdot\nabla d_{\mathrm{s}} - W'(\psi))\,\mathrm{d}x$$
$$= -\frac{1}{\varepsilon|\Omega|}\int_\Omega (\sigma B(\psi)B'(\psi)(\psi')^2 + W'(\psi))\,\mathrm{d}x, \tag{10.36}$$

Expression (10.30) in Lemma 10.5 leads us to the following equation

$$\begin{aligned} W'(\psi) &= \psi'' - \sigma B(\psi)\left(B'(\psi)(\psi')^2 + B(\psi)\psi''\right) \\ &= (1-\sigma W(\psi))\psi'' - \sigma B(\psi)B'(\psi)(\psi')^2 \end{aligned} \tag{10.37}$$

where we have used that $W(\psi) = (B(\psi))^2$. In addition, by taking the derivative of expression (10.27) with respect to ξ, we also obtain

$$\psi''(\xi) = \frac{f_\sigma{}'(\psi)}{\sqrt{2f_\sigma(\psi)}}\psi'(\xi), \tag{10.38}$$

where f_σ is defined in (10.28). Applying equation (10.37), followed by substitution of expression (10.38), the leading order term of the Lagrange multiplier becomes

$$-\frac{1}{\varepsilon|\Omega|}\int_\Omega (\sigma B(\psi)B'(\psi)(\psi')^2 + W'(\psi))\,\mathrm{d}x$$
$$\begin{aligned} &= -\frac{1}{\varepsilon|\Omega|}\int_\Omega (1-\sigma W(\psi))\psi''\,\mathrm{d}x \\ &= -\frac{1}{\varepsilon|\Omega|}\int_\Omega (1-\sigma W(\psi))\frac{f_\sigma{}'(\psi)}{\sqrt{2f_\sigma(\psi)}}\psi'\,\mathrm{d}x. \end{aligned} \tag{10.39}$$

Lastly, in view of the co-area formula for shared interfaces (10.17), we establish that

$$\lim_{\varepsilon\to 0}\left(-\frac{1}{\varepsilon|\Omega|}\int_\Omega (1-\sigma W(\psi))\psi''\,\mathrm{d}x\right)$$
$$\begin{aligned} &= -\frac{1}{|\Omega|}\int_{-\infty}^{\infty}(1-\sigma W(\psi))\frac{f_\sigma{}'(\psi)}{\sqrt{2f_\sigma(\psi)}}\psi'\,\mathrm{d}\xi\int_{\Gamma_{\mathrm{adh}}}\mathrm{d}a \\ &= -\frac{1}{|\Omega|}\int_{\varphi_-}^{\varphi_+}(1-\sigma W(\psi))\frac{f_\sigma{}'(\psi)}{\sqrt{2f_\sigma(\psi)}}\,\mathrm{d}\psi\int_{\Gamma_{\mathrm{adh}}}\mathrm{d}a = 0, \end{aligned} \tag{10.40}$$

noting that an integral of an odd function over a symmetric interval equals zero. □

10.6 Convergence to the sharp limit

To study the convergence of the diffuse-interface adhesion energy $\mathcal{E}^\varepsilon_{\mathrm{single}}(\varphi^*)$, we expand $\mathcal{E}^\varepsilon_{\mathrm{single}}(\varphi^*)$ using the ansatz for φ^* in Assumption (A.2) and the diffuse-interface interpretation of φ_{s} in Assumption (A.4). This yields

$$\begin{aligned}
\mathcal{E}^{\varepsilon}_{\text{single}}(\varphi^*) = & \int_\Omega \left(\frac{1}{\varepsilon}W(\varphi^\varepsilon) + \frac{\varepsilon}{2}|\nabla\varphi^\varepsilon|^2 + \varepsilon\sigma B(\varphi^\varepsilon)B(\varphi^\varepsilon_{\mathrm{s}})\nabla\varphi^\varepsilon\cdot\nabla\varphi^\varepsilon_{\mathrm{s}}\right)\,\mathrm{d}x \\
= & \frac{1}{\varepsilon}\int_\Omega \left(W(\psi) + \varepsilon W'(\psi)\left(h + \frac{1}{\varepsilon}g\right) + \mathcal{O}(\varepsilon^2)\right)\,\mathrm{d}x \\
& + \frac{\varepsilon}{2}\int_\Omega \left(\frac{1}{\varepsilon^2}(\psi')^2 + \mathcal{O}(1)\right)\,\mathrm{d}x \\
& + \varepsilon\int_\Omega \Bigg(\sigma\left(B(\psi) + \varepsilon B'(\psi)\left(h + \frac{1}{\varepsilon}g\right) + \mathcal{O}(\varepsilon^2)\right)B(\varphi^\varepsilon_{\mathrm{s}}) \\
& \qquad \left(\frac{1}{\varepsilon}\psi'\nabla d^\varepsilon + \varepsilon\nabla h + \nabla g\right)\cdot\left(\frac{1}{\varepsilon}\varphi^{\varepsilon\prime}_{\mathrm{s}}\nabla d_{\mathrm{s}}\right)\Bigg)\,\mathrm{d}x \\
= & \frac{1}{\varepsilon}\int_\Omega \left(W(\psi) + \frac{1}{2}(\psi')^2 + \sigma B(\psi)B(\varphi^\varepsilon_{\mathrm{s}})\psi'\varphi^{\varepsilon\prime}_{\mathrm{s}}\nabla d^\varepsilon\cdot\nabla d_{\mathrm{s}}\right)\,\mathrm{d}x \\
& + \int_\Omega \left(W'(\psi)h + \sigma B'(\psi)hB(\varphi^\varepsilon_{\mathrm{s}})\psi'\varphi^{\varepsilon\prime}_{\mathrm{s}}\nabla d^\varepsilon\cdot\nabla d_{\mathrm{s}}\right)\,\mathrm{d}x + \mathcal{O}(\varepsilon),
\end{aligned} \tag{10.41}$$

Using the above result, we demonstrate in Theorem 10.A that the diffuse-interface energy converges to a sharp-interface energy, as $\varepsilon \to 0$.

Theorem 10.A (Convergence to sharp-interface energy) *If φ^ε solves Problem 10.1 and additionally satisfies (A.1), (A.2) and (A.4) - (A.6), then,*

$$\mathcal{E}^0_{\text{single}}(\Gamma^0) := \lim_{\varepsilon\to 0}\mathcal{E}^\varepsilon_{\text{single}}(\varphi^\varepsilon) = C_W\int_{\Gamma^c_{\text{adh}}}\mathrm{d}a + C_\sigma\int_{\Gamma_{\text{adh}}}\mathrm{d}a, \tag{10.42}$$

bearing in mind that $\Gamma_{\text{adh}} := \Gamma^0\cap\Gamma_{\mathrm{s}}$ and $\Gamma^c_{\text{adh}} := \Gamma^0\backslash\Gamma_{\text{adh}}$. Furthermore, the constants are defined as follows

$$C_W := \sqrt{2}\int_{\varphi_-}^{\varphi_+}\sqrt{W(\psi)}\,\mathrm{d}\psi, \quad \textit{and} \quad C_\sigma := \int_{\varphi_-}^{\varphi_+} g_\sigma(\psi)\,\mathrm{d}\psi, \tag{10.43}$$

with

$$g_\sigma(\psi) := \begin{cases}\sqrt{2}\left(1 - \frac{3}{2}\sigma W(\psi)\right)\sqrt{\left(1-\sigma W(\psi)\right)^{-1}W(\psi)}, & \psi\in[\varphi_-,\varphi_+], \\ 0, & \textit{otherwise.}\end{cases} \tag{10.44}$$

□

Proof. Using Lemmas 9.4, 10.3 and 10.5, we write

$$
\begin{aligned}
&\lim_{\varepsilon\to 0} \mathcal{E}^{\varepsilon}_{\mathrm{single}}(\varphi^{\varepsilon}) \\
&= \lim_{\varepsilon\to 0} \left(\frac{1}{\varepsilon} \int_{\Omega} \left(W(\psi) + \frac{1}{2}(\psi')^2 + \sigma B(\psi) B(\varphi_{\mathrm{s}}^{\varepsilon}) \psi' \varphi_{\mathrm{s}}^{\varepsilon\prime} \nabla d^{\varepsilon} \cdot \nabla d_{\mathrm{s}} \right) \mathrm{d}x \right. \\
&\quad \left. + \int_{\Omega} \left(W'(\psi) h + \sigma B'(\psi) h B(\varphi_{\mathrm{s}}^{\varepsilon}) \psi' \varphi_{\mathrm{s}}^{\varepsilon\prime} \nabla d^{\varepsilon} \cdot \nabla d_{\mathrm{s}} \right) \mathrm{d}x + \mathcal{O}(\varepsilon) \right) \\
&= \int_{-\infty}^{\infty} (\psi'(\xi))^2 \, \mathrm{d}\xi \int_{\Gamma^c_{\mathrm{adh}}} \mathrm{d}a \\
&\quad + \int_{-\infty}^{\infty} \left(W(\psi(\xi)) + \frac{1}{2}(\psi'(\xi))^2 - \sigma W(\psi(\xi))(\psi'(\xi))^2 \right) \mathrm{d}\xi \int_{\Gamma_{\mathrm{adh}}} \mathrm{d}a \\
&= \sqrt{2} \int_{\varphi_-}^{\varphi_+} \sqrt{W(\psi)} \, \mathrm{d}\psi \int_{\Gamma^c_{\mathrm{adh}}} \mathrm{d}a \\
&\quad + \int_{-\infty}^{\infty} \left(\frac{1}{2} (1 - \sigma W(\psi(\xi))) (\psi'(\xi))^2 + \left(\frac{1}{2} - \sigma W(\psi(\xi)) \right) (\psi'(\xi))^2 \right) \mathrm{d}\xi \int_{\Gamma_{\mathrm{adh}}} \mathrm{d}a \\
&= C_W \int_{\Gamma^c_{\mathrm{adh}}} \mathrm{d}a + \int_{-\infty}^{\infty} \left(1 - \frac{3\sigma}{2} W(\psi(\xi)) \right) \sqrt{2 f_{\sigma}(\psi(\xi))} \psi'(\xi) \, \mathrm{d}\xi \int_{\Gamma_{\mathrm{adh}}} \mathrm{d}a \\
&= C_W \int_{\Gamma^c_{\mathrm{adh}}} \mathrm{d}a + \int_{\varphi_-}^{\varphi_+} g_{\sigma}(\psi) \, \mathrm{d}\psi \int_{\Gamma_{\mathrm{adh}}} \mathrm{d}a \\
&= C_W \int_{\Gamma^c_{\mathrm{adh}}} \mathrm{d}a + C_{\sigma} \int_{\Gamma_{\mathrm{adh}}} \mathrm{d}a,
\end{aligned}
$$

with $\Gamma_{\mathrm{adh}} := \Gamma^0 \cap \Gamma_{\mathrm{s}}$ and $g_{\sigma}(\psi)$ as defined in (10.44). Note that the $\mathcal{O}(1)$ terms vanish, because of arguments earlier presented in Remark 10.6 and Lemma 9.5. ■

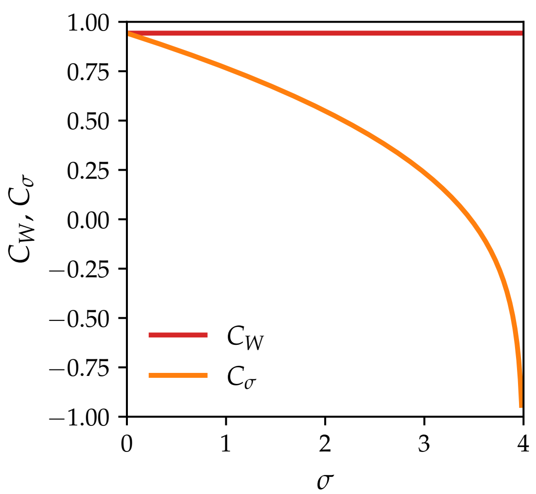

Figure 10.1: Constants in the sharp-interface energy plotted against the adhesion strength for the truncated double-well potential (10.2).

In Theorem 10.A, we have shown that the sharp-interface energy (10.42) is composed of two surface integrals, essentially splitting the outer boundary of the material into an adhered and non-adhered part. Each of the integral contributions is weighted by a constant. These constants depend on properties of the diffuse-interface problem. In particular, the constant weighting the non-adhered part of the limiting surface, that is C_W, has the same form as the constant C_W derived for the Cahn-Hilliard problem in Chapter 9, and represents the surface tension of the non-adhered boundary. The constant weighting the shared interface between material and substrate, that is C_σ, takes on a different form, and decreases for increasing values of σ. In Figure 10.1, both constants are plotted as a function of the adhesive strength σ, in which the truncated double-well potential (10.2) is considered. From this Figure, we can conclude that in absence of any adhesive interaction, that is for $\sigma = 0$, the sharp-interface energy functional (10.42) reduces to the sharp-interface energy functional for the Cahn-Hilliard problem (9.66). Furthermore, as σ approaches its limiting value, i.e. $\sigma \to 4$, the constant $C_\sigma \to -\infty$.

10.7 Minimizers of the sharp-interface energy

Using the sharp-interface energy functional derived in Theorem 10.A for the single-phase adhesion problem, we formulate the associated constrained minimization Problem 10.7. In this problem, the initial configuration of the system constrains the domain size enclosed by the sharp interface.

Problem 10.7 (Sharp-interface adhesion minimization problem) *Find* Γ^* *such that*

$$\mathcal{E}_{\text{single}}(\Gamma^*) = \inf_{\Gamma} \mathcal{E}_{\text{single}}(\Gamma), \tag{10.45}$$

subject to $|\Omega_+| := \int_{\Omega_+} \mathrm{d}x = M_{+,0}$, *with* $M_{+,0} := \int_{\Omega_+(t=0)} \mathrm{d}x$ *and* $\partial\Omega_+ := \Gamma$. □

Next, we define an equivalent saddle-point problem, using the following Lagrangian

$$\mathscr{L}(\Gamma, \lambda) = C_W \int_{\Gamma^c_{\text{adh}}} \mathrm{d}a + C_\sigma \int_{\Gamma_{\text{adh}}} \mathrm{d}a + \lambda(|\Omega_+| - M_{+,0}), \tag{10.46}$$

where the constants C_W and C_σ are specified through the associated diffuse-interface problem. Now, for a given Γ the Lagrangian satisfies

$$\sup_{\lambda\in\mathbb{R}} \mathscr{L}(\Gamma, \lambda) = \begin{cases} \mathcal{E}_{\text{single}}(\Gamma), & \text{if } |\Omega_+| = M_{+,0}, \quad \forall \lambda \in \mathbb{R}, \\ \infty, & \text{otherwise}, \end{cases} \tag{10.47}$$

which leads us the saddle-point Problem 10.8.

Problem 10.8 (Sharp-interface saddle-point problem) *Find* (Γ^*, λ^*) *such that*

$$\mathscr{L}(\Gamma^*, \lambda^*) = \inf_{\varphi\in\mathcal{L}} \sup_{\lambda\in\mathbb{R}} \mathscr{L}(\Gamma, \lambda). \tag{10.48}$$

□

To find the saddle points which solve Problem 10.8, and additionally minimize the energy in Problem 10.7, we consider the following expressions

$$\begin{cases} 0 = \mathscr{L}'(\Gamma^*, \lambda^*; \delta\lambda), & \forall \delta\lambda \in \mathbb{R}, \\ 0 = \mathscr{L}'(\Gamma^*, \lambda^*; \boldsymbol{v}), & \forall \boldsymbol{v} \in \mathcal{L}_v, \end{cases} \tag{10.49}$$

where we have used the velocity method introduced in Chapter 2 to take the Hadamard shape derivative. Bearing in mind that Γ is a piecewise smooth boundary, we consider perturbations in the tangential direction at the points where the boundary loses its

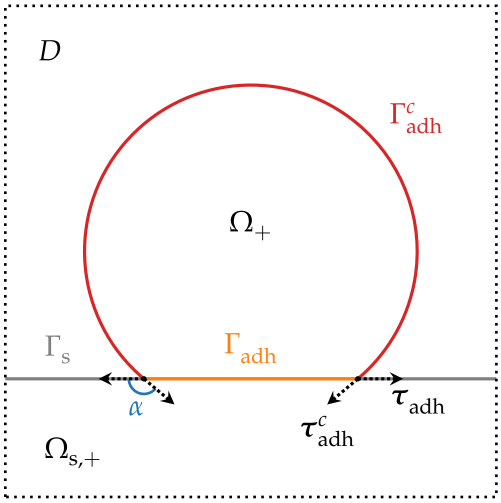

Figure 10.2: Shape of minimizers of the sharp-interface energy. The minimizer is a piecewise smooth surface, that is, $\Gamma^* = \Gamma^c_{\mathrm{adh}} \cup \Gamma_{\mathrm{adh}}$, where the adhered part of the surface is shared with the substrate surface Γ_{s}. At the edges $\partial\Gamma$ the tangential vectors to Γ_{adh} and Γ^c_{adh} are shown, which are denoted by $\boldsymbol{\tau}_{\mathrm{adh}}$ and $\boldsymbol{\tau}_{\mathrm{adh}}$ and define the angle α.

smoothness, see Figure 10.2. In particular, we define $\boldsymbol{\tau}_{\mathrm{adh}}$ as the outward unit tangent-normal to Γ_{adh} and $\boldsymbol{\tau}^c_{\mathrm{adh}}$ as the outward unit tangent-normal to Γ^c_{adh} at such points. At the non-adhered interface, we also consider perturbations given by the normal velocity $V := \boldsymbol{v} \cdot \boldsymbol{n}$.

Using the shape derivatives of the domain and boundary integral defined in Theorem 2.B and Theorem 2.C, respectively, we arrive at

$$\begin{cases} 0 = |\Omega_+| - M_{+,0}, \\ 0 = \displaystyle\int_{\partial\Gamma} \boldsymbol{v} \cdot (C_W \boldsymbol{\tau}^c_{\mathrm{adh}} + C_\sigma \boldsymbol{\tau}_{\mathrm{adh}})\, \mathrm{d}s + \int_{\Gamma^c_{\mathrm{adh}}} (C_W K + \lambda^*)(\boldsymbol{v} \cdot \boldsymbol{n})\, \mathrm{d}a, \end{cases} \tag{10.50}$$

where $\partial\Gamma$ are the points where Γ_{adh} and Γ^c_{adh} meet. If we consider the class of admissible velocity fields for which holds that $\boldsymbol{v} \cdot \boldsymbol{n} \neq 0$, we find that

$$C_W \boldsymbol{\tau}^c_{\mathrm{adh}} = -C_\sigma \boldsymbol{\tau}_{\mathrm{adh}}, \qquad \forall \boldsymbol{x} \in \partial\Gamma, \tag{10.51}$$

and also that

$$K = -\frac{\lambda^*}{C_W}, \qquad \forall \boldsymbol{x} \in \Gamma^c_{\mathrm{adh}}. \tag{10.52}$$

Here, expression (10.52) implies that the non-adhered part of the minimizing surface has a constant curvature, which value depends on the domain-size constraint. Furthermore, we can write (10.51) so that it defines the angle α, see Figure 10.2, that is

$$\alpha = \arccos\left(-\frac{\boldsymbol{\tau}^c_{\mathrm{adh}} \cdot \boldsymbol{\tau}_{\mathrm{adh}}}{|\boldsymbol{\tau}^c_{\mathrm{adh}}||\boldsymbol{\tau}_{\mathrm{adh}}|}\right) = \arccos\left(-\frac{C_\sigma}{C_W}\right), \qquad \forall \boldsymbol{x} \in \partial\Gamma. \tag{10.53}$$

From expression (10.53) follows that for $C_\sigma = C_W$, the angle is given by $\alpha = \pi$ radians, meaning that the limiting surface Γ^* is not adhered. For $C_\sigma = -C_W$, the angle $\alpha \to 0$, implying that the surface Γ^* is in its most adhered state. Thus, the values of the constants C_σ and C_W put a geometrical restriction on the angle between the adhered and non-adhered parts of the limiting surface.

In the following, we consider the two-dimensional configuration depicted in Figure 10.2 to further characterize the shapes of the minimizers of the sharp-interface energy functional for different adhesive strengths σ. For this purpose, we employ a geometrical approach, motivated by the results in (10.51) and (10.52), that is that minimizers can be geometrically parameterized by the combination of an adhesive curve length $L_{\text{adh}} := |\Gamma_{\text{adh}}|$, a non-adhesive curve length $L^c_{\text{adh}} := |\Gamma^c_{\text{adh}}|$ and an adhesion angle α. In our two-dimensional setting, the substrate is flat, and thus the adhesive curve length corresponds to the length of a straight line, whereas the non-adhesive curve length is part of the perimeter of an auxiliary circle with radius R. In its non-adhered configuration, the area of the domain enclosed by Γ^* is given by

$$A_0 = \pi R_0^2, \tag{10.54}$$

which we refer to as the initial area, as A_0 represents the constraint $M_{+,0}$. In what follows, let the initial radius be given by $R_0 = 0.45$. Then, for a given adhesion angle $\alpha \in (0, \pi]$, its corresponding lengths L_{adh} and L^c_{adh} can be found using

$$L_{\text{adh}} = 2R\sin(\pi - \alpha), \qquad \text{and} \qquad L^c_{\text{adh}} = 2\alpha R, \tag{10.55}$$

where the radius R of the auxiliary circle reads

$$R = \sqrt{\frac{A_0}{\alpha - \frac{1}{2}\sin(2\alpha)}}. \tag{10.56}$$

Next, we use the following numerical procedure to find for each adhesive strength $\sigma \in [0, 4)$ the geometric parameters $(L_{\text{adh}}, L^c_{\text{adh}}, \alpha)$ associated with the minimizer Γ^* of the sharp-interface energy functional:

(I) Looping over all $\alpha \in (0, \pi]$, the lengths L_{adh} and L^c_{adh} (10.55) are determined using the initial area (10.54). These computed pairs $(L_{\text{adh}}, L^c_{\text{adh}})$ represent the allowable geometries for the minimizers;

(II) Then, for each $\sigma \in [0, 4)$:

  (i) The value of the constant C_σ $(10.43)_2$ is determined, see Figure 10.1;

  (ii) Subsequently, the values of the adhesion energy

$$\mathcal{E} = C_W L^c_{\text{adh}} + C_\sigma L_{\text{adh}}, \tag{10.57}$$

  for all allowable pairs $(L_{\text{adh}}, L^c_{\text{adh}})$ are computed;

  (iii) Finally, the minimum energy over all values $\mathcal{E}$ is determined. Its associated geometric parameters $(L_{\text{adh}}, L^c_{\text{adh}}, \alpha)$ define the minimizer Γ^*.

Using the above approach, we find the values of the sharp-interface adhesion energy and plot these against the adhesive lengths, see Figure 10.3. In Figure 10.3, the minimum energies are marked for various σ, which demonstrate that (i) in the non-adhered case ($\sigma = 0$), the length of the adhesive part of Γ^* is zero; and that (ii) for σ tending to 4 the adhesive length tends to $+\infty$. Furthermore, the energy associated with the minimizers decreases for higher values of σ, yet seems bounded for $\sigma \to 4$. Lastly, in Figure 10.4 the values of the geometric parameters characterizing the minimizers for all $\sigma \in [0, 4)$ the are shown. We clearly observe that for $\sigma \to 4$, the material of interest spreads out over the flat substrate.

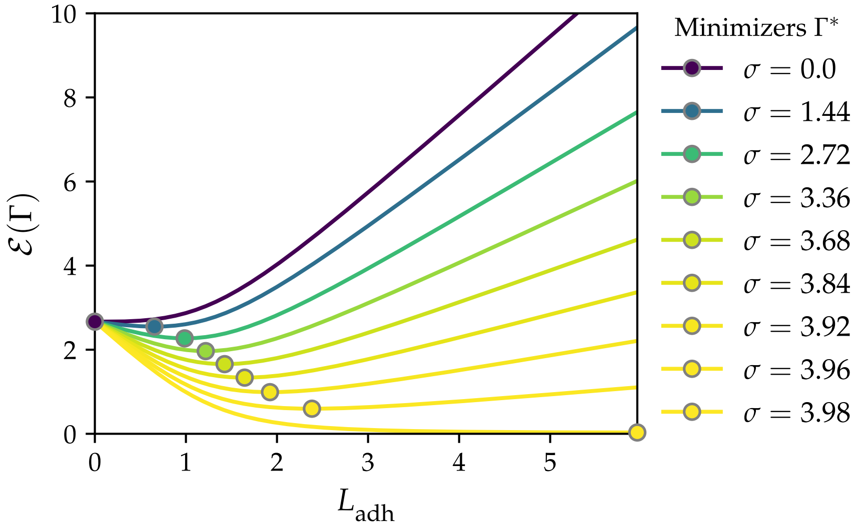

Figure 10.3: Sharp adhesion energy for different geometries using various σ. The adhered length L_{adh} represents the geometry. Minimizers Γ^* for the various adhesive strengths σ are indicated by the round markers.

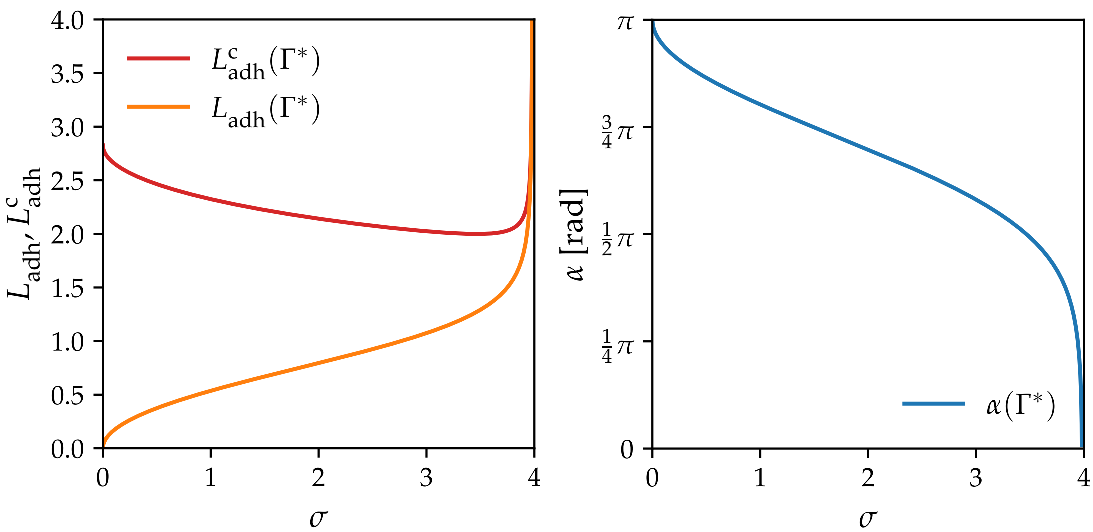

(a) Adhered L_{adh} and non-adhered length L^c_{adh}.

(b) Adhesion angle α.

Figure 10.4: Geometric parameters characterizing minimizers Γ^* for various σ: (a) adhered and non-adhered curve lengths and (b) angle between $\boldsymbol{\tau}_{\text{adh}}$ and $\boldsymbol{\tau}^c_{\text{adh}}$.

Chapter 11

Numerical Results

In this Chapter, we numerically solve the phase-field adhesion models presented in Chapter 8. To this end, we discretize the mixed form of the equations in space using the Finite Element method and in time using the so-called *scalar auxiliary variable* (SAV) approach. This SAV approach produces *energy-stable* results. An introduction to the scheme and the time-discretized version of the adhesion equations are provided in Section 11.1. In Section 11.2, we study the behaviour of the single-phase adhesion model in various numerical experiments. In particular, the effect of the curvature of the substrate's diffuse interface, the adhesion strength and the thickness of the diffuse interface on the steady states are numerically investigated. Lastly, Section 11.3 focusses on the multi-phase adhesion model and presents the numerical results of the adhesive interaction between two moving phase-field variables.

11.1 Time-discretization of the adhesion problem

In computational phase-field modelling, the time integration of the phase-field equations can be numerically challenging, as naively chosen time-discretization schemes may lack stability. In the first part of this Section, we introduce the reader to the notion of *time-discrete energy-stability*. In particular, we detail in Section 11.1.2 a recently proposed class of efficient and robust energy-stable schemes, known as the *scalar auxiliary variable* (SAV) approach. A first-order SAV scheme for a general class of phase-field based gradient flows is presented (Section 11.1.3), before it is applied to the single-phase adhesion (Section 11.1.4). Extension of this scheme provides us with an appropriate time-discretization scheme for the multi-phase adhesion problem (Section 11.1.5). These energy-stable systems are used to produce the numerical results in subsequent Sections.

11.1.1 Time-discretization methods for phase-field models

Phase-field theories are generally based on a free-energy functional that involve a non-convex term. These terms locally produce so-called *uphill* or *backward* diffusion, which standard time-integration schemes can not always adequately deal with. For this reason, the phase-field modelling community has taken much interest in the study and development of time-discretization methods.

To evaluate and compare the numerical performance of different time-discretization schemes, usually the following aspects are considered:

1. The order of accuracy of the scheme, i.e. whether the scheme is convergent and what error bounds can be established;

2. The stability of the scheme, i.e. whether the time-integration conserves the energy structure of the model;
3. The solvability of the time-discrete system, i.e. whether a solution exists and if that solution is unique;
4. The efficiency and the ease of implementation of the scheme.

For phase-field problems, the stability of the used time-discretization scheme is inherently dependent on the problem's energetic structure. In particular, we can say that a time-discretization scheme preserves the energy-dissipative property of the underlying phase-field model, if it dissipates[10] energy at each time step, see Definition 11.1. For a comprehensive overview of existing time-discretization schemes and their energy-dissipative properties, the reader is referred to Gomez & van der Zee (2017) [78].

Definition 11.1 (Energy stability of a time-discretization scheme) Let t^n, $n = 0, 1, \ldots,$ denote discrete time instances, $\tau = t^{n+1} - t^n$ define the time-step size, and $\varphi^n \approx \varphi(\cdot, t^n)$ the approximate solution at these discrete time instances. A numerical scheme for a phase-field model with an energy structure given by functional $\mathcal{E} : \mathcal{V} \to \mathbb{R}$ is said to be unconditionally energy-stable if

$$\mathcal{E}(\varphi^{n+1}) - \mathcal{E}(\varphi^n) \leq 0, \qquad \forall\, n \geq 0, \tag{11.1}$$

independent of the time-step size τ. If the stability holds under some constraint, e.g. for some τ, the scheme is said to be conditionally energy stable. □

In this work, we consider a time-discretization technique known as the scalar auxiliary variable (SAV) approach. The SAV scheme was originally proposed by Shen *et al.* (2018) [151] as an efficient and robust approach to construct energy-stable schemes for a general class of phase-field models. More specifically, it is based on the invariant energy quadratization (IEQ) approach, see recent work by [177, 179]. The IEQ approach is a generalization of the method of Lagrange multipliers, which act as auxiliary variables, and was first developed for phase-field models in [10, 80]. The IEQ method has made it possible to construct linear, unconditionally stable, as well as second-order unconditionally stable schemes for a large class of phase-field based gradient flows. Whilst the SAV approach enjoys all the advantages of the IEQ scheme, it also overcomes some of IEQ's shortcomings[11], thereby making it the more efficient and versatile approach of the two.

11.1.2 The SAV approach for gradient flows

Recall from Chapter 3 that phase-field gradient flows are evolutionary systems driven by a free-energy functional $\mathcal{E} : \mathcal{V} \to \mathbb{R}$ and a dissipation mechanism. Here, we consider energy functionals $\mathcal{E}$ of the following class

$$\mathcal{E}(\varphi) = \frac{1}{2}\langle \mathcal{L}\varphi, \varphi\rangle_{\mathcal{V}^*,\mathcal{V}} + \mathcal{E}_1(\varphi), \tag{11.2}$$

[10] Here, we additionally assume that no external work is acting on the system. Natural or periodic boundary conditions yield such a system.

[11] Using the SAV approach (i) the model's equations can be reduced in such way that a linear system with constant coefficients needs to be solved at each time step, instead of a linear system with variable coefficients; (ii) gradients flows with multiple variables no longer lead to IEQ's coupled system with variable coefficients, instead a system of decoupled linear equations with constant coefficients should be solved for each variable, and (iii) the class of gradient flows for which the scheme works is slightly larger, as certain restrictions on the bound of terms in the energy-functional are relaxed in the SAV scheme.

with $\mathcal{V}^*$ the dual of the vector space $\mathcal{V}$ and $\langle\cdot,\cdot\rangle_{\mathcal{V}^*,\mathcal{V}}$ the dual pairing $\mathcal{V}^* \times \mathcal{V} \to \mathbb{R}$. In the above, $\mathcal{L}$ is a symmetric non-negative linear operator, which is independent of φ. Furthermore, $\mathcal{E}_1 : \mathcal{V} \to \mathbb{R}$ is non-linear and typically only contains derivatives of lower order than $\mathcal{L}$. In addition, we assume that $\mathcal{E}_1$ is bounded from below as follows: there exists a constant C such that $\mathcal{E}_1 \geq C > 0$. Alternatively, we may add a constant $C_{\mathcal{E}}$ to $\mathcal{E}_1$ so that $\mathcal{E}_1 + C_{\mathcal{E}} \geq C > 0$ without altering the gradient flow. In contrast to Chapter 3, we here formulate the dissipation mechanism explicitly using the non-positive symmetric operator $\mathcal{G} : \mathcal{W} \to \mathcal{W}^*$. Then, the general structure of the gradient flows considered in this Chapter is given by

$$\frac{\partial \varphi}{\partial t} = \mathcal{G}\mu, \tag{11.3}$$

subject to suitable boundary conditions. Here, the variational derivative reads $\mu := \delta\mathcal{E}/\delta\varphi$, which we refer to as the chemical potential. Moreover, the operator $\mathcal{G}$ determines the dissipation mechanism of the gradient flow, which is characterized by the following energy-dissipation property

$$\frac{\mathrm{d}\mathcal{E}}{\mathrm{d}t} = \mathcal{E}'(\varphi; \frac{\partial \varphi}{\partial t}) = \langle \frac{\partial \varphi}{\partial t}, D\mathcal{E}(\varphi)\rangle_{\mathcal{W}^*,\mathcal{W}} = \langle \mathcal{G}\mu, \mu\rangle_{\mathcal{W}^*,\mathcal{W}} \leq 0. \tag{11.4}$$

Following Shen *et al.* (2019) [152], we introduce an auxiliary scalar variable $r = \sqrt{\mathcal{E}_1}$ to construct an energy-stable time-discretization scheme for the gradient flow (11.3). In case $\mathcal{E}_1$ is bounded by $C_{\mathcal{E}} > 0$, we may write $r = \sqrt{\mathcal{E}_1 + C_{\mathcal{E}}}$, without altering the structure of the gradient flow. Using this auxiliary variable, we rewrite the gradient flow (11.3) as

$$\begin{cases} \dfrac{\partial \varphi}{\partial t} = \mathcal{G}\mu, \\ \mu = \mathcal{L}\varphi + \dfrac{r}{\sqrt{\mathcal{E}_1(\varphi)}} U(\varphi), \\ \dfrac{\mathrm{d}r}{\mathrm{d}t} = \dfrac{1}{2\sqrt{\mathcal{E}_1(\varphi)}} \displaystyle\int_\Omega U(\varphi) \frac{\partial \varphi}{\partial t}\, \mathrm{d}x, \end{cases} \tag{11.5}$$

where auxiliary function

$$U(\varphi) = \frac{\delta \mathcal{E}_1}{\delta \varphi}, \tag{11.6}$$

denotes the variational derivative of the non-linear part of the energy functional. In Theorem 11.A, we establish that the system presented in (11.5) dissipates energy for the modified energy

$$\mathcal{E}_{\mathrm{mod}}(\varphi, r) = \frac{1}{2}\langle \mathcal{L}\varphi, \varphi\rangle_{\mathcal{V}^*,\mathcal{V}} + r^2, \tag{11.7}$$

and thus also for the general energy functional (11.2).

Theorem 11.A (Energy-dissipation of a SAV based gradient flow) *Let $\mathcal{E}(\varphi)$ be of the class of energy-functionals defined in* (11.2)*, where $\mathcal{E}_1(\varphi)$ is bounded from below. For a symmetric non-negative linear operator $\mathcal{L}$ and a non-positive symmetric operator $\mathcal{G}$, the system in* (11.5) *is energy-dissipative.* □

Proof. In view of the mixed system (11.5), we arrive at the following dissipation law for the energy functional (11.2)

$$\begin{aligned}
\frac{\mathrm{d}\mathcal{E}(\varphi)}{\mathrm{d}t} &= \frac{\mathrm{d}}{\mathrm{d}t}\Big(\frac{1}{2}\langle\mathcal{L}\varphi,\varphi\rangle_{\mathcal{V}^*,\mathcal{V}} + r^2\Big) \\
&= \langle\mathcal{L}\varphi,\frac{\partial\varphi}{\partial t}\rangle_{\mathcal{V}^*,\mathcal{V}} + 2r\frac{\mathrm{d}r}{\mathrm{d}t} \\
&= \langle\mathcal{G}\mu,\mu\rangle_{\mathcal{W}^*,\mathcal{W}} - \Big(\frac{\partial\varphi}{\partial t},\frac{r}{\sqrt{\mathcal{E}_1(\varphi)}}U(\varphi)\Big)_{L^2(\Omega)} + \frac{r}{\sqrt{\mathcal{E}_1(\varphi)}}\int_\Omega U(\varphi)\frac{\partial\varphi}{\partial t}\,\mathrm{d}x \\
&= \langle\mathcal{G}\mu,\mu\rangle_{\mathcal{W}^*,\mathcal{W}} \le 0,
\end{aligned} \tag{11.8}$$

bearing in mind that the energy functional $\mathcal{E}(\varphi)$ in (11.2) with $r = \sqrt{\mathcal{E}_1}$ corresponds to the modified energy functional $\mathcal{E}_{\mathrm{mod}}(\varphi,r)$ in (11.7). ∎

11.1.3 First-order SAV scheme

To arrive at a time-discrete system, we apply a first order time-integration scheme to the (φ,μ,r)-system in (11.5). The resulting system reads

$$\begin{cases}
\dfrac{\varphi^{n+1}-\varphi^n}{\tau} = \mathcal{G}\mu^{n+1}, \\[2ex]
\mu^{n+1} = \mathcal{L}\varphi^{n+1} + \dfrac{r^{n+1}}{\sqrt{\mathcal{E}_1(\varphi^n)}}U(\varphi^n), \\[2ex]
\dfrac{r^{n+1}-r^n}{\tau} = \dfrac{1}{2\sqrt{\mathcal{E}_1(\phi^n)}}\displaystyle\int_\Omega U(\varphi^n)\frac{\varphi^{n+1}-\varphi^n}{\tau}\,\mathrm{d}x,
\end{cases} \tag{11.9}$$

with $U(\varphi^n) = \delta\mathcal{E}_1(\varphi^n)/\delta\varphi$. This discrete system (11.9) is unconditionally energy-stable for the modified energy $\mathcal{E}_{\mathrm{mod}}$ (11.7), see Theorem 11.B. Moreover, the system that needs to be solved to find the solution $(\varphi^{n+1},\mu^{n+1},r^{n+1})$ is linear, making it an efficient and scheme, which is easy to implement.

Theorem 11.B (Unconditional energy stability of the first-order SAV scheme) *For the modified energy $\mathcal{E}_{\mathrm{mod}}(\varphi,r)$ in* (11.7)*, the scheme in* (11.9) *is unconditionally energy stable.* □

Proof. To arrive at the discrete modified energy dissipation, we multiply the expressions in (11.9) by μ^{n+1}, $(\varphi^{n+1}-\varphi^n)/\tau$ and $2r^{n+1}$, respectively, followed by integration over the domain of the first two expressions. Via these newly obtained identities, we find

$$\begin{aligned}
&\frac{1}{\tau}\Big(\mathcal{E}_{\mathrm{mod}}(\varphi^{n+1},r^{n+1}) - \mathcal{E}_{\mathrm{mod}}(\varphi^n,r^n)\Big) \\
&\quad= \frac{1}{2\tau}\langle\mathcal{L}\varphi^{n+1},\varphi^{n+1}\rangle_{\mathcal{V}^*,\mathcal{V}} - \frac{1}{2\tau}\langle\mathcal{L}\varphi^n,\varphi^n\rangle_{\mathcal{V}^*,\mathcal{V}} + \frac{(r^{n+1})^2-(r^n)^2}{\tau} \\
&\quad= \langle\mathcal{G}\mu^{n+1},\mu^{n+1}\rangle_{\mathcal{W}^*,\mathcal{W}} \\
&\qquad - \frac{1}{2\tau}\langle\mathcal{L}(\varphi^{n+1}-\varphi^n),(\varphi^{n+1}-\varphi^n)\rangle_{\mathcal{V}^*,\mathcal{V}} - \frac{(r^{n+1}-r^n)^2}{\tau} \le 0,
\end{aligned} \tag{11.10}$$

where we have used that $a^2-b^2 = 2a(a-b)-(a-b)^2$. Here, last term represents artificial dissipation of $\mathcal{O}(\tau^2)$. ∎

11.1.4 Time-discretization of single-phase field adhesion problem

In this Section, we present a first-order SAV scheme for the single-phase field adhesion problem. To write the single-phase adhesion energy functional $\mathcal{E}_{\text{single}}$ (10.1) as a functional of the class (11.2), we consider the operators

$$\mathcal{L} := -\varepsilon\Delta, \qquad \text{and} \qquad \mathcal{G} := \Delta. \tag{11.11}$$

For these operators, the first-order scheme (11.9) reads

$$\begin{cases} \dfrac{\varphi^{n+1}-\varphi^n}{\tau} = \Delta\mu^{n+1}, \\ \mu^{n+1} = -\varepsilon\Delta\varphi^{n+1} + \dfrac{r^{n+1}}{\sqrt{\mathcal{E}_1(\varphi^n)}}U(\varphi^n), \\ \dfrac{r^{n+1}-r^n}{\tau} = \dfrac{1}{2\sqrt{\mathcal{E}_1(\phi^n)}}\displaystyle\int_\Omega U(\varphi^n)\frac{\varphi^{n+1}-\varphi^n}{\tau}\,\mathrm{d}x, \end{cases} \tag{11.12}$$

with

$$\mathcal{E}_1(\varphi^n) := \int_\Omega \left(\frac{1}{\varepsilon}W(\varphi^n) + \sigma\varepsilon B(\varphi^n)B(\varphi_{\mathrm{s}})\nabla\varphi^n \cdot \nabla\varphi_{\mathrm{s}}\right)\mathrm{d}x, \tag{11.13}$$

so that the auxiliary function $U(\varphi^n)$ is given by

$$U(\varphi^n) := \frac{\delta\mathcal{E}_1(\varphi^n)}{\delta\varphi} = \frac{1}{\varepsilon}W'(\varphi^n) - \sigma\varepsilon B(\varphi^n)(B(\varphi_{\mathrm{s}})\Delta\varphi_{\mathrm{s}} + B'(\varphi_{\mathrm{s}})|\nabla\varphi_{\mathrm{s}}|^2). \tag{11.14}$$

11.1.5 First-order SAV scheme for the multi-phase field adhesion problem

The SAV approach presented for a gradient flow involving a single phase-field variable in Section 11.1.2-11.1.4 can be extended to multi-phase field gradient flows, see Section 2.2 in [152] for more details. Here, we present the first-order SAV scheme for the multi-phase adhesion problem. First, we write the multi-phase adhesion energy functional $\mathcal{E}^{\varepsilon}_{\text{multi}}$ (8.14) into the following general form

$$\mathcal{E}_{\text{multi}}(\varphi_i, \dots, \varphi_k) = \sum_{i=1}^{k}\left(\frac{1}{2}\langle\mathcal{L}_i\varphi_i, \varphi_i\rangle_{\mathcal{V}^*,\mathcal{V}}\right) + \mathcal{E}_1(\varphi_i, \dots, \varphi_k), \tag{11.15}$$

using that $\mathcal{L}_i := -\varepsilon\Delta$ and

$$\mathcal{E}_1(\varphi_i, \dots, \varphi_k) := \sum_{i=1}^{k}\sum_{j\neq i}^{k}\int_\Omega \frac{\varepsilon\sigma_{ij}}{2}B(\varphi_i)B(\varphi_j)\nabla\varphi_i \cdot \nabla\varphi_j\,\mathrm{d}x. \tag{11.16}$$

Furthermore, for the adhesion problem we have that $\mathcal{G}_i = \Delta$ for all $i = 1, \dots, k$. Then, using the SAV approach, a first-order scheme is given by

$$\begin{cases} \dfrac{\varphi_i^{n+1}-\varphi_i^n}{\tau} = \Delta\mu_i^{n+1}, \\ \mu_i^{n+1} = -\varepsilon\Delta\varphi_i^{n+1} + \dfrac{r^{n+1}}{\sqrt{\mathcal{E}_1(\varphi_i^n, \dots, \varphi_k^n)}}U_i(\varphi_i^n, \dots, \varphi_k^n), \\ \dfrac{r^{n+1}-r^n}{\tau} = \displaystyle\int_\Omega \sum_{i=1}^{k}\left(\frac{U_i(\phi_i^n, \dots, \phi_k^n)}{2\sqrt{\mathcal{E}_1(\phi_i^n, \dots, \phi_k^n)}}\frac{\varphi_i^{n+1}-\varphi_i^n}{\tau}\right)\mathrm{d}x, \end{cases} \tag{11.17}$$

for all $i = 1, \ldots, k$. Here, the auxiliary function U_i reads

$$U_i(\varphi_i^n, \ldots, \varphi_k^n) := \frac{\delta \mathcal{E}_1(\varphi_i^k, \ldots, \varphi_k^n)}{\delta \varphi_i}$$
$$= \frac{1}{\varepsilon} W'(\varphi^n) - \sum_{j \neq i}^{k} \varepsilon \sigma_{ij} B(\varphi_i^n)(B(\varphi_j^n)\Delta \varphi_j^n + B'(\varphi_j^n)|\nabla \varphi_j^n|^2), \tag{11.18}$$

bearing in mind that we consider symmetric adhesion strengths, that is $\sigma_{ij} = \sigma_{ji}$.

11.2 2-D single phase-field adhesion

In this Section, we present two-dimensional numerical results for the single-phase adhesion model detailed in Section 8.1. First, we present the results of a numerical experiment involving the interaction of the phase field with a flat steady substrate in Section 11.2.1. In Section 11.2.2 and 11.2.3, we consider the effect of curvature, as we study the interaction of the phase-field with a convex and concave substrate field, respectively.

All numerical results in this Section are obtained using the first-order SAV schemes presented in Section 11.1. Furthermore, we employed the standard Galerkin Finite Element Method for the discretization in space. More specifically, we used linear basis functions ($p = 1$) on quadrilateral elements and a uniform mesh size $h := L/n_{\text{elem}}$. Here, L is the (larger) domain length and n_{elem} denotes the number of elements along the (longer) domain boundary, chosen so that $\epsilon \geq 2h$ for all experiments. Lastly, the results were computed using Nutils: a free and open source Python programming library for Finite Element Method computations [169].

11.2.1 Flat substrate

In this Section, we consider a flat substrate field onto which a moving phase-field adheres. Let the computational domain be given by $\Omega = [-L, L]^2$ with $L = 1.0$, and let $t \in [0, T]$ with final time $T = 0.8$. Furthermore, we consider the initial configuration depicted in Figure 8.1. Then, the initial condition of the phase-field variable is given by

$$\varphi(\boldsymbol{x}, 0) = \tanh\left(\frac{R_0 - |\boldsymbol{x}|}{\sqrt{2}\varepsilon}\right), \tag{11.19}$$

whereas the steady substrate field reads

$$\phi_{\text{s}}(\boldsymbol{x}) = -\tanh\left(\frac{h_{\text{s}} + y}{\sqrt{2}\varepsilon}\right), \tag{11.20}$$

so that at $t = 0$ the only point of contact between the phase-field's and substrate's 0-level sets is the origin. Here, the initial radius of this circular shape of the phase field is given by $R_0 = 0.45$. Furthermore, $h_{\text{s}} = R_0$ is the translation of the substrate field in the negative y-direction.

In the numerical experiments presented in this Section, the following double-well function is employed

$$W(\varphi) = \frac{1}{4}(1 - \varphi^2)^2, \tag{11.21}$$

with minima located at $\varphi_- = -1$ and $\varphi_+ = 1$. Additionally, we use

$$B(\varphi) := \begin{cases} \sqrt{W(\varphi)} = \frac{1}{2}(1 - \varphi^2), & \varphi \in [-1, 1], \\ 0, & \text{otherwise}, \end{cases} \tag{11.22}$$

as regularizing function.

We solve the single-phase field adhesion problem for various values of the interfacial thickness ε and also use different values for the adhesive strength σ. The simulation parameters used for each of these simulations are provided in Table 11.1.

Figures 11.1, 11.3, and 11.5 show the evolution of the phase-field variable over time for $\sigma = 1.0$ and $\sigma = 2.0$, using $\varepsilon = 0.10$, $\varepsilon = 0.05$ and $\varepsilon = 0.025$, respectively. Then, Figures 11.2, 11.4, and 11.6 show the evolution of the phase-field variable over time for higher values of the adhesion strength, that is $\sigma = 3.0$ and $\sigma = 4.0$, again using $\varepsilon = 0.10$, $\varepsilon = 0.05$ and $\varepsilon = 0.025$, respectively. At the final time $T = 0.8$, the adhered length L_{adh} is depicted in these Figures, which exact value is based on the sharp-interface results in Section 10.7 and varies for different values for the adhesive strength σ. In general, we observe that for each interfacial thickness ε, the phase-field adheres onto the substrate: the domain enclosed by the diffuse interface moves closer to the substrate field and flattens on top of it, thereby increasing the overlapping area between the diffuse regions of the two fields. In the numerical limit, the diffuse interpretation of the adhesive length (at $T = 0.8$) corresponds well with the predicted L_{adh} by the sharp-interface analysis in Section 10.7, especially for lower values of σ. However, for $\sigma = 4.0$ no fully adhered configuration is recovered by the phase-field model, while this was predicted by the sharp-interface analysis. Furthermore, a comparison between the results for different ε reveals that ε scales the adhesive effect, as the diffuse interpretation of the adhesive length gets larger for smaller values of ε.

In Figures 11.7, 11.8, 11.9, the energy results over time for $\varepsilon = 0.10$, $\varepsilon = 0.05$ and $\varepsilon = 0.025$, respectively, are plotted. These results show that the phase field results at $T = 0.8$ can indeed be considered as steady states, as the energies converge to constant values over time. Furthermore, we see that the adhesive process is mainly associated with a (strong) decrease in adhesive energy, lowering the total energy in the system. In the numerical limit, we see that hardly any changes in the homogeneous part of the energy functional should be expected over time, whereas changes in interfacial energy reflect the changes in adhesive energy, as the diffuse interpretation of the perimeter grows due to the adhesive effect.

Table 11.1: Simulation parameters used in the flat substrate simulations.

interfacial thickness ε	time step size τ	number of elements along the domain boundary n_{elem}
0.10	$2 \cdot 10^{-4}$	80
0.05	$2 \cdot 10^{-4}$ ($1 \cdot 10^{-4}$ for $\sigma = 1.0$)	80
0.025	$25 \cdot 10^{-6}$ ($125 \cdot 10^{-7}$ for $\sigma \geq 3.0$)	160

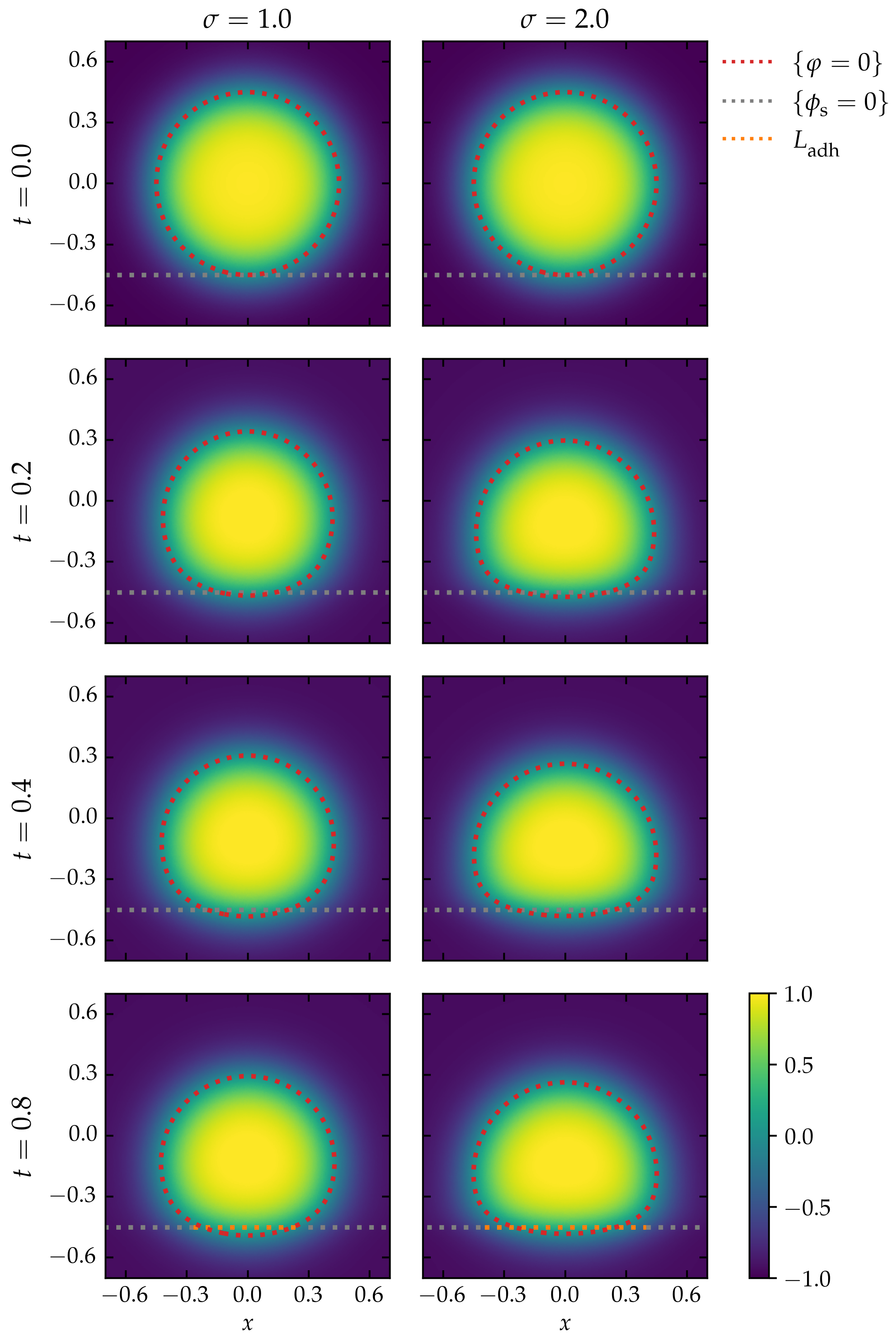

Figure 11.1: Adhesion on a flat substrate for $\varepsilon = 0.10$**.** 2-D results at various times for lower values of the adhesive strength σ. The 0-level set of the adhesive phase-field φ and the substrate ϕ_s are plotted as dotted lines.

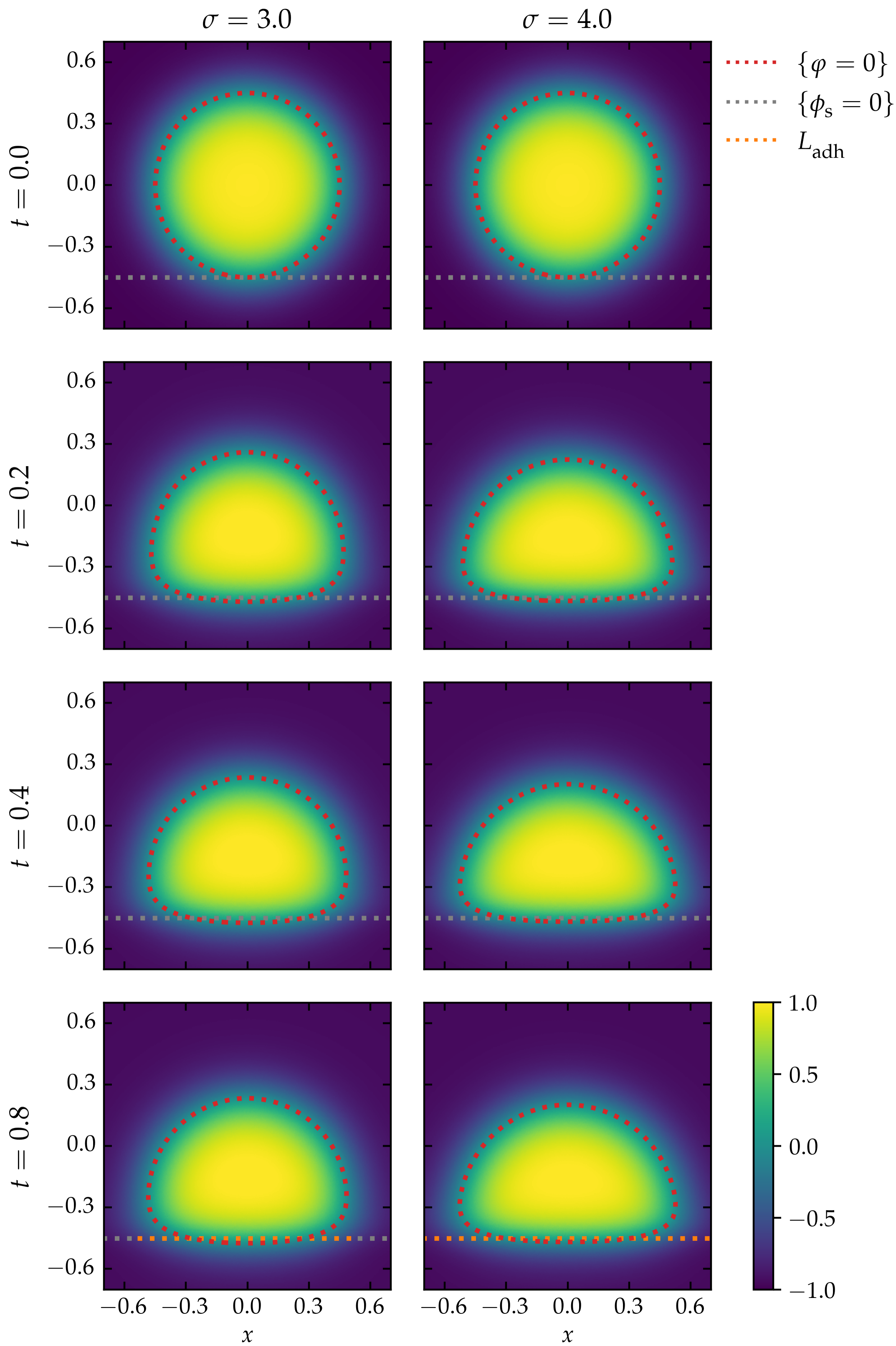

Figure 11.2: Adhesion on a flat substrate for $\varepsilon = 0.10$. 2-D results at various times for higher values of the adhesive strength σ. The 0-level set of the adhesive phase-field φ and the substrate ϕ_s are plotted as dotted lines.

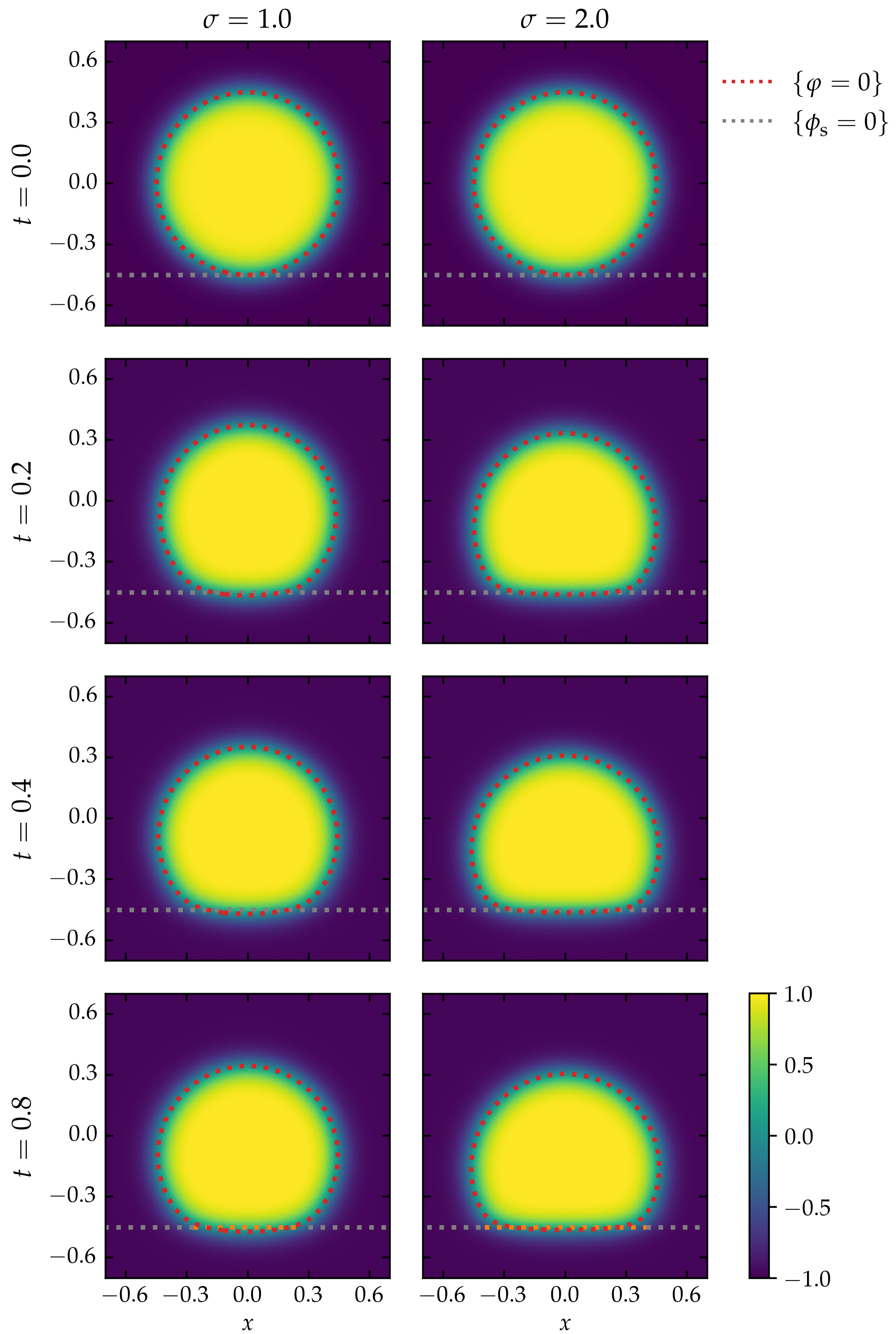

Figure 11.3: Adhesion on a flat substrate for $\varepsilon = 0.05$**.** 2-D results at various times for lower values of the adhesive strength σ. The 0-level set of the adhesive phase-field φ and the substrate ϕ_s are plotted as dotted lines.

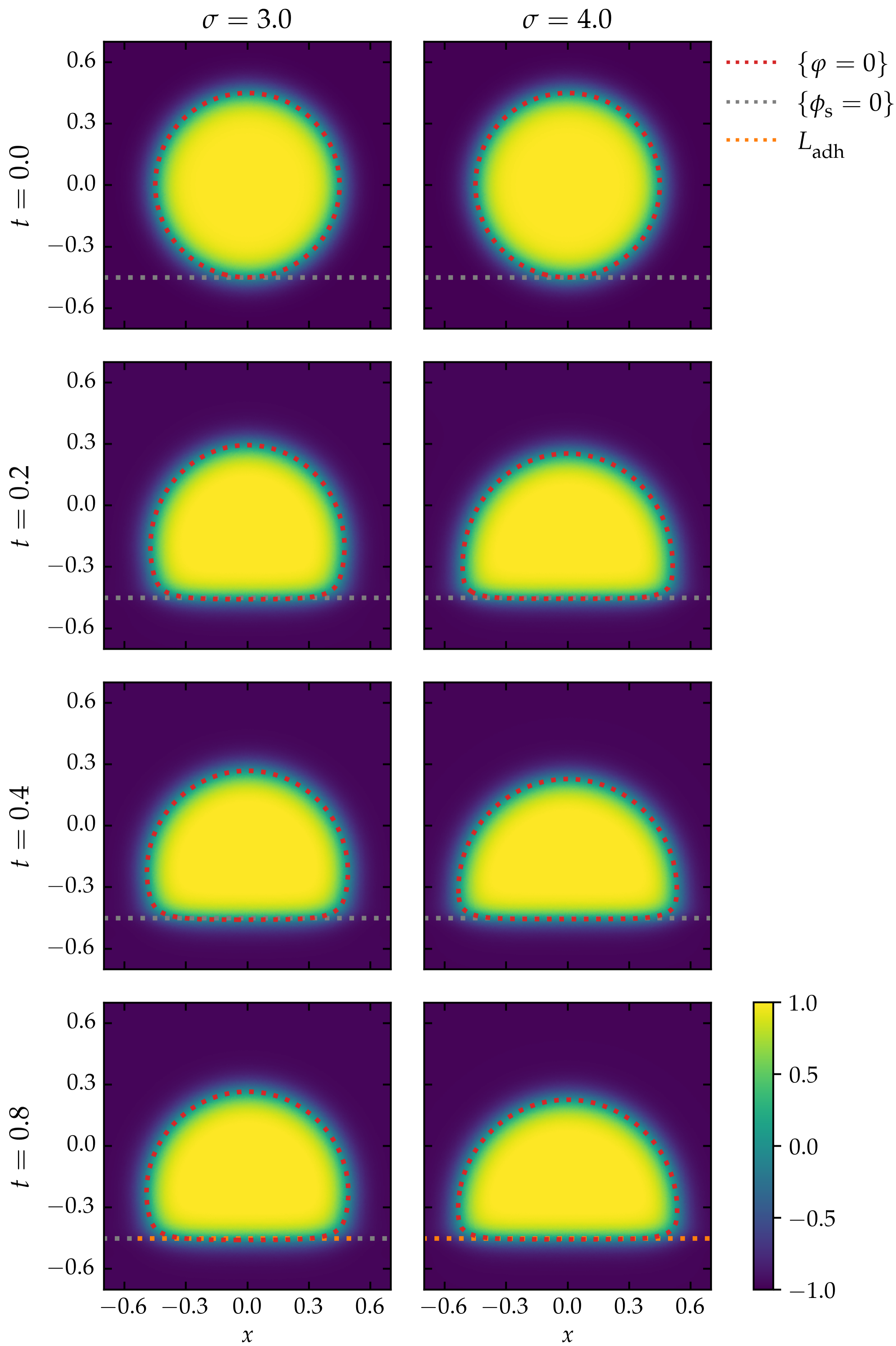

Figure 11.4: Adhesion on a flat substrate for $\varepsilon = 0.05$**.** 2-D results at various times for higher values of the adhesive strength σ. The 0-level set of the adhesive phase-field φ and the substrate ϕ_s are plotted as dotted lines.

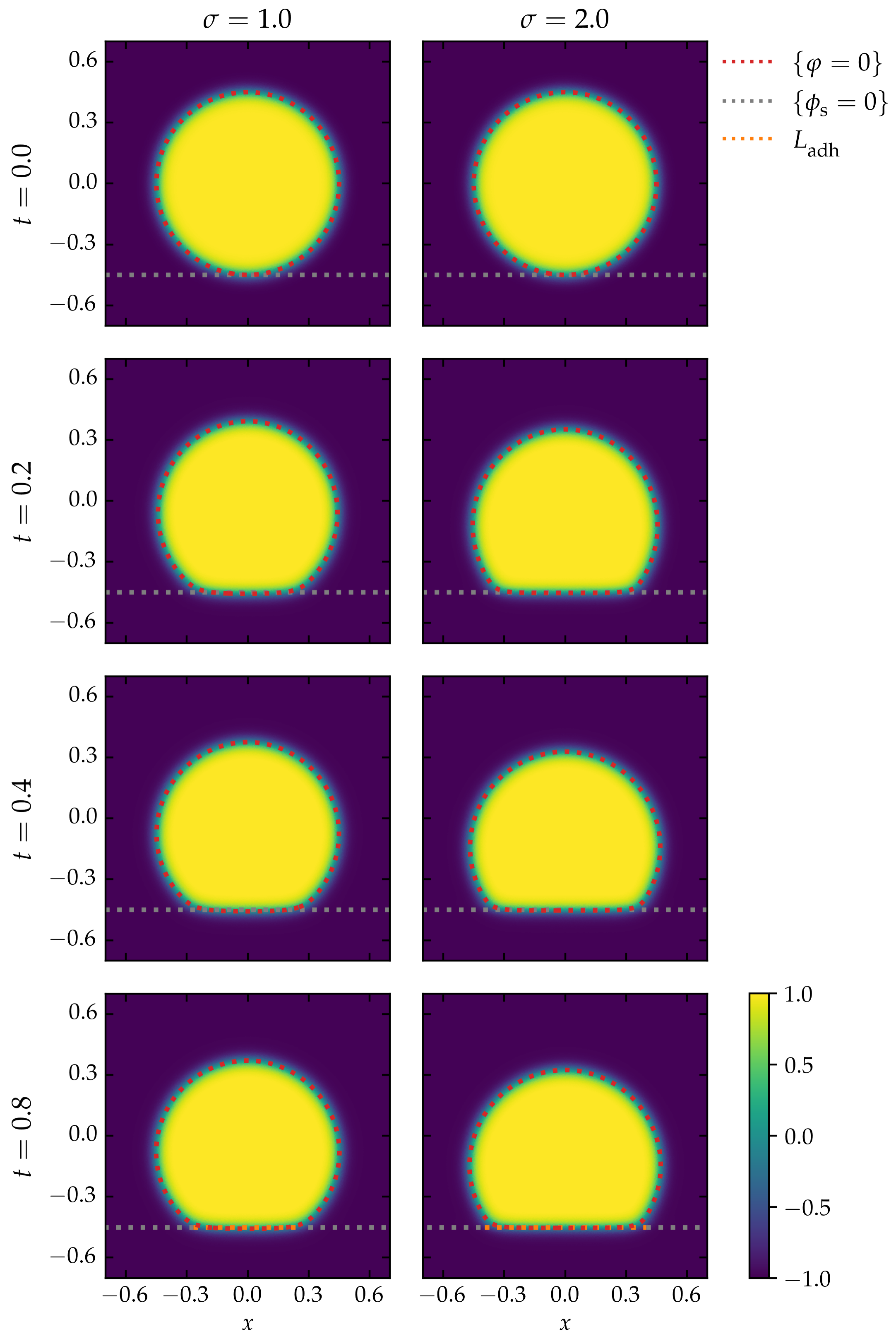

Figure 11.5: Adhesion on a flat substrate for $\varepsilon = 0.025$. 2-D results at various times for lower values of the adhesive strength σ. The 0-level set of the adhesive phase-field φ and the substrate ϕ_s are plotted as dotted lines.

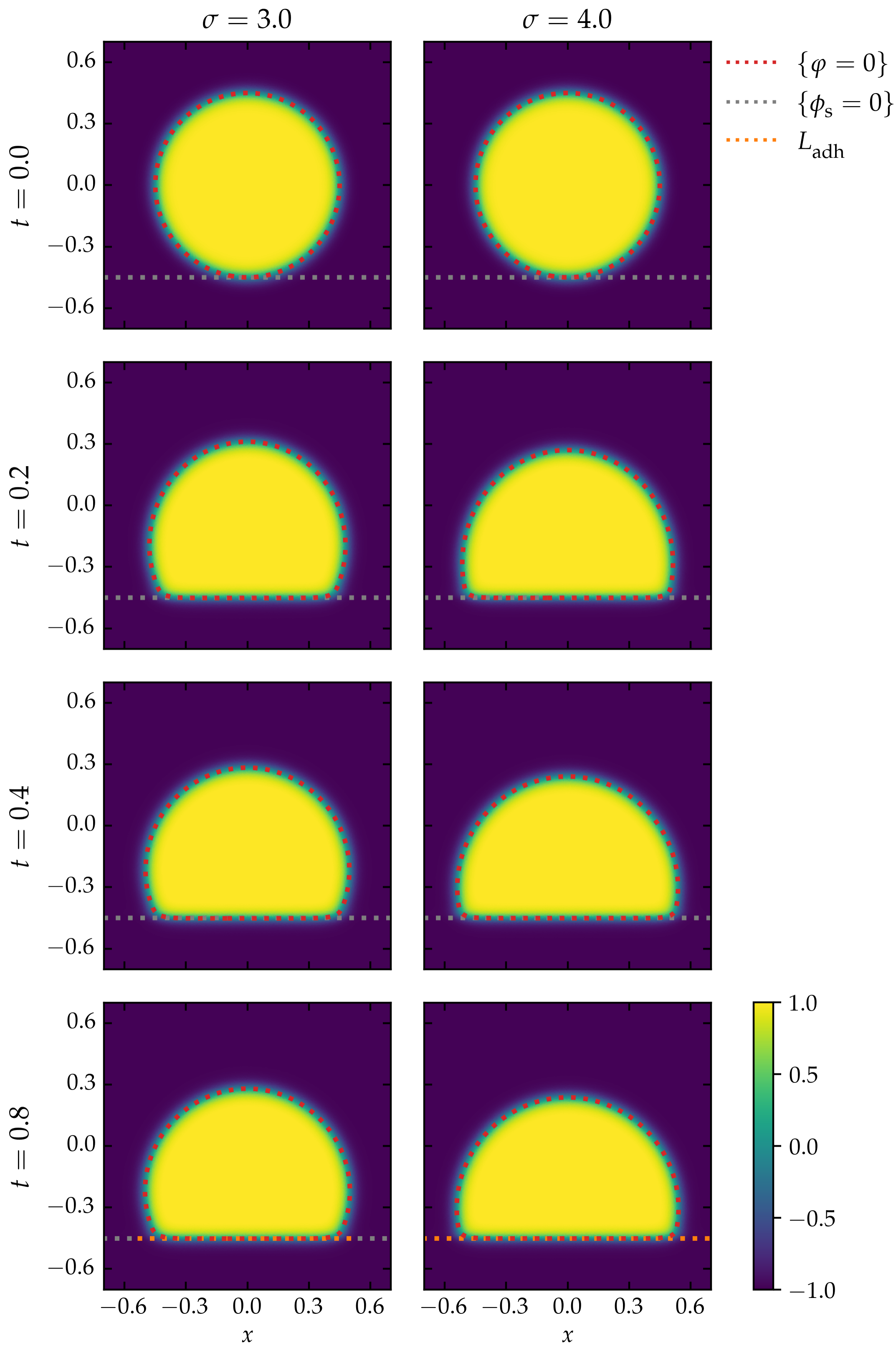

Figure 11.6: Adhesion on a flat substrate for $\varepsilon = 0.025$**.** 2-D results at various times for higher values of the adhesive strength σ. The 0-level set of the adhesive phase-field φ and the substrate ϕ_s are plotted as dotted lines.

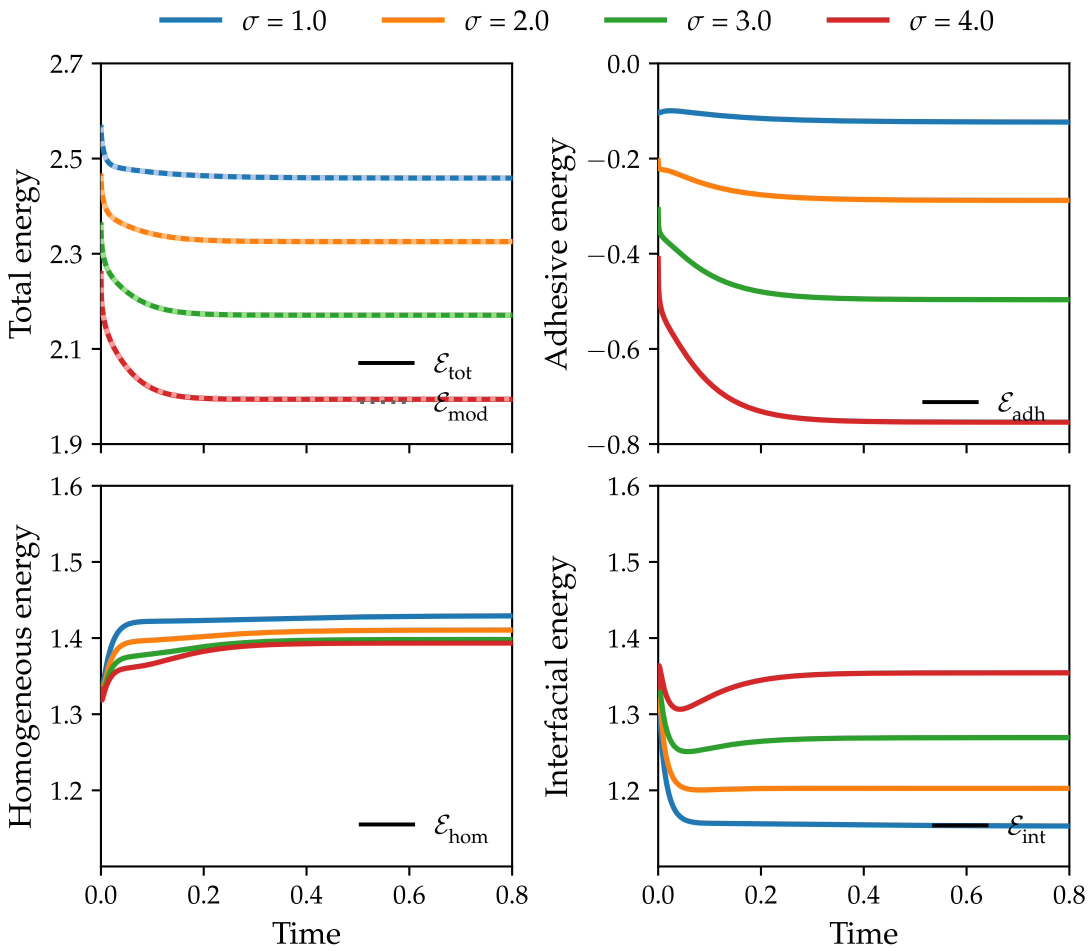

Figure 11.7: Adhesion on a flat substrate for $\varepsilon = 0.10$**.** Energy results showing the total energy $\mathcal{E}_{\text{tot}}$, modified energy $\mathcal{E}_{\text{mod}}$, adhesive energy $\mathcal{E}_{\text{adh}}$, homogeneous energy $\mathcal{E}_{\text{hom}}$ and interfacial energy $\mathcal{E}_{\text{int}}$ over time for various adhesive strengths σ.

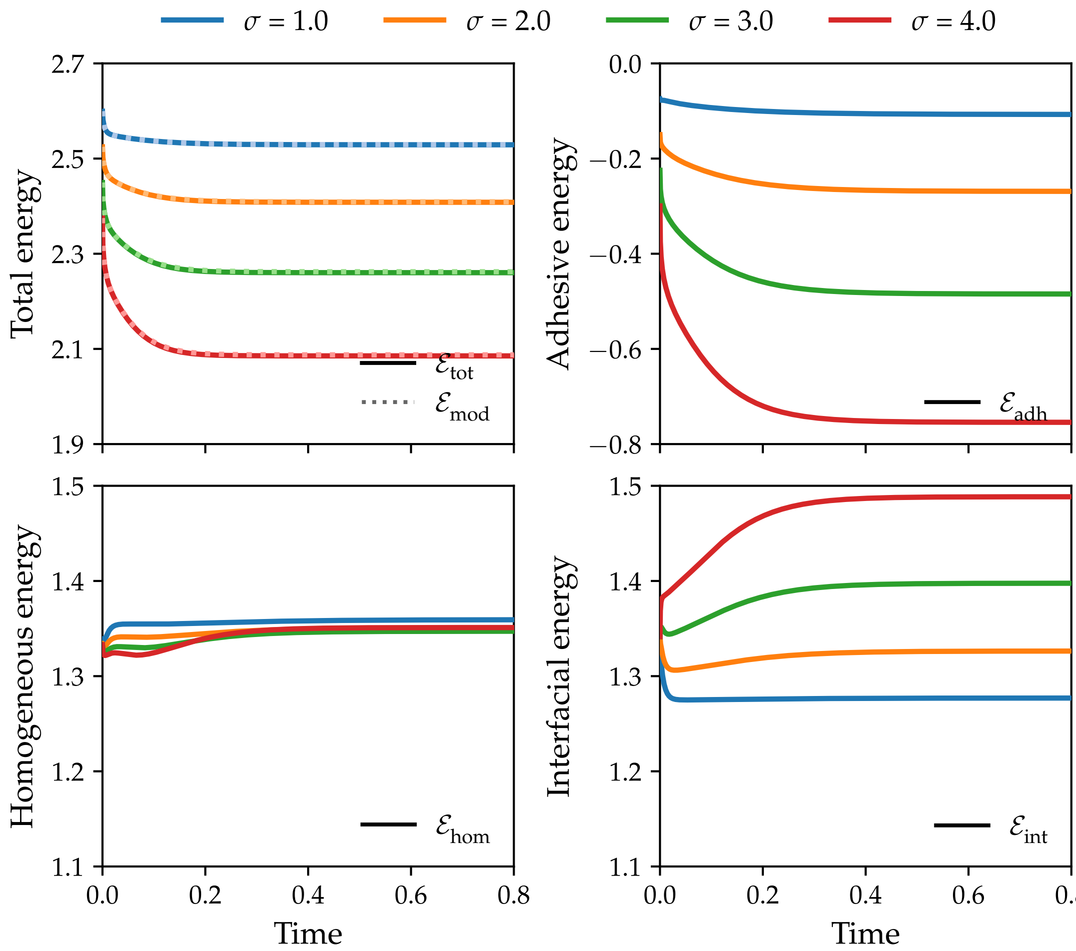

Figure 11.8: Adhesion on a flat substrate for $\varepsilon = 0.05$**.** Energy results showing the total energy $\mathcal{E}_{\text{tot}}$, modified energy $\mathcal{E}_{\text{mod}}$, adhesive energy $\mathcal{E}_{\text{adh}}$, homogeneous energy $\mathcal{E}_{\text{hom}}$ and interfacial energy $\mathcal{E}_{\text{int}}$ over time for various adhesive strengths σ.

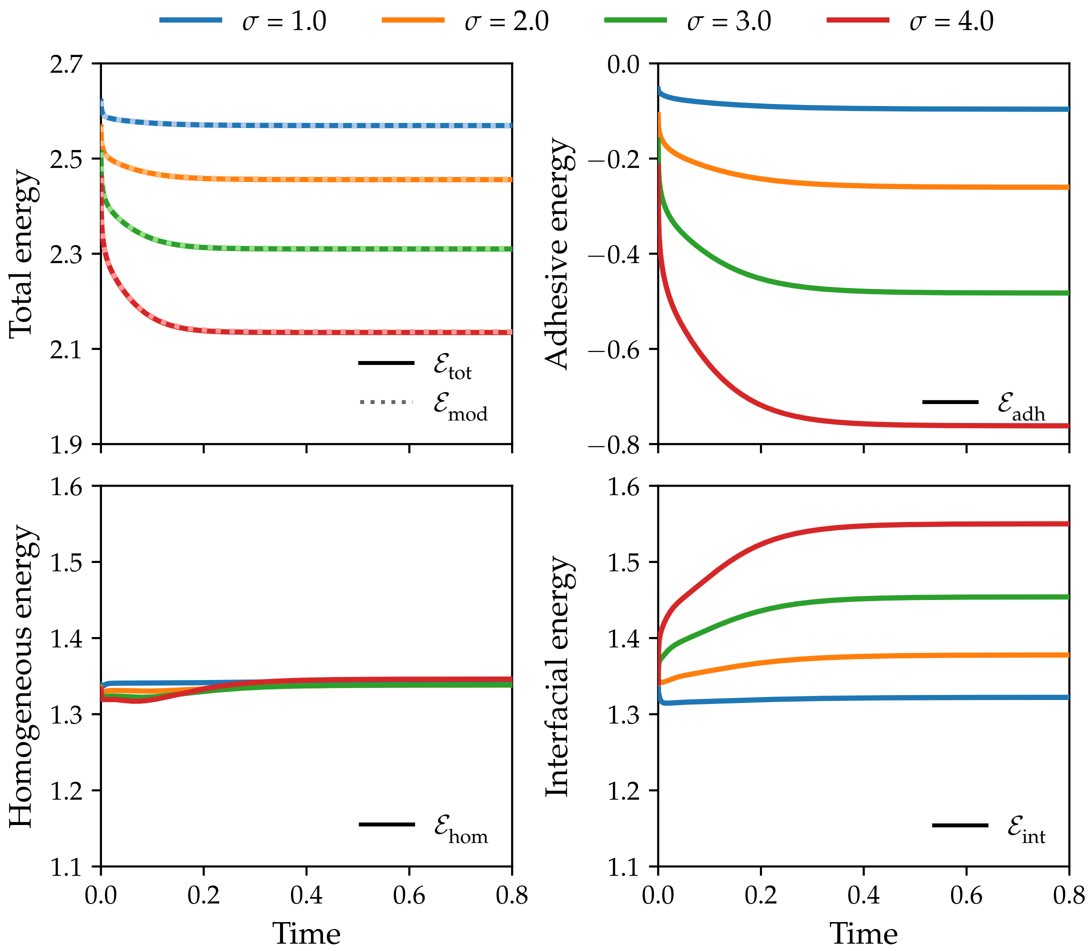

Figure 11.9: Adhesion on a flat substrate for $\varepsilon = 0.025$**.** Energy results showing the total energy $\mathcal{E}_{\mathrm{tot}}$, modified energy $\mathcal{E}_{\mathrm{mod}}$, adhesive energy $\mathcal{E}_{\mathrm{adh}}$, homogeneous energy $\mathcal{E}_{\mathrm{hom}}$ and interfacial energy $\mathcal{E}_{\mathrm{int}}$ over time for various adhesive strengths σ.

11.2.2 Convex substrate

In this Section, we present the numerical results for a convexly shaped substrate field. Here, we consider a steady substrate field

$$\phi_{\mathrm{s}}(\boldsymbol{x}) = \tanh\left(\frac{R_{\mathrm{s}} - \sqrt{x^2 + (C_y - y)^2}}{\sqrt{2}\varepsilon}\right), \tag{11.23}$$

with R_{s} governing the curvature and $C_y = -(R_{\mathrm{s}} - R_0)$. The rest of the parameters and settings are taken from the experiment described in Section 11.2.1, except that for all simulations here $\tau = 2 \cdot 10^{-4}$ is used for $\varepsilon = 0.05$ and $\tau = 25 \cdot 10^{-6}$ for $\varepsilon = 0.025$.

Figures 11.10 and 11.14 shows the phase field at $T = 0.8$ for lower values of R_{s} and various σ, using $\varepsilon = 0.05$ and $\varepsilon = 0.025$, respectively. Then, Figures 11.11 and 11.15 show the steady states for higher values of R_{s}, again using $\varepsilon = 0.05$ and $\varepsilon = 0.025$, respectively. Furthermore, in Figures 11.12, 11.13, 11.16 and 11.17 the energetic contributions over time are plotted.

Similar effects to the ones discussed in Section 11.2.1 can be observed in these Figures. For this numerical experiment involving a convex substrate, however, the part of the diffuse interface of the phase field that adheres onto the substrate has to become concave. We observe that the diffuse adhesion lengths increase for larger values of σ. The energy plots show that higher values of R_{s} are associated with lower adhesion energies (and thus also total energies). Furthermore, larger interfacial energies are found, hinting at larger diffuse perimeters, for larger values of R_{s}, in other words, for less curved substrate fields.

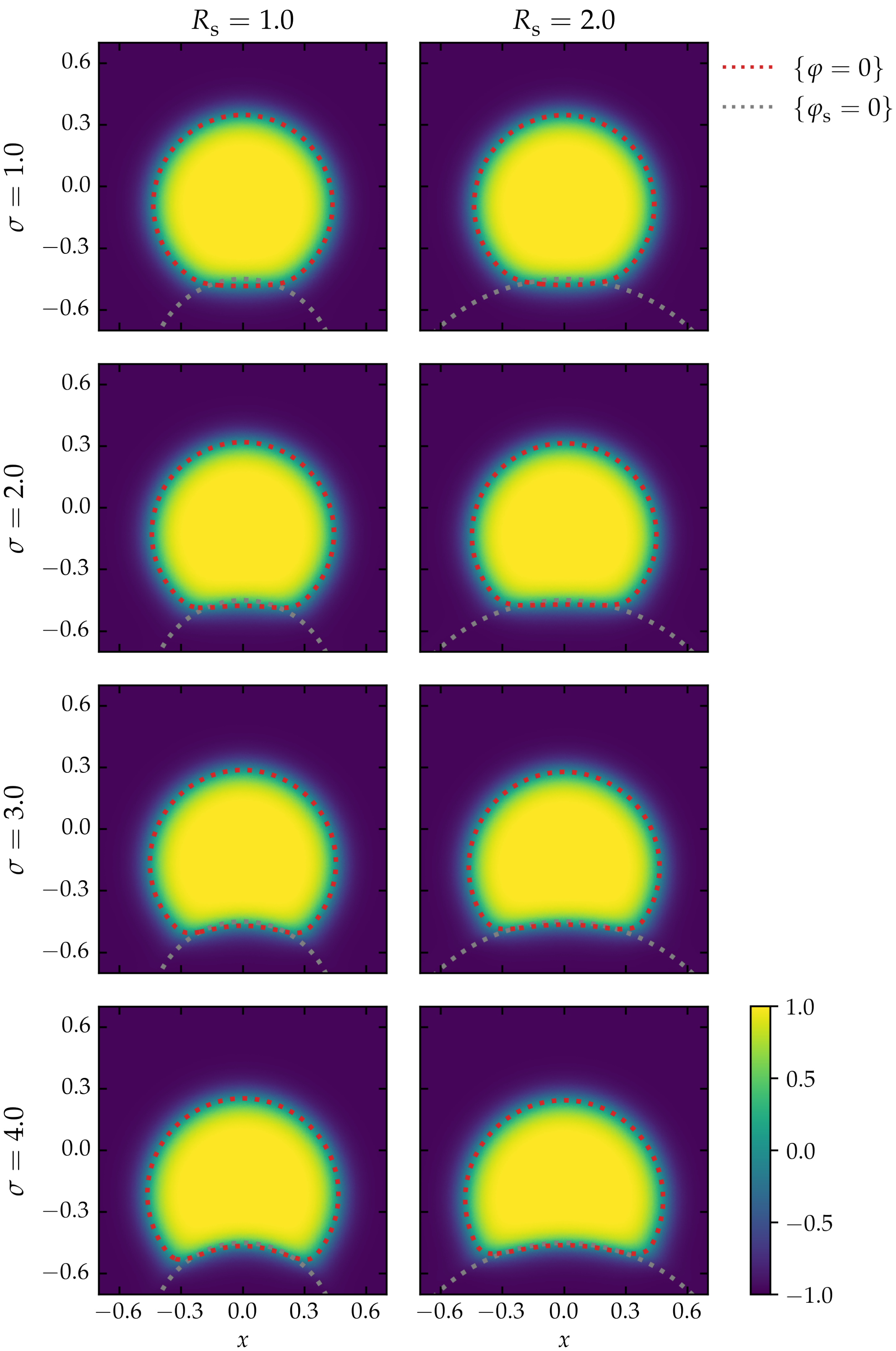

Figure 11.10: Adhesion on a convex substrate for $\varepsilon = 0.05$**.** 2-D results at $T = 0.8$ for lower values of R_s and for various adhesive strengths σ. The 0-level set of the adhesive phase-field φ and the substrate ϕ_s are plotted as dotted lines.

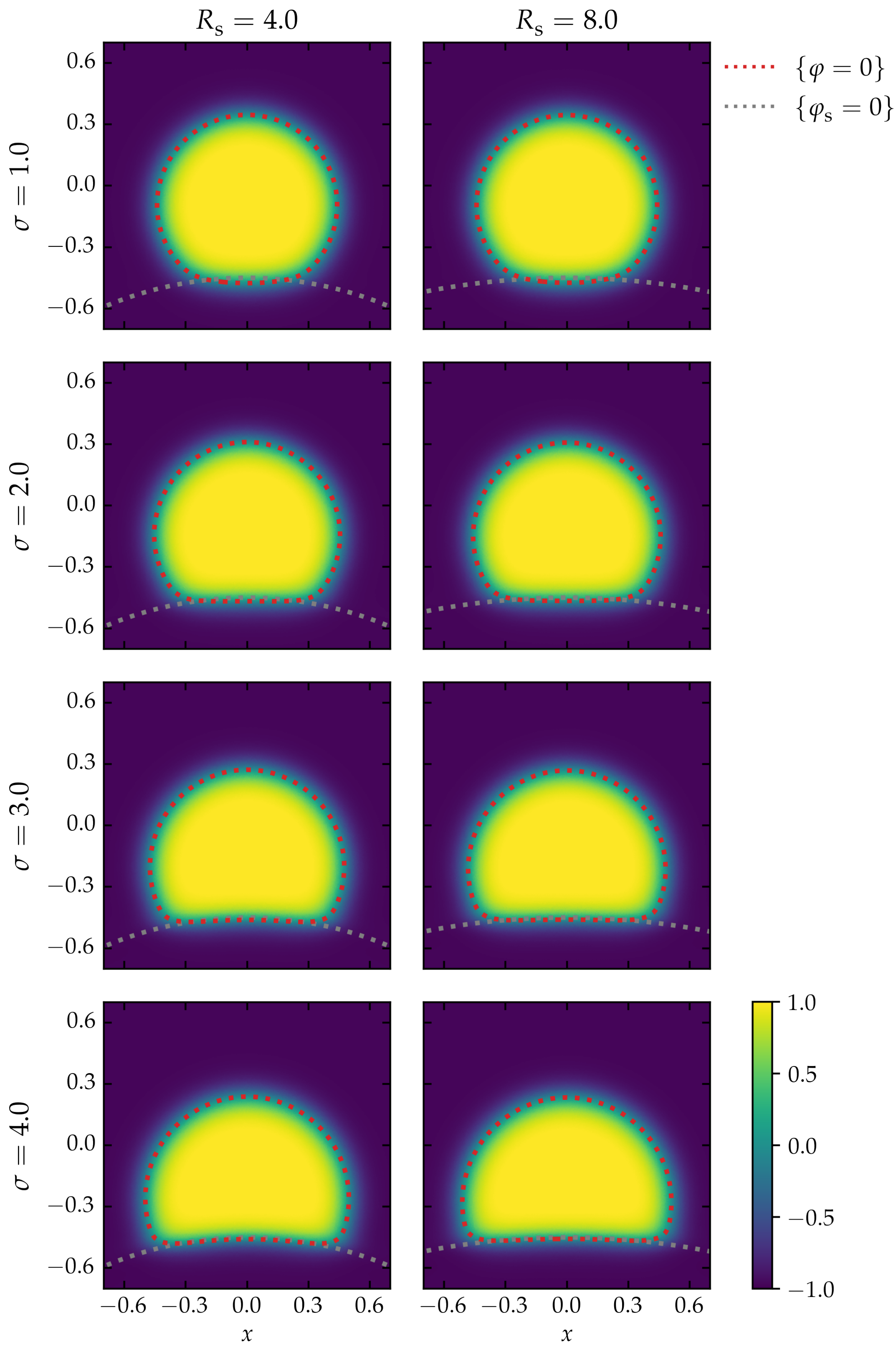

Figure 11.11: Adhesion on a convex substrate for $\varepsilon = 0.05$**.** 2-D results at $T = 0.8$ for higher values of R_s and for various adhesive strengths σ. The 0-level set of the adhesive phase-field φ and the substrate ϕ_s are plotted as dotted lines.

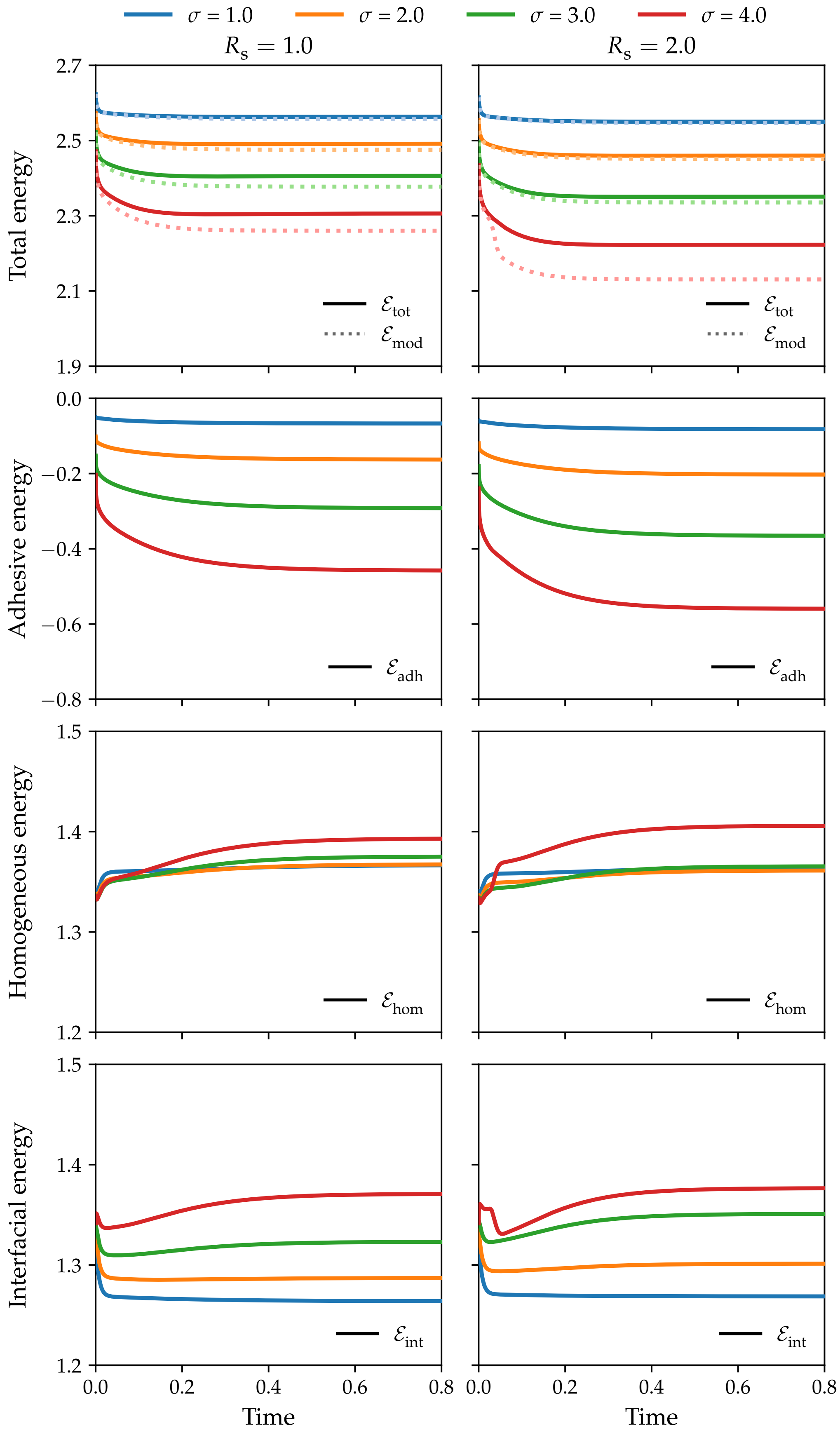

Figure 11.12: Adhesion on a convex substrate for $\varepsilon = 0.05$**.** Energy results showing the total energy $\mathcal{E}_{tot}$, modified energy $\mathcal{E}_{mod}$, adhesive energy $\mathcal{E}_{adh}$, homogeneous energy $\mathcal{E}_{hom}$ and interfacial energy $\mathcal{E}_{int}$ over time for various adhesive strengths σ and for lower values R_s governing the substrate's curvature.

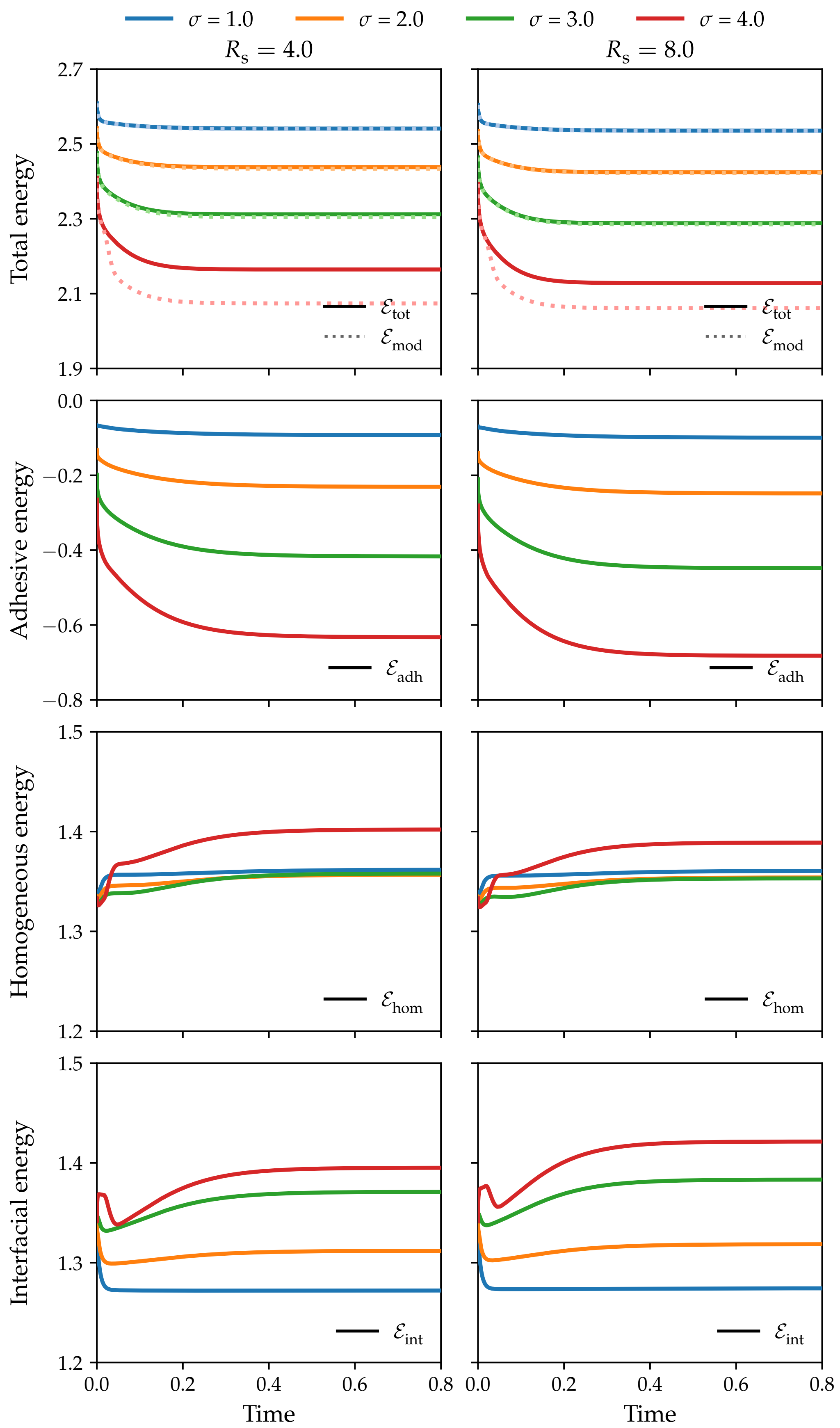

Figure 11.13: Adhesion on a convex substrate for $\varepsilon = 0.05$. Energy results showing the total energy $\mathcal{E}_{\text{tot}}$, modified energy $\mathcal{E}_{\text{mod}}$, adhesive energy $\mathcal{E}_{\text{adh}}$, homogeneous energy $\mathcal{E}_{\text{hom}}$ and interfacial energy $\mathcal{E}_{\text{int}}$ over time for various adhesive strengths σ and for higher values R_s governing the substrate's curvature.

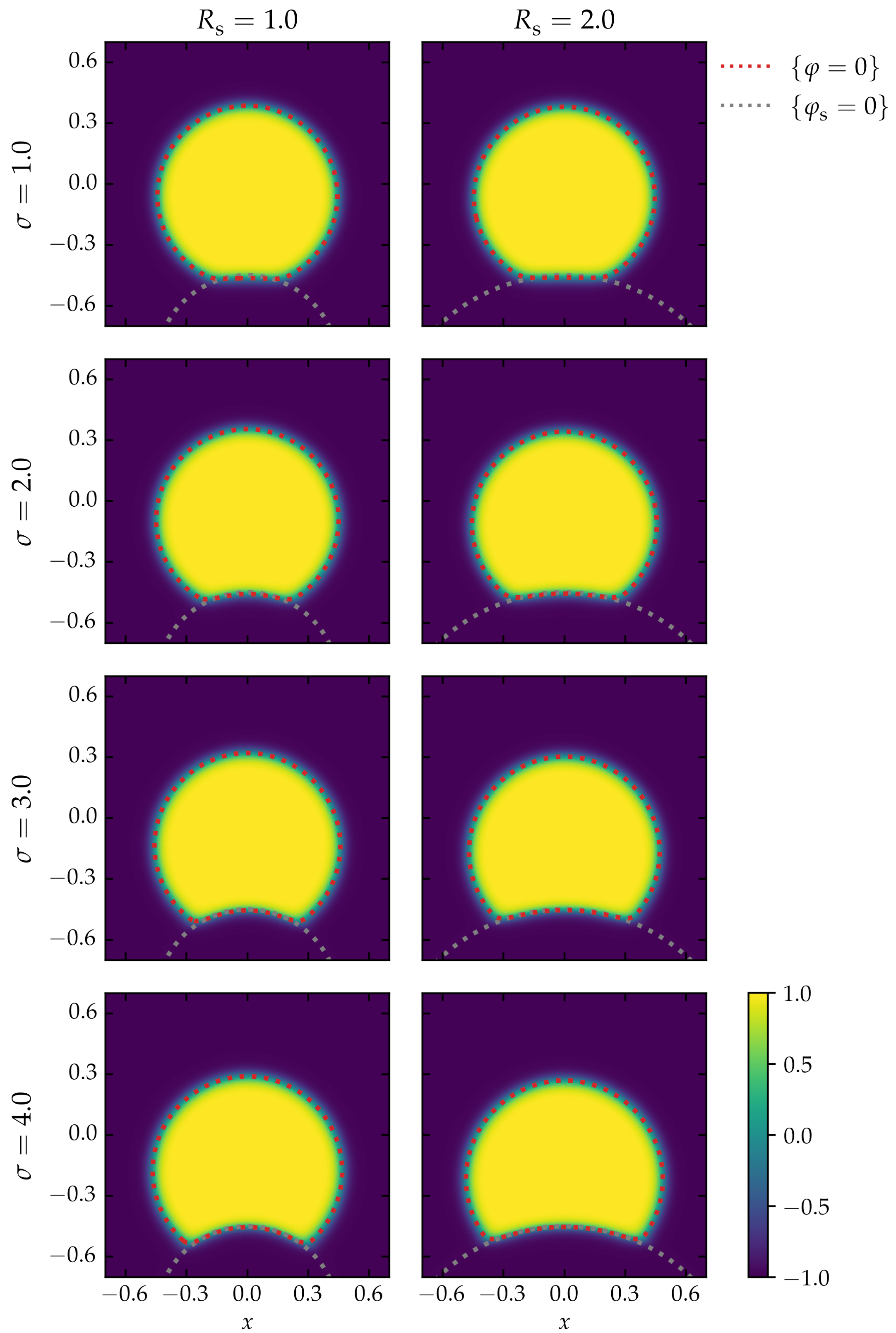

Figure 11.14: Adhesion on a convex substrate for $\varepsilon = 0.025$**.** 2-D results at $T = 0.8$ for lower values of R_s and for various adhesive strengths σ. The 0-level set of the adhesive phase-field φ and the substrate ϕ_s are plotted as dotted lines.

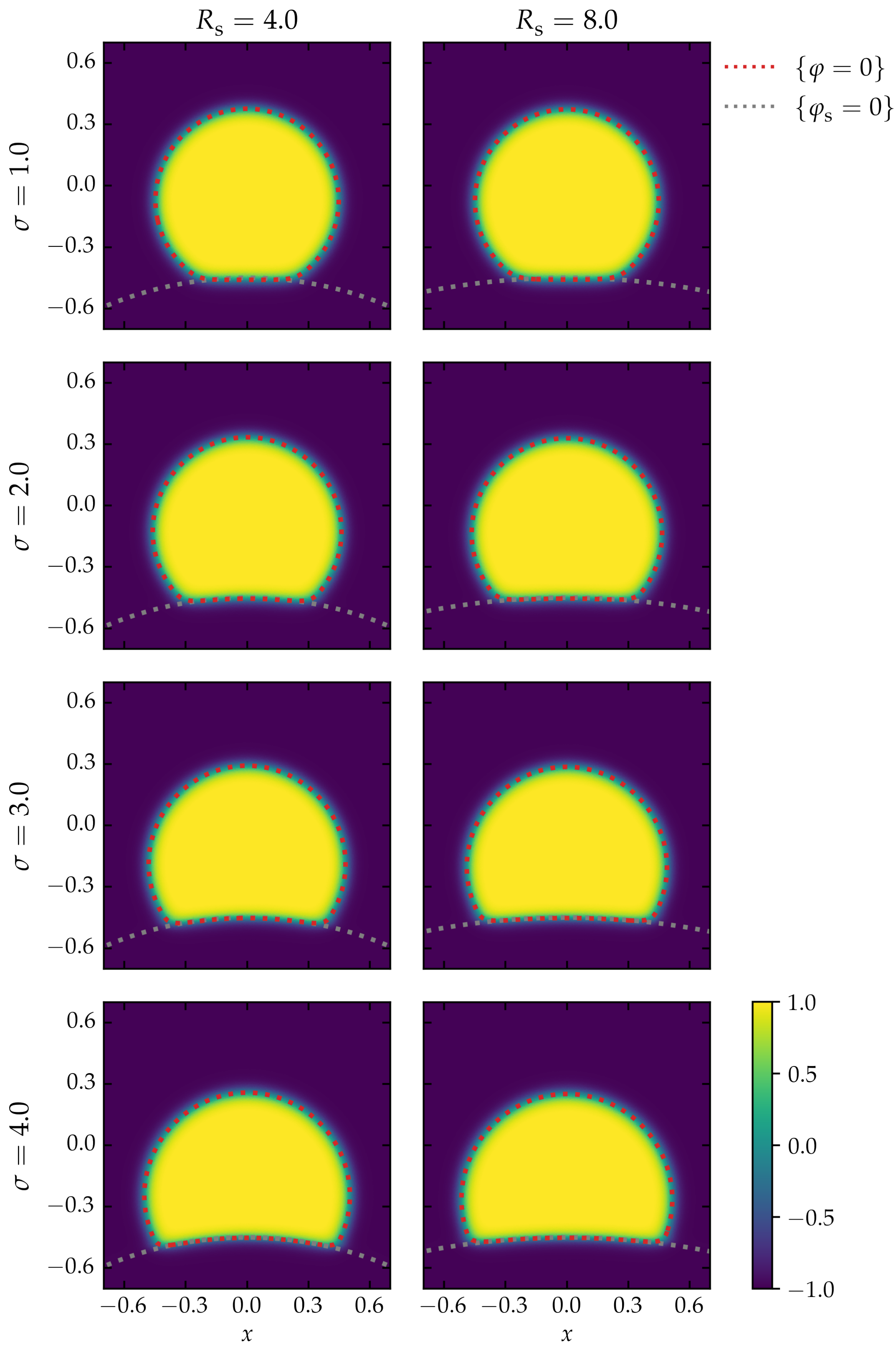

Figure 11.15: Adhesion on a convex substrate for $\varepsilon = 0.025$**.** 2-D results at $T = 0.8$ for higher values of R_s and for various adhesive strengths σ. The 0-level set of the adhesive phase-field φ and the substrate ϕ_s are plotted as dotted lines.

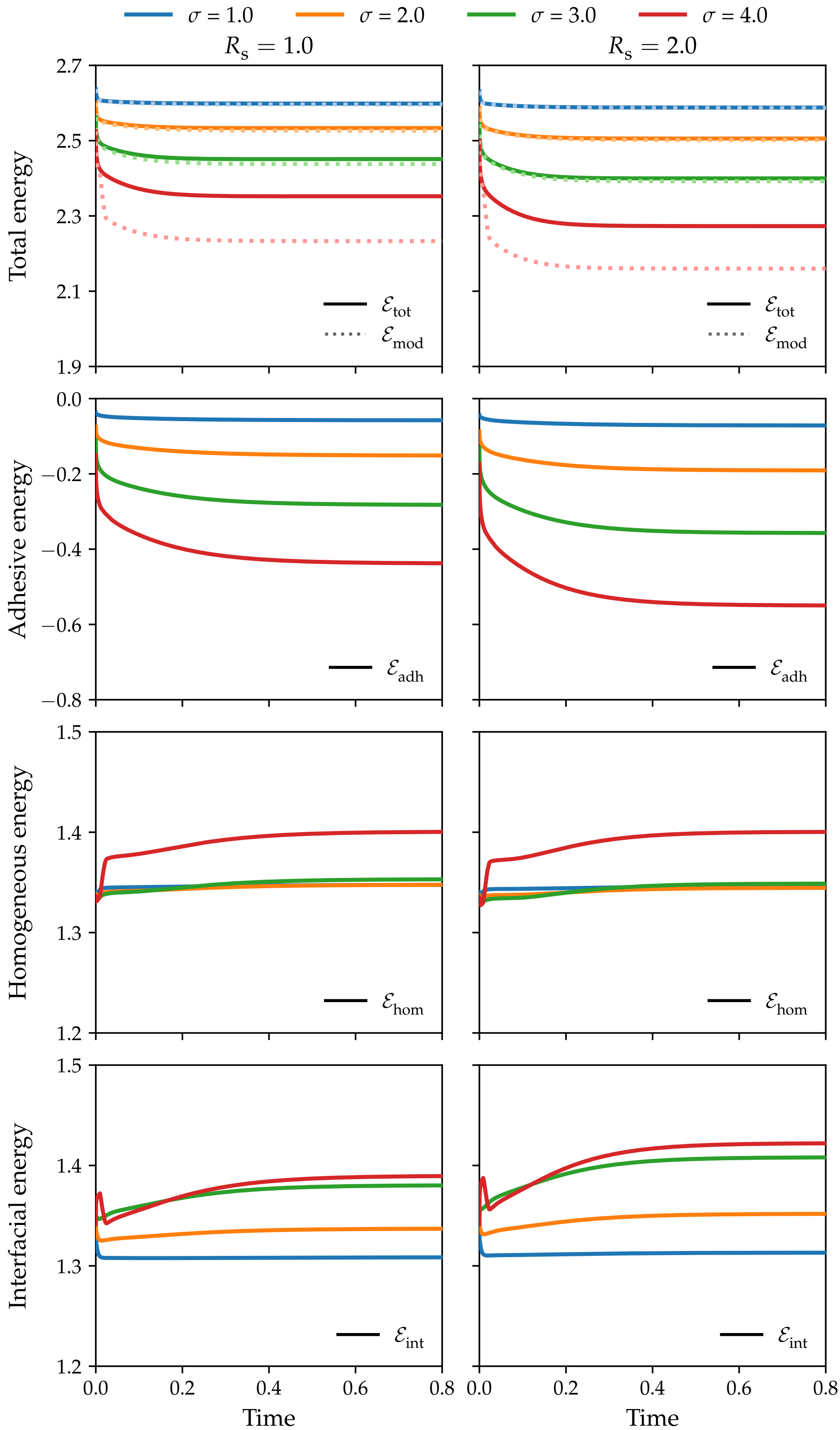

Figure 11.16: Adhesion on a convex substrate for $\varepsilon = 0.025$. Energy results showing the total energy $\mathcal{E}_{tot}$, modified energy $\mathcal{E}_{mod}$, adhesive energy $\mathcal{E}_{adh}$, homogeneous energy $\mathcal{E}_{hom}$ and interfacial energy $\mathcal{E}_{int}$ over time for various adhesive strengths σ and for lower values R_s governing the substrate's curvature.

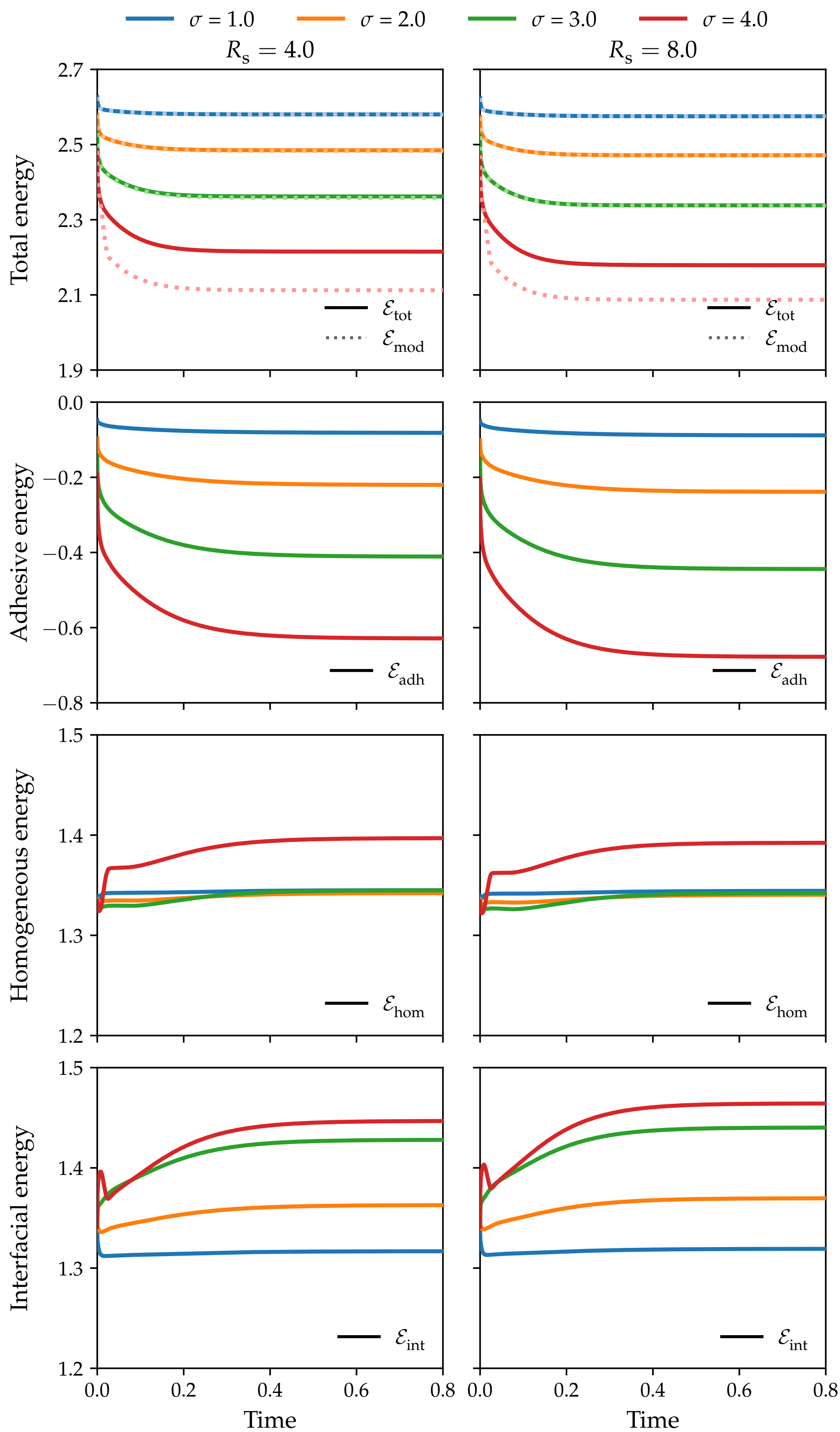

Figure 11.17: Adhesion on a convex substrate for $\varepsilon = 0.025$. Energy results showing the total energy $\mathcal{E}_{tot}$, modified energy $\mathcal{E}_{mod}$, adhesive energy $\mathcal{E}_{adh}$, homogeneous energy $\mathcal{E}_{hom}$ and interfacial energy $\mathcal{E}_{int}$ over time for various adhesive strengths σ and for higher values R_s governing the substrate's curvature.

11.2.3 Concave substrate

In this Section, we present the numerical results for a concave substrate field. Here, we let the steady substrate field given by

$$\phi_{\mathrm{s}}(\boldsymbol{x}) = -\tanh\left(\frac{R_{\mathrm{s}} - \sqrt{x^2 + (C_y - y)^2}}{\sqrt{2}\varepsilon}\right), \tag{11.24}$$

with R_{s} as a measure of its curvature and $C_y = (R_{\mathrm{s}} - R_0)$. The rest of the settings are copied from Section 11.2.1, except that for the results presented here $\tau = 2 \cdot 10^{-4}$ is used for $\varepsilon = 0.05$ and $\tau = 25 \cdot 10^{-6}$ for $\varepsilon = 0.025$. For the simulations involving $R_{\mathrm{s}} = 1.0$ and $\varepsilon = 0.025$, we used $C_{\mathcal{E}} = 1.0$ for $\sigma = 3.0$ and $C_{\mathcal{E}} = 0.5$ for $\sigma = 4.0$.

In Figures 11.18 and 11.22, the phase field at $T = 0.8$ is plotted for lower values of R_s and various σ, using $\varepsilon = 0.05$ and $\varepsilon = 0.025$, respectively. Figures 11.19 and 11.23 show the steady states for higher values of R_s, again using $\varepsilon = 0.05$ and $\varepsilon = 0.025$, respectively. Furthermore, in Figures 11.20, 11.21, 11.24 and 11.25 the energetic contributions over time are plotted.

In these results for a concave substrate field, we again observe similar trends to the ones described in Section 11.2.1 and 11.2.2. Here, the adhered part of the diffuse surface follows the curvature of the concave substrate field. Lower values of R_s are associated with longer adhered lengths of the diffuse interface, as well as lower adhesive energies.

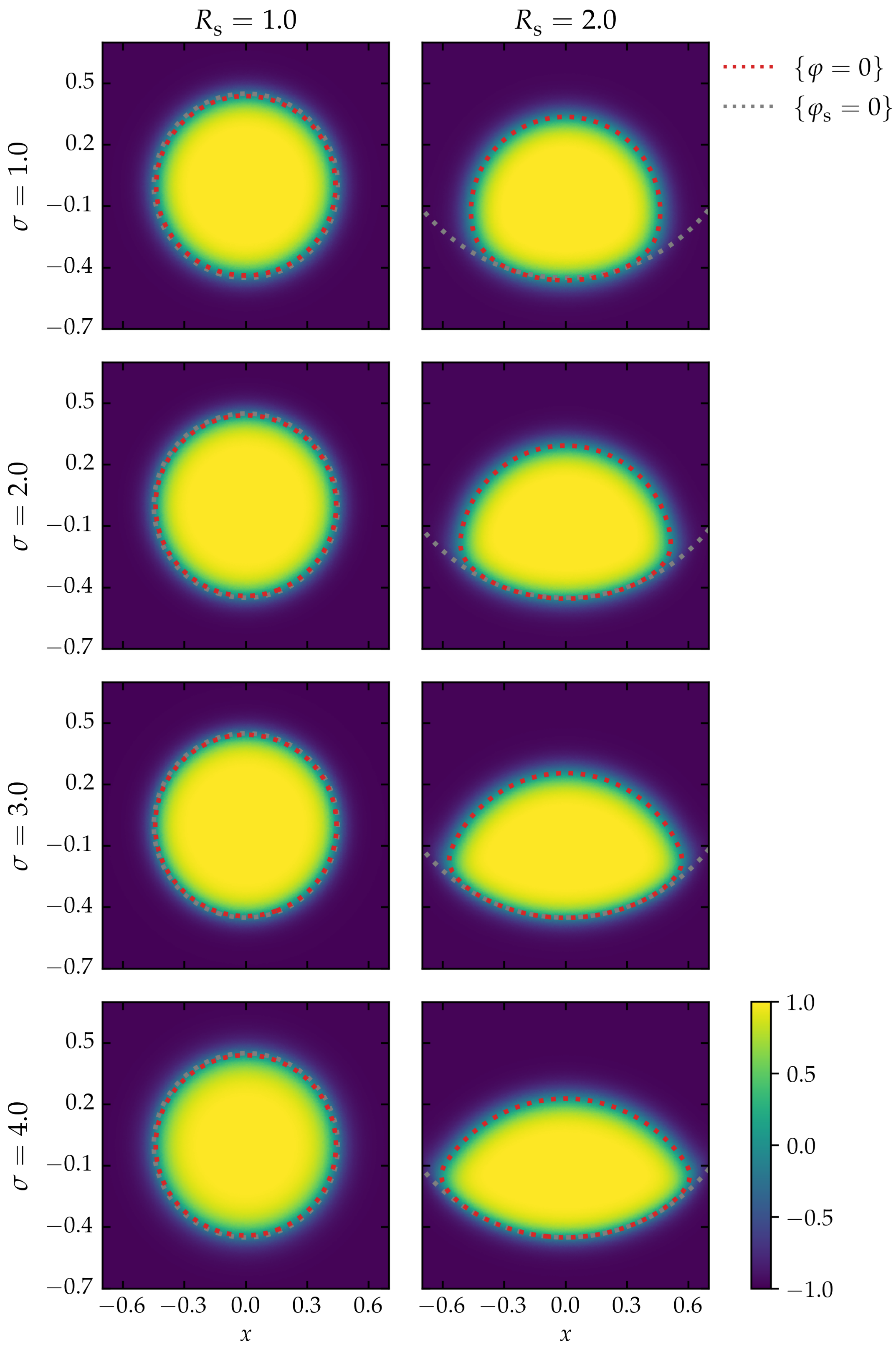

Figure 11.18: Adhesion on a concave substrate for $\varepsilon = 0.05$**.** 2-D results at $T = 0.8$ for lower values of R_s and for various adhesive strengths σ. The 0-level set of the adhesive phase-field φ and the substrate ϕ_s are plotted as dotted lines.

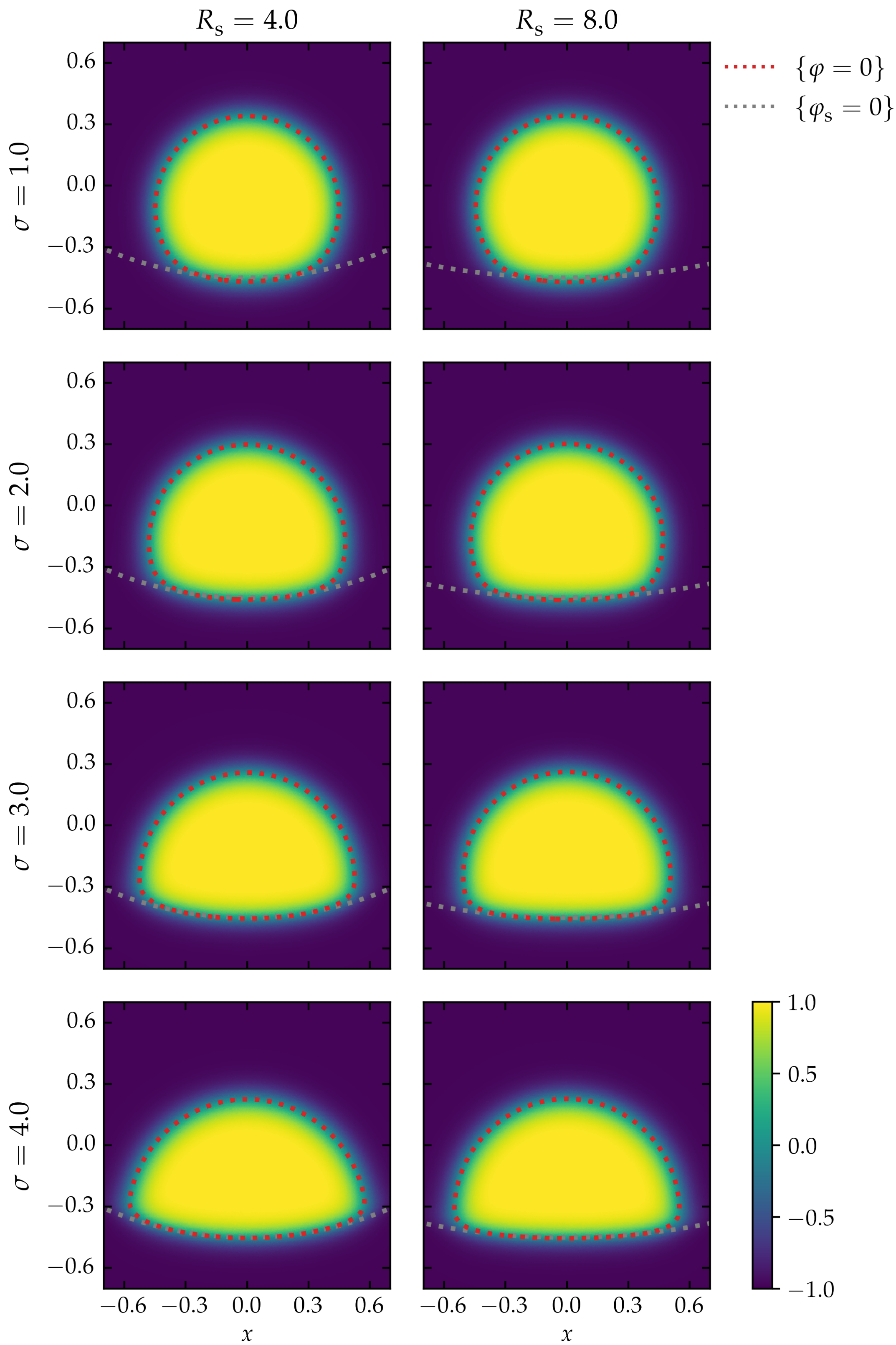

Figure 11.19: Adhesion on a concave substrate for $\varepsilon = 0.05$**.** 2-D results at $T = 0.8$ for higher values of R_s and for various adhesive strengths σ. The 0-level set of the adhesive phase-field φ and the substrate ϕ_s are plotted as dotted lines.

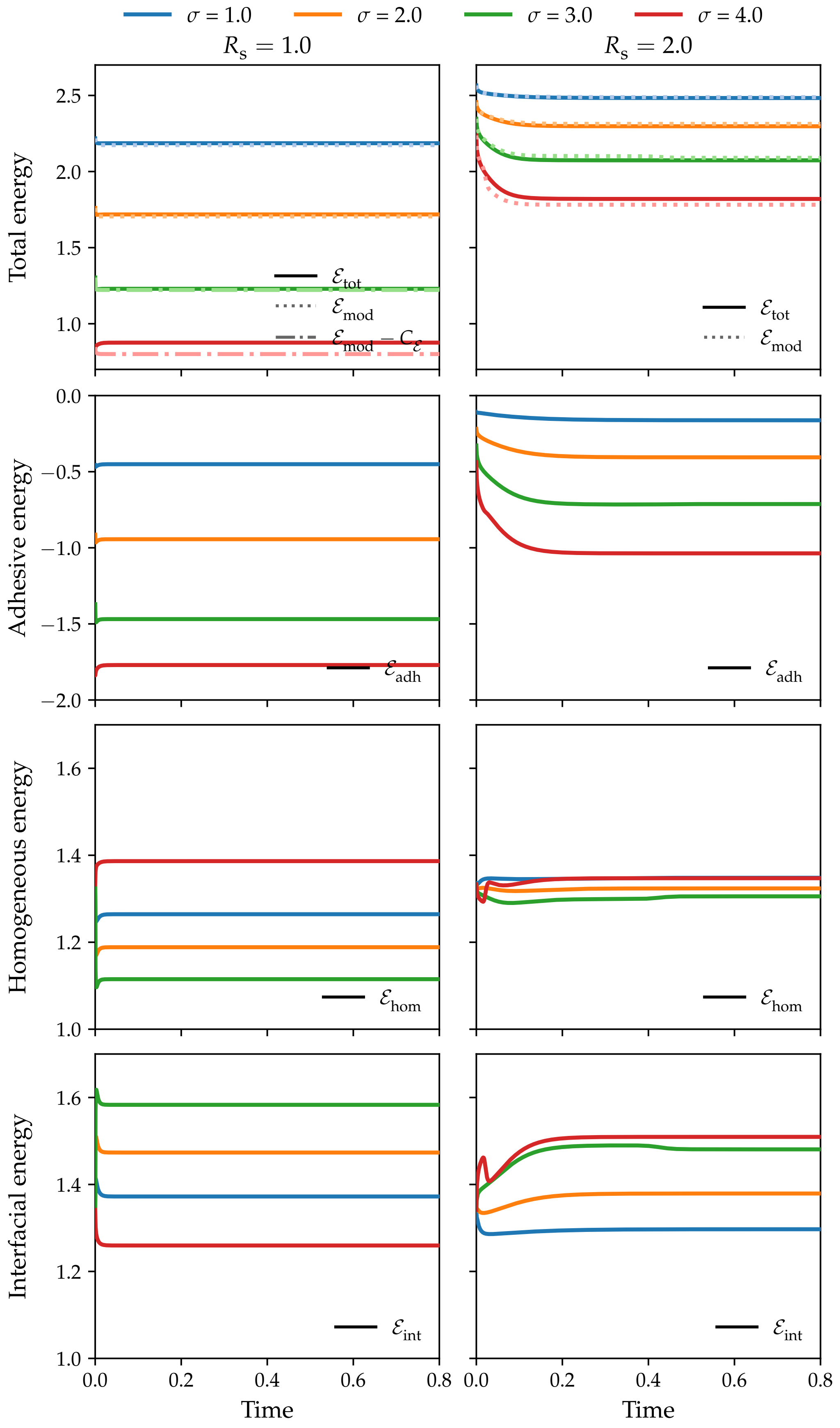

Figure 11.20: Adhesion on a concave substrate for $\varepsilon = 0.05$**.** Energy results showing the total energy $\mathcal{E}_{\text{tot}}$, modified energy $\mathcal{E}_{\text{mod}}$, adhesive energy $\mathcal{E}_{\text{adh}}$, homogeneous energy $\mathcal{E}_{\text{hom}}$ and interfacial energy $\mathcal{E}_{\text{int}}$ over time for various adhesive strengths σ and for lower values R_s governing the substrate's curvature.

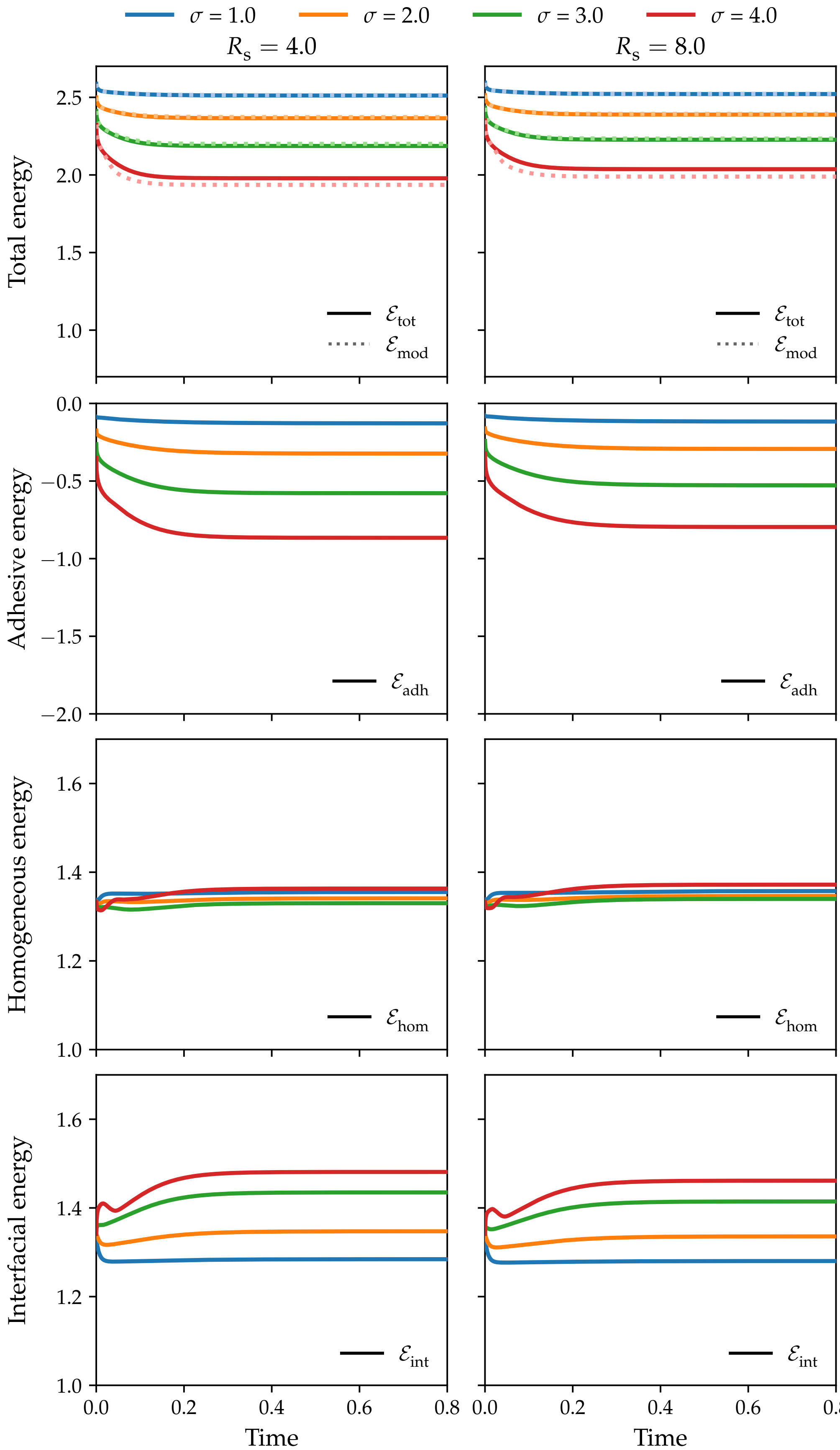

Figure 11.21: Adhesion on a concave substrate for $\varepsilon = 0.05$. Energy results showing the total energy $\mathcal{E}_{\text{tot}}$, modified energy $\mathcal{E}_{\text{mod}}$, adhesive energy $\mathcal{E}_{\text{adh}}$, homogeneous energy $\mathcal{E}_{\text{hom}}$ and interfacial energy $\mathcal{E}_{\text{int}}$ over time for various adhesive strengths σ and for higher values R_s governing the substrate's curvature.

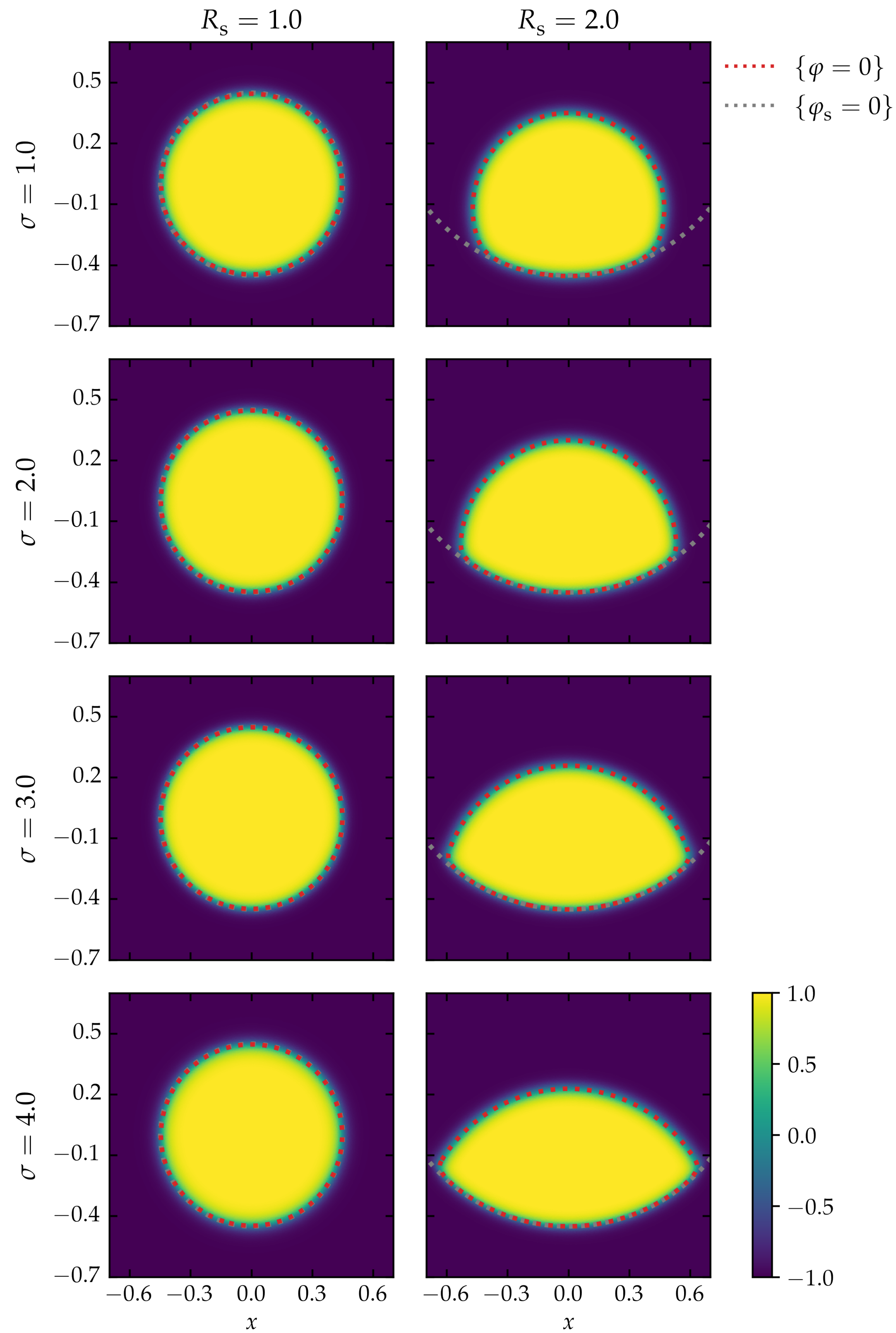

Figure 11.22: Adhesion on a concave substrate for $\varepsilon = 0.025$**.** 2-D results at $T = 0.8$ for lower values of R_s and for various adhesive strengths σ. The 0-level set of the adhesive phase-field φ and the substrate ϕ_s are plotted as dotted lines.

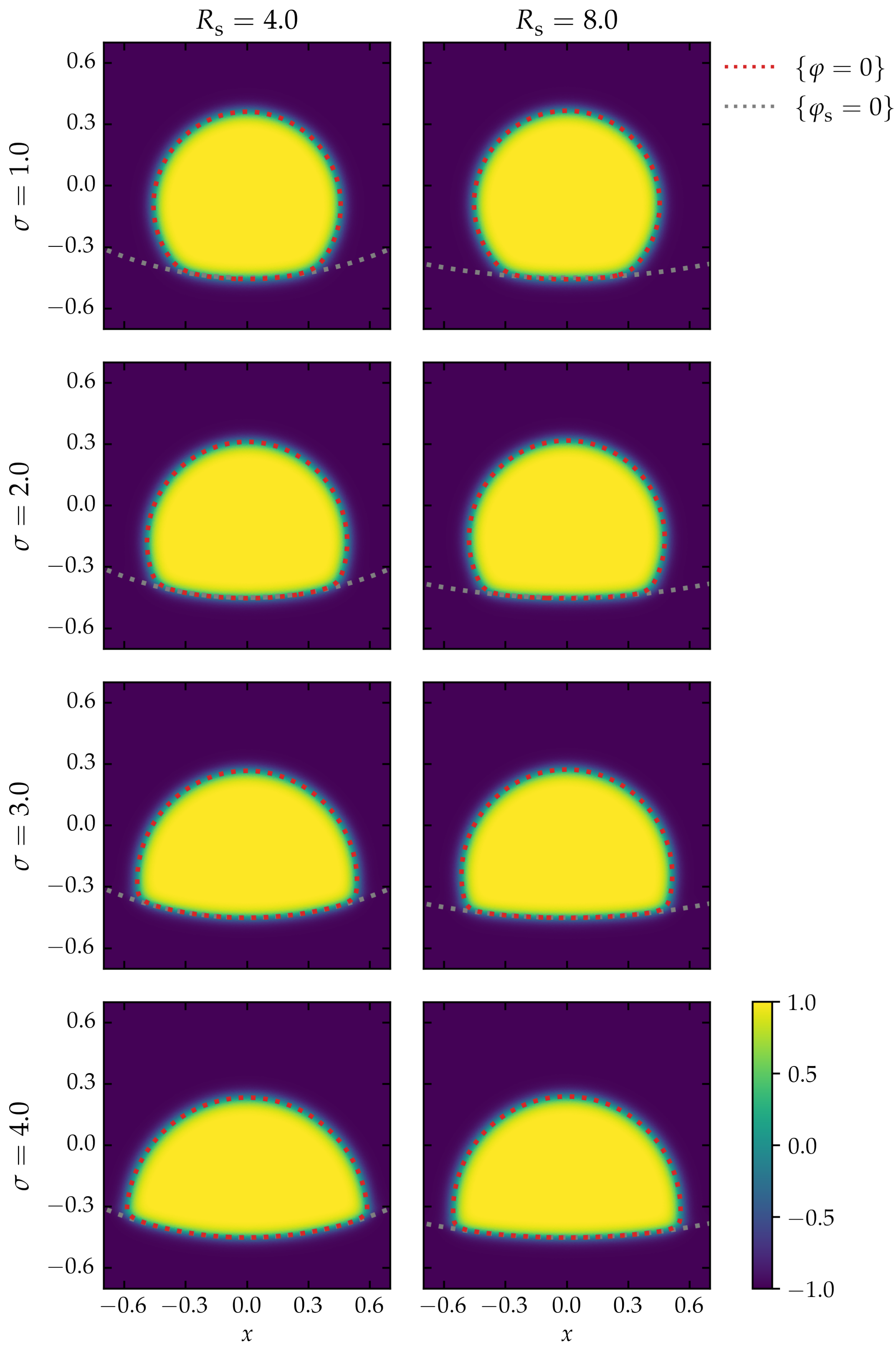

Figure 11.23: Adhesion on a concave substrate for $\varepsilon = 0.025$**.** 2-D results at $T = 0.8$ for higher values of R_s and for various adhesive strengths σ. The 0-level set of the adhesive phase-field φ and the substrate ϕ_s are plotted as dotted lines.

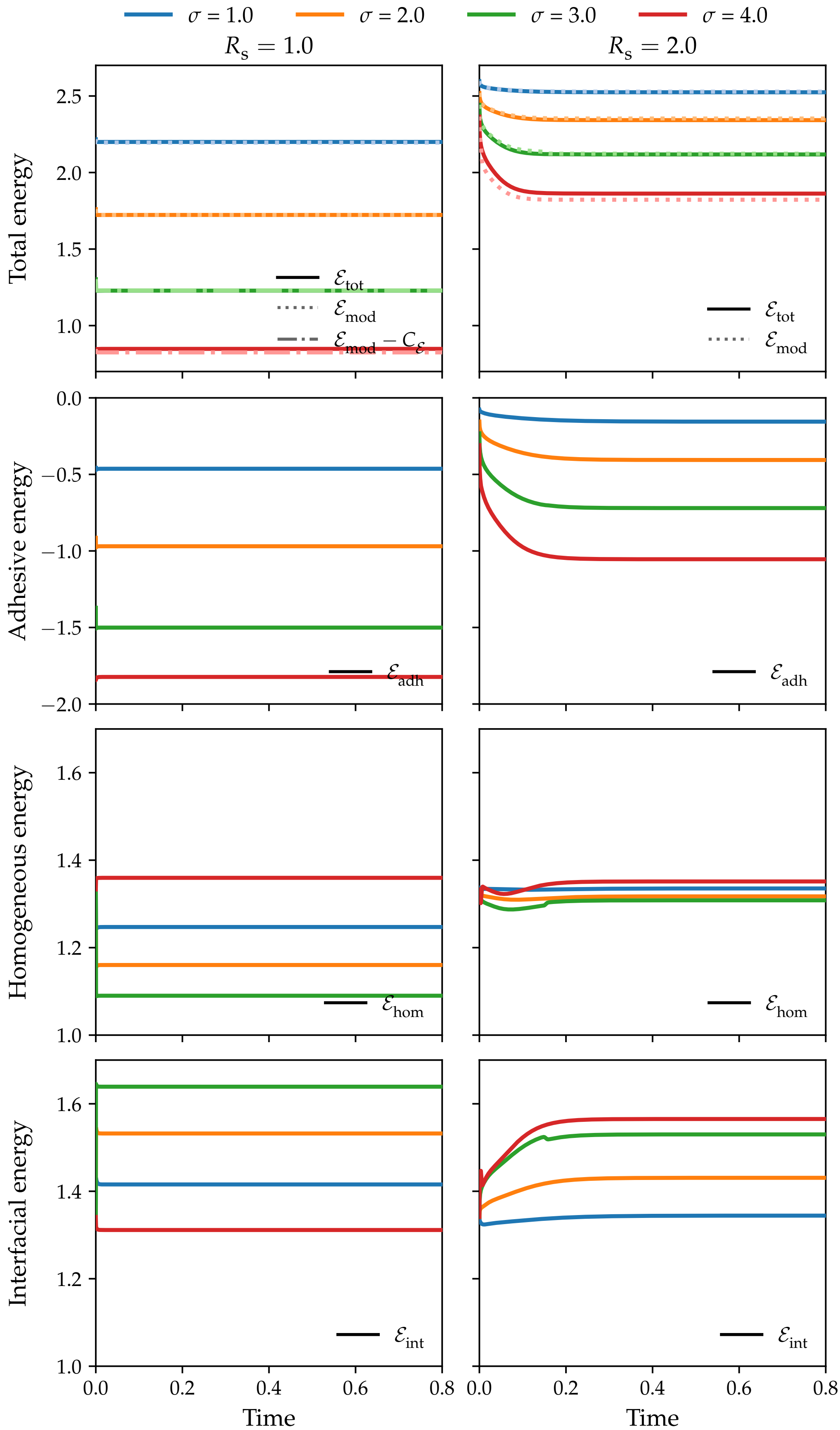

Figure 11.24: Adhesion on a concave substrate for $\varepsilon = 0.025$**.** Energy results showing the total energy $\mathcal{E}_{\text{tot}}$, modified energy $\mathcal{E}_{\text{mod}}$, adhesive energy $\mathcal{E}_{\text{adh}}$, homogeneous energy $\mathcal{E}_{\text{hom}}$ and interfacial energy $\mathcal{E}_{\text{int}}$ over time for various adhesive strengths σ and for lower values R_s governing the substrate's curvature.

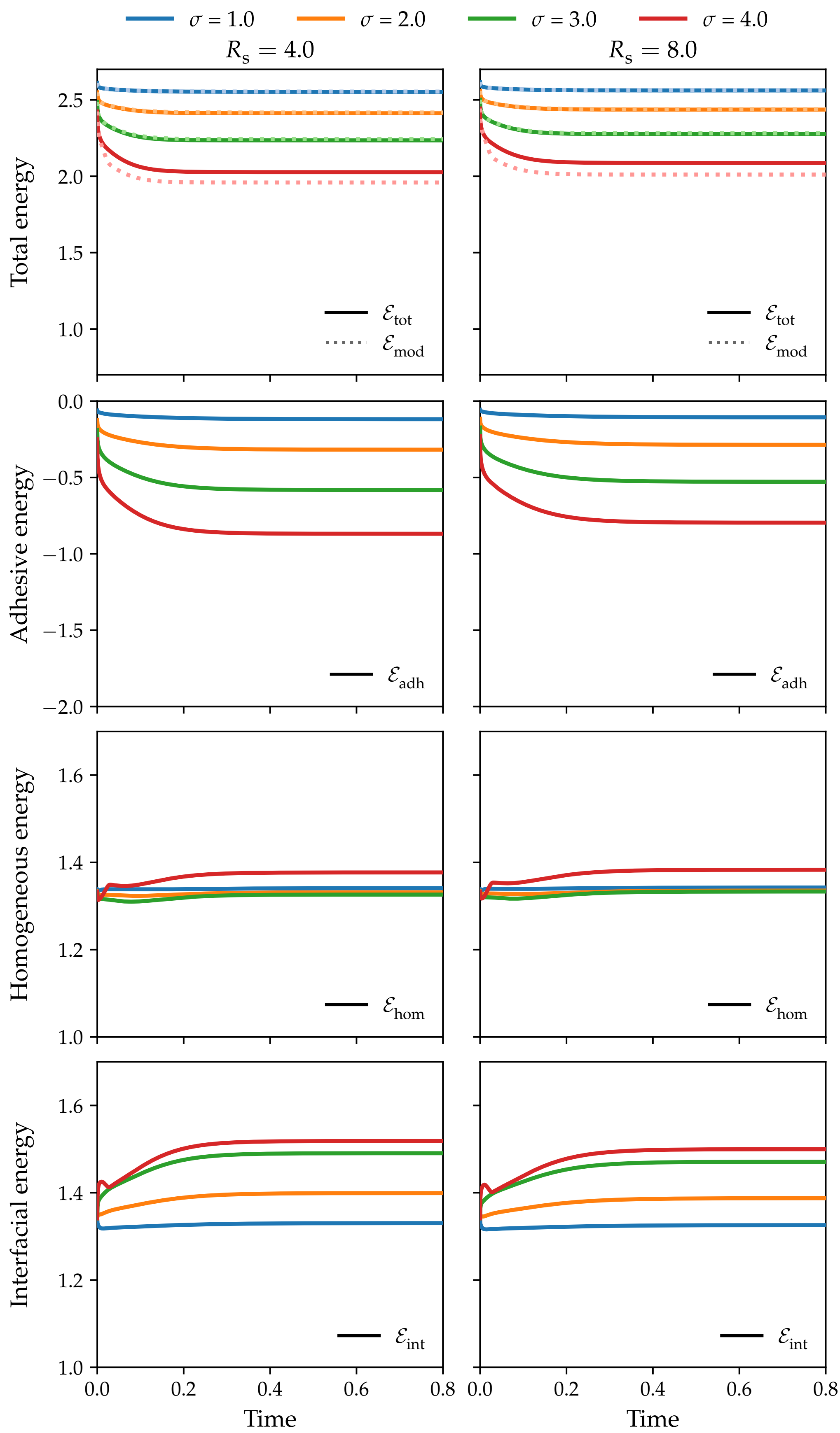

Figure 11.25: Adhesion on a concave substrate for $\varepsilon = 0.025$**.** Energy results showing the total energy $\mathcal{E}_{\text{tot}}$, modified energy $\mathcal{E}_{\text{mod}}$, adhesive energy $\mathcal{E}_{\text{adh}}$, homogeneous energy $\mathcal{E}_{\text{hom}}$ and interfacial energy $\mathcal{E}_{\text{int}}$ over time for various adhesive strengths σ and for higher values R_{s} governing the substrate's curvature.

11.3 2-D two phase-field adhesion

We consider the multi-phase adhesion problem presented in Section 8.2 for two phase-field variables ($k = 2$) on the domain $\Omega = [-1.5, 1.5] \times [-1.0, 1.0]$ for $t \in [0, T]$, with final time $T = 0.8$. We supply the system with the following initial condition

$$\varphi_i(\boldsymbol{x}, 0) = \tanh\left(\frac{R - |\boldsymbol{C}_i - \boldsymbol{x}|}{\sqrt{2}\varepsilon}\right), \qquad i = 1, 2. \tag{11.25}$$

with $R = 0.45$, $\boldsymbol{C}_1 = (-R, 0)$ and $\boldsymbol{C}_2 = (R, 0)$. In addition, we consider the double-well function (11.21) and regularizing function (11.22) in Section 11.2.1. The simulation parameters used to obtain the numerical results presented in this Section are provided in Table 11.2.

Table 11.2: Simulation parameters used in the two-phase adhesion simulations.

interfacial thickness ε	time step size τ	number of elements along the (longer) domain boundary n_{elem}
0.05	$2 \cdot 10^{-4}$	120
0.025	$25 \cdot 10^{-6}$	240

In Figures 11.26 and 11.27 the phase-field variables over time are plotted on a subregion of the domain $\Omega_{\text{sub}} = [-0.4, 1.0] \times [-0.7, 0.7]$ for $\varepsilon = 0.05$. The 0-level sets show that the shared part of the diffuse interface becomes larger for larger values of the adhesive strength $\sigma := \sigma_{12} = \sigma_{21}$. Similar results can be found in Figures 11.28 and 11.29, where the phase-field variables over time are plotted for $\varepsilon = 0.025$ on Ω_{sub}. From the energy plots in Figure 11.30 for $\varepsilon = 0.05$ and in Figure 11.31, we conclude that the solution at $t = 0.8$ has reached its steady state. Again, similar to the results presented in Section 11.2, we find that the adhesive interaction is stronger for smaller ε in terms of diffuse adhesion length, yet that this does not per se imply lower absolute values in adhesion (and total) energy. Lastly, although only a subregion of the domain is shown in Figures 11.26, 11.27, 11.28 and 11.29, both phase-field variables show the same shape evolution over time in a reflected manner about the y-axis.

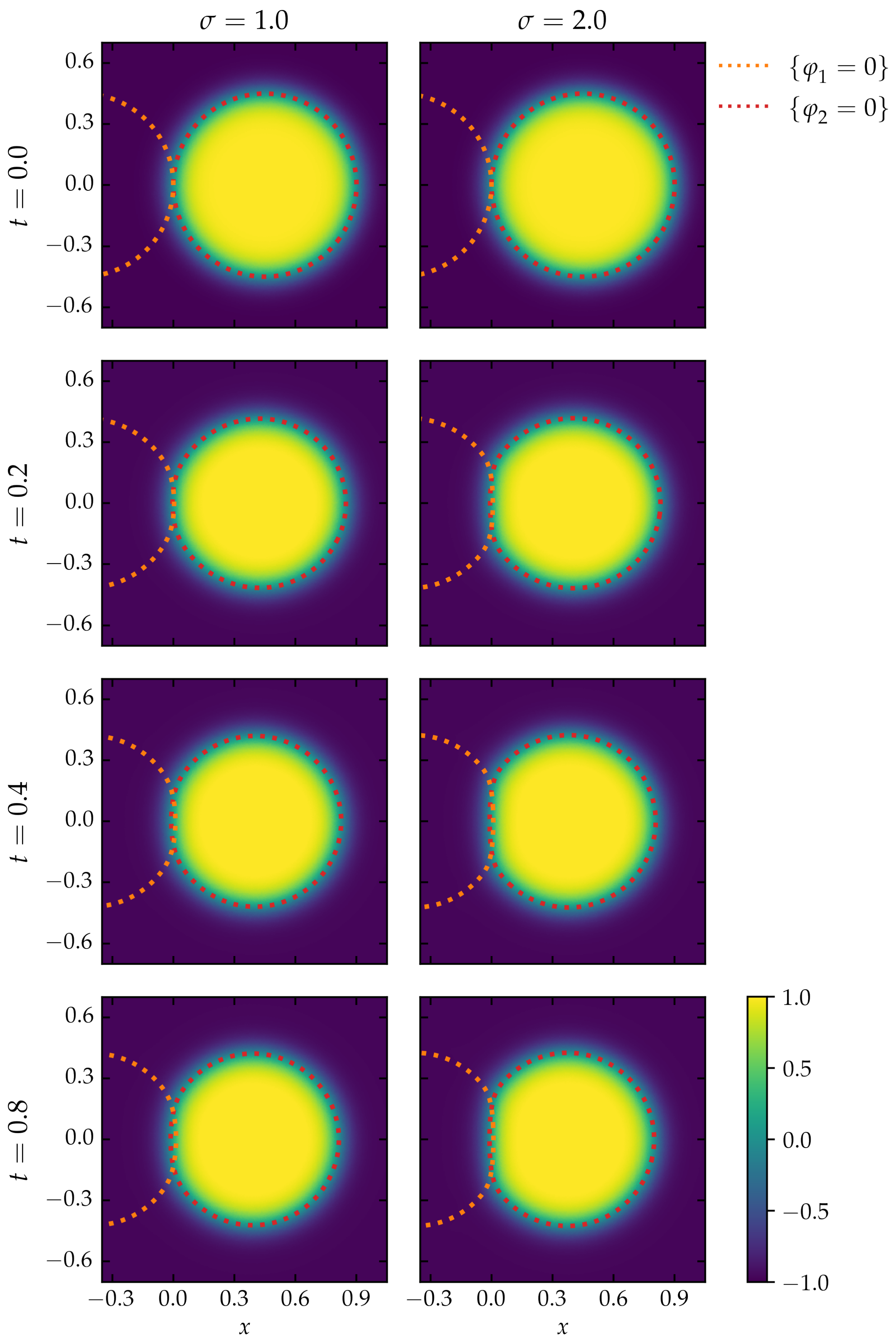

Figure 11.26: Adhesion between two phase fields for $\varepsilon = 0.05$. 2-D results at various times for lower values of the adhesive strength σ. The 0-level set of both phase fields are plotted as dotted lines.

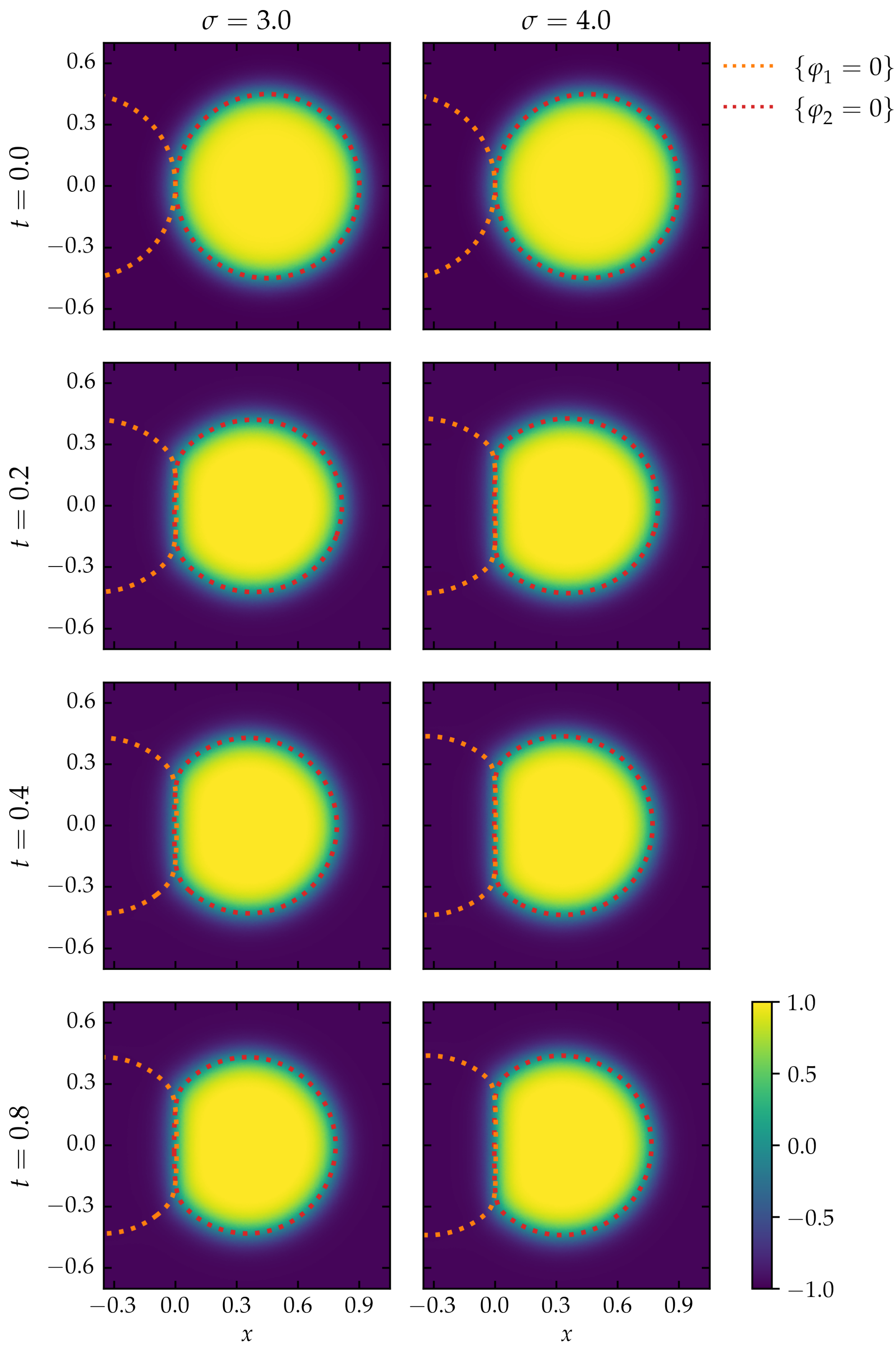

Figure 11.27: Adhesion between two phase fields for $\varepsilon = 0.05$**.** 2-D results at various times for higher values of the adhesive strength σ. The 0-level set of both phase fields are plotted as dotted lines.

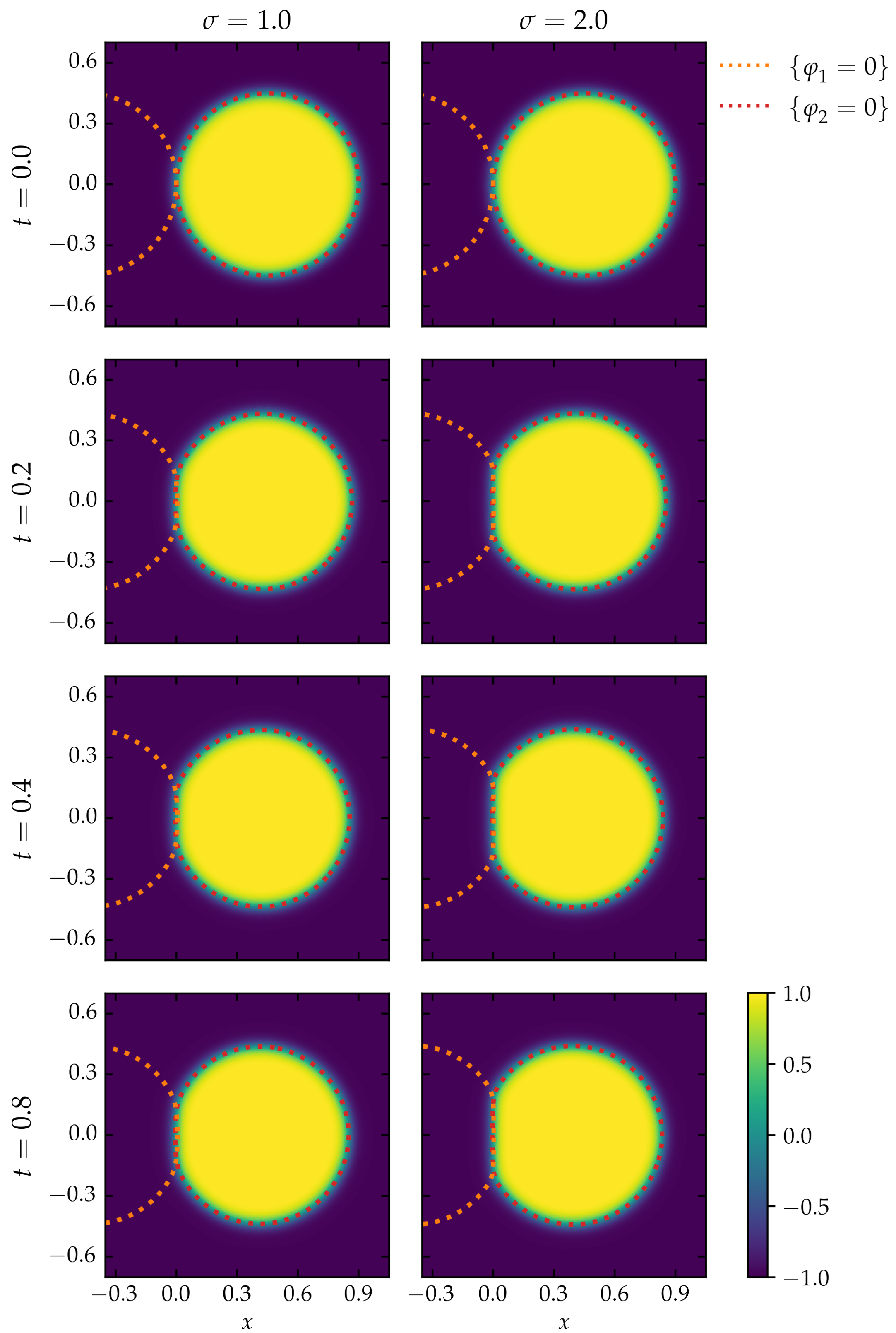

Figure 11.28: Adhesion between two phase fields for $\varepsilon = 0.025$**.** 2-D results at various times for lower values of the adhesive strength σ. The 0-level set of both phase fields are plotted as dotted lines.

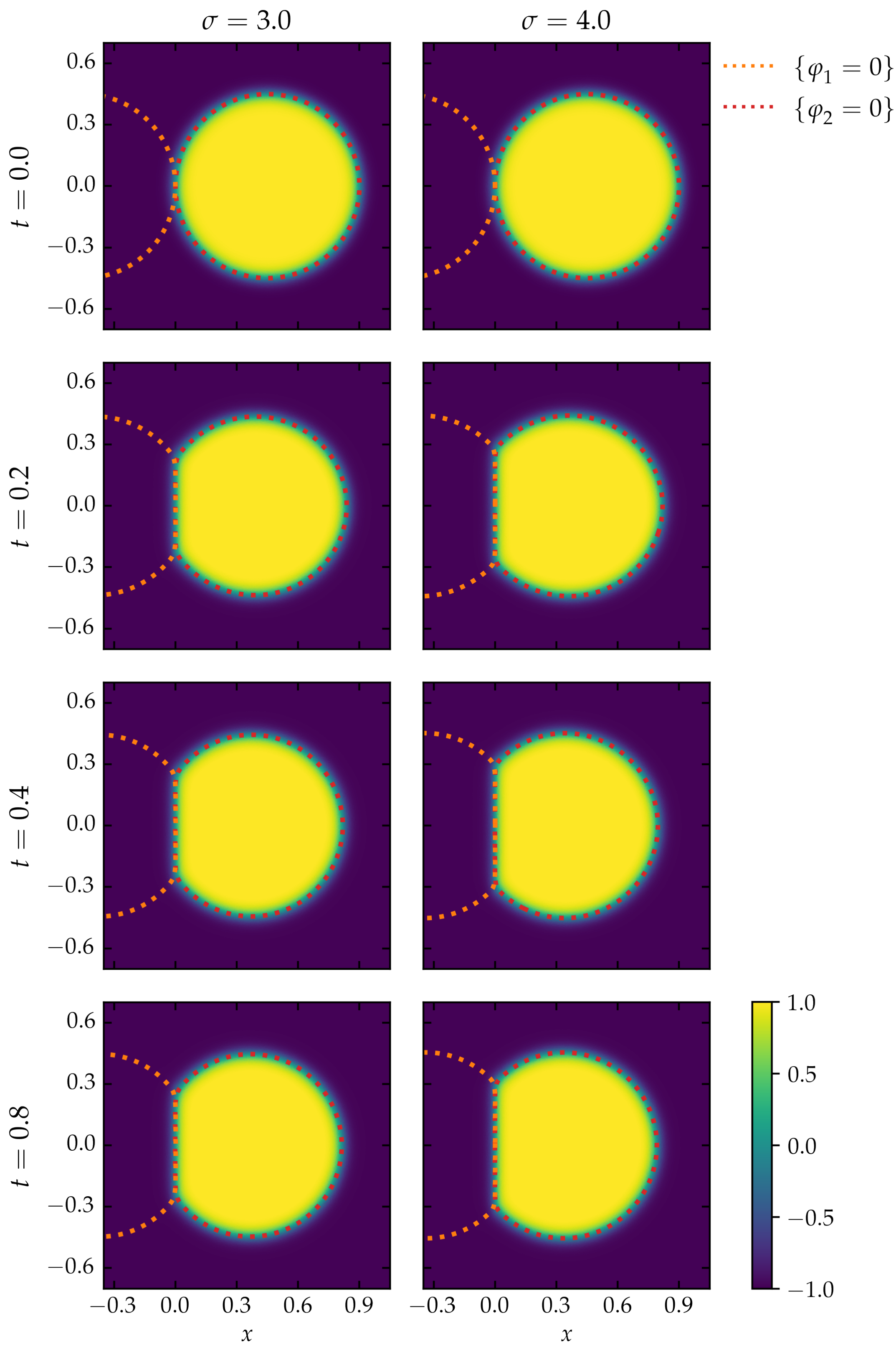

Figure 11.29: Adhesion between two phase fields for $\varepsilon = 0.025$**.** 2-D results at various times for higher values of the adhesive strength σ. The 0-level set of both phase fields are plotted as dotted lines.

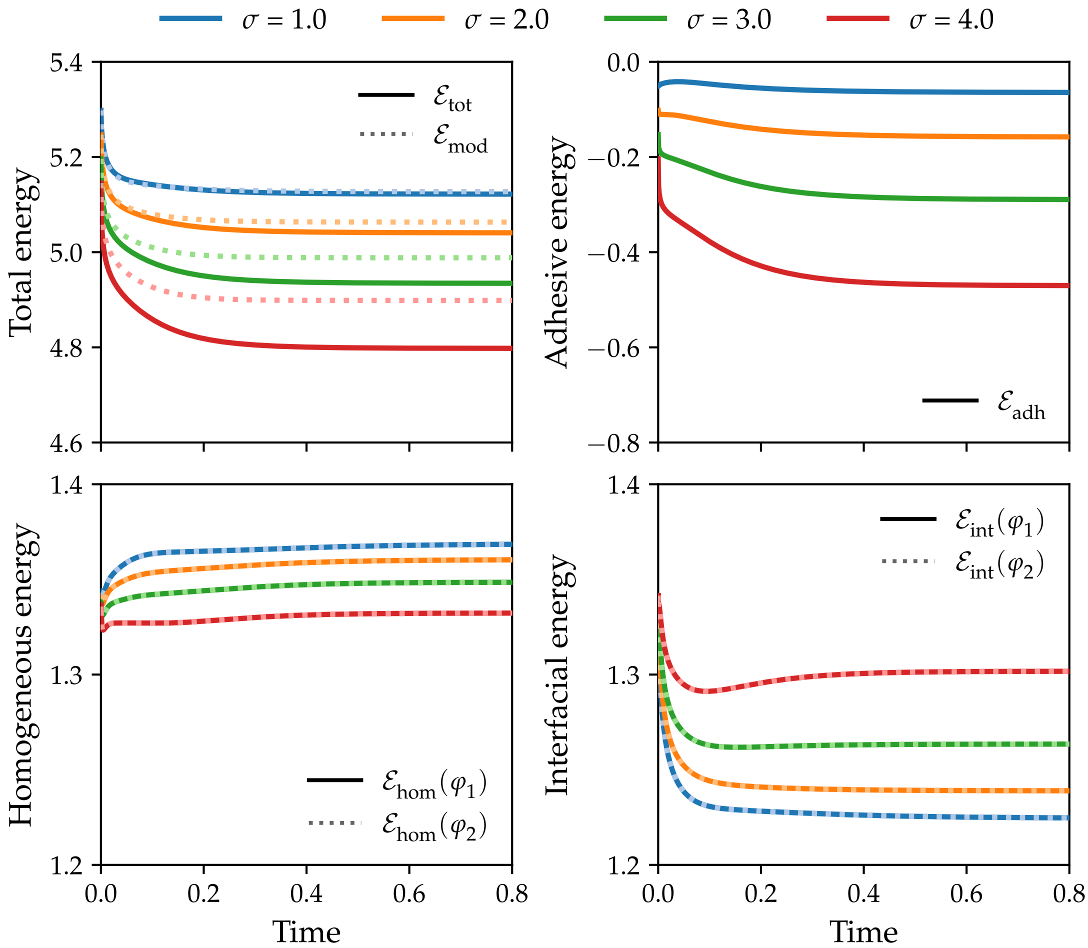

Figure 11.30: Energies over time for adhesion between two phase fields for $\varepsilon = 0.05$. Energy results showing the total energy $\mathcal{E}_{\mathrm{tot}}$, modified energy $\mathcal{E}_{\mathrm{mod}}$, adhesive energy $\mathcal{E}_{\mathrm{adh}}$, homogeneous energy $\mathcal{E}_{\mathrm{hom}}$ and interfacial energy $\mathcal{E}_{\mathrm{int}}$ over time for various adhesive strengths σ.

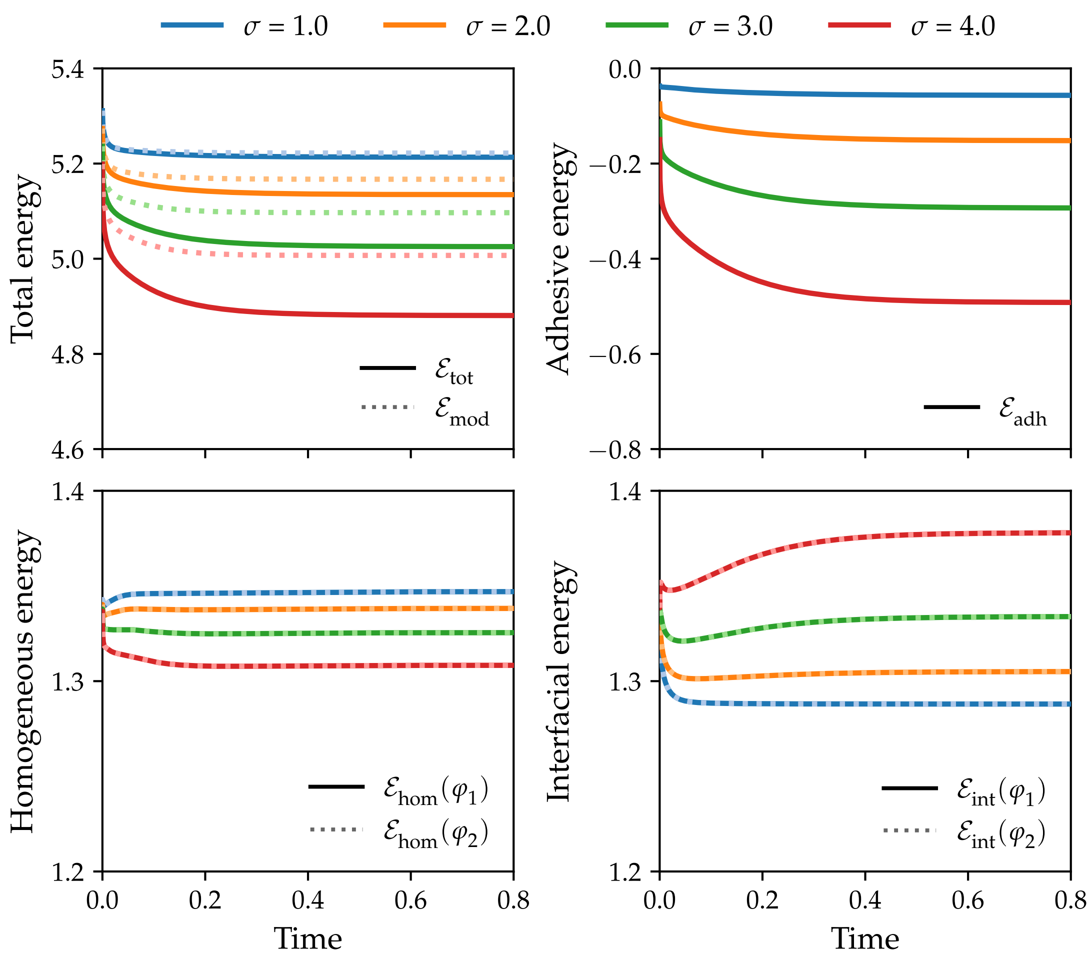

Figure 11.31: Adhesion between two phase fields for $\varepsilon = 0.025$. Energy results showing the total energy $\mathcal{E}_{tot}$, modified energy $\mathcal{E}_{mod}$, adhesive energy $\mathcal{E}_{adh}$, homogeneous energy $\mathcal{E}_{hom}$ and interfacial energy $\mathcal{E}_{int}$ over time for various adhesive strengths σ.

Chapter 12

Concluding Remarks

In this Part, we developed phase-field models that capture adhesive interactions between steady and moving diffuse interfaces. The mathematical framework of this theory is based on the variational framework detailed in Chapter 4. The adhesion model is founded on the classical Ginzburg-Landau energy functional with an additional contribution accounting for the adhesive effect between the two interacting interfaces. This effect is restricted to the shared diffuse interfaces using regularizing terms. By making appropriate choices for the constitutive equations, we arrive at a set of thermodynamically-consistent phase-field equations.

To characterize the behaviour of steady states, we presented a formal asymptotic framework, which is extendable to a wider class of phase-field problems. Within this framework, we studied the adhesion energy functional and its associated minimizers in the sharp-interface limit. In particular, we established bounds on the parameter regulating the adhesive interaction. Furthermore, we demonstrated that the sharp-interface minimizers are piecewise smooth surfaces consisting of a non-adhered boundary part and a non-trivial adhered boundary part. The adhesion angle and curvature of the non-adhered part are determined by the adhesion strength and the mass constraint. The effect of the adhesion strength, curvature and interface thickness have also been numerically investigated using energy-stable schemes, which can efficiently deal with the underlying gradient-flow structure of these phase-field adhesion models.

We envision that the phase-field theories presented in this work may particularly be interesting to use in the context of active interfaces. The current framework can be extended in a straightforward manner to allow for additional surface dynamics through regularized surface partial differential equations [140]. It is known that heterogeneities on the surface may lead to contact angle and adhesion hysteresis. [94]. Furthermore, in cellular biomechanics, transmembrane proteins are essential for the formation of bonds between the cell membrane they live on and entities exterior to the cell membrane [93, 95]. An additional surface partial differential equation could be introduced accounting for the transport and dynamics of these transmembrane proteins. Then, the adhesion strength parameter should be made dependent on the surface concentration of these membrane proteins in an appropriate manner, so that the local adhesive interactions are induced by the presence of the dynamics of these proteins.

Part III

A Bulk-Surface Continuum Theory for Fluid Flows and Phase Separation

The Chapters in this Part have been accepted for publication as A. BOSCHMAN, L. ESPATH, AND K. VAN DER ZEE, *A bulk-surface continuum theory for fluid flows and phase segregation with finite surface thickness*, Physica D (2024) [16].

Chapter 13

Introduction and Preliminaries

The last Part of this work focusses on bulk-surface materials undergoing deformation and phase separation. The motivation to develop a continuum framework for these coupled materials is presented in Section 13.1. The main objectives and outline of this last Part are detailed in Section 13.2. In Section 13.3, preliminary concepts are defined, which are relevant for the development of the continuum theory presented in the subsequent Chapters.

13.1 Bulk-surface systems with material interfaces

Bulk-surface models have been developed to study a wide range of interfacial phenomena, from flows of emulsions, foams stabilized by surfactants to cell dynamics governed by proteins at the cell membrane. Key to these models is the idea that the dynamics are not solely restricted to a bulk material, but that an active surface coating the bulk material, that is, a surface with its own dynamics, also dictates the overall material behaviour. Typically, these systems involve species adsorption from a bulk material onto a surface, giving rise to the particular dynamics on the surface. These interactions may result in the motion of the surface, which in turn can cause bulk material deformation and vice versa. This bulk-surface reciprocal interplay is the focus of this Part.

In modelling approaches, these interfaces are either treated as *material* surfaces or as *non-material* surfaces that migrate with the bulk material. Non-material interfaces are defined through a microscopic viewpoint of the surface, in which the surface is seen as a thin diffuse three-dimensional transition region between two relatively homogeneous bulk phases. The material approach, on the other hand, considers a macroscopic viewpoint, in which the surface appears as a two-dimensional, singular surface. Characteristic of the material approach is that it does not allow for bulk mass transfer across the material surface, yet, diffusive transport of solute species is still possible.

There is a vast literature on the physics and thermochemistry of these surfaces, including studies into adsorption phenomena, see for instance the works by Adam [3], Adamson & Gast [4] and Edwards, Brenner & Wasan [48]. Key contributions, in which the underlying rational mechanics of material surfaces were systematically derived using modern continuum mechanics, were made by Gurtin & Murdoch (1975) [82]. They developed a mathematical framework to study the elastic behaviour of material surfaces. According to Gurtin & Murdoch, arguments for the validity of such a macroscopic approach and its use in understanding surface behaviour were already presented by Herring (1953) [90].

Another important contribution to the study of surface dynamics is the work by Scriven (1960) [148] on fluid films. In this work, a general formulation for the dynamics of a Newtonian fluid interface is derived. In line with Boussinesq's stipulations (1913)

[18], a linear dependence of stress on the rate of strain in the interface is considered, resulting in interfacial fluid behaviour characterized by Boussinesq's two coefficients of surface viscosity, as well as a coefficient representing its interfacial tension. In addition, consideration of the coupling between the surface and bulk material by Scriven yields dynamic boundary conditions for two-phase bulk flows. Later, Levich (1962) [106] proposed that surface stresses may be induced by surface tension gradients, which are in turn due to the presence of surfactants.

Motivation for these bulk-surface continuum theories can for instance be found in biological systems. Cells may mathematically be described as a bulk material (cytoplasm) enclosed by a surface (cell membrane). Their mechanobiology involves various complex processes, as Ladoux & Mège [101, Figure 1a] illustrate, which in turn determine the shape of these cells. In particular, during adhesion cells may take saucer-shaped forms. To fully understand the underlying mechanical behaviour of these cells and such adhesive processes, the tractions developed on the edges need to be accounted for. Considering arbitrary geometries, including those with a boundary that may lose its smoothness, requires certain modifications and further generalization of continuum theories, as shown by Espath [52] for the Navier-Stokes equations. Furthermore, Brangwynne [19] and Shin & Brangwynne [153] suggest that membrane-less organelles are formed by regulated phase-segregation processes within the cytoplasm. In these works, the authors capitalize on the physics of polymer phase separation. Current frameworks that may capture the dynamics of these biological cells to some extent include the work by Madzvamuse et al. [117], who present a reaction-diffusion for bulk-surface systems suitable to model cell polarization but do not include phase segregation and motion. Similarly, Duda et al. [45] investigate bulk-surface systems for cell adsorption/desorption and chemical reactions for classical diffusion.

13.2 Objectives and outline

The objective of this work is to present a comprehensive continuum theory for bulk-surface materials undergoing deformation and phase separation. In particular, we consider an immiscible binary bulk fluid enclosed by a thin immiscible binary fluid film. We treat this thin film as a material surface with a small, yet finite, surface thickness. This surface fluid exhibits its own dynamics, and as a result the mechanical laws ruling the bulk and surface dynamics are coupled.

Both the bulk fluid and the enclosing thin film of fluid are only allowed to undergo isochoric motions, that is, both flows are incompressible. Isochoric motion within the bulk implies no change in volume. In addition, the pressure found in the bulk fluid does not affect the stress power. However, isochoric motion within the surface fluid does not impose the same restrictions on changes in surface area, as the thickness of the thin fluid film may change. Based on this hypothesis, we derive the mass balance equations for the bulk and surface material. This formalism is detailed in Chapter 14, in which we also present the balances accounting for the mass transport of the two species present in the bulk-surface system.

Next, in Chapter 15, we extend the principle of virtual power presented for phase-fields with bulk-surface dynamics by Espath [53, 54], and present the coupled bulk-surface principle of virtual power for systems undergoing deformation. We postulate the virtual power balance assuming that the material surface may lose smoothness, viz. the normal field may be discontinuous at an edge, thereby accounting for power expenditures across edges.

In Chapter 16, the thermodynamics of the system and its implications in terms of constitutive equations are discussed. Among other things, we derive the general form for the bulk and surface fluid stresses depending linearly on the rate of strain in the bulk or surface material, respectively. We conclude this Chapter by presenting the specialized equations for a bulk-surface system undergoing phase separation.

In Chapter 17, we supplement the system with appropriate boundary conditions, including a set of mixed boundary conditions that allow for slip between the surface and the bulk material, which are dissipative in nature. These boundary conditions are employed to arrive at the Lyapunov decay relation for the coupled bulk-surface material, which characterizes the dissipative nature of the bulk-surface system and its interaction with the environment.

Lastly, Chapter 18 bears concluding remarks and directions for future research.

13.3 Preliminary definitions

In the following Subsections, we present the preliminary definitions used to the develop the mathematical framework in the subsequent Chapters. In Subsection 13.3.1, we define the differential operators on surfaces, and in Subsection 13.3.2 the integral theorems on surfaces are presented. Lastly, in Subsection 13.3.3 the material and spatial time derivatives of both bulk and surface fields are defined.

13.3.1 Differential operators on surfaces

Consider the smooth scalar, vector, and tensor fields denoted by κ, $\boldsymbol{\kappa}$, and $\mathbf{K}$, respectively, defined on a smooth surface $\mathcal{S}$ oriented by the outward unit normal $\boldsymbol{n}$ at $\boldsymbol{x} \in \mathcal{S}$. In what follows, we define the differential operators. Bear in mind that we allow the fields κ, $\boldsymbol{\kappa}$, and $\mathbf{K}$ to have smooth normal extensions, enabling us to define the relevant differential operators in a neighbourhood of $\mathcal{S}$ along all directions. The gradients can be written in the following form

$$\operatorname{grad}\kappa = \partial_n\kappa\,\boldsymbol{n} + \partial_p\kappa\,\boldsymbol{e}^p, \qquad \text{with} \qquad p = 1,2, \tag{13.1}$$

and

$$\operatorname{grad}\boldsymbol{\kappa} = \partial_n\boldsymbol{\kappa} \otimes \boldsymbol{n} + \partial_p\boldsymbol{\kappa} \otimes \boldsymbol{e}^p, \qquad \text{with} \qquad p = 1,2, \tag{13.2}$$

where $\boldsymbol{e}^p$ are tangential to $\mathcal{S}$ and defined by $\boldsymbol{e}_p = \partial_p\boldsymbol{x}$ for all $\boldsymbol{x} \in \mathcal{S}$. Next, let $\mathbf{P}_n := \mathbf{P}_n(\boldsymbol{n})$ denote the projector onto the plane defined by $\boldsymbol{n}$ at $\boldsymbol{x} \in \mathcal{S}$, which reads

$$\mathbf{P}_n := \mathbf{1} - \boldsymbol{n} \otimes \boldsymbol{n} = \mathbf{P}_n^\top, \tag{13.3}$$

where $(\cdot)^\top$ represents the transposition. In view of (13.3) and the expressions (13.1) and (13.2), the surface gradient of a scalar and vector field are, respectively, written as

$$\operatorname{grad}_{\mathcal{S}}\kappa := \partial_p\kappa\,\boldsymbol{e}^p = \mathbf{P}_n\operatorname{grad}\kappa, \qquad \text{with} \qquad p = 1,2, \tag{13.4}$$

and

$$\operatorname{grad}_{\mathcal{S}}\boldsymbol{\kappa} := \partial_p\boldsymbol{\kappa} \otimes \boldsymbol{e}^p = (\operatorname{grad}\boldsymbol{\kappa})\mathbf{P}_n, \qquad \text{with} \qquad p = 1,2. \tag{13.5}$$

Furthermore, the surface divergence for a vector field reads

$$\operatorname{div}_{\mathcal{S}}\boldsymbol{\kappa} := \partial_p\boldsymbol{\kappa} \cdot \boldsymbol{e}^p = \operatorname{grad}\boldsymbol{\kappa} : \mathbf{P}_n, \qquad \text{with} \qquad p = 1,2, \tag{13.6}$$

and is for a tensor field given by

$$\operatorname{div}_{\mathcal{S}}\mathbf{K} := \partial_p\mathbf{K} \cdot \boldsymbol{e}^p = \operatorname{grad}\mathbf{K} : \mathbf{P}_n, \qquad \text{with} \qquad p = 1,2. \tag{13.7}$$

Lastly, the Laplace–Beltrami operator may be written as

$$\triangle_{\mathcal{S}}\kappa := \operatorname{div}_{\mathcal{S}}\operatorname{grad}_{\mathcal{S}}\kappa = \operatorname{grad}(\mathbf{P}_n\operatorname{grad}\kappa) : \mathbf{P}_n, \tag{13.8}$$

and

$$\triangle_{\mathcal{S}}\boldsymbol{\kappa} := \operatorname{div}_{\mathcal{S}}\operatorname{grad}_{\mathcal{S}}\boldsymbol{\kappa} = \operatorname{grad}((\operatorname{grad}\boldsymbol{\kappa})\mathbf{P}_n) : \mathbf{P}_n. \tag{13.9}$$

13.3.2 Integral theorems on surfaces

On a smooth, closed and oriented surface $\mathcal{S}$, the surface divergence theorem for the smooth vector and tensor fields $\boldsymbol{\kappa}$ and $\mathbf{K}$ states that

$$\int_{\mathcal{S}} \operatorname{div}_{\mathcal{S}}(\mathbf{P}_n\boldsymbol{\kappa})\,\mathrm{d}a = 0, \qquad \text{and} \qquad \int_{\mathcal{S}} \operatorname{div}_{\mathcal{S}}(\mathbf{K}\mathbf{P}_n)\,\mathrm{d}a = \mathbf{0}, \tag{13.10}$$

whereas, on a smooth, open and oriented surface $\mathcal{S}$, the surface divergence theorem reads

$$\int_{\mathcal{S}} \operatorname{div}_{\mathcal{S}}(\mathbf{P}_n\boldsymbol{\kappa})\,\mathrm{d}a = \int_{\partial\mathcal{S}} \boldsymbol{\kappa}\cdot\boldsymbol{\nu}\,\mathrm{d}\sigma, \qquad \text{and} \qquad \int_{\mathcal{S}} \operatorname{div}_{\mathcal{S}}(\mathbf{K}\mathbf{P}_n)\,\mathrm{d}a = \int_{\partial\mathcal{S}} \mathbf{K}\boldsymbol{\nu}\,\mathrm{d}\sigma, \tag{13.11}$$

with $\boldsymbol{\nu}$ the outward unit tangent-normal at the boundary $\partial\mathcal{S}$.

Lastly, consider a non-smooth oriented surface $\mathcal{S}$ for which smoothness of the normal vector field is lost on an edge $\mathcal{C}$. The edge $\mathcal{C}$ is defined by the limiting outward unit tangent-normals $\boldsymbol{\nu}^+$ and $\boldsymbol{\nu}^-$, yet we only consider smooth $\mathcal{C}$. The surface $\mathcal{S}$ has to be understood as the union of open sets $\mathcal{S} := \mathcal{S}^+ \cup \mathcal{S}^-$, or in general $\mathcal{S} := \bigcup_\alpha \mathcal{S}_\alpha$. Additionally, we abandon the smoothness hypotheses of $\boldsymbol{\kappa}$ and $\mathbf{K}$ and allow these fields to be discontinuous across $\mathcal{C}$, and denote by $\boldsymbol{\kappa}^\pm$ and $\mathbf{K}^\pm$, respectively, the limiting values of $\boldsymbol{\kappa}$ and $\mathbf{K}$ when approaching $\mathcal{C}$ from $\mathcal{S}^\pm$. Owing to the lack of smoothness on the edge $\mathcal{C}$, the surface divergence theorem exhibits a surplus, that is,

$$\int_{\mathcal{S}} \operatorname{div}_{\mathcal{S}}(\mathbf{P}_n\boldsymbol{\kappa})\,\mathrm{d}a = \int_{\mathcal{C}} \{\!\{\boldsymbol{\kappa}\cdot\boldsymbol{\nu}\}\!\}\,\mathrm{d}\sigma, \qquad \text{and} \qquad \int_{\mathcal{S}} \operatorname{div}_{\mathcal{S}}(\mathbf{K}\mathbf{P}_n)\,\mathrm{d}a = \int_{\mathcal{C}} \{\!\{\mathbf{K}\boldsymbol{\nu}\}\!\}\,\mathrm{d}\sigma, \tag{13.12}$$

where $\{\!\{\boldsymbol{\kappa}\cdot\boldsymbol{\nu}\}\!\} := \boldsymbol{\kappa}^+\cdot\boldsymbol{\nu}^+ + \boldsymbol{\kappa}^-\cdot\boldsymbol{\nu}^-$ and $\{\!\{\mathbf{K}\boldsymbol{\nu}\}\!\} := \mathbf{K}^+\boldsymbol{\nu}^+ + \mathbf{K}^-\boldsymbol{\nu}^-$. Conversely, for open non-smooth oriented surfaces, the surface divergence theorem (13.12) is extended, that is, for the vector field $\boldsymbol{\kappa}$ we have

$$\int_{\mathcal{S}} \operatorname{div}_{\mathcal{S}}(\mathbf{P}_n\boldsymbol{\kappa})\,\mathrm{d}a = \int_{\partial\mathcal{S}} \boldsymbol{\kappa}\cdot\boldsymbol{\nu}\,\mathrm{d}\sigma + \int_{\mathcal{C}} \{\!\{\boldsymbol{\kappa}\cdot\boldsymbol{\nu}\}\!\}\,\mathrm{d}\sigma, \tag{13.13}$$

and for the tensor field $\mathbf{K}$

$$\int_{\mathcal{S}} \operatorname{div}_{\mathcal{S}}(\mathbf{K}\mathbf{P}_n)\,\mathrm{d}a = \int_{\partial\mathcal{S}} \mathbf{K}\boldsymbol{\nu}\,\mathrm{d}\sigma + \int_{\mathcal{C}} \{\!\{\mathbf{K}\boldsymbol{\nu}\}\!\}\,\mathrm{d}\sigma. \tag{13.14}$$

13.3.3 Material and spatial time-derivatives

Given are the material scalar and vector fields $k_{\mathcal{P}}(\boldsymbol{x}, t)$ and $\boldsymbol{k}_{\mathcal{P}}(\boldsymbol{x}, t)$ defined in a bulk material body $\mathcal{P}$ that occupies a region of a three-dimensional point space $\mathscr{E}$. Furthermore, we consider the smooth motion $\boldsymbol{y}_{\mathcal{P}}(\boldsymbol{x}_{\mathcal{P}}, t)$ of the material body, so that the region of space occupied by the body at a time $t = \tau$ is denoted by $\mathcal{P}_\tau = \boldsymbol{y}_{\mathcal{P}}(\mathcal{P})$. Given any material fields $k_{\mathcal{P}}(\boldsymbol{x}_{\mathcal{P}}, t)$ and $\boldsymbol{k}_{\mathcal{P}}(\boldsymbol{x}_{\mathcal{P}}, t)$, their respective bulk material time-derivatives are defined as

$$\dot{k}_{\mathcal{P}} := \frac{\partial k_{\mathcal{P}}(\boldsymbol{x}_{\mathcal{P}}, t)}{\partial t}, \qquad \text{and} \qquad \dot{\boldsymbol{k}}_{\mathcal{P}} := \frac{\partial \boldsymbol{k}_{\mathcal{P}}(\boldsymbol{x}_{\mathcal{P}}, t)}{\partial t}, \qquad \text{(holding } \boldsymbol{x}_{\mathcal{P}} \text{ fixed).} \tag{13.15}$$

We introduce $\kappa_{\mathcal{P}}(\boldsymbol{y}_{\mathcal{P}}, t)$ and $\boldsymbol{\kappa}_{\mathcal{P}}(\boldsymbol{y}_{\mathcal{P}}, t)$ as the spatial scalar and vector fields defined on the spatial bulk part $\mathcal{P}_\tau$. The corresponding spatial time-derivatives read

$$\kappa'_{\mathcal{P}} := \frac{\partial \kappa_{\mathcal{P}}(\boldsymbol{y}_{\mathcal{P}}, t)}{\partial t}, \qquad \text{and} \qquad \boldsymbol{\kappa}'_{\mathcal{P}} := \frac{\partial \boldsymbol{\kappa}_{\mathcal{P}}(\boldsymbol{y}_{\mathcal{P}}, t)}{\partial t}, \qquad \text{(holding } \boldsymbol{y}_{\mathcal{P}} \text{ fixed).} \tag{13.16}$$

The material and spatial time-derivatives for the spatial bulk fields $\kappa_{\mathcal{P}}(\boldsymbol{y}_{\mathcal{P}}, t)$ and $\boldsymbol{\kappa}_{\mathcal{P}}(\boldsymbol{y}_{\mathcal{P}}, t)$ are related through the following time-derivative identities

$$\dot{\kappa}_{\mathcal{P}} = \kappa'_{\mathcal{P}} + \operatorname{grad}\kappa_{\mathcal{P}} \cdot \boldsymbol{v}_{\mathcal{P}}, \qquad \text{and} \qquad \dot{\boldsymbol{\kappa}}_{\mathcal{P}} = \boldsymbol{\kappa}'_{\mathcal{P}} + (\operatorname{grad}\boldsymbol{\kappa}_{\mathcal{P}})\boldsymbol{v}_{\mathcal{P}}, \tag{13.17}$$

where $\boldsymbol{v}_{\mathcal{P}}(\boldsymbol{y}_{\mathcal{P}}, t) = \dot{\boldsymbol{y}}_{\mathcal{P}}(\boldsymbol{y}_{\mathcal{P}}{}^{-1}(\boldsymbol{y}_{\mathcal{P}}, t), t)$ denotes the spatial description of the bulk velocity. More information on material and spatial descriptions of fields and their time-derivatives can be found in [86].

For fields defined on moving surfaces, special attention should be paid to their time derivatives. To arrive at the surface counterparts of the spatial and material time-derivatives in (13.16) and (13.17), we follow the theory presented by Cermelli et al. [31].

First, let $\kappa_{\partial\mathcal{P}}(\boldsymbol{y}_{\partial\mathcal{P}}, t)$ and $\boldsymbol{\kappa}_{\partial\mathcal{P}}(\boldsymbol{y}_{\partial\mathcal{P}}, t)$ be the smooth spatial scalar and vector fields defined on a surface $\partial\mathcal{P}_\tau$, with $\partial\mathcal{P}_\tau$ the region occupied by the deformed surface material at $t = \tau$. Furthermore, let $\boldsymbol{v}_{\partial\mathcal{P}}(\boldsymbol{y}_{\partial\mathcal{P}}, t)$ denote the migrational velocity of the surface $\partial\mathcal{P}_\tau$, and let its corresponding trajectory $\boldsymbol{z}(t)$ through a fixed $\boldsymbol{x}_{\partial\mathcal{P}} \in \partial\mathcal{P}$ at time t_0 be defined as

$$\frac{\mathrm{d}\boldsymbol{z}(t)}{\mathrm{d}t} = \boldsymbol{v}_{\partial\mathcal{P}}(\boldsymbol{z}(t), t), \qquad \boldsymbol{z}(t_0) = \boldsymbol{x}_{\partial\mathcal{P}}. \tag{13.18}$$

Then, the normal trajectories, which are the trajectories corresponding to the normal velocity, read

$$\frac{\mathrm{d}\boldsymbol{z}_{\boldsymbol{n}}(t)}{\mathrm{d}t} = (\boldsymbol{v}_{\partial\mathcal{P}}(\boldsymbol{z}_{\boldsymbol{n}}(t), t) \cdot \boldsymbol{n}(\boldsymbol{y}_{\partial\mathcal{P}}, t))\boldsymbol{n}(\boldsymbol{y}_{\partial\mathcal{P}}, t), \qquad \boldsymbol{z}_{\boldsymbol{n}}(t_0) = \boldsymbol{x}_{\partial\mathcal{P}}. \tag{13.19}$$

Next, we introduce $\hat{\kappa}_{\partial\mathcal{P}}(\boldsymbol{y}_{\partial\mathcal{P}}, t)$ and $\hat{\boldsymbol{\kappa}}_{\partial\mathcal{P}}(\boldsymbol{y}_{\partial\mathcal{P}}, t)$ as the normally constant extensions of the fields $\kappa_{\partial\mathcal{P}}(\boldsymbol{y}_{\partial\mathcal{P}}, t)$ and $\boldsymbol{\kappa}_{\partial\mathcal{P}}(\boldsymbol{y}_{\partial\mathcal{P}}, t)$, respectively. That is, the fields $\hat{\kappa}_{\partial\mathcal{P}}(\boldsymbol{y}_{\partial\mathcal{P}}, t)$ and $\hat{\boldsymbol{\kappa}}_{\partial\mathcal{P}}(\boldsymbol{y}_{\partial\mathcal{P}}, t)$ are constant on the lines in the normal direction $\boldsymbol{n}(\boldsymbol{y}_{\partial\mathcal{P}}, t)$ of any $\boldsymbol{y}_{\partial\mathcal{P}} \in \partial\mathcal{P}_\tau$. Then, given any scalar field $\kappa_{\partial\mathcal{P}}(\boldsymbol{y}_{\partial\mathcal{P}}, t)$, the normal time-derivative reads

$$\overset{\square}{\kappa}_{\partial\mathcal{P}} := \frac{\mathrm{d}}{\mathrm{d}t}\kappa_{\partial\mathcal{P}}(\boldsymbol{z}_{\boldsymbol{n}}(t), t) = \frac{\mathrm{d}}{\mathrm{d}t}\hat{\kappa}_{\partial\mathcal{P}}(\boldsymbol{z}_{\boldsymbol{n}}(t), t) = \frac{\partial\hat{\kappa}_{\partial\mathcal{P}}(\boldsymbol{y}_{\partial\mathcal{P}}, t)}{\partial t}\bigg|_{\boldsymbol{y}_{\partial\mathcal{P}} = \boldsymbol{z}_{\boldsymbol{n}}(t)}, \tag{13.20}$$

and, similarly, for any vector field $\boldsymbol{\kappa}_{\partial\mathcal{P}}(\boldsymbol{y}_{\partial\mathcal{P}}, t)$, it is defined as

$$\overset{\square}{\boldsymbol{\kappa}}_{\partial\mathcal{P}} := \frac{\mathrm{d}}{\mathrm{d}t}\boldsymbol{\kappa}_{\partial\mathcal{P}}(\boldsymbol{z}_{\boldsymbol{n}}(t), t) = \frac{\mathrm{d}}{\mathrm{d}t}\hat{\boldsymbol{\kappa}}_{\partial\mathcal{P}}(\boldsymbol{z}_{\boldsymbol{n}}(t), t) = \frac{\partial\hat{\boldsymbol{\kappa}}_{\partial\mathcal{P}}(\boldsymbol{y}_{\partial\mathcal{P}}, t)}{\partial t}\bigg|_{\boldsymbol{y}_{\partial\mathcal{P}} = \boldsymbol{z}_{\boldsymbol{n}}(t)}. \tag{13.21}$$

Lastly, the migrationally normal time-derivative of the fields $\kappa_{\partial\mathcal{P}}(\boldsymbol{x}_{\partial\mathcal{P}}, t)$ and $\boldsymbol{\kappa}_{\partial\mathcal{P}}(\boldsymbol{x}_{\partial\mathcal{P}}, t)$ following the moving material surface $\partial\mathcal{P}_\tau$ at a time t_0 and a point $\boldsymbol{x}_{\partial\mathcal{P}}$ are defined as

$$\mathring{\kappa}_{\partial\mathcal{P}} := \frac{\mathrm{d}}{\mathrm{d}t}\Big(\kappa_{\partial\mathcal{P}}(\boldsymbol{z}(t), t)\Big)\Big|_{t=t_0}, \qquad \text{and} \qquad \mathring{\boldsymbol{\kappa}}_{\partial\mathcal{P}} := \frac{\mathrm{d}}{\mathrm{d}t}\Big(\boldsymbol{\kappa}_{\partial\mathcal{P}}(\boldsymbol{z}(t), t)\Big)\Big|_{t=t_0}. \tag{13.22}$$

In view of relations (13.20) - (13.22), we obtain the identities

$$\mathring{\kappa}_{\partial\mathcal{P}} = \overset{\square}{\kappa}_{\partial\mathcal{P}} + (\mathbf{P}_{\boldsymbol{n}}\boldsymbol{v}_{\partial\mathcal{P}}) \cdot \operatorname{grad}_{\mathcal{S}}\kappa_{\partial\mathcal{P}}, \qquad \text{and} \qquad \mathring{\boldsymbol{\kappa}}_{\partial\mathcal{P}} = \overset{\square}{\boldsymbol{\kappa}}_{\partial\mathcal{P}} + (\operatorname{grad}_{\mathcal{S}}\boldsymbol{\kappa}_{\partial\mathcal{P}})(\mathbf{P}_{\boldsymbol{n}}\boldsymbol{v}_{\partial\mathcal{P}}), \tag{13.23}$$

which are analogous to the bulk time-derivative identities in (13.17). Notice that we can also write expression $(13.23)_1$ as

$$\mathring{\kappa}_{\partial\mathcal{P}} = \overset{\square}{\kappa}_{\partial\mathcal{P}} + \boldsymbol{v}_{\partial\mathcal{P}} \cdot \operatorname{grad}_{\mathcal{S}}\kappa_{\partial\mathcal{P}}. \tag{13.24}$$

Chapter 14

Isochoric Motion and Mass Balance

In this Chapter, we focus on the motion and mass transfer in a binary immiscible bulk fluid enclosed by a thin film of surface fluid. We assume that both the bulk and surface material undergo *isochoric motion*, and present the implications of this assumption in Section 14.1. Using these results, we derive the *mass balance* equations in the coupled bulk-surface material in Section 14.2. In Section 14.3, we consider the *mass transport of species* in the bulk-surface system and present a partwise species mass balance.

14.1 Isochoric motion

In this Section, we consider the motion of a coupled bulk-surface material and present its kinematics. To this end, we consider the material body $\mathcal{P}$ occupying a region of a three-dimensional point space $\mathscr{E}$ as the reference configuration. Furthermore, we let $\partial\mathcal{P}$ denote its closed surface boundary, which may lose smoothness along a curve, namely an edge $\partial^2\mathcal{P}$. In the neighbourhood of an edge $\partial^2\mathcal{P}$ two smooth surfaces $\partial\mathcal{P}^{\pm}$ are defined. The limiting unit normals of $\partial\mathcal{P}^{\pm}$ on $\partial^2\mathcal{P}$ are denoted by the pair $\{\boldsymbol{n}^+, \boldsymbol{n}^-\}$, which characterize the edge $\partial^2\mathcal{P}$. Similarly, the limiting outward unit tangent-normal of $\partial\mathcal{P}^{\pm}$ on $\partial^2\mathcal{P}$ are $\{\boldsymbol{\nu}^+, \boldsymbol{\nu}^-\}$. Additionally, $\partial^2\mathcal{P}$ is oriented by the unit tangent $\boldsymbol{\sigma} := \boldsymbol{\sigma}^+$ such that $\boldsymbol{\sigma}^+ := \boldsymbol{n}^+ \times \boldsymbol{\nu}^+$. Following the notational agreement in Section 13.3.3, we use the subscript τ to refer to spatial entities in the current configuration. More specifically, $\mathcal{P}_\tau$ denotes the spatial part, we write $\partial\mathcal{P}_\tau$ for the boundary of $\mathcal{P}_\tau$ and use $\partial^2\mathcal{P}_\tau$ for the boundary of $\partial\mathcal{P}_\tau$. Note that $\mathcal{P}$, $\partial\mathcal{P}$ and $\partial^2\mathcal{P}$ are reserved for their counterparts in the reference configuration, respectively.

In this continuum theory, the bulk and surface material are endowed with two distinct kinematic descriptors, namely, the fluid velocities $\boldsymbol{v}_{\mathcal{P}}$ in the bulk and $\boldsymbol{v}_{\partial\mathcal{P}}$ on the surface. Furthermore, let the density of the bulk material be given by $\varrho_{\mathcal{P}}$, and let $\varrho_{\partial\mathcal{P}}$ denote the apparent surface density of the surface material endowed with a finite thickness ℓ_τ. The bulk-surface framework developed in this Part is based on two important assumptions. That is, we assume that:

(A.1) The bulk-surface motion is *isochoric*. For the bulk material, this means that motion preserves volume. For the surface material, we assume that isochoric motion implies volume conservation on a microscopic scale;

(A.2) The normal components of the velocities are continuous, i.e.

$$\boldsymbol{v}_{\mathcal{P}} \cdot \boldsymbol{n}\big|_{\partial\mathcal{P}} = \boldsymbol{v}_{\partial\mathcal{P}} \cdot \boldsymbol{n}. \tag{14.1}$$

Notice that we do not impose such a continuity assumption on the tangential velocities $\mathbf{P}_n \boldsymbol{v}_{\mathcal{P}}\big|_{\partial\mathcal{P}}$ and $\mathbf{P}_n \boldsymbol{v}_{\partial\mathcal{P}}$.

Remark 14.1 (On the kinematical assumption (A.2)) The kinematic constraint (14.1) is imposed to guarantee that the bulk and the surface material's boundary coincide at all times and never detach from one another. As we do not endow edges with their own kinematic descriptors, it is not needed to define additional kinematic constraints. Moreover, as a consequence of the kinematic constraint (14.1), we find on $\partial^2\mathcal{P}$ that

$$\boldsymbol{v}_{\mathcal{P}} \cdot \boldsymbol{n}^+\big|_{\partial^2\mathcal{P}} = \boldsymbol{v}_{\partial\mathcal{P}} \cdot \boldsymbol{n}^+\big|_{\partial^2\mathcal{P}}, \qquad \text{and} \qquad \boldsymbol{v}_{\mathcal{P}} \cdot \boldsymbol{n}^-\big|_{\partial^2\mathcal{P}} = \boldsymbol{v}_{\partial\mathcal{P}} \cdot \boldsymbol{n}^-\big|_{\partial^2\mathcal{P}}. \tag{14.2}$$

□

Bearing in mind Assumptions (A.1) - (A.2), let the bulk and surface deformation gradient be denoted by

$$\mathbf{F}_{\mathcal{P}} := \operatorname{grad}^x \boldsymbol{y}_{\mathcal{P}}, \qquad \text{and} \qquad \mathbf{F}_{\partial\mathcal{P}} := \operatorname{grad}^x_{\mathcal{S}} \boldsymbol{y}_{\partial\mathcal{P}}, \tag{14.3}$$

where $\boldsymbol{y}_{\mathcal{P}}$ represents the motion of $\mathcal{P}_\tau$ and $\boldsymbol{y}_{\partial\mathcal{P}}$ the motion of $\partial\mathcal{P}_\tau$, such that $\mathcal{P}_\tau = \boldsymbol{y}_{\mathcal{P}}(\mathcal{P})$ and $\partial\mathcal{P}_\tau = \boldsymbol{y}_{\partial\mathcal{P}}(\partial\mathcal{P})$, respectively. In expression (14.3), the gradients are defined with respect to the reference configuration, either $\boldsymbol{x}_{\mathcal{P}} \in \mathcal{P}$ or $\boldsymbol{x}_{\partial\mathcal{P}} \in \partial\mathcal{P}$, respectively. If not made explicit, differential operators are computed with respect to the current configuration, either $\boldsymbol{y}_{\mathcal{P}}$ or $\boldsymbol{y}_{\partial\mathcal{P}}$.

As $\mathbf{F}_{\partial\mathcal{P}}$ is rank deficient, we introduce the pseudo-inverse of the surface deformation gradient as

$$\mathbf{F}^{-1}_{\partial\mathcal{P}} := \mathbf{P}_{n}(\boldsymbol{x}_{\partial\mathcal{P}})(\mathbf{F}_{\partial\mathcal{P}} + \boldsymbol{n}(\boldsymbol{y}_{\partial\mathcal{P}}) \otimes \boldsymbol{n}(\boldsymbol{x}_{\partial\mathcal{P}}))^{-1}, \tag{14.4}$$

where we explicitly show the dependency on either the reference configuration $\boldsymbol{x}_{\partial\mathcal{P}} \in \partial\mathcal{P}$ or the current configuration $\boldsymbol{y}_{\partial\mathcal{P}} \in \partial\mathcal{P}_\tau$. Note that $\mathbf{F}_{\partial\mathcal{P}} + \boldsymbol{n}(\boldsymbol{y}_{\partial\mathcal{P}}) \otimes \boldsymbol{n}(\boldsymbol{x}_{\partial\mathcal{P}})$ is full rank since $\boldsymbol{n}(\boldsymbol{y}_{\partial\mathcal{P}})$ is not in the range of $\mathbf{F}_{\partial\mathcal{P}}$. Additionally, we have that

$$\mathbf{F}^{-1}_{\partial\mathcal{P}}\mathbf{F}_{\partial\mathcal{P}} = \mathbf{P}_{n}(\boldsymbol{x}_{\partial\mathcal{P}}), \quad \mathbf{F}_{\partial\mathcal{P}}\mathbf{F}^{-1}_{\partial\mathcal{P}} = \mathbf{P}_{n}(\boldsymbol{y}_{\partial\mathcal{P}}), \quad \text{and} \quad \mathbf{F}^{-1}_{\partial\mathcal{P}}\boldsymbol{n}(\boldsymbol{y}_{\partial\mathcal{P}}) = \mathbf{F}^{-\top}_{\partial\mathcal{P}}\boldsymbol{n}(\boldsymbol{x}_{\partial\mathcal{P}}) = \mathbf{0}. \tag{14.5}$$

For further details on this pseudo-inverse, the reader is referred to the work by Šilhavý [173] on interactions of shells with bulk matter, and also to the more recent work by Tomassetti [162] on a coordinate-free description for thin shells.

Next, we introduce $\mathbf{L}_{\mathcal{P}} := \operatorname{grad} \boldsymbol{v}_{\mathcal{P}}$ and $\mathbf{L}_{\partial\mathcal{P}} := \operatorname{grad}_{\mathcal{S}} \boldsymbol{v}_{\partial\mathcal{P}}$ as the bulk and surface velocity gradient, respectively. We consider the following classical identity in continuum mechanics (c.f. Gurtin [83, Eq. (8) on page 23]), also known as Jacobi's formula,

$$\dot{\overline{|\mathbf{F}_{\mathcal{P}}|}} = |\mathbf{F}_{\mathcal{P}}|\operatorname{tr}(\dot{\mathbf{F}}_{\mathcal{P}}\mathbf{F}^{-1}_{\mathcal{P}}), \tag{14.6}$$

where $|\mathbf{F}_{\mathcal{P}}|$ denotes the determinant of $\mathbf{F}_{\mathcal{P}}$. In addition, the dot over the line indicates the derivative of the quantity under the line. The surface counterpart of expression (14.6) reads

$$\mathring{\overline{|\mathbf{F}_{\partial\mathcal{P}}|}} = |\mathbf{F}_{\partial\mathcal{P}}|\operatorname{tr}(\mathring{\mathbf{F}}_{\partial\mathcal{P}}\mathbf{F}^{-1}_{\partial\mathcal{P}}). \tag{14.7}$$

Furthermore, we have the volumetric and areal Jacobian of deformation, respectively, defined as

$$J_{\mathcal{P}} := \frac{\mathrm{d}v_\tau}{\mathrm{d}v} = |\mathbf{F}_{\mathcal{P}}|, \tag{14.8}$$

and

$$J_{\partial\mathcal{P}} := \frac{\mathrm{d}a_\tau}{\mathrm{d}a} = |\mathbf{F}_{\partial\mathcal{P}}|. \tag{14.9}$$

where $\mathrm{d}v_\tau$ and $\mathrm{d}v$ are the differential of the volume at the current and reference configuration, while $\mathrm{d}a_\tau$ and $\mathrm{d}a$ denote the differential of the area at the current and reference configuration. Finally, in view of (14.6) and (14.7) and bearing in mind that $\dot{\mathbf{F}}_{\mathcal{P}} = \mathbf{L}_{\mathcal{P}}\mathbf{F}_{\mathcal{P}}$ and $\mathring{\mathbf{F}}_{\partial\mathcal{P}} = \mathbf{L}_{\partial\mathcal{P}}\mathbf{F}_{\partial\mathcal{P}}$, we arrive at

$$\begin{aligned} \dot{J}_{\mathcal{P}} &= J_{\mathcal{P}}\,\mathrm{tr}(\dot{\mathbf{F}}_{\mathcal{P}}\mathbf{F}_{\mathcal{P}}^{-1}) \\ &= J_{\mathcal{P}}\,\mathrm{tr}(\mathbf{L}_{\mathcal{P}}\mathbf{F}_{\mathcal{P}}\mathbf{F}_{\mathcal{P}}^{-1}) \\ &= J_{\mathcal{P}}\,\mathrm{div}\,\boldsymbol{v}_{\mathcal{P}}, \end{aligned} \tag{14.10}$$

and

$$\begin{aligned} \mathring{J}_{\partial\mathcal{P}} &= J_{\partial\mathcal{P}}\,\mathrm{tr}(\mathring{\mathbf{F}}_{\partial\mathcal{P}}\mathbf{F}_{\partial\mathcal{P}}^{-1}) \\ &= J_{\partial\mathcal{P}}\,\mathrm{tr}(\mathbf{L}_{\partial\mathcal{P}}\mathbf{F}_{\partial\mathcal{P}}\mathbf{F}_{\partial\mathcal{P}}^{-1}) \\ &= J_{\partial\mathcal{P}}\,\mathrm{div}_{\mathcal{S}}\boldsymbol{v}_{\partial\mathcal{P}}. \end{aligned} \tag{14.11}$$

Next, following Assumption (A.1), we consider the isochoric motion of the bulk material

$$\overline{|\mathcal{P}_\tau|}^{\boldsymbol{\cdot}} := \overline{\mathrm{vol}(\mathcal{P}_\tau)}^{\boldsymbol{\cdot}} = 0, \tag{14.12}$$

Assuming that expression (14.12) holds for any $\mathcal{R}_\tau \subseteq \mathcal{P}_\tau$, we are led to

$$0 = \overline{\int_{\mathcal{R}_\tau} \mathrm{d}v_\tau}^{\boldsymbol{\cdot}} = \int_{\mathcal{R}} \dot{J}_{\mathcal{P}}\,\mathrm{d}v = \int_{\mathcal{R}_\tau} \mathrm{div}\,\boldsymbol{v}_{\mathcal{P}}\,\mathrm{d}v_\tau, \tag{14.13}$$

where we have used expression (14.10). Thus, it follows by localization that

$$\mathrm{div}\,\boldsymbol{v}_{\mathcal{P}} = 0, \qquad \text{in } \mathcal{P}_\tau, \tag{14.14}$$

which is a well-known constraint for incompressible bulk materials.

In view of Assumption (A.1), microscopic isochoric motion for the surface material $\partial\mathcal{P}_\tau$ with current thickness ℓ_τ implies

$$\overline{|\ell_\tau\partial\mathcal{P}_\tau|}^{\boldsymbol{\cdot}} := \overline{\mathrm{area}(\ell_\tau\partial\mathcal{P}_\tau)}^{\boldsymbol{\cdot}} = 0. \tag{14.15}$$

Let the above expression (14.15) hold for any $\mathcal{S}_\tau \subseteq \partial\mathcal{P}_\tau$. This leads us to the following

$$\begin{aligned} 0 &= \overline{\int_{\mathcal{S}_\tau} \ell_\tau\,\mathrm{d}a_\tau}^{\boldsymbol{\cdot}} \\ &= \int_{\mathcal{S}} \overline{\ell_\tau J_{\partial\mathcal{P}}}^{\circ}\,\mathrm{d}a \\ &= \int_{\mathcal{S}} (\mathring{\ell}_\tau J_{\partial\mathcal{P}} + \ell_\tau \mathring{J}_{\partial\mathcal{P}})\,\mathrm{d}a \\ &= \int_{\mathcal{S}_\tau} (\mathring{\ell}_\tau + \ell_\tau \mathrm{div}_{\mathcal{S}}\boldsymbol{v}_{\partial\mathcal{P}})\,\mathrm{d}a_\tau, \end{aligned} \tag{14.16}$$

where we have used the result in (14.11). Localization of (14.16) renders

$$\mathring{\ell}_\tau + \ell_\tau \mathrm{div}_{\mathcal{S}}\boldsymbol{v}_{\partial\mathcal{P}} = 0, \qquad \text{on } \partial\mathcal{P}_\tau. \tag{14.17}$$

Thus, the microscopically incompressible surface body can only undergo microscopic isochoric motion, a requirement which imposes the constraint (14.17) on all motions the surface material may undergo. Further motivation for this microscopic viewpoint leading to the definition in (14.15) and the corresponding constraint (14.17) is based on the partwise mass balance for the surface, which is defined in the next Section.

14.2 Mass Balance

In this Section, we present the bulk and surface *mass balances* of the bulk-surface material undergoing isochoric motion. Using the transport theorem, the partwise bulk balance of mass is given by

$$\overline{\int_{\mathcal{R}_\tau} \varrho_{\mathcal{P}}\, \mathrm{d}v_\tau}^{\boldsymbol{\cdot}} = \int_{\mathcal{R}_\tau} (\dot{\varrho}_{\mathcal{P}} + \varrho_{\mathcal{P}} \operatorname{div} \boldsymbol{v}_{\mathcal{P}})\, \mathrm{d}v_\tau = 0, \tag{14.18}$$

and by localization we arrive at the pointwise bulk mass balance

$$\dot{\varrho}_{\mathcal{P}} + \varrho_{\mathcal{P}} \operatorname{div} \boldsymbol{v}_{\mathcal{P}} = 0, \qquad \text{in } \mathcal{P}_\tau, \tag{14.19}$$

In terms of specific volume $\nu_{\mathcal{P}} := \varrho_{\mathcal{P}}^{-1}$, the pointwise bulk balance of mass (14.19) reads

$$\dot{\nu}_{\mathcal{P}} = \nu_{\mathcal{P}} \operatorname{div} \boldsymbol{v}_{\mathcal{P}}, \qquad \text{in } \mathcal{P}_\tau. \tag{14.20}$$

Using the isochoric constraint (14.14), $\operatorname{div} \boldsymbol{v}_{\mathcal{P}} = 0$, we obtain

$$\dot{\varrho}_{\mathcal{P}} = 0, \qquad \text{and} \qquad \dot{\nu}_{\mathcal{P}} = 0, \tag{14.21}$$

implying that the bulk mass density $\varrho_{\mathcal{P}}$ and specific bulk volume $\nu_{\mathcal{P}}$ are constant on particle paths. Moreover, we further restrict $\varrho_{\mathcal{P}}$ and $\nu_{\mathcal{P}}$ by assuming that

$$\varrho_{\mathcal{P}} = \text{constant}, \qquad \text{and} \qquad \nu_{\mathcal{P}} = \text{constant}, \tag{14.22}$$

which means that applications in which spatial variations of the density are important, such as oceanic and mantle convection, are excluded [86]. Based on these results for the bulk material, it would be natural to assume that the surface density $\varrho_{\partial\mathcal{P}}$ is constant as well for all motions. However, this would imply that the only motions possible are those of the class in which both the volume and surface area do not change. This hypothesis for the material motion is far too restrictive, and provides the main motivation for employing a microscopic approach for the surface material's motion.

Thus, from a microscopic viewpoint, we consider that the surface fluid has a constant density ρ, defined as

$$\rho := \frac{\mathrm{d}m_\tau}{\mathrm{d}v_\tau} = \text{constant}, \tag{14.23}$$

where $\mathrm{d}m_\tau$ and $\mathrm{d}v_\tau$ are the differential of mass and volume, and the subscript τ refers to the deformed configuration. When the surface fluid deforms the actual thickness should change to maintain the constant microscopic volume. Accordingly, we define the apparent surface density $\varrho_{\partial\mathcal{P}}$, a macroscopic quantity, as

$$\varrho_{\partial\mathcal{P}} := \frac{\mathrm{d}m_\tau}{\mathrm{d}a_\tau} = \frac{\mathrm{d}m_\tau}{\mathrm{d}v_\tau}\ell_\tau = \rho\, \ell_\tau, \tag{14.24}$$

where ℓ_τ and $\mathrm{d}a_\tau$ are the current thickness and current differential of area, respectively. Furthermore, let ℓ be the initial thickness and $\mathrm{d}a$ denote the differential area. Given that the microscopic surface motion is isochoric, we have that

$$\mathrm{d}a_\tau \times \ell_\tau = \mathrm{d}a \times \ell, \tag{14.25}$$

leading us to the definition for microscopic isochoric motion

$$\overline{|\ell_\tau \partial\mathcal{P}_\tau|}^{\boldsymbol{\cdot}} := \overline{\operatorname{area}(\ell_\tau \partial\mathcal{P}_\tau)}^{\boldsymbol{\cdot}} = 0, \tag{14.26}$$

which we already defined in (14.15) to arrive at the constraint $\mathring{\ell}_\tau + \ell_\tau \mathrm{div}_{\mathcal{S}} \boldsymbol{v}_{\partial\mathcal{P}} = 0$ in (14.17).

In view of (14.24), we have that

$$\frac{\varrho_{\partial\mathcal{P}}}{\ell_\tau} = \rho, \qquad \varrho_{\partial\mathcal{P}} \times \mathrm{d}a_\tau = \rho \times \mathrm{d}a \times \ell, \qquad \text{and} \qquad \nu \times \mathrm{d}a_\tau = \nu_{\partial\mathcal{P}} \times \mathrm{d}a \times \ell, \tag{14.27}$$

where $\nu := \rho^{-1}$ is the constant microscopic specific volume and $\nu_{\partial\mathcal{P}} := \varrho_{\partial\mathcal{P}}^{-1}$ is the apparent specific area. Moreover, (14.27) yields

$$\nu_{\partial\mathcal{P}} = \frac{J_{\partial\mathcal{P}}}{\ell}\nu. \tag{14.28}$$

Additionally, in view of (14.25) and the areal Jacobian (14.9), we have

$$J_{\partial\mathcal{P}} = \frac{\ell}{\ell_\tau}. \tag{14.29}$$

Lastly, the balance of mass for a spatial convecting region $\mathcal{S}_\tau \subseteq \partial\mathcal{P}_\tau$ is given by

$$\begin{aligned} 0 &= \overline{\int_{\mathcal{S}_\tau} \varrho_{\partial\mathcal{P}} \, \mathrm{d}a_\tau}^{\boldsymbol{\cdot}} \\ &= \int_{\mathcal{S}} (\mathring{\varrho}_{\partial\mathcal{P}} J_{\partial\mathcal{P}} + \varrho_{\partial\mathcal{P}} \mathring{J}_{\partial\mathcal{P}}) \, \mathrm{d}a \\ &= \int_{\mathcal{S}_\tau} (\mathring{\varrho}_{\partial\mathcal{P}} + \varrho_{\partial\mathcal{P}} \mathrm{div}_{\mathcal{S}} \boldsymbol{v}_{\partial\mathcal{P}}) \, \mathrm{d}a_\tau, \end{aligned} \tag{14.30}$$

and thus, after localization, we arrive at the pointwise balance of surface mass

$$\mathring{\varrho}_{\partial\mathcal{P}} + \varrho_{\partial\mathcal{P}} \mathrm{div}_{\mathcal{S}} \boldsymbol{v}_{\partial\mathcal{P}} = 0, \qquad \text{on } \partial\mathcal{P}_\tau, \tag{14.31}$$

where $\mathrm{div}_{\mathcal{S}} \boldsymbol{v}_{\partial\mathcal{P}} = \mathrm{div}_{\mathcal{S}}(\mathbf{P}_n \boldsymbol{v}_{\partial\mathcal{P}}) - 2K\, \boldsymbol{v}_{\partial\mathcal{P}} \cdot \boldsymbol{n}$, in which $K := -\frac{1}{2}\mathrm{div}_{\mathcal{S}} \boldsymbol{n}$ denotes the mean curvature. Notice that the definition for density ρ (14.23) is consistent with the pointwise balance of surface mass (14.31) and the isochoric constraint (14.17): combining both expressions leads to $\mathring{\rho}\ell_\tau = 0$. Hence, one can also arrive at the pointwise balance of mass (14.31) through multiplication of the isochoric constraint (14.17) by ρ. Alternatively, we can write (14.31) in terms of the specific area, that is,

$$\mathring{\nu}_{\partial\mathcal{P}} = \nu_{\partial\mathcal{P}}(\mathrm{div}_{\mathcal{S}}(\mathbf{P}_n \boldsymbol{v}_{\partial\mathcal{P}}) - 2K\, \boldsymbol{v}_{\partial\mathcal{P}} \cdot \boldsymbol{n}), \qquad \text{on } \partial\mathcal{P}_\tau. \tag{14.32}$$

14.3 Conserved species transport

In this Section, we consider two diffusing species in the coupled bulk-surface material, and characterize their transport by means of a *partwise bulk-surface balance of species mass*. We define $\varphi_{\mathcal{P}}$ as the bulk mass fraction of one of the species in the bulk, and let $\varphi_{\partial\mathcal{P}}$ be its surface counterpart. Moreover, since the sum of the mass fractions of both species in the bulk is one, we write $\varphi_{\mathcal{P}}$ for one of the bulk mass fraction and $1 - \varphi_{\mathcal{P}}$ for the other bulk mass fraction. Similarly, on the surface, the surface mass fraction of one species is $\varphi_{\partial\mathcal{P}}$ and the other one is $1 - \varphi_{\partial\mathcal{P}}$.

Bearing in mind that $\varrho_{\partial\mathcal{P}} = \rho\ell_\tau$ (14.24), the partwise bulk-surface balance of species mass is given by

$$\overline{\int_{\mathcal{P}_\tau} \varrho_{\mathcal{P}} \varphi_{\mathcal{P}} \, \mathrm{d}v_\tau}^{\boldsymbol{\cdot}} + \overline{\int_{\partial\mathcal{P}_\tau} \rho \ell_\tau \varphi_{\partial\mathcal{P}} \, \mathrm{d}a_\tau}^{\boldsymbol{\cdot}} = \int_{\mathcal{P}_\tau} s_{\mathcal{P}} \, \mathrm{d}v_\tau + \int_{\partial\mathcal{P}_\tau} s_{\partial\mathcal{P}} \, \mathrm{d}a_\tau - \int_{\partial^2\mathcal{P}_\tau} \{\!\{ \boldsymbol{\jmath}_{\partial\mathcal{P}} \cdot \boldsymbol{\nu} \}\!\} \, \mathrm{d}\sigma_\tau, \tag{14.33}$$

where $s_{\mathcal{P}}$ and $s_{\partial\mathcal{P}}$ are the bulk and surface species mass supply, respectively, and $\jmath_{\partial\mathcal{P}}$ denotes the surface species mass flux across the edge.

Letting $\jmath_{\mathcal{P}}$ denote the bulk species mass flux, we stipulate that the partwise bulk-surface species mass balance (14.33) can be uncoupled into

$$\overline{\int_{\mathcal{P}_\tau} \varrho_{\mathcal{P}} \varphi_{\mathcal{P}} \, \mathrm{d}v_\tau}^{\boldsymbol{\cdot}} = \int_{\mathcal{P}_\tau} \varrho_{\mathcal{P}} \dot{\varphi}_{\mathcal{P}} \, \mathrm{d}v_\tau = \int_{\mathcal{P}_\tau} s_{\mathcal{P}} \, \mathrm{d}v_\tau - \int_{\partial\mathcal{P}_\tau} \jmath_{\mathcal{P}} \cdot \boldsymbol{n} \, \mathrm{d}a_\tau, \tag{14.34}$$

and

$$\begin{aligned} \overline{\int_{\partial\mathcal{P}_\tau} \rho \ell_\tau \varphi_{\partial\mathcal{P}} \, \mathrm{d}a_\tau}^{\boldsymbol{\cdot}} &= \int_{\partial\mathcal{P}_\tau} \rho \ell_\tau \mathring{\varphi}_{\partial\mathcal{P}} \, \mathrm{d}a_\tau + \int_{\partial\mathcal{P}_\tau} \rho \varphi_{\partial\mathcal{P}} (\mathring{\ell}_\tau + \ell_\tau \mathrm{div}_{\mathcal{S}} \boldsymbol{v}_{\partial\mathcal{P}}) \, \mathrm{d}a_\tau \\ &= \int_{\partial\mathcal{P}_\tau} \rho \ell_\tau \mathring{\varphi}_{\partial\mathcal{P}} \, \mathrm{d}a_\tau \\ &= \int_{\partial\mathcal{P}_\tau} \jmath_{\mathcal{P}} \cdot \boldsymbol{n} \, \mathrm{d}a_\tau + \int_{\partial\mathcal{P}_\tau} s_{\partial\mathcal{P}} \, \mathrm{d}a_\tau - \int_{\partial^2\mathcal{P}_\tau} \{\!\{\jmath_{\partial\mathcal{P}} \cdot \boldsymbol{\nu}\}\!\} \, \mathrm{d}\sigma_\tau. \end{aligned} \tag{14.35}$$

Next, we apply the divergence and surface divergence theorems to the uncoupled partwise balance of species mass (14.34) and (14.35), respectively. After localization, we are led to the following pointwise balance of bulk species mass

$$\varrho_{\mathcal{P}} \dot{\varphi}_{\mathcal{P}} = s_{\mathcal{P}} - \mathrm{div}\, \jmath_{\mathcal{P}}, \qquad \text{in } \mathcal{P}_\tau, \tag{14.36}$$

and for the surface holds

$$\rho \ell_\tau \mathring{\varphi}_{\partial\mathcal{P}} = \jmath_{\mathcal{P}} \cdot \boldsymbol{n} + s_{\partial\mathcal{P}} - \mathrm{div}_{\mathcal{S}}(\mathbf{P}_{\!n} \jmath_{\partial\mathcal{P}}), \qquad \text{on } \partial\mathcal{P}_\tau. \tag{14.37}$$

Note that the pointwise bulk species mass balance (14.36) has a standard form, motivating our choice for the uncoupling. However, the pointwise balance of surface species mass (14.37) contains a contribution from the bulk in the form of the term $\jmath_{\mathcal{P}} \cdot \boldsymbol{n}$. Additionally, the term $\mathrm{div}_{\mathcal{S}}(\mathbf{P}_{\!n} \jmath_{\partial\mathcal{P}})$ may be split as $\mathrm{div}_{\mathcal{S}}(\mathbf{P}_{\!n} \jmath_{\partial\mathcal{P}}) = \mathrm{div}_{\mathcal{S}} \jmath_{\partial\mathcal{P}} + 2K \jmath_{\partial\mathcal{P}} \cdot \boldsymbol{n}$. Then, we arrive at the following expression for the pointwise balance of surface species mass

$$\rho \ell_\tau \mathring{\varphi}_{\partial\mathcal{P}} = \jmath_{\mathcal{P}} \cdot \boldsymbol{n} + s_{\partial\mathcal{P}} - \mathrm{div}_{\mathcal{S}} \jmath_{\partial\mathcal{P}} - 2K \jmath_{\partial\mathcal{P}} \cdot \boldsymbol{n}, \qquad \text{on } \partial\mathcal{P}_\tau. \tag{14.38}$$

Chapter 15

Principle of Virtual Power

The aim of this Chapter is to derive the governing equations for a bulk-surface material undergoing motion and phase separation within a framework that is independent of constitutive equations. For this purpose, we use the *principle of virtual power*. For readers unfamiliar with the principle of virtual power, a general introduction to this formalism is presented in Section 15.1, detailing its use and illustrating its implications by applying the principle to a simple material. In Section 15.2, we employ the principle of virtual power to determine the *structure of the microtractions and tractions*, as well as of the *pointwise balance of microforces and forces* in our coupled bulk and surface material. In Section 15.3, we demonstrate how the requirement of *frame indifference* for the internal virtual power implies symmetry for the stresses in the bulk-surface material. Lastly, in Section 15.4 we present the *partwise balance of microforces, forces, microtorques, and torques*, which complement the theory.

15.1 Introduction to the principle of virtual power's formalism

The principle of virtual power is a powerful and natural approach to formulate continuum theories for standard and complex materials. In this Subsection, we provide the reader with an introduction to this method. To this end, we discuss the use of the virtual power formalism and its application in literature in Subsection 15.1.1. To illustrate this approach in more detail, we apply the principle to a simple material and discuss its consequences in Subsection 15.1.2. The statement of virtual power in Section 15.2 for the bulk-surface material can be seen as an extension of the theory presented for the simple material in Subsection 15.1.2.

15.1.1 From balance laws to the virtual power principle

Classical continuum mechanics is based on balance equations, such as the balance laws of linear and angular momentum, which form the fundamental postulates on which theory for classical continua resides. In particular, the balance laws of linear and angular momentum can be combined to form an integral relation: the so-called *equation of virtual power* or *virtual power balance*. This integral identity represents the weak formulation of the equations of motion.

The approach outlined above lacks generality, and can not be easily extended to non-classical continua, i.e. continua with a particular microstructure. Difficulties encountered in postulating new balance equations for these non-standard continua involve the choice of the structure of these balance laws, as well as their underlying motivation. To address this, more novel approaches take the virtual power balance as a fundamental principle, rather than to deduce it from the balance laws. This alternative perspective is known as the *virtual power principle* and proves valuable in formulating generalized balance laws for non-classical continua.

There exists a large set of literature on the principle of virtual power. In the following, we provide an incomplete overview of the main and more recent contributions to the development and application of the principle of virtual powers' formalism. Although it is not our aim to present a literature overview of recent developments in continuum theories of enriched continua[12], much of the more modern virtual power machinery has been developed and applied within this field. For further historical background, the reader is referred to Capecchi's study (2012) [30] into the history of virtual work laws. Capecchi discusses the law of virtual work from its early Greek formulations (fourth century BC) to its evolved state in the contributions of Pierre Duhem (late 19th century/early 20th century) to thermodynamics.

In the early 1960s, Toupin [163, 164] was one of the first to base a continuum theory for non-simple materials on the virtual power principle. Using the principle of virtual power machinery, Toupin derived the general balance equations and associated traction relations for an elastic body. In Toupin's theory, the strain energy of the elastic body depends on first and second gradients of the deformation, thereby equipping the material with a so-called couple stress, in addition to the regular Cauchy stress.

Using the virtual work machinery, Mindlin (& Eshel) [121, 122] applied Toupin's work on second-grade materials with couple-stresses to linear elastostatics. In the early 1970s, Germain [70, 71, 72] extended these ideas even further. For this purpose, Germain formalized the principle of virtual work and demonstrated its use by applying it to second-gradient and micropolar continua.

Antman & Osborn (1979) [9] show in their fundamental work that the principle of virtual work and the integral laws of motion are equivalent and independent of constitutive equations. Around the same time, Maugin (1980) [118] presented the formal structure underlying the principle of virtual power before applying it to the study of coupled electro-magneto-mechanical effects in electronic components.

Further generalization of Toupin's theory was achieved by Fried & Gurtin (2006) [65], who developed general balance equations and boundary conditions for second-grade materials, including fluid flows. They employed a nonstandard form of the principle of virtual power based on Gurtin (2002) [85], where a microforce and force balance describing single-crystal viscoplasticity with geometrically necessary dislocations are derived using the principle of virtual power on arbitrary subregions deforming with the material. Fried & Gurtin's work [65] was followed up by a paper by Podio-Guidugli & Vianello (2010) [136], who strengthen and generalize the virtual power principle machinery by demonstrating that hyperstresses and hypertractions convey the same mechanical information.

Two more recent overviews of the virtual power principle are the works by DelPiero (2009) [135] and Lidström (2010) [110]. DelPiero presented a broad overview of the principle, including first and second gradient continuum theories, whereas Lidström includes the possibility of jump discontinuities (shocks) in its formulation, as well as internal and external constraint conditions.

Most recently, Espath (2023) [54] has presented a comprehensive and geometric framework for the theoretical description and modelling of enriched continua using the principle of virtual work machinery. The work presented in this Chapter is an extension of the principle of virtual power for phase-fields with bulk-surface dynamics by Espath [53, 54].

[12]Continua which contain a type of enrichment, for instance due to their underlying microstructure.

Remark 15.1 (Note on nomenclature) In literature, the principle of virtual power is also called the *principle of virtual work*, the *principle of virtual velocities*, or even the *principle of virtual displacements*. Usually, the term virtual work is encountered when the principle describes an equilibrium, whereas the notion of virtual power is used when the principle describes the kinematic processes for an evolving body, thereby allowing for inertia. Throughout this work, we use the term principle of virtual power to refer to the formalism, as we account in our theory for an evolving body and corresponding inertial effects. Furthermore, we disregard the notion of virtual velocity or displacement, as this is coupled to the constitutive response of the material, i.e. whether the material behaves as a solid or fluid. □

15.1.2 Principle of virtual power for a simple material

In this Subsection, we consider a material body $\mathcal{B}$ occupying a three-dimensional region of space and let $\mathcal{B}_\tau$ denote its deformed state at some fixed time τ. Let $\mathcal{P}_\tau$ denote an arbitrary subregion of the deformed body $\mathcal{B}_\tau$ with $\boldsymbol{n}$ the outward unit normal on the boundary $\partial\mathcal{P}_\tau$ of $\mathcal{P}_\tau$. In the following, we present a continuum theory for a *simple material*, in which a single vector field field describes the kinematics. For this purpose, we introduce the admissible virtual vector field χ on $\mathcal{P}_\tau$, which should be thought of as a virtual displacement or velocity field. Furthermore, we wish to emphasize that our choice of arbitrary parts is restricted to those with continuous outward unit normal fields, meaning that additional interactions at points where the boundary $\partial\mathcal{P}_\tau$ loses its smoothness are not considered, and thus do not appear in the virtual power principle presented in this Subsection.

In classical continuum mechanics, the power expended within an arbitrary part $\mathcal{P}_\tau$ migrating with the deformed body of a simple material reads

$$\mathcal{V}_{\text{int}}(\mathcal{P}_\tau;\chi) := \int_{\mathcal{P}_\tau} \mathbf{T} : \operatorname{grad}\chi \, \mathrm{d}v_\tau, \tag{15.1}$$

where $\mathbf{T}$ denotes the Cauchy stress. Notice that we have replaced the classical displacement or velocity field by the virtual vector field χ, thereby arriving at the *internal virtual power* in (15.1). In the above expression (15.1), the term $\mathbf{T} : \operatorname{grad}\chi$ represents the stress power, in which $\mathbf{T}$ is acting on $\operatorname{grad}\chi$, and we say that $\mathbf{T}$ is power conjugate to $\operatorname{grad}\chi$. To complement the internal power expenditure (15.1), we postulate that the *external virtual power expenditure* is defined as

$$\mathcal{V}_{\text{ext}}(\mathcal{P}_\tau;\chi) := \int_{\mathcal{P}_\tau} \boldsymbol{b}\cdot\chi \, \mathrm{d}v_\tau + \int_{\partial\mathcal{P}_\tau} \boldsymbol{t}_{\mathcal{S}}\cdot\chi \, \mathrm{d}a_\tau, \tag{15.2}$$

where $\boldsymbol{b} = \boldsymbol{b}^{\text{ni}} + \boldsymbol{b}^{\text{in}}$ denotes the inertial and non-inertial body force acting within the body [129], while $\boldsymbol{t}_{\mathcal{S}}$ represents the traction acting on the boundary $\partial\mathcal{P}_\tau$ of $\mathcal{P}_\tau$. We can say that both $\boldsymbol{t}_{\mathcal{S}}$ and $\boldsymbol{b}$ are power conjugate to the virtual vector field χ.

Now, the *principle of virtual power* is the requirement that the postulated internal (15.1) and external (15.2) power expenditures are balanced, that is, that the virtual power balance

$$\mathcal{V}_{\text{ext}}(\mathcal{P}_\tau;\chi) = \mathcal{V}_{\text{int}}(\mathcal{P}_\tau;\chi), \tag{15.3}$$

is satisfied for all admissible virtual fields χ and any spatial part $\mathcal{P}_\tau$.

To elucidate the consequences of the principle (15.3), we apply the divergence theorem to the internal power expenditure (15.1), which yields the following expression for the internal power

$$\mathcal{V}_{\text{int}}(\mathcal{P}_\tau;\chi) = \int_{\mathcal{P}_\tau} \mathbf{T} : \operatorname{grad}\chi \, \mathrm{d}v_\tau = -\int_{\mathcal{P}_\tau} \operatorname{div}\mathbf{T}\cdot\chi \, \mathrm{d}v_\tau + \int_{\partial\mathcal{P}_\tau} \mathbf{T}\boldsymbol{n}\cdot\chi \, \mathrm{d}a_\tau. \tag{15.4}$$

Thus, in view of (15.2) and (15.4), the virtual power balance (15.3) becomes

$$\int_{\mathcal{P}_\tau} (\operatorname{div}\mathbf{T} + \boldsymbol{b})\cdot\chi \, \mathrm{d}v_\tau + \int_{\partial\mathcal{P}_\tau} (\boldsymbol{t}_{\mathcal{S}} - \mathbf{T}\boldsymbol{n})\cdot\chi \, \mathrm{d}a_\tau = 0. \tag{15.5}$$

The arbitrary choice of spatial part $\mathcal{P}_\tau$ and virtual field χ allows us to call upon the fundamental lemma of the calculus of variations. As a result, we arrive at the pointwise field equations

$$\operatorname{div}\mathbf{T} + \boldsymbol{b} = \mathbf{0}, \qquad \text{in } \mathcal{P}_\tau, \tag{15.6}$$

which we recognize as the pointwise balance of forces. Moreover, writing the inertial body force as $\boldsymbol{b}^{\text{in}} := -\varrho_{\mathcal{P}}\dot{\boldsymbol{v}}$ results in the classical balance

$$\operatorname{div}\mathbf{T} + \boldsymbol{b}^{\text{ni}} = \varrho_{\mathcal{P}}\dot{\boldsymbol{v}}, \qquad \text{in } \mathcal{P}_\tau, \tag{15.7}$$

with $\varrho_{\mathcal{P}}$ being the material's mass density. A second consequence of the localization of (15.5) is that the surface traction is given by

$$\boldsymbol{t}_{\mathcal{S}}(\boldsymbol{n}) = \mathbf{T}\boldsymbol{n}, \qquad \text{on } \partial\mathcal{P}_\tau, \tag{15.8}$$

which is Cauchy's classical relation for traction across a surface with unit normal $\boldsymbol{n}$ [62].

Notice that the pointwise balance of forces (15.6) and surface traction condition (15.8) are independent of constitutive choices, and hence valid for both solids and fluids. Most importantly, since the choice of the part $\mathcal{P}_\tau$ is arbitrary, these results must hold throughout the deformed material body $\mathcal{B}_\tau$.

Remark 15.2 (Additional requirement: frame indifference) The virtual power principle, i.e. the requirement that the virtual power balance holds, is often accompanied by an additional requirement: the requirement of frame indifference of the expended power. The latter requirement has important consequences. For instance, for the simple material considered in this Subsection, requiring frame indifference of the virtual power expenditure (15.1) implies that the Cauchy stress is symmetric, i.e. $\mathbf{T} = \mathbf{T}^\top$, which represents the pointwise balance of angular momentum. The reader is referred to [86] for more details. In Section 15.3, we detail the consequences of the requirement of frame indifference for the coupled bulk-surface material. □

15.2 Statement of the virtual power principle

The aim of this Section is to derive the field equations of the continuum framework for bulk-surface materials undergoing motion and phase separation. For this purpose, we devise a principle of virtual power on the material part $\mathcal{P}_\tau$, where the surface $\partial\mathcal{P}_\tau$ may lose smoothness along a curve, viz. the edge $\partial^2\mathcal{P}_\tau$. In our principle, kinematical processes in the form of scalar and vector fields in the deformed bulk and surface material are considered. Then, the principle of virtual power requires that the following virtual power balance holds

$$\mathcal{V}_{\text{ext}}(\mathcal{P}_\tau, \partial\mathcal{P}_\tau; \chi_{\mathcal{P}}, \chi_{\mathcal{P}}, \chi_{\partial\mathcal{P}}, \chi_{\partial\mathcal{P}}) = \mathcal{V}_{\text{int}}(\mathcal{P}_\tau, \partial\mathcal{P}_\tau; \chi_{\mathcal{P}}, \chi_{\mathcal{P}}, \chi_{\partial\mathcal{P}}, \chi_{\partial\mathcal{P}}), \tag{15.9}$$

where $\chi_{\mathcal{P}}$ and $\boldsymbol{\chi}_{\mathcal{P}}$ are, respectively, sufficiently smooth scalar and vector fields representing the kinematical processes on $\mathcal{P}_\tau$, and similarly, $\chi_{\mathcal{P}}$ and $\boldsymbol{\chi}_{\mathcal{P}}$ denote sufficiently smooth scalar and vector fields representing the kinematical processes on $\partial\mathcal{P}_\tau$. We consider the following internal virtual power

$$\begin{aligned}
\mathcal{V}_{\text{int}}(\mathcal{P}_\tau, \partial\mathcal{P}_\tau; \boldsymbol{\chi}_{\mathcal{P}}, \chi_{\mathcal{P}}, \boldsymbol{\chi}_{\partial\mathcal{P}}, \chi_{\partial\mathcal{P}}) \coloneqq & \int_{\mathcal{P}_\tau} \mathbf{T} : \operatorname{grad}\boldsymbol{\chi}_{\mathcal{P}}\, \mathrm{d}v_\tau + \int_{\partial\mathcal{P}_\tau} \mathbf{H} : \operatorname{grad}_{\mathcal{S}}\boldsymbol{\chi}_{\partial\mathcal{P}}\, \mathrm{d}a_\tau \\
& - \int_{\mathcal{P}_\tau} \pi\chi_{\mathcal{P}}\, \mathrm{d}v_\tau - \int_{\partial\mathcal{P}_\tau} \varpi\chi_{\partial\mathcal{P}}\, \mathrm{d}a_\tau \\
& + \int_{\mathcal{P}_\tau} \boldsymbol{\xi} \cdot \operatorname{grad}\chi_{\mathcal{P}}\, \mathrm{d}v_\tau + \int_{\partial\mathcal{P}_\tau} \boldsymbol{\tau} \cdot \operatorname{grad}_{\mathcal{S}}\chi_{\partial\mathcal{P}}\, \mathrm{d}a_\tau, \quad (15.10)
\end{aligned}$$

where $\mathbf{T}$ and $\mathbf{H}$ denote the stresses in the bulk and surface material, respectively, and similarly, $\boldsymbol{\xi}$ and $\boldsymbol{\tau}$ represent the bulk and surface microstresses. In the above, the scalar fields π and ϖ are internal microforces acting on the bulk and surface material, respectively. To complement the internal virtual power (15.9), we define the external virtual power as

$$\begin{aligned}
\mathcal{V}_{\text{ext}}(\mathcal{P}_\tau, \partial\mathcal{P}_\tau; \boldsymbol{\chi}_{\mathcal{P}}, \chi_{\mathcal{P}}, \boldsymbol{\chi}_{\partial\mathcal{P}}, \chi_{\partial\mathcal{P}}) \coloneqq & \int_{\mathcal{P}_\tau} \boldsymbol{b} \cdot \boldsymbol{\chi}_{\mathcal{P}}\, \mathrm{d}v_\tau + \int_{\partial\mathcal{P}_\tau} (\boldsymbol{g} - \boldsymbol{t}_{\mathcal{S}}) \cdot \boldsymbol{\chi}_{\partial\mathcal{P}}\, \mathrm{d}a_\tau \\
& + \int_{\partial\mathcal{P}_\tau} \boldsymbol{t}_{\mathcal{S}} \cdot \boldsymbol{\chi}_{\mathcal{P}}\, \mathrm{d}a_\tau + \int_{\partial^2\mathcal{P}_\tau} \boldsymbol{h}_{\partial\mathcal{S}} \cdot \boldsymbol{\chi}_{\partial\mathcal{P}}\, \mathrm{d}\sigma_\tau \\
& + \int_{\mathcal{P}_\tau} \gamma\chi_{\mathcal{P}}\, \mathrm{d}v_\tau + \int_{\partial\mathcal{P}_\tau} (\zeta - \xi_{\mathcal{S}})\chi_{\partial\mathcal{P}}\, \mathrm{d}a_\tau \\
& + \int_{\partial\mathcal{P}_\tau} \xi_{\mathcal{S}}\chi_{\mathcal{P}}\, \mathrm{d}a_\tau + \int_{\partial^2\mathcal{P}_\tau} \tau_{\partial\mathcal{S}}\chi_{\partial\mathcal{P}}\, \mathrm{d}\sigma_\tau, \quad (15.11)
\end{aligned}$$

where $\boldsymbol{b}$ is the external body force acting on the bulk material, while $\boldsymbol{g} - \boldsymbol{t}_{\mathcal{S}}$ represents the effective external force acting on the surface material, with $\boldsymbol{g}$ being the external surface body force and the surface traction $\boldsymbol{t}_{\mathcal{S}}$ representing the contribution from the bulk material. Furthermore, $\boldsymbol{h}_{\partial\mathcal{S}}$ denotes the edge traction. Similarly, for the scalar fields, we have that γ denotes the external microforce acting on the bulk material via the scalar bulk field $\chi_{\mathcal{P}}$, whereas $(\zeta - \xi_{\mathcal{S}})$ is power conjugate with $\chi_{\partial\mathcal{P}}$. Here, ζ is the contribution from the environment and referred to as the surface external microforce, whereas $\xi_{\mathcal{S}}$ is the surface microtraction across the surface originating from the bulk. Lastly, the field $\tau_{\partial\mathcal{S}}$ in the external virtual power expenditure (15.11) represents the edge microtraction.

Next, by combining the external (15.11) and internal (15.10) virtual power through the virtual power balance (15.9), we are led to

$$\begin{aligned}
& \int_{\mathcal{P}_\tau} \boldsymbol{\chi}_{\mathcal{P}} \cdot (\operatorname{div}\mathbf{T} + \boldsymbol{b})\, \mathrm{d}v_\tau + \int_{\partial\mathcal{P}_\tau} \boldsymbol{\chi}_{\mathcal{P}} \cdot (\boldsymbol{t}_{\mathcal{S}} - \mathbf{T}\cdot\boldsymbol{n})\, \mathrm{d}a_\tau \\
& \quad + \int_{\mathcal{P}_\tau} \chi_{\mathcal{P}}(\operatorname{div}\boldsymbol{\xi} + \pi + \gamma)\, \mathrm{d}v_\tau + \int_{\partial\mathcal{P}_\tau} \chi_{\mathcal{P}}(\xi_{\mathcal{S}} - \boldsymbol{\xi}\cdot\boldsymbol{n})\, \mathrm{d}a_\tau \\
& \quad + \int_{\partial\mathcal{P}_\tau} \boldsymbol{\chi}_{\partial\mathcal{P}} \cdot (\operatorname{div}_{\mathcal{S}}(\mathbf{H}\mathbf{P}_n) + \boldsymbol{g} - \boldsymbol{t}_{\mathcal{S}})\, \mathrm{d}a_\tau + \int_{\partial^2\mathcal{P}_\tau} \boldsymbol{\chi}_{\partial\mathcal{P}} \cdot (\boldsymbol{h}_{\partial\mathcal{S}} - \{\!\{\mathbf{H}\boldsymbol{\nu}\}\!\})\, \mathrm{d}\sigma_\tau \\
& \quad + \int_{\partial\mathcal{P}_\tau} \chi_{\partial\mathcal{P}}(\operatorname{div}_{\mathcal{S}}(\mathbf{P}_n\boldsymbol{\tau}) + \varpi + \zeta - \xi_{\mathcal{S}})\, \mathrm{d}a_\tau + \int_{\partial^2\mathcal{P}_\tau} \chi_{\partial\mathcal{P}}(\tau_{\partial\mathcal{S}} - \{\!\{\boldsymbol{\tau}\cdot\boldsymbol{\nu}\}\!\})\, \mathrm{d}\sigma_\tau = 0, \quad (15.12)
\end{aligned}$$

where we have used the divergence theorem and surface divergence theorem for non-smooth closed surfaces (13.12).

Bearing in mind that the virtual power principle (15.9), and thus (15.12), holds for all admissible kinematical processes, we arrive at the following consequences for the continuum theory. First, the field equations read

$$\operatorname{div}\mathbf{T}+\boldsymbol{b}=\mathbf{0},\quad \text{in } \mathcal{P}_\tau,\quad \text{and}\quad \operatorname{div}_{\mathcal{S}}(\mathbf{H}\mathbf{P}_{n})+\boldsymbol{g}-\boldsymbol{t}_{\mathcal{S}}=\mathbf{0},\quad \text{on } \partial\mathcal{P}_\tau, \tag{15.13}$$

and

$$\operatorname{div}\boldsymbol{\xi}+\pi+\gamma=0,\quad \text{in } \mathcal{P}_\tau,\quad \text{and}\quad \operatorname{div}_{\mathcal{S}}(\mathbf{P}_{n}\boldsymbol{\tau})+\varpi+\zeta-\xi_{\mathcal{S}}=0,\quad \text{on } \partial\mathcal{P}_\tau. \tag{15.14}$$

In the above, we recognize the pointwise force balances (15.13) and the pointwise microforce balances (15.14) on the bulk and surface parts. Secondly, as a result of the variational arguments, the tractions are given by

$$\boldsymbol{t}_{\mathcal{S}}=\mathbf{T}\boldsymbol{n},\qquad \text{on } \partial\mathcal{P}_\tau,\qquad \text{and}\qquad \boldsymbol{h}_{\partial\mathcal{S}}=\{\!\{\mathbf{H}\boldsymbol{\nu}\}\!\},\qquad \text{on } \partial^2\mathcal{P}_\tau, \tag{15.15}$$

while the microtractions read

$$\xi_{\mathcal{S}}=\boldsymbol{\xi}\cdot\boldsymbol{n},\qquad \text{on } \partial\mathcal{P}_\tau,\qquad \text{and}\qquad \tau_{\partial\mathcal{S}}=\{\!\{\boldsymbol{\tau}\cdot\boldsymbol{\nu}\}\!\},\qquad \text{on } \partial^2\mathcal{P}_\tau. \tag{15.16}$$

Lastly, decomposition of the external bulk and surface forces into an inertial and non-inertial part allows us to write

$$\boldsymbol{b}:=\boldsymbol{b}^{\mathrm{ni}}+\boldsymbol{b}^{\mathrm{in}},\qquad \text{and}\qquad \boldsymbol{g}:=\boldsymbol{g}^{\mathrm{ni}}+\boldsymbol{g}^{\mathrm{in}}. \tag{15.17}$$

Furthermore, we consider the following expressions for the inertial body forces

$$\boldsymbol{b}^{\mathrm{in}}:=-\varrho_{\partial\mathcal{P}}\dot{\boldsymbol{v}}_{\mathcal{P}},\qquad \text{and}\qquad \boldsymbol{g}^{\mathrm{in}}:=-\varrho_{\partial\mathcal{P}}\mathring{\boldsymbol{v}}_{\partial\mathcal{P}}=-\rho\ell_\tau\mathring{\boldsymbol{v}}_{\partial\mathcal{P}}, \tag{15.18}$$

so that the pointwise force balances in (15.13) can be written as

$$\varrho_{\mathcal{P}}\dot{\boldsymbol{v}}_{\mathcal{P}}=\operatorname{div}\mathbf{T}+\boldsymbol{b}^{\mathrm{ni}},\qquad \text{in } \mathcal{P}_\tau, \tag{15.19}$$

and

$$\rho\ell_\tau\mathring{\boldsymbol{v}}_{\partial\mathcal{P}}=\operatorname{div}_{\mathcal{S}}(\mathbf{H}\mathbf{P}_{n})+\boldsymbol{g}^{\mathrm{ni}}-\boldsymbol{t}_{\mathcal{S}},\qquad \text{on } \partial\mathcal{P}_\tau. \tag{15.20}$$

In addition, by splitting $\operatorname{div}_{\mathcal{S}}(\mathbf{H}\mathbf{P}_{n})=\operatorname{div}_{\mathcal{S}}\mathbf{H}+2K\mathbf{H}\boldsymbol{n}$ and $\operatorname{div}_{\mathcal{S}}(\mathbf{P}_{n}\boldsymbol{\tau})=\operatorname{div}_{\mathcal{S}}\boldsymbol{\tau}+2K\boldsymbol{\tau}\cdot\boldsymbol{n}$, the field equation (15.20) can be written as

$$\rho\ell_\tau\mathring{\boldsymbol{v}}_{\partial\mathcal{P}}=\operatorname{div}_{\mathcal{S}}\mathbf{H}+2K\mathbf{H}\boldsymbol{n}+\boldsymbol{g}^{\mathrm{ni}}-\boldsymbol{t}_{\mathcal{S}},\qquad \text{on } \partial\mathcal{P}_\tau, \tag{15.21}$$

while equation $(15.14)_2$ becomes

$$\operatorname{div}_{\mathcal{S}}\boldsymbol{\tau}+2K\boldsymbol{\tau}\cdot\boldsymbol{n}+\varpi+\zeta-\xi_{\mathcal{S}}=0,\qquad \text{on } \partial\mathcal{P}_\tau. \tag{15.22}$$

Remark 15.3 (Discontinuous surface microstress and stress) Note that the surface microstress and stress may be discontinuous across the edge $\partial^2\mathcal{P}_\tau$. In what follows, we further motivate what allows for these discontinuities. In literature on higher-order continua, edge tractions and edge microtractions can be written as

$$\boldsymbol{h}_{\partial\mathcal{S}}:=\{\!\{(\mathbb{G}\boldsymbol{n})\boldsymbol{\nu}\}\!\},\qquad \text{and}\qquad \tau_{\partial\mathcal{S}}:=\{\!\{(\boldsymbol{\Sigma}\boldsymbol{n})\cdot\boldsymbol{\nu}\}\!\}, \tag{15.23}$$

where $\mathbb{G}$ and $\boldsymbol{\Sigma}$ are the hyperstress and the hypermicrostress, respectively, see for instance [61, 55]. Therefore, although one assumes that $\mathbb{G}$ and $\boldsymbol{\Sigma}$ are continuous, it is expected that $\mathbb{G}\boldsymbol{n}^+\neq\mathbb{G}\boldsymbol{n}^-$ and $\boldsymbol{\Sigma}\boldsymbol{n}^+\neq\boldsymbol{\Sigma}\boldsymbol{n}^-$ on $\partial^2\mathcal{P}_\tau$. Conversely, in bulk-surface systems, edge tractions $(15.15)_2$ and edge microtraction $(15.16)_2$ take the form

$$\boldsymbol{h}_{\partial\mathcal{S}}:=\{\!\{\mathbf{H}\boldsymbol{\nu}\}\!\},\qquad \text{and}\qquad \tau_{\partial\mathcal{S}}:=\{\!\{\boldsymbol{\tau}\cdot\boldsymbol{\nu}\}\!\},\qquad \text{on } \partial^2\mathcal{P}_\tau. \tag{15.24}$$

Thus, one may argue that the surface stress $\mathbf{H}$ and surface microstress $\boldsymbol{\tau}$ have a similar role as the fields $\mathbb{G}\boldsymbol{n}^\pm$ and $\boldsymbol{\Sigma}\boldsymbol{n}^\pm$. Therefore, we consider that the surface stress $\mathbf{H}$ and surface microstress $\boldsymbol{\tau}$ are piecewise smooth, but can be discontinuous on an edge $\partial^2\mathcal{P}_\tau$.□

15.3 Frame indifference principle

Here, we discuss the consequences of the frame indifference requirement of the virtual powers. Consider a change of frame given by the following mappings

$$\chi_{\mathcal{P}} \mapsto \chi_{\mathcal{P}} + \boldsymbol{\beta} + \boldsymbol{\Omega}\boldsymbol{y}_{\mathcal{P}}, \quad \text{in } \mathcal{P}_\tau, \quad \text{and} \quad \chi_{\partial\mathcal{P}} \mapsto \chi_{\partial\mathcal{P}} + \boldsymbol{\beta} + \boldsymbol{\Omega}\boldsymbol{y}_{\partial\mathcal{P}}, \quad \text{on } \partial\mathcal{P}_\tau, \tag{15.25}$$

where $\boldsymbol{\beta}$ denotes the velocity of frame and the skew-symmetric tensor $\boldsymbol{\Omega}$ represents the rotation of frame, both independent of time. From (15.25) follows that

$$\operatorname{grad}\chi_{\mathcal{P}} \mapsto \operatorname{grad}\chi_{\mathcal{P}} + \boldsymbol{\Omega}, \qquad \text{in } \mathcal{P}_\tau, \qquad \text{and} \tag{15.26}$$

$$\operatorname{grad}_{\mathcal{S}}\chi_{\partial\mathcal{P}} \mapsto \operatorname{grad}_{\mathcal{S}}\chi_{\partial\mathcal{P}} + \boldsymbol{\Omega}\mathbf{P}_n, \qquad \text{on } \partial\mathcal{P}_\tau. \tag{15.27}$$

We emphasize that scalar vector fields are not affected by a change in observer, i.e.

$$\chi_{\mathcal{P}} \mapsto \chi_{\mathcal{P}}, \quad \text{in } \mathcal{P}_\tau, \quad \text{and} \quad \chi_{\partial\mathcal{P}} \mapsto \chi_{\partial\mathcal{P}}, \quad \text{on } \partial\mathcal{P}_\tau. \tag{15.28}$$

We now postulate that the internal virtual power defined in (15.10) is indifferent to the changes in frame specified in (15.25). This implies that

$$\begin{aligned}
&\mathcal{V}_{\text{int}}(\mathcal{P}_\tau, \partial\mathcal{P}_\tau; \boldsymbol{\chi}_{\mathcal{P}}, \chi_{\mathcal{P}}, \boldsymbol{\chi}_{\partial\mathcal{P}}, \chi_{\partial\mathcal{P}}) \\
&\qquad = \mathcal{V}_{\text{int}}(\mathcal{P}_\tau, \partial\mathcal{P}_\tau; \boldsymbol{\chi}_{\mathcal{P}} + \boldsymbol{\beta} + \boldsymbol{\Omega}\boldsymbol{y}, \chi_{\mathcal{P}}, \boldsymbol{\chi}_{\partial\mathcal{P}} + \boldsymbol{\beta} + \boldsymbol{\Omega}\boldsymbol{y}, \chi_{\partial\mathcal{P}}),
\end{aligned} \tag{15.29}$$

with $\boldsymbol{y} \in \mathcal{P}_\tau \cup \partial\mathcal{P}_\tau$. Using expressions (15.26) and (15.27), we arrive at

$$\begin{aligned}
&\int_{\mathcal{P}_\tau} \mathbf{T} : \operatorname{grad}\boldsymbol{\chi}_{\mathcal{P}} \, \mathrm{d}v_\tau + \int_{\partial\mathcal{P}_\tau} \mathbf{H} : \operatorname{grad}_{\mathcal{S}}\boldsymbol{\chi}_{\partial\mathcal{P}} \, \mathrm{d}a_\tau \\
&\qquad = \int_{\mathcal{P}_\tau} \mathbf{T} : (\operatorname{grad}\boldsymbol{\chi}_{\mathcal{P}} + \boldsymbol{\Omega}) \, \mathrm{d}v_\tau + \int_{\partial\mathcal{P}_\tau} \mathbf{H} : (\operatorname{grad}_{\mathcal{S}}\boldsymbol{\chi}_{\partial\mathcal{P}} + \boldsymbol{\Omega}\mathbf{P}_n) \, \mathrm{d}a_\tau.
\end{aligned} \tag{15.30}$$

Equation (15.30) holds for

$$\mathbf{T} : \boldsymbol{\Omega} = \mathbf{0}, \quad \text{in } \mathcal{P}_\tau, \quad \text{and} \quad \mathbf{H} : \boldsymbol{\Omega}\mathbf{P}_n = \mathbf{0}, \quad \text{on } \partial\mathcal{P}_\tau, \tag{15.31}$$

where $(15.31)_2$ can be written as

$$\mathbf{H} : \boldsymbol{\Omega} = \mathbf{H}\boldsymbol{n} \cdot \boldsymbol{\Omega}\boldsymbol{n}, \quad \text{on } \partial\mathcal{P}_\tau, \tag{15.32}$$

using $\mathbf{P}_n := \mathbf{1} - \boldsymbol{n} \otimes \boldsymbol{n}$. As $(15.31)_1$ holds for all skew-symmetric tensors $\boldsymbol{\Omega}$, we find that the bulk stress $\mathbf{T}$ is symmetric, i.e.

$$\mathbf{T} = \mathbf{T}^\top, \quad \text{in } \mathcal{P}_\tau. \tag{15.33}$$

Similarly, from $(15.31)_2$ follows

$$\mathbf{H}\mathbf{P}_n = (\mathbf{H}\mathbf{P}_n)^\top = \mathbf{P}_n\mathbf{H}^\top, \quad \text{on } \partial\mathcal{P}_\tau. \tag{15.34}$$

Moreover, expression (15.34) implies that the surface stress tensor is symmetric, that is $\mathbf{H} = \mathbf{H}^\top$ and requires simultaneously that it annihilates the normal, i.e. $\mathbf{H}\boldsymbol{n} = \mathbf{0}$. Thus, the symmetry implications for the bulk and surface stress in (15.33) and (15.34), respectively, are consequences of the frame indifference postulate for the internal virtual work (15.29).

Lastly, frame indifference of the internal virtual power also implies that the external virtual power is frame indifferent, see Remark 15.4.

Remark 15.4 (Frame indifference of the external virtual power) Frame indifference of the external virtual power in (15.11) is the requirement that

$$\begin{aligned}\mathcal{V}_{\text{ext}}(\mathcal{P}_\tau, \partial\mathcal{P}_\tau; \boldsymbol{\chi}_{\mathcal{P}}, \chi_{\mathcal{P}}, \boldsymbol{\chi}_{\partial\mathcal{P}}, \chi_{\partial\mathcal{P}}) \\ = \mathcal{V}_{\text{ext}}(\mathcal{P}_\tau, \partial\mathcal{P}_\tau; \boldsymbol{\chi}_{\mathcal{P}} + \boldsymbol{\beta} + \boldsymbol{\Omega}\boldsymbol{y}, \chi_{\mathcal{P}}, \boldsymbol{\chi}_{\partial\mathcal{P}} + \boldsymbol{\beta} + \boldsymbol{\Omega}\boldsymbol{y}, \chi_{\partial\mathcal{P}}),\end{aligned} \tag{15.35}$$

holds under all changes of frame (15.25). This requirement is satisfied through the frame indifference postulate for the internal virtual power (15.29) and the virtual power principle (15.9), that is

$$\begin{aligned}\mathcal{V}_{\text{ext}}(\mathcal{P}_\tau, \partial\mathcal{P}_\tau; \boldsymbol{\chi}_{\mathcal{P}} + \boldsymbol{\beta} + \boldsymbol{\Omega}\boldsymbol{y}, \chi_{\mathcal{P}}, \boldsymbol{\chi}_{\partial\mathcal{P}} + \boldsymbol{\beta} + \boldsymbol{\Omega}\boldsymbol{y}, \chi_{\partial\mathcal{P}}) \\ = \mathcal{V}_{\text{int}}(\mathcal{P}_\tau, \partial\mathcal{P}_\tau; \boldsymbol{\chi}_{\mathcal{P}} + \boldsymbol{\beta} + \boldsymbol{\Omega}\boldsymbol{y}, \chi_{\mathcal{P}}, \boldsymbol{\chi}_{\partial\mathcal{P}} + \boldsymbol{\beta} + \boldsymbol{\Omega}\boldsymbol{y}, \chi_{\partial\mathcal{P}}) \\ = \mathcal{V}_{\text{int}}(\mathcal{P}_\tau, \partial\mathcal{P}_\tau; \boldsymbol{\chi}_{\mathcal{P}}, \chi_{\mathcal{P}}, \boldsymbol{\chi}_{\partial\mathcal{P}}, \chi_{\partial\mathcal{P}}) \\ = \mathcal{V}_{\text{ext}}(\mathcal{P}_\tau, \partial\mathcal{P}_\tau; \boldsymbol{\chi}_{\mathcal{P}}, \chi_{\mathcal{P}}, \boldsymbol{\chi}_{\partial\mathcal{P}}, \chi_{\partial\mathcal{P}}).\end{aligned} \tag{15.36}$$

□

15.4 Complementary partwise balances

The aim of this Section is to construct the partwise integral balances using the field equations (15.13) and (15.14) presented in Section 15.2. We present the partwise balances of microforces and forces in Subsection 15.4.1, and in Subsection 15.4.2 we derive the partwise balances of microtorques and torques.

15.4.1 Partwise balance of microforces and forces

To arrive at the partwise bulk-surface balance of forces, we integrate the field equations, namely the pointwise balance of forces (15.13), on their respective parts, and find

$$\int_{\mathcal{P}_\tau} (\operatorname{div}\mathbf{T} + \boldsymbol{b})\,\mathrm{d}v_\tau + \int_{\partial\mathcal{P}_\tau} (\operatorname{div}_{\mathcal{S}}(\mathbf{H}\mathbf{P}_{\!n}) + \boldsymbol{g} - \boldsymbol{t}_{\mathcal{S}})\,\mathrm{d}a_\tau = \mathbf{0}. \tag{15.37}$$

Next, using the divergence theorem and the divergence theorem on non-smooth closed surfaces (13.12), we arrive at

$$\int_{\mathcal{P}_\tau} \boldsymbol{b}\,\mathrm{d}v_\tau + \int_{\partial\mathcal{P}_\tau} \mathbf{T}\boldsymbol{n}\,\mathrm{d}a_\tau + \int_{\partial\mathcal{P}_\tau} (\boldsymbol{g} - \boldsymbol{t}_{\mathcal{S}})\,\mathrm{d}a_\tau + \int_{\partial^2\mathcal{P}_\tau} \{\!\{\mathbf{H}\boldsymbol{\nu}\}\!\}\,\mathrm{d}\sigma_\tau = \mathbf{0}. \tag{15.38}$$

In view of the expression $(15.15)_1$ for the surface traction, we find the partwise bulk-surface balance of forces

$$\mathcal{F}^\sharp(\mathcal{P}_\tau, \partial\mathcal{P}_\tau) := \int_{\mathcal{P}_\tau} \boldsymbol{b}\,\mathrm{d}v_\tau + \int_{\partial\mathcal{P}_\tau} \boldsymbol{g}\,\mathrm{d}a_\tau + \int_{\partial^2\mathcal{P}_\tau} \boldsymbol{h}_{\partial\mathcal{S}}\,\mathrm{d}\sigma_\tau = \mathbf{0}. \tag{15.39}$$

Similarly, for the remaining field equations, viz. the pointwise balances of microforce (15.14), emulating the above procedure, we arrive at the partwise bulk-surface balance of microforces

$$\mathcal{F}^\flat(\mathcal{P}_\tau, \partial\mathcal{P}_\tau) := \int_{\mathcal{P}_\tau} (\pi + \gamma)\,\mathrm{d}v_\tau + \int_{\partial\mathcal{P}_\tau} (\varpi + \zeta)\,\mathrm{d}a_\tau + \int_{\partial^2\mathcal{P}_\tau} \tau_{\partial\mathcal{S}}\,\mathrm{d}\sigma_\tau = 0. \tag{15.40}$$

15.4.2 Partwise balance of microtorques and torques

To arrive at the partwise bulk-surface balances of microtorques and torques of the bulk-surface material, we introduce the position vector $\boldsymbol{r} := \boldsymbol{y} - \boldsymbol{o}$ identifying each point $\boldsymbol{y} \in \mathcal{P}_\tau \cup \partial\mathcal{P}_\tau$, where the origin $\boldsymbol{o} \in \mathscr{E}$ is arbitrarily chosen and fixed.

First, we construct the partwise bulk-surface balance of microtorques. For this purpose, we multiply the pointwise balance of microforces in (15.14) by the position vector $\boldsymbol{r}$, integrate the resulting expressions over their respective parts, and obtain

$$\int_{\mathcal{P}_\tau} \boldsymbol{r}(\operatorname{div}\boldsymbol{\xi} + \pi + \gamma)\,\mathrm{d}v_\tau + \int_{\partial\mathcal{P}_\tau} \boldsymbol{r}(\operatorname{div}_{\mathcal{S}}(\mathbf{P}_n\boldsymbol{\tau}) + \varpi + \zeta - \xi_{\mathcal{S}})\,\mathrm{d}a_\tau = \mathbf{0}. \tag{15.41}$$

Bearing in mind that $\operatorname{grad}\boldsymbol{r} = \mathbf{1}$ and $\operatorname{grad}_{\mathcal{S}}\boldsymbol{r} = \mathbf{P}_n$, we employ the following identities

$$\operatorname{div}(\boldsymbol{r}\otimes\boldsymbol{\xi}) = \boldsymbol{\xi} + \boldsymbol{r}\operatorname{div}\boldsymbol{\xi}, \qquad \text{and} \qquad \operatorname{div}_{\mathcal{S}}(\boldsymbol{r}\otimes\mathbf{P}_n\boldsymbol{\tau}) = \mathbf{P}_n\boldsymbol{\tau} + \boldsymbol{r}\operatorname{div}_{\mathcal{S}}(\mathbf{P}_n\boldsymbol{\tau}), \tag{15.42}$$

followed by the application of the divergence theorems, to write (15.41) as

$$\begin{aligned}\int_{\mathcal{P}_\tau} (\boldsymbol{r}(\pi+\gamma) - \boldsymbol{\xi})\,\mathrm{d}v_\tau + \int_{\partial\mathcal{P}_\tau} (\boldsymbol{r}\otimes\boldsymbol{\xi})\cdot\boldsymbol{n}\,\mathrm{d}a_\tau + \int_{\partial\mathcal{P}_\tau} (\boldsymbol{r}(\varpi+\zeta-\xi_{\mathcal{S}}) - \mathbf{P}_n\boldsymbol{\tau})\,\mathrm{d}a_\tau \\ + \int_{\partial^2\mathcal{P}_\tau} \{\!\{(\boldsymbol{r}\otimes\boldsymbol{\tau})\cdot\boldsymbol{\nu}\}\!\}\,\mathrm{d}\sigma_\tau = \mathbf{0}.\end{aligned} \tag{15.43}$$

Then, in view of the expression for the surface and edge microtraction (15.16), the partwise bulk-surface balance of microtorques reads

$$\begin{aligned}\mathcal{T}^\flat(\mathcal{P}_\tau, \partial\mathcal{P}_\tau) := \int_{\mathcal{P}_\tau} (\boldsymbol{r}(\pi+\gamma) - \boldsymbol{\xi})\,\mathrm{d}v_\tau \\ + \int_{\partial\mathcal{P}_\tau} (\boldsymbol{r}(\varpi+\zeta) - \mathbf{P}_n\boldsymbol{\tau})\,\mathrm{d}a_\tau + \int_{\partial^2\mathcal{P}_\tau} \boldsymbol{r}\tau_{\partial\mathcal{S}}\,\mathrm{d}\sigma_\tau = \mathbf{0}.\end{aligned} \tag{15.44}$$

To derive the partwise bulk-surface balance of torques, we take the tensor product between $\boldsymbol{r}$ and the pointwise balances of force in (15.13). The resulting expressions are integrated over the respective parts, yielding the balance

$$\int_{\mathcal{P}_\tau} \boldsymbol{r}\otimes(\operatorname{div}\mathbf{T} + \boldsymbol{b})\,\mathrm{d}v_\tau + \int_{\partial\mathcal{P}_\tau} \boldsymbol{r}\otimes(\operatorname{div}_{\mathcal{S}}(\mathbf{H}\mathbf{P}_n) + \boldsymbol{g} - \boldsymbol{t}_{\mathcal{S}})\,\mathrm{d}a_\tau = \mathbf{0}, \tag{15.45}$$

Next, we consider the identities

$$\operatorname{div}(\boldsymbol{r}\otimes\mathbf{T}) = \mathbf{T} + \boldsymbol{r}\otimes\operatorname{div}\mathbf{T}, \tag{15.46}$$

and

$$\operatorname{div}_{\mathcal{S}}(\boldsymbol{r}\otimes\mathbf{H}\mathbf{P}_n) = \mathbf{P}_n\mathbf{H}\mathbf{P}_n + \boldsymbol{r}\otimes\operatorname{div}_{\mathcal{S}}(\mathbf{H}\mathbf{P}_n) = \mathbf{H}\mathbf{P}_n + \boldsymbol{r}\otimes\operatorname{div}_{\mathcal{S}}(\mathbf{H}\mathbf{P}_n), \tag{15.47}$$

where we have used the frame-indifference result for the surface stress, i.e. $\mathbf{H}\mathbf{P}_n = \mathbf{P}_n\mathbf{H}^\top$ in (15.34), as well as $\mathbf{P}_n\mathbf{P}_n = \mathbf{P}_n$. The use of these identities in (15.45), followed by application of the divergence theorem and the divergence theorem on non-smooth closed surfaces (13.12), yields

$$\begin{aligned}\int_{\mathcal{P}_\tau} (\boldsymbol{r}\otimes\boldsymbol{b} - \mathbf{T})\,\mathrm{d}v_\tau + \int_{\partial\mathcal{P}_\tau} \boldsymbol{r}\otimes\mathbf{T}\boldsymbol{n}\,\mathrm{d}a_\tau + \int_{\partial\mathcal{P}_\tau} (\boldsymbol{r}\otimes(\boldsymbol{g} - \boldsymbol{t}_{\mathcal{S}}) - \mathbf{H}\mathbf{P}_n)\,\mathrm{d}a_\tau \\ + \int_{\partial^2\mathcal{P}_\tau} \{\!\{\boldsymbol{r}\otimes\mathbf{H}\boldsymbol{\nu}\}\!\}\,\mathrm{d}\sigma_\tau = \mathbf{0}.\end{aligned} \tag{15.48}$$

Then, using the definitions for the surface traction and edge traction (15.15), we arrive at

$$\int_{\mathcal{P}_\tau} (\boldsymbol{r} \otimes \boldsymbol{b} - \mathbf{T})\, \mathrm{d}v_\tau + \int_{\partial\mathcal{P}_\tau} (\boldsymbol{r} \otimes \boldsymbol{g} - \mathbf{HP}_{n})\, \mathrm{d}a_\tau + \int_{\partial^2\mathcal{P}_\tau} \boldsymbol{r} \otimes \boldsymbol{h}_{\partial\mathcal{S}}\, \mathrm{d}\sigma_\tau = \mathbf{0}. \tag{15.49}$$

Lastly, by taking (15.49) and subtracting its transposed form, we obtain the partwise bulk-surface balance of torques

$$\mathcal{T}^\sharp(\mathcal{P}_\tau, \partial\mathcal{P}_\tau) := \int_{\mathcal{P}_\tau} \boldsymbol{r} \wedge \boldsymbol{b}\, \mathrm{d}v_\tau + \int_{\partial\mathcal{P}_\tau} \boldsymbol{r} \wedge \boldsymbol{g}\, \mathrm{d}a_\tau + \int_{\partial^2\mathcal{P}_\tau} \boldsymbol{r} \wedge \boldsymbol{h}_{\partial\mathcal{S}}\, \mathrm{d}\sigma_\tau = \mathbf{0}, \tag{15.50}$$

where we have used the implications of frame-indifference, i.e. $\mathbf{T} = \mathbf{T}^\top$ in (15.33) and $\mathbf{HP}_{n} = (\mathbf{HP}_{n})^\top$ in (15.34). Additionally, we used the wedge product defined as $\boldsymbol{a} \wedge \boldsymbol{b} := \boldsymbol{a} \otimes \boldsymbol{b} - \boldsymbol{b} \otimes \boldsymbol{a}$.

Chapter 16

Free-Energy Imbalance and Constitutive Response Functions

The objective of this Chapter is to present the thermodynamics of the coupled bulk-surface material and to consider its implications in terms of constitutive equations. In Section 16.1, we present the free-energy imbalance for this system. Guided by the free-energy imbalance, we discuss thermodynamically-consistent constitutive response functions in Section 16.2. We conclude this Chapter in Section 16.3 by using a canonical form for the free-energy densities and arrive at the specialized equations for a bulk-surface system undergoing phase separation.

16.1 Free-energy imbalance

In Section 15.2, we presented the internal (15.10) and external power (15.11) for the virtual fields $\boldsymbol{\chi}_{\mathcal{P}}$, $\chi_{\mathcal{P}}$, $\boldsymbol{\chi}_{\partial\mathcal{P}}$ and $\chi_{\partial\mathcal{P}}$ describing the kinematical processes in the coupled bulk-surface material. To obtain the actual external power for a bulk-surface material exhibiting fluidic material behaviour, we need to replace $\boldsymbol{\chi}_{\mathcal{P}}$ and $\boldsymbol{\chi}_{\partial\mathcal{P}}$ by the velocity fields $\boldsymbol{v}_{\mathcal{P}}$ and $\boldsymbol{v}_{\partial\mathcal{P}}$, respectively. Furthermore, we substitute the scalar fields $\chi_{\mathcal{P}}$ and $\chi_{\partial\mathcal{P}}$ by $\dot{\varphi}_{\mathcal{P}}$ and $\mathring{\varphi}_{\partial\mathcal{P}}$, respectively, which capture changes in the underlying microstructure of the materials. From this follows that the actual external power is given by

$$\mathcal{W}_{\text{ext}}(\mathcal{P}_\tau, \partial\mathcal{P}_\tau) := \mathcal{V}_{\text{ext}}(\mathcal{P}_\tau, \partial\mathcal{P}_\tau; \boldsymbol{v}_{\mathcal{P}}, \dot{\varphi}_{\mathcal{P}}, \boldsymbol{v}_{\partial\mathcal{P}}, \mathring{\varphi}_{\partial\mathcal{P}}). \tag{16.1}$$

Furthermore, we introduce the conventional power $\mathcal{W}^{\text{conv}}_{\text{ext}}(\mathcal{P}_\tau, \partial\mathcal{P}_\tau)$, as the actual external power that does not include inertial effects, i.e.

$$\begin{aligned}\mathcal{W}^{\text{conv}}_{\text{ext}}(\mathcal{P}_\tau, \partial\mathcal{P}_\tau) := &\int_{\mathcal{P}_\tau} \boldsymbol{b}^{\text{ni}} \cdot \boldsymbol{v}_{\mathcal{P}} \, \mathrm{d}v_\tau + \int_{\partial\mathcal{P}_\tau} (\boldsymbol{g}^{\text{ni}} - \boldsymbol{t}_{\mathcal{S}}) \cdot \boldsymbol{v}_{\partial\mathcal{P}} \, \mathrm{d}a_\tau \\ &+ \int_{\partial\mathcal{P}_\tau} \boldsymbol{t}_{\mathcal{S}} \cdot \boldsymbol{v}_{\mathcal{P}} \, \mathrm{d}a_\tau + \int_{\partial^2\mathcal{P}_\tau} \boldsymbol{h}_{\partial\mathcal{S}} \cdot \boldsymbol{v}_{\partial\mathcal{P}} \, \mathrm{d}\sigma_\tau \\ &+ \int_{\mathcal{P}_\tau} \gamma \dot{\varphi}_{\mathcal{P}} \, \mathrm{d}v_\tau + \int_{\partial\mathcal{P}_\tau} (\zeta - \xi_{\mathcal{S}}) \mathring{\varphi}_{\partial\mathcal{P}} \, \mathrm{d}a_\tau \\ &+ \int_{\partial\mathcal{P}_\tau} \xi_{\mathcal{S}} \dot{\varphi}_{\mathcal{P}} \, \mathrm{d}a_\tau + \int_{\partial^2\mathcal{P}_\tau} \tau_{\partial\mathcal{S}} \mathring{\varphi}_{\partial\mathcal{P}} \, \mathrm{d}\sigma_\tau.\end{aligned} \tag{16.2}$$

Lastly, the actual internal power in the system reads

$$\mathcal{W}_{\text{int}}(\mathcal{P}_\tau, \partial\mathcal{P}_\tau) := \mathcal{V}_{\text{int}}(\mathcal{P}_\tau, \partial\mathcal{P}_\tau; \boldsymbol{v}_{\mathcal{P}}, \dot{\varphi}_{\mathcal{P}}, \boldsymbol{v}_{\partial\mathcal{P}}, \mathring{\varphi}_{\partial\mathcal{P}}). \tag{16.3}$$

Now, the free energy in the bulk-surface material is given by

$$\mathcal{F}(\mathcal{P}_\tau, \partial\mathcal{P}_\tau) := \int_{\mathcal{P}_\tau} \varrho_{\mathcal{P}} \psi_{\mathcal{P}} \, \mathrm{d}v_\tau + \int_{\partial\mathcal{P}_\tau} \rho \ell_\tau \psi_{\partial\mathcal{P}} \, \mathrm{d}a_\tau, \tag{16.4}$$

where $\psi_{\mathcal{P}}$ and $\psi_{\partial\mathcal{P}}$ denote the bulk and surface specific free-energy, respectively, while the kinetic energy reads

$$\mathcal{K}(\mathcal{P}_\tau, \partial\mathcal{P}_\tau) := \int_{\mathcal{P}_\tau} \tfrac{1}{2} \varrho_{\mathcal{P}} |\boldsymbol{v}_{\mathcal{P}}|^2 \, \mathrm{d}v_\tau + \int_{\partial\mathcal{P}_\tau} \tfrac{1}{2} \rho \ell_\tau |\boldsymbol{v}_{\partial\mathcal{P}}|^2 \, \mathrm{d}a_\tau. \tag{16.5}$$

Then, for isothermal processes, the dissipation is given by

$$\begin{aligned}
\mathcal{D}(\mathcal{P}_\tau, \partial\mathcal{P}_\tau) := \mathcal{W}^{\mathrm{conv}}_{\mathrm{ext}} &- \overline{\mathcal{F}(\mathcal{P}_\tau, \partial\mathcal{P}_\tau) + \mathcal{K}(\mathcal{P}_\tau, \partial\mathcal{P}_\tau)}^{\boldsymbol{\cdot}} \\
&+ \int_{\mathcal{P}_\tau} \mu_{\mathcal{P}} s_{\mathcal{P}} \, \mathrm{d}v_\tau - \int_{\partial\mathcal{P}_\tau} \mu_{\mathcal{P}} \boldsymbol{\jmath}_{\mathcal{P}} \cdot \boldsymbol{n} \, \mathrm{d}a_\tau \\
&+ \int_{\partial\mathcal{P}_\tau} \mu_{\partial\mathcal{P}} \boldsymbol{\jmath}_{\mathcal{P}} \cdot \boldsymbol{n} \, \mathrm{d}a_\tau + \int_{\partial\mathcal{P}_\tau} \mu_{\partial\mathcal{P}} s_{\partial\mathcal{P}} \, \mathrm{d}a_\tau - \int_{\partial^2\mathcal{P}_\tau} \{\!\{ \mu_{\partial\mathcal{P}} \boldsymbol{\jmath}_{\partial\mathcal{P}} \cdot \boldsymbol{\nu} \}\!\} \, \mathrm{d}\sigma_\tau,
\end{aligned} \tag{16.6}$$

where we have accounted for the species production of energy. Here, $\mu_{\mathcal{P}}$ denotes the bulk chemical potential and $\mu_{\partial\mathcal{P}}$ is the surface chemical potential. Moreover, the dissipation is required to be non-negative, i.e. $\mathcal{D}(\mathcal{P}_\tau, \partial\mathcal{P}_\tau) \geq 0$. Thus, the partwise free-energy imbalance reads

$$\begin{aligned}
\overline{\mathcal{F}(\mathcal{P}_\tau, \partial\mathcal{P}_\tau) + \mathcal{K}(\mathcal{P}_\tau, \partial\mathcal{P}_\tau)}^{\boldsymbol{\cdot}} &- \mathcal{W}^{\mathrm{conv}}_{\mathrm{ext}}(\mathcal{P}_\tau, \partial\mathcal{P}_\tau) - \int_{\mathcal{P}_\tau} \mu_{\mathcal{P}} s_{\mathcal{P}} \, \mathrm{d}v_\tau + \int_{\partial\mathcal{P}_\tau} \mu_{\mathcal{P}} \boldsymbol{\jmath}_{\mathcal{P}} \cdot \boldsymbol{n} \, \mathrm{d}a_\tau \\
&- \int_{\partial\mathcal{P}_\tau} \mu_{\partial\mathcal{P}} \boldsymbol{\jmath}_{\mathcal{P}} \cdot \boldsymbol{n} \, \mathrm{d}a_\tau - \int_{\partial\mathcal{P}_\tau} \mu_{\partial\mathcal{P}} s_{\partial\mathcal{P}} \, \mathrm{d}a_\tau + \int_{\partial^2\mathcal{P}_\tau} \{\!\{ \mu_{\partial\mathcal{P}} \boldsymbol{\jmath}_{\partial\mathcal{P}} \cdot \boldsymbol{\nu} \}\!\} \, \mathrm{d}\sigma_\tau \\
&= -\mathcal{D}(\mathcal{P}_\tau, \partial\mathcal{P}_\tau) \leq 0.
\end{aligned} \tag{16.7}$$

Introducing the pointwise species mass balances (14.36) and (14.37) in the above inequality, followed by application of the divergence theorems on the terms accounting for species transport, we obtain

$$\begin{aligned}
\overline{\mathcal{F}(\mathcal{P}_\tau, \partial\mathcal{P}_\tau) + \mathcal{K}(\mathcal{P}_\tau, \partial\mathcal{P}_\tau)}^{\boldsymbol{\cdot}} - \mathcal{W}^{\mathrm{conv}}_{\mathrm{ext}}(\mathcal{P}_\tau, \partial\mathcal{P}_\tau) &- \int_{\mathcal{P}_\tau} (\varrho_{\partial\mathcal{P}} \dot{\varphi}_{\mathcal{P}} \mu_{\mathcal{P}} - \boldsymbol{\jmath}_{\mathcal{P}} \cdot \operatorname{grad} \mu_{\mathcal{P}}) \, \mathrm{d}v_\tau \\
&- \int_{\partial\mathcal{P}_\tau} (\rho \ell_\tau \mathring{\varphi}_{\partial\mathcal{P}} \mu_{\partial\mathcal{P}} - \boldsymbol{\jmath}_{\partial\mathcal{P}} \cdot \operatorname{grad}_{\mathcal{S}} \mu_{\partial\mathcal{P}}) \, \mathrm{d}a_\tau \leq 0,
\end{aligned} \tag{16.8}$$

bearing in mind that $\mathbf{P}_{n} \boldsymbol{\jmath}_{\partial\mathcal{P}} \cdot \operatorname{grad}_{\mathcal{S}} \mu_{\partial\mathcal{P}} = \boldsymbol{\jmath}_{\partial\mathcal{P}} \cdot \operatorname{grad}_{\mathcal{S}} \mu_{\partial\mathcal{P}}$. Next, in view of the virtual power balance (15.9) and the decomposition of the bulk and surface external body force (15.17), the conventional external power expenditure (16.2) can be written as

$$\begin{aligned}
\mathcal{W}^{\mathrm{conv}}_{\mathrm{ext}}(\mathcal{P}_\tau, \partial\mathcal{P}_\tau) &= \mathcal{W}_{\mathrm{int}}(\mathcal{P}_\tau, \partial\mathcal{P}_\tau) - \int_{\mathcal{P}_\tau} \boldsymbol{b}^{\mathrm{in}} \cdot \boldsymbol{v}_{\mathcal{P}} \, \mathrm{d}v_\tau - \int_{\partial\mathcal{P}_\tau} \boldsymbol{g}^{\mathrm{in}} \cdot \boldsymbol{v}_{\partial\mathcal{P}} \, \mathrm{d}a_\tau \\
&= \int_{\mathcal{P}_\tau} \mathbf{T} : \operatorname{grad} \boldsymbol{v}_{\mathcal{P}} \, \mathrm{d}v_\tau + \int_{\partial\mathcal{P}_\tau} \mathbf{H} : \operatorname{grad}_{\mathcal{S}} \boldsymbol{v}_{\partial\mathcal{P}} \, \mathrm{d}a_\tau \\
&\quad - \int_{\mathcal{P}_\tau} \pi \dot{\varphi}_{\mathcal{P}} \, \mathrm{d}v_\tau - \int_{\partial\mathcal{P}_\tau} \varpi \mathring{\varphi}_{\partial\mathcal{P}} \, \mathrm{d}a_\tau \\
&\quad + \int_{\mathcal{P}_\tau} \boldsymbol{\xi} \cdot \operatorname{grad} \dot{\varphi}_{\mathcal{P}} \, \mathrm{d}v_\tau + \int_{\partial\mathcal{P}_\tau} \boldsymbol{\tau} \cdot \operatorname{grad}_{\mathcal{S}} \mathring{\varphi}_{\partial\mathcal{P}} \, \mathrm{d}a_\tau + \overline{\mathcal{K}(\mathcal{P}_\tau, \partial\mathcal{P}_\tau)}^{\boldsymbol{\cdot}},
\end{aligned} \tag{16.9}$$

where we have used the relations for the inertial body forces (15.18) and the actual internal power (16.3). Using the free energy definition (16.4) and the above expression for the conventional external power (16.9), we arrive at the following partwise free-energy imbalance

$$\begin{aligned}
&\int_{\mathcal{P}_\tau} (\varrho_{\mathcal{P}}\dot{\psi}_{\mathcal{P}} - \mathbf{T} : \operatorname{grad} \boldsymbol{v}_{\mathcal{P}})\,\mathrm{d}v_\tau + \int_{\partial\mathcal{P}_\tau} (\rho\ell_\tau \mathring{\psi}_{\partial\mathcal{P}} - \mathbf{H} : \operatorname{grad}_{\mathcal{S}} \boldsymbol{v}_{\partial\mathcal{P}})\,\mathrm{d}a_\tau \\
&+ \int_{\mathcal{P}_\tau} (\pi\dot{\varphi}_{\mathcal{P}} - \boldsymbol{\xi} \cdot \operatorname{grad} \dot{\varphi}_{\mathcal{P}})\,\mathrm{d}v_\tau + \int_{\partial\mathcal{P}_\tau} (\varpi\mathring{\varphi}_{\partial\mathcal{P}} - \boldsymbol{\tau} \cdot \operatorname{grad}_{\mathcal{S}} \mathring{\varphi}_{\partial\mathcal{P}})\,\mathrm{d}a_\tau \\
&- \int_{\mathcal{P}_\tau} (\varrho_{\partial\mathcal{P}}\dot{\varphi}_{\mathcal{P}}\mu_{\mathcal{P}} - \boldsymbol{\jmath}_{\mathcal{P}} \cdot \operatorname{grad} \mu_{\mathcal{P}})\,\mathrm{d}v_\tau - \int_{\partial\mathcal{P}_\tau} (\rho\ell_\tau \mathring{\varphi}_{\partial\mathcal{P}}\mu_{\partial\mathcal{P}} - \boldsymbol{\jmath}_{\partial\mathcal{P}} \cdot \operatorname{grad}_{\mathcal{S}} \mu_{\partial\mathcal{P}})\,\mathrm{d}a_\tau \le 0. \quad (16.10)
\end{aligned}$$

The following uncoupled pointwise imbalances satisfy the above partwise free-energy imbalance, that is the pointwise bulk free-energy imbalance reads

$$\varrho_{\mathcal{P}}\dot{\psi}_{\mathcal{P}} - \mathbf{T} : \operatorname{grad} \boldsymbol{v}_{\mathcal{P}} + (\pi - \varrho_{\mathcal{P}}\mu_{\mathcal{P}})\dot{\varphi}_{\mathcal{P}} - \boldsymbol{\xi} \cdot \operatorname{grad} \dot{\varphi}_{\mathcal{P}} + \boldsymbol{\jmath}_{\mathcal{P}} \cdot \operatorname{grad} \mu_{\mathcal{P}} \le 0, \quad \text{in } \mathcal{P}_\tau, \quad (16.11)$$

while the pointwise surface free-energy imbalance is given by

$$\begin{aligned}
\rho\ell_\tau \mathring{\psi}_{\partial\mathcal{P}} - \mathbf{H} : \operatorname{grad}_{\mathcal{S}} \boldsymbol{v}_{\partial\mathcal{P}} + (\varpi - \rho\ell_\tau\mu_{\partial\mathcal{P}})\mathring{\varphi}_{\partial\mathcal{P}} - \boldsymbol{\tau} \cdot \operatorname{grad}_{\mathcal{S}} \mathring{\varphi}_{\partial\mathcal{P}} \\
+ \boldsymbol{\jmath}_{\partial\mathcal{P}} \cdot \operatorname{grad}_{\mathcal{S}} \mu_{\partial\mathcal{P}} \le 0, \quad \text{on } \partial\mathcal{P}_\tau. \quad (16.12)
\end{aligned}$$

Lastly, using the following identities

$$\operatorname{grad} \dot{\varphi}_{\mathcal{P}} = (\operatorname{grad} \varphi_{\mathcal{P}})^{\boldsymbol{\cdot}} + (\operatorname{grad} \boldsymbol{v}_{\mathcal{P}})^{\top} \operatorname{grad} \varphi_{\mathcal{P}}, \tag{16.13}$$

and

$$\operatorname{grad}_{\mathcal{S}} \mathring{\varphi}_{\partial\mathcal{P}} = (\operatorname{grad}_{\mathcal{S}} \varphi_{\partial\mathcal{P}})^{\circ} + (\operatorname{grad}_{\mathcal{S}} \boldsymbol{v}_{\partial\mathcal{P}})^{\top} \operatorname{grad}_{\mathcal{S}} \varphi_{\partial\mathcal{P}},^{13} \tag{16.14}$$

the pointwise free-energy imbalances become

$$\begin{aligned}
\varrho_{\mathcal{P}}\dot{\psi}_{\mathcal{P}} - (\mathbf{T} + \operatorname{grad} \varphi_{\mathcal{P}} \otimes \boldsymbol{\xi}) : \operatorname{grad} \boldsymbol{v}_{\mathcal{P}} + (\pi - \varrho_{\mathcal{P}}\mu_{\mathcal{P}})\dot{\varphi}_{\mathcal{P}} \\
- \boldsymbol{\xi} \cdot (\operatorname{grad} \varphi_{\mathcal{P}})^{\boldsymbol{\cdot}} + \boldsymbol{\jmath}_{\mathcal{P}} \cdot \operatorname{grad} \mu_{\mathcal{P}} \le 0, \quad \text{in } \mathcal{P}_\tau, \quad (16.15)
\end{aligned}$$

and

$$\begin{aligned}
\rho\ell_\tau \mathring{\psi}_{\partial\mathcal{P}} - (\mathbf{H} + \operatorname{grad}_{\mathcal{S}} \varphi_{\partial\mathcal{P}} \otimes \boldsymbol{\tau}) : \operatorname{grad}_{\mathcal{S}} \boldsymbol{v}_{\partial\mathcal{P}} + (\varpi - \rho\ell_\tau\mu_{\partial\mathcal{P}})\mathring{\varphi}_{\partial\mathcal{P}} \\
- \boldsymbol{\tau} \cdot (\operatorname{grad}_{\mathcal{S}} \varphi_{\partial\mathcal{P}})^{\circ} + \boldsymbol{\jmath}_{\partial\mathcal{P}} \cdot \operatorname{grad}_{\mathcal{S}} \mu_{\partial\mathcal{P}} \le 0, \quad \text{on } \partial\mathcal{P}_\tau. \quad (16.16)
\end{aligned}$$

16.2 Constitutive response functions

Guided by the pointwise free-energy imbalances (16.15) and (16.16) in Section 16.1, we here present the constitutive response functions, specifying the class of processes that the bulk-surface fluid may undergo. The set of independent variables is given by $\{\varrho_{\partial\mathcal{P}}, \varphi_{\mathcal{P}}, \varphi_{\partial\mathcal{P}}, \operatorname{grad} \varphi_{\mathcal{P}}, \operatorname{grad}_{\mathcal{S}} \varphi_{\partial\mathcal{P}}, \mu_{\mathcal{P}}, \mu_{\partial\mathcal{P}}, \operatorname{grad} \boldsymbol{v}_{\mathcal{P}}, \operatorname{grad}_{\mathcal{S}} \boldsymbol{v}_{\partial\mathcal{P}}\}$, whereas the set of dependent constitutive functions reads $\{\pi, \varpi, \boldsymbol{\xi}, \boldsymbol{\tau}, \boldsymbol{\jmath}_{\mathcal{P}}, \boldsymbol{\jmath}_{\partial\mathcal{P}}, \mathbf{T}, \mathbf{H}\}$. Thus, we find that the pointwise inequalities (16.15) and (16.16) are satisfied in all processes if:

[13] This identity may be obtained from the previous one in (16.13) by premultiplying by $\mathbf{P}_n$ and assuming a normal constant extension of $\boldsymbol{v}_{\partial\mathcal{P}}$ and $\varphi_{\partial\mathcal{P}}$, while noting that $\partial_n \varphi_{\partial\mathcal{P}} = 0$.

- The bulk and surface free-energy densities $\psi_{\mathcal{P}}$ and $\psi_{\partial\mathcal{P}}$ are, respectively, given by constitutive response functions that are independent of $\mu_{\mathcal{P}}$, $\mu_{\partial\mathcal{P}}$, $\operatorname{grad}\mu_{\mathcal{P}}$, and $\operatorname{grad}_{\mathcal{S}}\mu_{\partial\mathcal{P}}$, $\operatorname{grad}\boldsymbol{v}_{\mathcal{P}}$, $\operatorname{grad}_{\mathcal{S}}\boldsymbol{v}_{\partial\mathcal{P}}$, i.e.

$$\psi_{\mathcal{P}} := \psi_{\mathcal{P}}(\varphi_{\mathcal{P}}, \operatorname{grad}\varphi_{\mathcal{P}}), \qquad \text{and} \qquad \psi_{\partial\mathcal{P}} := \psi_{\partial\mathcal{P}}(\varrho_{\partial\mathcal{P}}, \varphi_{\partial\mathcal{P}}, \operatorname{grad}_{\mathcal{S}}\varphi_{\partial\mathcal{P}}). \tag{16.17}$$

Thus, with

$$\dot{\psi}_{\mathcal{P}} = \partial_{\varphi_{\mathcal{P}}}\psi_{\mathcal{P}}\dot{\varphi}_{\mathcal{P}} + \partial_{\operatorname{grad}\varphi_{\mathcal{P}}}\psi_{\mathcal{P}} \cdot (\operatorname{grad}\varphi_{\mathcal{P}})^{\dot{}}, \tag{16.18}$$

and through $(14.27)_1$ and (14.31) also

$$\begin{aligned}\mathring{\psi}_{\partial\mathcal{P}} &= \partial_{\varrho_{\partial\mathcal{P}}}\psi_{\partial\mathcal{P}}\mathring{\varrho}_{\partial\mathcal{P}} + \partial_{\varphi_{\partial\mathcal{P}}}\psi_{\partial\mathcal{P}}\mathring{\varphi}_{\partial\mathcal{P}} + \partial_{\operatorname{grad}_{\mathcal{S}}\varphi_{\partial\mathcal{P}}}\psi_{\partial\mathcal{P}} \cdot (\operatorname{grad}_{\mathcal{S}}\varphi_{\partial\mathcal{P}})^{\circ} \\ &= -\ell_\tau\partial_{\ell_\tau}\psi_{\partial\mathcal{P}}\operatorname{div}_{\mathcal{S}}\boldsymbol{v}_{\partial\mathcal{P}} + \partial_{\varphi_{\partial\mathcal{P}}}\psi_{\partial\mathcal{P}}\mathring{\varphi}_{\partial\mathcal{P}} + \partial_{\operatorname{grad}_{\mathcal{S}}\varphi_{\partial\mathcal{P}}}\psi_{\partial\mathcal{P}} \cdot (\operatorname{grad}_{\mathcal{S}}\varphi_{\partial\mathcal{P}})^{\circ},\end{aligned} \tag{16.19}$$

the pointwise free-energy imbalances in (16.15) and (16.16) become

$$\begin{aligned}&(\mathbf{T} + \operatorname{grad}\varphi_{\mathcal{P}} \otimes \boldsymbol{\xi}) : \operatorname{grad}\boldsymbol{v}_{\mathcal{P}} + (\varrho_{\mathcal{P}}\mu_{\mathcal{P}} - \pi - \varrho_{\mathcal{P}}\partial_{\varphi}\psi_{\mathcal{P}})\dot{\varphi}_{\mathcal{P}} \\ &\qquad + (\boldsymbol{\xi} - \varrho_{\mathcal{P}}\partial_{\operatorname{grad}\varphi_{\mathcal{P}}}\psi_{\mathcal{P}}) \cdot (\operatorname{grad}\varphi_{\mathcal{P}})^{\dot{}} - \boldsymbol{\jmath}_{\mathcal{P}} \cdot \operatorname{grad}\mu_{\mathcal{P}} \geq 0, \quad \text{in } \mathcal{P}_\tau,\end{aligned} \tag{16.20}$$

and

$$\begin{aligned}&(\mathbf{H} + \operatorname{grad}_{\mathcal{S}}\varphi_{\partial\mathcal{P}} \otimes \boldsymbol{\tau}) : \operatorname{grad}_{\mathcal{S}}\boldsymbol{v}_{\partial\mathcal{P}} + \rho\ell_\tau^2\partial_{\ell_\tau}\psi_{\partial\mathcal{P}}\operatorname{div}_{\mathcal{S}}\boldsymbol{v}_{\partial\mathcal{P}} \\ &\qquad + (\rho\ell_\tau\mu_{\partial\mathcal{P}} - \varpi - \rho\ell_\tau\partial_{\varphi_{\partial\mathcal{P}}}\psi_{\partial\mathcal{P}})\mathring{\varphi}_{\partial\mathcal{P}} \\ &\qquad + (\boldsymbol{\tau} - \rho\ell_\tau\partial_{\operatorname{grad}_{\mathcal{S}}\varphi_{\partial\mathcal{P}}}\psi_{\partial\mathcal{P}}) \cdot (\operatorname{grad}_{\mathcal{S}}\varphi_{\partial\mathcal{P}})^{\circ} - \boldsymbol{\jmath}_{\partial\mathcal{P}} \cdot \operatorname{grad}_{\mathcal{S}}\mu_{\partial\mathcal{P}} \geq 0, \quad \text{on } \partial\mathcal{P}_\tau.\end{aligned} \tag{16.21}$$

From a microscopic viewpoint, one expects to have a constant microscopic free-energy density for a fixed $\varphi_{\partial\mathcal{P}}$ and $\operatorname{grad}_{\mathcal{S}}\varphi_{\partial\mathcal{P}}$ in the thin film of fluid surrounding the bulk fluid. However, since the thickness may change, one may stipulate that the surface free-energy density, therefore, a macroscopic quantity, depends linearly on thickness ℓ_τ. That is, we may define the surface free-energy density as

$$\psi_{\partial\mathcal{P}}(\varrho_{\partial\mathcal{P}}, \varphi_{\partial\mathcal{P}}, \operatorname{grad}_{\mathcal{S}}\varphi_{\partial\mathcal{P}}) := \frac{\varrho_{\partial\mathcal{P}}}{\rho}\psi(\varphi_{\partial\mathcal{P}}, \operatorname{grad}_{\mathcal{S}}\varphi_{\partial\mathcal{P}}) = \ell_\tau\psi(\varphi_{\partial\mathcal{P}}, \operatorname{grad}_{\mathcal{S}}\varphi_{\partial\mathcal{P}}), \tag{16.22}$$

where ψ is the microscopic free-energy density in the thin film of the fluid. The corresponding pointwise free-energy imbalance is given by

$$\begin{aligned}&(\mathbf{H} + \operatorname{grad}_{\mathcal{S}}\varphi_{\partial\mathcal{P}} \otimes \boldsymbol{\tau}) : \operatorname{grad}_{\mathcal{S}}\boldsymbol{v}_{\partial\mathcal{P}} + \rho\ell_\tau^2\psi\operatorname{div}_{\mathcal{S}}\boldsymbol{v}_{\partial\mathcal{P}} + (\rho\ell_\tau\mu_{\partial\mathcal{P}} - \varpi - \rho\ell_\tau^2\partial_{\varphi_{\partial\mathcal{P}}}\psi)\mathring{\varphi}_{\partial\mathcal{P}} \\ &\qquad + (\boldsymbol{\tau} - \rho\ell_\tau^2\partial_{\operatorname{grad}_{\mathcal{S}}\varphi_{\partial\mathcal{P}}}\psi) \cdot \operatorname{grad}_{\mathcal{S}}\mathring{\varphi}_{\partial\mathcal{P}} - \boldsymbol{\jmath}_{\partial\mathcal{P}} \cdot \operatorname{grad}_{\mathcal{S}}\mu_{\partial\mathcal{P}} \geq 0.\end{aligned} \tag{16.23}$$

- The bulk and surface microstress $\boldsymbol{\xi}$ and $\boldsymbol{\tau}$ are, respectively, given by

$$\boldsymbol{\xi} := \varrho_{\mathcal{P}}\partial_{\operatorname{grad}\varphi}\psi_{\mathcal{P}}, \qquad \text{and} \qquad \boldsymbol{\tau} := \rho\ell_\tau\partial_{\operatorname{grad}_{\mathcal{S}}\varphi_{\partial\mathcal{P}}}\psi_{\partial\mathcal{P}}. \tag{16.24}$$

- The internal bulk and surface microforces π and ϖ are, respectively, given by constitutive response functions that differ from the bulk and surface chemical potential by a contribution derived from the response functions $\psi_{\mathcal{P}}$ and $\psi_{\partial\mathcal{P}}$, i.e.

$$\pi := \varrho_{\mathcal{P}}(\mu_{\mathcal{P}} - \partial_{\varphi_{\mathcal{P}}}\psi_{\mathcal{P}}), \qquad \text{and} \qquad \varpi := \rho\ell_\tau(\mu_{\partial\mathcal{P}} - \partial_{\varphi_{\partial\mathcal{P}}}\psi_{\partial\mathcal{P}}). \tag{16.25}$$

- Granted that the species bulk and surface fluxes $\jmath_{\mathcal{P}}$ and $\jmath_{\partial\mathcal{P}}$ depend smoothly on the gradient of the bulk chemical potential, $\operatorname{grad}\mu_{\mathcal{P}}$, and the surface gradient of the surface chemical potential, $\operatorname{grad}_{\mathcal{S}}\mu_{\partial\mathcal{P}}$, these fluxes are, respectively, given by a constitutive response function of the form

$$\jmath_{\mathcal{P}} := -\boldsymbol{M}_{\mathcal{P}}\operatorname{grad}\mu_{\mathcal{P}}, \qquad \text{and} \qquad \jmath_{\partial\mathcal{P}} := -\boldsymbol{M}_{\partial\mathcal{P}}\operatorname{grad}_{\mathcal{S}}\mu_{\partial\mathcal{P}}, \tag{16.26}$$

where the mobility tensors $\boldsymbol{M}_{\mathcal{P}}$ and $\boldsymbol{M}_{\partial\mathcal{P}}$ must obey the residual dissipation inequalities

$$\operatorname{grad}\mu_{\mathcal{P}}\cdot\boldsymbol{M}_{\mathcal{P}}\operatorname{grad}\mu_{\mathcal{P}}\geq 0, \qquad \text{and} \qquad \operatorname{grad}_{\mathcal{S}}\mu_{\partial\mathcal{P}}\cdot\boldsymbol{M}_{\partial\mathcal{P}}\operatorname{grad}_{\mathcal{S}}\mu_{\partial\mathcal{P}}\geq 0. \tag{16.27}$$

Oftentimes one finds in the literature that $\boldsymbol{M}_{\mathcal{P}} := m_{\mathcal{P}}\mathbf{1}$ and $\boldsymbol{M}_{\partial\mathcal{P}} := m_{\partial\mathcal{P}}\mathbf{P}_{\!n}$, where $m_{\mathcal{P}}$ and $m_{\partial\mathcal{P}}$ denote the scalar bulk and surface mobilities, respectively. With this choice for $\boldsymbol{M}_{\partial\mathcal{P}}$, the surface flux $\jmath_{\partial\mathcal{P}}$ remains proportional to $\operatorname{grad}_{\mathcal{S}}\mu_{\partial\mathcal{P}}$ and therefore tangential to $\partial\mathcal{P}_\tau$. As a result of the vanishing contributions of $\boldsymbol{M}_{\partial\mathcal{P}}$ to the normal component of $\jmath_{\partial\mathcal{P}}$, the pointwise surface species balance (14.38) can be rewritten as follows

$$\rho\ell_\tau\mathring{\varphi}_{\partial\mathcal{P}} = \jmath_{\mathcal{P}}\cdot\boldsymbol{n} + s_{\partial\mathcal{P}} - \operatorname{div}_{\mathcal{S}}\jmath_{\partial\mathcal{P}}, \qquad \text{on } \partial\mathcal{P}_\tau. \tag{16.28}$$

- The bulk and surface stress are, respectively, given by

$$\begin{cases}\mathbf{T} := \mathbf{T}^{\text{vis}}(\mathbf{D}_{\mathcal{P}}) - p_{\mathcal{P}}^{\text{mech}}\mathbf{1} - \operatorname{grad}\varphi_{\mathcal{P}}\otimes\boldsymbol{\xi}, \qquad \text{and}\\ \mathbf{H} := \mathbf{H}^{\text{vis}}(\varrho_{\partial\mathcal{P}},\mathbf{D}_{\partial\mathcal{P}}) - p_{\partial\mathcal{P}}^{\text{therm}}\mathbf{P}_{\!n} - \operatorname{grad}_{\mathcal{S}}\varphi_{\partial\mathcal{P}}\otimes\boldsymbol{\tau},\end{cases} \tag{16.29}$$

where the rate of deformation is defined as $\mathbf{D}_{\mathcal{P}} := \operatorname{sym}\operatorname{grad}\boldsymbol{v}_{\mathcal{P}}$ and $\mathbf{D}_{\partial\mathcal{P}} := \operatorname{sym}\operatorname{grad}_{\mathcal{S}}\boldsymbol{v}_{\partial\mathcal{P}}$, with sym being the symmetric operator. Furthermore, $p_{\mathcal{P}}^{\text{mech}}$ denotes the mechanical bulk pressure and $p_{\partial\mathcal{P}}^{\text{therm}}$ the thermodynamical surface pressure, which is also oftentimes called the surface tension. In what follows we discuss these pressures in more detail. We consider linearly viscous response functions, that is we consider a viscous bulk and surface stress $\mathbf{T}^{\text{vis}}$ and $\mathbf{H}^{\text{vis}}$ that are linear in $\mathbf{D}_{\mathcal{P}}$ and $\mathbf{D}_{\partial\mathcal{P}}$, respectively, which we write as

$$\begin{cases}\mathbf{T}^{\text{vis}} := 2\bar{\mu}_{\mathcal{P}}\,\mathbf{D}_{\mathcal{P}},\\ \mathbf{H}^{\text{vis}} := 2\bar{\mu}_{\partial\mathcal{P}}\,\mathbf{P}_{\!n}\mathbf{D}_{\partial\mathcal{P}}\mathbf{P}_{\!n} + (\bar{\kappa}_{\partial\mathcal{P}} - \bar{\mu}_{\partial\mathcal{P}})(\operatorname{div}_{\mathcal{S}}\boldsymbol{v}_{\partial\mathcal{P}})\mathbf{P}_{\!n},\end{cases} \tag{16.30}$$

where $\bar{\mu}_{\mathcal{P}}$ and $\bar{\mu}_{\partial\mathcal{P}}(\varrho_{\partial\mathcal{P}})$ denote the bulk and surface dynamic viscosities[14], and $\bar{\kappa}_{\partial\mathcal{P}}(\varrho_{\partial\mathcal{P}})$ is the surface dilatational viscosity[15]. Next, we decompose $\mathbf{D}_{\mathcal{P}}$ and $\mathbf{D}_{\partial\mathcal{P}}$ into a deviatoric and spherical part, i.e. $\mathbf{D}_{\mathcal{P}} = \mathbf{D}_{\mathcal{P}}^0 + \frac{1}{3}(\operatorname{tr}\mathbf{D}_{\mathcal{P}})\mathbf{1}$ and $\mathbf{D}_{\partial\mathcal{P}} = \mathbf{D}_{\partial\mathcal{P}}^0 + \frac{1}{2}(\operatorname{tr}\mathbf{D}_{\partial\mathcal{P}})\mathbf{P}_{\!n}$, with $\operatorname{tr}(\mathbf{D}_{\mathcal{P}}^0) = \operatorname{tr}(\mathbf{D}_{\partial\mathcal{P}}^0) = 0$. Then, we may compute the viscous dissipation as

$$\begin{cases}\mathbf{T}^{\text{vis}}:\mathbf{D}_{\mathcal{P}} = \Big(2\bar{\mu}_{\mathcal{P}}\,\mathbf{D}_{\mathcal{P}}\Big):\Big(\mathbf{D}_{\mathcal{P}}^0 + \frac{1}{3}(\operatorname{tr}\mathbf{D}_{\mathcal{P}})\mathbf{1}\Big)\\ \qquad\qquad = 2\bar{\mu}_{\mathcal{P}}|\mathbf{D}_{\mathcal{P}}^0|^2,\\ \mathbf{H}^{\text{vis}}:\mathbf{D}_{\partial\mathcal{P}} = \Big(2\bar{\mu}_{\partial\mathcal{P}}\,\mathbf{P}_{\!n}\mathbf{D}_{\partial\mathcal{P}}\mathbf{P}_{\!n} + (\bar{\kappa}_{\partial\mathcal{P}} - \bar{\mu}_{\partial\mathcal{P}})(\operatorname{div}_{\mathcal{S}}\boldsymbol{v}_{\partial\mathcal{P}})\mathbf{P}_{\!n}\Big)\\ \qquad\qquad\qquad\qquad\qquad\qquad : \Big(\mathbf{D}_{\partial\mathcal{P}}^0 + \frac{1}{2}(\operatorname{tr}\mathbf{D}_{\partial\mathcal{P}})\mathbf{P}_{\!n}\Big)\\ \qquad\qquad = 2\bar{\mu}_{\partial\mathcal{P}}|\mathbf{P}_{\!n}\mathbf{D}_{\partial\mathcal{P}}^0|^2 + \bar{\kappa}_{\partial\mathcal{P}}(\operatorname{div}_{\mathcal{S}}\boldsymbol{v}_{\partial\mathcal{P}})^2,\end{cases} \tag{16.31}$$

[14] $\bar{\mu}_{\mathcal{P}}$ and $\bar{\mu}_{\partial\mathcal{P}}(\varrho_{\partial\mathcal{P}})$ are also referred to as the bulk and surface shear viscosities, respectively.
[15] $\bar{\kappa}_{\partial\mathcal{P}}$ is also referred to as the bulk viscosity of the surface fluid.

where we have taken into account that $\mathrm{tr}(\mathbf{D}_{\mathcal{P}}) = \mathrm{div}\,\boldsymbol{v}_{\mathcal{P}} = 0$ and $\mathrm{tr}(\mathbf{D}_{\partial\mathcal{P}}) = \mathrm{div}_{\mathcal{S}}\boldsymbol{v}_{\partial\mathcal{P}} = -\frac{\mathring{\ell}_\tau}{\ell_\tau}$. In view of the free-energy inequalities in (16.20) and (16.21), we conclude that $\bar{\mu}_{\mathcal{P}} \geq 0$, $\bar{\mu}_{\partial\mathcal{P}}(\rho\ell_\tau) \geq 0$ and $\bar{\kappa}_{\partial\mathcal{P}}(\rho\ell_\tau) \geq 0$.

- The total pressure in the bulk and surface fluids are, respectively, given by

$$\begin{cases} p^{\mathrm{tot}}_{\mathcal{P}} := -\frac{1}{3}\mathrm{tr}(\mathbf{T}) = p^{\mathrm{mech}}_{\mathcal{P}} + p^{\mathrm{cap}}_{\mathcal{P}}, \\ p^{\mathrm{tot}}_{\partial\mathcal{P}} := -\frac{1}{2}\mathrm{tr}(\mathbf{H}) = p^{\mathrm{therm}}_{\partial\mathcal{P}} + p^{\mathrm{mech}}_{\partial\mathcal{P}} + p^{\mathrm{cap}}_{\partial\mathcal{P}}. \end{cases} \tag{16.32}$$

In the above, the mechanical bulk pressure $p^{\mathrm{mech}}_{\mathcal{P}}$ is indeterminate, whereas the bulk capillary-like pressure is defined as $p^{\mathrm{cap}}_{\mathcal{P}} := -\frac{1}{3}\mathrm{tr}(\mathrm{grad}\,\varphi_{\mathcal{P}} \otimes \boldsymbol{\xi})$. For the surface, we find $p^{\mathrm{cap}}_{\partial\mathcal{P}} := -\frac{1}{2}\mathrm{tr}(\mathrm{grad}_{\mathcal{S}}\varphi_{\partial\mathcal{P}} \otimes \boldsymbol{\tau})$. In view of the surface free-energy imbalance (16.23) and the viscous surface dissipation $(16.31)_2$, the thermodynamical surface pressure is given by

$$p^{\mathrm{therm}}_{\partial\mathcal{P}} := \rho\ell_\tau^2\psi, \tag{16.33}$$

and, lastly, $p^{\mathrm{mech}}_{\partial\mathcal{P}} := -\frac{1}{2}\mathrm{tr}(\mathbf{H}^{\mathrm{vis}}) = -\bar{\kappa}_{\partial\mathcal{P}}\mathrm{div}_{\mathcal{S}}\boldsymbol{v}_{\partial\mathcal{P}}$. Thus, the total bulk and surface pressure read

$$\begin{cases} p^{\mathrm{tot}}_{\mathcal{P}} := p^{\mathrm{mech}}_{\mathcal{P}} - \frac{1}{3}\mathrm{tr}(\mathrm{grad}\,\varphi_{\mathcal{P}} \otimes \boldsymbol{\xi}), \\ p^{\mathrm{tot}}_{\partial\mathcal{P}} := \rho\ell_\tau^2\psi - \bar{\kappa}_{\partial\mathcal{P}}\mathrm{div}_{\mathcal{S}}\boldsymbol{v}_{\partial\mathcal{P}} - \frac{1}{2}\mathrm{tr}(\mathrm{grad}_{\mathcal{S}}\varphi_{\partial\mathcal{P}} \otimes \boldsymbol{\tau}). \end{cases} \tag{16.34}$$

- In view of (16.30) and (16.33), we conclude that stresses in (16.29) can be rewritten as

$$\begin{cases} \mathbf{T} := 2\bar{\mu}_{\mathcal{P}}\,\mathbf{D}_{\mathcal{P}} - p^{\mathrm{mech}}_{\mathcal{P}}\mathbf{1} - \mathrm{grad}\,\varphi_{\mathcal{P}} \otimes \boldsymbol{\xi}, \qquad \text{and} \\ \mathbf{H} := 2\bar{\mu}_{\partial\mathcal{P}}\,\mathbf{P}_{\!n}\mathbf{D}^0_{\partial\mathcal{P}}\mathbf{P}_{\!n} - (\rho\ell_\tau^2\psi - \bar{\kappa}_{\partial\mathcal{P}}\mathrm{div}_{\mathcal{S}}\boldsymbol{v}_{\partial\mathcal{P}})\mathbf{P}_{\!n} - \mathrm{grad}_{\mathcal{S}}\varphi_{\partial\mathcal{P}} \otimes \boldsymbol{\tau}. \end{cases} \tag{16.35}$$

Notice that the surface stress in $(16.35)_2$ is symmetric, i.e. $\mathbf{H} = \mathbf{H}^\top$, and annihilates the normal, i.e. $\mathbf{H}\boldsymbol{n} = \mathbf{0}$, which makes it consistent with the frame-indifference result in (15.34).

Lastly, we use the above results to present the explicit form of the bulk and surface chemical potentials. Substitution of (15.16) and (15.14) in (16.25) yields

$$\varrho_{\mathcal{P}}\mu_{\mathcal{P}} = -\mathrm{div}\,\boldsymbol{\xi} - \gamma + \varrho_{\mathcal{P}}\partial_{\varphi_{\mathcal{P}}}\psi_{\mathcal{P}}, \quad \text{in } \mathcal{P}_\tau, \tag{16.36}$$

and

$$\rho\ell_\tau\mu_{\partial\mathcal{P}} = -\mathrm{div}_{\mathcal{S}}(\mathbf{P}_{\!n}\boldsymbol{\tau}) - \zeta + \boldsymbol{\xi}\cdot\boldsymbol{n} + \rho\ell_\tau\partial_{\varphi_{\partial\mathcal{P}}}\psi_{\partial\mathcal{P}}, \quad \text{on } \partial\mathcal{P}_\tau. \tag{16.37}$$

In view of (16.24), these expressions take the following form

$$\varrho_{\mathcal{P}}\mu_{\mathcal{P}} = \varrho_{\mathcal{P}}\partial_{\varphi_{\mathcal{P}}}\psi_{\mathcal{P}} - \mathrm{div}\left(\varrho_{\mathcal{P}}\partial_{\mathrm{grad}\,\varphi}\psi_{\mathcal{P}}\right) - \gamma, \quad \text{in } \mathcal{P}_\tau, \tag{16.38}$$

and, bearing in mind (16.22), we obtain

$$\rho\ell_\tau\mu_{\partial\mathcal{P}} = \rho\ell_\tau^2\partial_{\varphi_{\partial\mathcal{P}}}\psi - \mathrm{div}_{\mathcal{S}}\left(\rho\ell_\tau^2\partial_{\mathrm{grad}_{\mathcal{S}}\varphi_{\partial\mathcal{P}}}\psi\right) - \zeta + \varrho_{\mathcal{P}}\partial_{\mathrm{grad}\,\varphi}\psi_{\mathcal{P}}\cdot\boldsymbol{n}, \quad \text{on } \partial\mathcal{P}_\tau. \tag{16.39}$$

Additionally, the term $\mathrm{div}_{\mathcal{S}}(\rho\ell_\tau^2\partial_{\mathrm{grad}_{\mathcal{S}}\varphi_{\partial\mathcal{P}}}\psi)$ may be split as follows

$$\mathrm{div}_{\mathcal{S}}(\rho\ell_\tau^2\partial_{\mathrm{grad}_{\mathcal{S}}\varphi_{\partial\mathcal{P}}}\psi) = \rho\ell_\tau^2\mathrm{div}_{\mathcal{S}}(\partial_{\mathrm{grad}_{\mathcal{S}}\varphi_{\partial\mathcal{P}}}\psi) + 2\rho\ell_\tau\partial_{\mathrm{grad}_{\mathcal{S}}\varphi_{\partial\mathcal{P}}}\psi\cdot\mathrm{grad}_{\mathcal{S}}\ell_\tau. \tag{16.40}$$

Finally, using (16.40) in expression (16.39), we arrive at

$$\begin{aligned} \rho\ell_\tau\mu_{\partial\mathcal{P}} &= \rho\ell_\tau^2\partial_{\varphi_{\partial\mathcal{P}}}\psi - \rho\ell_\tau^2\mathrm{div}_{\mathcal{S}}(\partial_{\mathrm{grad}_{\mathcal{S}}\varphi_{\partial\mathcal{P}}}\psi) \\ &\quad - 2\rho\ell_\tau\partial_{\mathrm{grad}_{\mathcal{S}}\varphi_{\partial\mathcal{P}}}\psi\cdot\mathrm{grad}_{\mathcal{S}}\ell_\tau - \zeta + \varrho_{\mathcal{P}}\partial_{\mathrm{grad}\,\varphi_{\mathcal{P}}}\psi_{\mathcal{P}}\cdot\boldsymbol{n}, \quad \text{on } \partial\mathcal{P}_\tau. \end{aligned} \tag{16.41}$$

16.3 Specialized equations

To exemplify our bulk-surface continuum theory for fluid flow undergoing phase separation, we consider the following free-energy densities

$$\psi_{\mathcal{P}} := \frac{1}{\epsilon} f(\varphi_{\mathcal{P}}) + \frac{\epsilon}{2}|\mathrm{grad}\,\varphi_{\mathcal{P}}|^2, \quad \text{and} \quad \psi_{\partial\mathcal{P}} := \ell_\tau\Big(\frac{1}{\delta} g(\varphi_{\partial\mathcal{P}}) + \frac{\iota\delta}{2}|\mathrm{grad}_{\mathcal{S}}\,\varphi_{\partial\mathcal{P}}|^2\Big), \tag{16.42}$$

so that the total free-energy functional reads

$$\begin{aligned}\mathcal{F}(\mathcal{P}_\tau, \partial\mathcal{P}_\tau) &:= \int_{\mathcal{P}_\tau} \varrho_{\mathcal{P}} \psi_{\mathcal{P}}\,\mathrm{d}v_\tau + \int_{\partial\mathcal{P}_\tau} \rho\ell_\tau\psi_{\partial\mathcal{P}}\,\mathrm{d}a_\tau \\ &= \int_{\mathcal{P}_\tau} \varrho_{\mathcal{P}}\Big(\frac{1}{\epsilon} f(\varphi_{\mathcal{P}}) + \frac{\epsilon}{2}|\mathrm{grad}\,\varphi_{\mathcal{P}}|^2\Big)\,\mathrm{d}v_\tau \\ &\quad + \int_{\partial\mathcal{P}_\tau} \rho\ell_\tau^2\Big(\frac{1}{\delta} g(\varphi_{\partial\mathcal{P}}) + \frac{\iota\delta}{2}|\mathrm{grad}_{\mathcal{S}}\varphi_{\partial\mathcal{P}}|^2\Big)\,\mathrm{d}a_\tau,\end{aligned} \tag{16.43}$$

which describes the phase separation in our bulk-surface system. Here, ϵ, δ, and ι are real positive constant parameters, while f and g denote the bulk and surface potentials, respectively. With this choice for the free-energy densities (16.42), the bulk and surface microstress (16.24) specialize to

$$\boldsymbol{\xi} := \epsilon\varrho_{\mathcal{P}}\mathrm{grad}\,\varphi_{\mathcal{P}}, \qquad \text{and} \qquad \boldsymbol{\tau} := \iota\delta\rho\ell_\tau^2\mathrm{grad}_{\mathcal{S}}\varphi_{\partial\mathcal{P}}, \tag{16.44}$$

while the internal bulk and surface microforce (16.25) become

$$\pi := \varrho_{\mathcal{P}}\Big(\mu_{\mathcal{P}} - \frac{1}{\epsilon} f'(\varphi_{\mathcal{P}})\Big), \qquad \text{and} \qquad \varpi := \rho\ell_\tau\Big(\mu_{\partial\mathcal{P}} - \ell_\tau\frac{1}{\delta} g'(\varphi_{\partial\mathcal{P}})\Big). \tag{16.45}$$

Furthermore, we consider the following bulk and surface species fluxes

$$\jmath_{\mathcal{P}} := -\boldsymbol{M}_{\mathcal{P}}\mathrm{grad}\,\mu_{\mathcal{P}}, \qquad \text{and} \qquad \jmath_{\partial\mathcal{P}} := -\boldsymbol{M}_{\partial\mathcal{P}}\mathrm{grad}_{\mathcal{S}}\mu_{\partial\mathcal{P}}, \tag{16.46}$$

where, for the sake of simplicity, we use $\boldsymbol{M}_{\mathcal{P}} := m_{\mathcal{P}}\boldsymbol{I}$ and $\boldsymbol{M}_{\partial\mathcal{P}} := m_{\partial\mathcal{P}}\mathbf{P}_{\boldsymbol{n}}$ with scalar functions $m_{\mathcal{P}}, m_{\partial\mathcal{P}} \geq 0$ to ensure that bulk and surface mobilities satisfy the residual dissipation inequalities (16.27).

Thus, in view of expressions (16.44) and (16.46), the bulk field equation $(15.14)_1$ takes on the following form

$$\varrho_{\mathcal{P}}\mu_{\mathcal{P}} = \frac{1}{\epsilon}\varrho_{\mathcal{P}} f'(\varphi_{\mathcal{P}}) - \epsilon\varrho_{\mathcal{P}}\triangle\varphi_{\mathcal{P}} - \gamma, \qquad \text{in } \mathcal{P}_\tau, \tag{16.47}$$

where $\triangle := \mathrm{div}\,\mathrm{grad}$ denotes the Laplace operator. Additionally, for the above choices the surface species equation (15.22) can be written as

$$\begin{aligned}\rho\ell_\tau\mu_{\partial\mathcal{P}} = \frac{1}{\delta}\rho\ell_\tau^2 g'(\varphi_{\partial\mathcal{P}}) &- \iota\delta\rho\ell_\tau(\ell_\tau\triangle_{\mathcal{S}}\varphi_{\partial\mathcal{P}} \\ &+ 2\,\mathrm{grad}_{\mathcal{S}}\varphi_{\partial\mathcal{P}}\cdot\mathrm{grad}_{\mathcal{S}}\ell_\tau) + \epsilon\varrho_{\mathcal{P}}\,\mathrm{grad}\,\varphi_{\mathcal{P}}\cdot\boldsymbol{n} - \zeta, \qquad \text{on } \partial\mathcal{P}_\tau,\end{aligned} \tag{16.48}$$

with $\triangle_{\mathcal{S}} := \mathrm{div}_{\mathcal{S}}\mathrm{grad}_{\mathcal{S}}$ denoting the Laplace-Beltrami operator, see also definition (13.8). Note that we have arrived at equation (16.48) using the surface microtraction $(15.16)_1$, as well as $\mathrm{grad}_{\mathcal{S}}\varphi_{\partial\mathcal{P}}\cdot\boldsymbol{n} = 0$. Note that we could also have obtained expression (16.48) by substitution of the free-energy densities (16.42) into the equation for the surface chemical potential (16.41).

Next, we derive the specialized equations of motion. First, using the surface free-energy density $(16.42)_2$ and the microstresses (16.44), the bulk and surface stresses (16.35) specialize to

$$\begin{cases} \mathbf{T} := 2\bar{\mu}_{\mathcal{P}}\,\mathbf{D}_{\mathcal{P}} - p^{\text{mech}}_{\mathcal{P}}\mathbf{1} - \epsilon\varrho_{\mathcal{P}}\operatorname{grad}\varphi_{\mathcal{P}}\otimes\operatorname{grad}\varphi_{\mathcal{P}}, \qquad \text{and} \\ \mathbf{H} := 2\bar{\mu}_{\partial\mathcal{P}}\,\mathbf{P}_{n}\mathbf{D}^{0}_{\partial\mathcal{P}}\mathbf{P}_{n} - \left(\rho\ell^{2}_{\tau}\Big(\dfrac{1}{\delta}g(\varphi_{\partial\mathcal{P}}) + \dfrac{\iota\delta}{2}|\operatorname{grad}_{\mathcal{S}}\varphi_{\partial\mathcal{P}}|^{2}\Big) + \bar{\kappa}_{\partial\mathcal{P}}\dfrac{\mathring{\ell}_{\tau}}{\ell_{\tau}}\right)\mathbf{P}_{n} \\ \qquad - \iota\delta\rho\ell_{\tau}\operatorname{grad}_{\mathcal{S}}\varphi_{\partial\mathcal{P}}\otimes\operatorname{grad}_{\mathcal{S}}\varphi_{\partial\mathcal{P}}, \end{cases} \tag{16.49}$$

recalling that $\mathbf{D}_{\mathcal{P}} := \operatorname{sym}\operatorname{grad}\boldsymbol{v}_{\mathcal{P}}$, $\mathbf{D}_{\partial\mathcal{P}} := \operatorname{sym}\operatorname{grad}_{\mathcal{S}}\boldsymbol{v}_{\partial\mathcal{P}}$ and that $\mathbf{D}^{0}_{\partial\mathcal{P}}$ is the deviatoric part of $\mathbf{D}_{\partial\mathcal{P}}$. Using these bulk stress $(16.49)_1$, the bulk equation of motion (15.19) takes on the form

$$\begin{aligned} \varrho_{\mathcal{P}}\dot{\boldsymbol{v}}_{\mathcal{P}} &= \operatorname{div}\mathbf{T} + \boldsymbol{b}^{\text{ni}} &&(16.50)\\ &= 2\operatorname{div}(\bar{\mu}_{\mathcal{P}}\,\mathbf{D}_{\mathcal{P}}) - \operatorname{grad}p^{\text{mech}}_{\mathcal{P}} - \epsilon\varrho_{\mathcal{P}}\operatorname{div}(\operatorname{grad}\varphi_{\mathcal{P}}\otimes\operatorname{grad}\varphi_{\mathcal{P}}) + \boldsymbol{b}^{\text{ni}}, \qquad \text{in } \mathcal{P}_{\tau}. \end{aligned}$$

Conversely, we arrive at the specialized surface equation of motion by using the surface traction $(15.15)_1$ into surface equation (15.21), followed by substitution of the stresses (16.49), yielding

$$\begin{aligned} \rho\ell_{\tau}\mathring{\boldsymbol{v}}_{\partial\mathcal{P}} &= \operatorname{div}_{\mathcal{S}}\mathbf{H} + 2K\mathbf{H}\boldsymbol{n} + \boldsymbol{g}^{\text{ni}} - \mathbf{T}\boldsymbol{n} \\ &= 2\operatorname{div}_{\mathcal{S}}(\bar{\mu}_{\partial\mathcal{P}}\mathbf{P}_{n}\mathbf{D}^{0}_{\partial\mathcal{P}}\mathbf{P}_{n}) - \rho\ell^{2}_{\tau}\operatorname{grad}_{\mathcal{S}}\Big(\frac{1}{\delta}g(\varphi_{\partial\mathcal{P}}) + \frac{\iota\delta}{2}|\operatorname{grad}_{\mathcal{S}}\varphi_{\partial\mathcal{P}}|^{2}\Big) \\ &\quad - 2\rho\ell_{\tau}\Big(\frac{1}{\delta}g(\varphi_{\partial\mathcal{P}}) + \frac{\iota\delta}{2}|\operatorname{grad}_{\mathcal{S}}\varphi_{\partial\mathcal{P}}|^{2}\Big)\operatorname{grad}_{\mathcal{S}}\ell_{\tau} - \operatorname{grad}_{\mathcal{S}}\Big(\bar{\kappa}_{\partial\mathcal{P}}\frac{\mathring{\ell}_{\tau}}{\ell_{\tau}}\Big) \\ &\quad - \iota\delta\rho\ell_{\tau}\operatorname{div}_{\mathcal{S}}\Big(\operatorname{grad}_{\mathcal{S}}\varphi_{\partial\mathcal{P}}\otimes\operatorname{grad}_{\mathcal{S}}\varphi_{\partial\mathcal{P}}\Big) - \iota\delta\rho\operatorname{grad}_{\mathcal{S}}\ell_{\tau}\cdot\Big(\operatorname{grad}_{\mathcal{S}}\varphi_{\partial\mathcal{P}}\otimes\operatorname{grad}_{\mathcal{S}}\varphi_{\partial\mathcal{P}}\Big) \\ &\quad + \boldsymbol{g}^{\text{ni}} - 2\bar{\mu}_{\mathcal{P}}\,\mathbf{D}_{\mathcal{P}}\boldsymbol{n} + p^{\text{mech}}_{\mathcal{P}}\boldsymbol{n} + \epsilon\varrho_{\mathcal{P}}\operatorname{grad}\varphi_{\mathcal{P}}\otimes\operatorname{grad}\varphi_{\mathcal{P}}\boldsymbol{n}, \qquad \text{on } \partial\mathcal{P}_{\tau}, \end{aligned} \tag{16.51}$$

where we have additionally used that $\mathbf{P}_{n}\boldsymbol{n} = \mathbf{0}$.

Lastly, supplementing the specialized field equations (16.47), (16.48), (16.50), and (16.51) with the isochoric constraints in (14.14) and (14.17) renders a system of equations that describes the dynamics of the bulk-surface system in terms of the state variables $\varphi_{\mathcal{P}}$, $\varphi_{\partial\mathcal{P}}$, $\boldsymbol{v}_{\mathcal{P}}$, $\boldsymbol{v}_{\partial\mathcal{P}}$, $p^{\text{mech}}_{\mathcal{P}}$ and ℓ_{τ}.

Chapter 17

Boundary Conditions and Dissipation Inequalities

In this Chapter, we supplement the system with appropriate boundary conditions, so that we can further characterize its thermodynamics. In Section 17.1 of this Chapter, we postulate an *environmental surface imbalance*, which we employ to formulate thermodynamically-consistent boundary conditions. These boundary conditions describe the dynamic coupling of the bulk and surface fluid at the surface (Section 17.2), as well as the interaction of the surface fluid with the environment across the edges (Section 17.3). In Section 17.4, we use these boundary conditions to derive the *Lyapunov decay relation*, which characterizes the dissipative nature of our bulk-surface system and its interaction with the environment.

17.1 Environmental surface imbalance

In the following, we use a similar approach to the *surface imbalance* presented by Espath [54] based on arguments presented by Fried & Gurtin in [65, Equation (92)] to define dynamic boundary conditions on the migrating boundary $\partial\mathcal{P}_\tau$. Procedures based on analogous mechanical and thermodynamical arguments can be found in [66, 55, 46, 54]. In this work specifically, we stipulate that

$$\mathcal{T}_{\text{surf}}(-\partial\mathcal{P}_\tau) + \mathcal{T}_{\text{env}}(\partial\mathcal{P}_\tau) \geq 0, \tag{17.1}$$

where $\mathcal{T}_{\text{surf}}(-\partial\mathcal{P}_\tau)$ represents the power expended on $\partial\mathcal{P}_\tau$ by the material inside $\mathcal{P}_\tau$ and $\partial\mathcal{P}_\tau$, as well as the rate at which energy is transferred from $\mathcal{P}_\tau$ to $\partial\mathcal{P}_\tau$. In addition, $\mathcal{T}_{\text{env}}(\partial\mathcal{P}_\tau)$ combines the power expended by the environment on $\partial\mathcal{P}_\tau$ and the rate at which energy is transferred from the environment to $\partial\mathcal{P}_\tau$. Therefore, we define

$$\begin{aligned}\mathcal{T}_{\text{surf}}(-\partial\mathcal{P}_\tau) := &- \int_{\partial\mathcal{P}_\tau} (\boldsymbol{v}_{\mathcal{P}} - \boldsymbol{v}_{\partial\mathcal{P}}) \cdot \boldsymbol{t}_{\mathcal{S}} \, \mathrm{d}a_\tau - \int_{\partial^2\mathcal{P}_\tau} \boldsymbol{h}_{\partial\mathcal{S}} \cdot \boldsymbol{v}_{\partial\mathcal{P}} \, \mathrm{d}\sigma_\tau \\ &- \int_{\partial\mathcal{P}_\tau} (\dot{\varphi}_{\mathcal{P}} - \mathring{\varphi}_{\partial\mathcal{P}})\xi_{\mathcal{S}} \, \mathrm{d}a_\tau - \int_{\partial^2\mathcal{P}_\tau} \tau_{\partial\mathcal{S}} \mathring{\varphi}_{\partial\mathcal{P}} \, \mathrm{d}\sigma_\tau \\ &- \int_{\partial\mathcal{P}_\tau} (\mu_{\partial\mathcal{P}} - \mu_{\mathcal{P}}) \boldsymbol{\jmath}_{\mathcal{P}} \cdot \boldsymbol{n} \, \mathrm{d}a_\tau + \int_{\partial^2\mathcal{P}_\tau} \{\!\{ \mu_{\partial\mathcal{P}} \boldsymbol{\jmath}_{\partial\mathcal{P}} \cdot \boldsymbol{\nu} \}\!\} \, \mathrm{d}\sigma_\tau,\end{aligned} \tag{17.2}$$

where $\mathcal{T}_{\text{surf}}(-\partial\mathcal{P}_\tau) = -\mathcal{T}_{\text{surf}}(\partial\mathcal{P}_\tau)$, see Remark 17.1.

Remark 17.1 (Action-reaction principle and its consequences) As a result of (15.15) and (15.16), all tractions and microtractions are locally defined, i.e. for the bulk material we have that

$$\left.\begin{aligned} \boldsymbol{t}_{\mathcal{S}} &= \mathbf{T}\boldsymbol{n} \\ \xi_{\mathcal{S}} &= \boldsymbol{\xi}\cdot\boldsymbol{n} \end{aligned}\right\} \quad \text{on } \partial\mathcal{P}_\tau, \tag{17.3}$$

whilst for the surface material holds

$$\left.\begin{aligned} \boldsymbol{h}_{\partial\mathcal{S}} &= \{\!\{\mathbf{H}\boldsymbol{\nu}\}\!\} \\ \tau_{\partial\mathcal{S}} &= \{\!\{\boldsymbol{\tau}\cdot\boldsymbol{\nu}\}\!\} \end{aligned}\right\} \quad \text{on } \partial^2\mathcal{P}_\tau. \tag{17.4}$$

Then, let $-\partial\mathcal{P}_\tau$ denote the surface adjacent to $\partial\mathcal{P}_\tau$ and be oriented by $-\boldsymbol{n}(\boldsymbol{x},t)$. At this surface $-\partial\mathcal{P}_\tau$, we find

$$\left.\begin{aligned} \boldsymbol{t}_{-\mathcal{S}} &= -\mathbf{T}\boldsymbol{n} = -\boldsymbol{t}_{\mathcal{S}} \\ \xi_{-\mathcal{S}} &= -\boldsymbol{\xi}\cdot\boldsymbol{n} = -\xi_{\mathcal{S}} \end{aligned}\right\} \quad \text{on } -\partial\mathcal{P}_\tau, \tag{17.5}$$

whereas at the opposite edge $-\partial^2\mathcal{P}_\tau$, which is oriented by $-\boldsymbol{\nu}(\boldsymbol{x},t)$, we have that

$$\left.\begin{aligned} \boldsymbol{h}_{-\partial\mathcal{S}} &= -\{\!\{\mathbf{H}\boldsymbol{\nu}\}\!\} = -\boldsymbol{h}_{\partial\mathcal{S}} \\ \tau_{-\partial\mathcal{S}} &= -\{\!\{\boldsymbol{\tau}\cdot\boldsymbol{\nu}\}\!\} = -\tau_{\partial\mathcal{S}} \end{aligned}\right\} \quad \text{on } -\partial^2\mathcal{P}_\tau. \tag{17.6}$$

The relations in (17.5) and (17.6) represent the *action-reaction principles* for oppositely oriented surfaces and edges, respectively. More details on these principles in the context of enriched continua can be found in [65, 54].

As a consequence of the action-reaction principles in (17.5) and (17.6), the surface power acting on $-\partial\mathcal{P}_\tau$ can be rewritten as follows

$$\begin{aligned} \mathcal{T}_{\text{surf}}(-\partial\mathcal{P}_\tau) =& \int_{-\partial\mathcal{P}_\tau} (\boldsymbol{v}_{\mathcal{P}} - \boldsymbol{v}_{\partial\mathcal{P}})\cdot\boldsymbol{t}_{-\mathcal{S}}\,\mathrm{d}a_\tau + \int_{-\partial^2\mathcal{P}_\tau} \boldsymbol{h}_{-\partial\mathcal{S}}\cdot\boldsymbol{v}_{\partial\mathcal{P}}\,\mathrm{d}\sigma_\tau \\ &+ \int_{-\partial\mathcal{P}_\tau} (\dot{\varphi}_{\mathcal{P}} - \mathring{\varphi}_{\partial\mathcal{P}})\xi_{-\mathcal{S}}\,\mathrm{d}a_\tau + \int_{-\partial^2\mathcal{P}_\tau} \tau_{-\partial\mathcal{S}}\mathring{\varphi}_{\partial\mathcal{P}}\,\mathrm{d}\sigma_\tau \\ &+ \int_{-\partial\mathcal{P}_\tau} (\mu_{\partial\mathcal{P}} - \mu_{\mathcal{P}})\boldsymbol{\jmath}_{\mathcal{P}}\cdot\boldsymbol{n}\,\mathrm{d}a_\tau - \int_{-\partial^2\mathcal{P}_\tau} \{\!\{\mu_{\partial\mathcal{P}}\boldsymbol{\jmath}_{\partial\mathcal{P}}\cdot\boldsymbol{\nu}\}\!\}\,\mathrm{d}\sigma_\tau \\ =& -\int_{\partial\mathcal{P}_\tau} (\boldsymbol{v}_{\mathcal{P}} - \boldsymbol{v}_{\partial\mathcal{P}})\cdot\boldsymbol{t}_{\mathcal{S}}\,\mathrm{d}a_\tau - \int_{\partial^2\mathcal{P}_\tau} \boldsymbol{h}_{\partial\mathcal{S}}\cdot\boldsymbol{v}_{\partial\mathcal{P}}\,\mathrm{d}\sigma_\tau \\ &- \int_{\partial\mathcal{P}_\tau} (\dot{\varphi}_{\mathcal{P}} - \mathring{\varphi}_{\partial\mathcal{P}})\xi_{\mathcal{S}}\,\mathrm{d}a_\tau - \int_{\partial^2\mathcal{P}_\tau} \tau_{\partial\mathcal{S}}\mathring{\varphi}_{\partial\mathcal{P}}\,\mathrm{d}\sigma_\tau \\ &- \int_{\partial\mathcal{P}_\tau} (\mu_{\partial\mathcal{P}} - \mu_{\mathcal{P}})\boldsymbol{\jmath}_{\mathcal{P}}\cdot\boldsymbol{n}\,\mathrm{d}a_\tau + \int_{\partial^2\mathcal{P}_\tau} \{\!\{\mu_{\partial\mathcal{P}}\boldsymbol{\jmath}_{\partial\mathcal{P}}\cdot\boldsymbol{\nu}\}\!\}\,\mathrm{d}\sigma_\tau \\ =& -\mathcal{T}_{\text{surf}}(\partial\mathcal{P}_\tau). \end{aligned} \tag{17.7}$$

Thus, $\mathcal{T}_{\text{surf}}(\partial\mathcal{P}_\tau) + \mathcal{T}_{\text{surf}}(-\partial\mathcal{P}_\tau) = 0$ constitutes a balance at the surface. □

Furthermore, we define the contribution from the environment as follows

$$\mathcal{T}_{\text{env}}(\partial\mathcal{P}_\tau) := \int_{\partial^2\mathcal{P}_\tau} \boldsymbol{h}^{\text{env}}_{\partial\mathcal{S}}\cdot\boldsymbol{v}^{\text{env}}_{\partial^2\mathcal{P}}\,\mathrm{d}\sigma_\tau + \int_{\partial^2\mathcal{P}_\tau} \tau^{\text{env}}_{\partial\mathcal{S}}\dot{\varphi}^{\text{env}}_{\partial^2\mathcal{P}}\,\mathrm{d}\sigma_\tau - \int_{\partial^2\mathcal{P}_\tau} \mu^{\text{env}}_{\partial^2\mathcal{P}}\jmath^{\text{env}}_{\partial^2\mathcal{P}}\,\mathrm{d}\sigma_\tau. \tag{17.8}$$

Next, on $\partial^2\mathcal{P}_\tau$, we set $\boldsymbol{h}^{\text{env}}_{\partial\mathcal{S}} = \boldsymbol{h}_{\partial\mathcal{S}}$, $\boldsymbol{v}^{\text{env}}_{\partial^2\mathcal{P}} = \boldsymbol{v}_{\partial\mathcal{P}}$, $\tau^{\text{env}}_{\partial\mathcal{S}} = \tau_{\partial\mathcal{S}}$, $\dot{\varphi}^{\text{env}}_{\partial^2\mathcal{P}} = \mathring{\varphi}_{\partial\mathcal{P}}$, $\mu^{\text{env}}_{\partial^2\mathcal{P}} = \mu_{\partial\mathcal{P}}$, and $\jmath^{\text{env}}_{\partial^2\mathcal{P}} = \{\!\{\boldsymbol{\jmath}_{\partial\mathcal{P}}\cdot\boldsymbol{\nu}\}\!\}$. Granted this, the surface free-energy imbalance (17.1) becomes

$$-\int_{\partial\mathcal{P}_\tau} \big((\boldsymbol{v}_{\mathcal{P}} - \boldsymbol{v}_{\partial\mathcal{P}})\cdot\boldsymbol{t}_{\mathcal{S}} + (\dot{\varphi}_{\mathcal{P}} - \mathring{\varphi}_{\partial\mathcal{P}})\,\xi_{\mathcal{S}} + (\mu_{\partial\mathcal{P}} - \mu_{\mathcal{P}})\,\boldsymbol{\jmath}_{\mathcal{P}}\cdot\boldsymbol{n}\big)\,\mathrm{d}a_\tau \geq 0. \tag{17.9}$$

Uncoupling the above expression provides us with

$$\int_{\partial\mathcal{P}_\tau} (\boldsymbol{v}_{\mathcal{P}} - \boldsymbol{v}_{\partial\mathcal{P}}) \cdot \boldsymbol{t}_{\mathcal{S}} \, \mathrm{d}a_\tau \leq 0, \tag{17.10}$$

$$\int_{\partial\mathcal{P}_\tau} (\dot{\varphi}_{\mathcal{P}} - \mathring{\varphi}_{\partial\mathcal{P}}) \, \xi_{\mathcal{S}} \, \mathrm{d}a_\tau \leq 0, \tag{17.11}$$

$$\int_{\partial\mathcal{P}_\tau} (\mu_{\partial\mathcal{P}} - \mu_{\mathcal{P}}) \, \jmath_{\mathcal{P}} \cdot \boldsymbol{n} \, \mathrm{d}a_\tau \leq 0. \tag{17.12}$$

17.2 Dynamic surface boundary conditions

Using the inequalities in (17.10) - (17.12), we formulate three types of dynamic boundary conditions on $\partial\mathcal{P}_\tau$: essential, natural and mixed boundary conditions, which we present in the upcoming subsections.

17.2.1 Essential boundary conditions

Essential (Dirichlet) boundary conditions result from the prescription of the surface fields onto the bulk fields, i.e.

$$\left.\begin{aligned} \boldsymbol{v}_{\mathcal{P}} &= \boldsymbol{v}_{\partial\mathcal{P}} \\ \varphi_{\mathcal{P}} &= \varphi_{\partial\mathcal{P}} \\ \mu_{\mathcal{P}} &= \mu_{\partial\mathcal{P}} \end{aligned}\right\} \quad \text{on } \partial\mathcal{P}_\tau^{\text{ess}}. \tag{17.13}$$

Note that there is no dissipation contribution from the normal components of $\boldsymbol{v}_{\mathcal{P}}$ and $\boldsymbol{v}_{\partial\mathcal{P}}$ at $\partial\mathcal{P}_\tau^{\text{ess}}$: this can only be the result of any non-zero tangential components. Thus, because of assumption (A.2), we arrive at $(17.13)_1$.

17.2.2 Natural boundary conditions

Natural (Neumann) boundary conditions arise by specifying that the normal component of the bulk stress (given by the surface traction) and the normal component of the bulk microstress (described by the surface microtraction) are equal to the normal components of the surface stress and surface microstress, respectively. In addition, the normal component of the bulk species flux equals the normal component of the surface species flux on $\partial\mathcal{P}_\tau^{\text{nat}}$. Thus, the natural boundary conditions read

$$\left.\begin{aligned} \boldsymbol{t}_{\mathcal{S}} &= \mathbf{H}\boldsymbol{n} \\ \xi_{\mathcal{S}} &= \boldsymbol{\tau} \cdot \boldsymbol{n} \\ \jmath_{\mathcal{P}} \cdot \boldsymbol{n} &= \jmath_{\partial\mathcal{P}} \cdot \boldsymbol{n} \end{aligned}\right\} \quad \text{on } \partial\mathcal{P}_\tau^{\text{nat}}. \tag{17.14}$$

However, $\mathbf{H}$ annihilates the normal, i.e. $\mathbf{H}\boldsymbol{n} = \mathbf{0}$, in view of $(16.35)_2$, in addition to the frame-indifference requirement (15.34). Furthermore, we have $\boldsymbol{\tau} \cdot \boldsymbol{n} = 0$ and $\jmath_{\partial\mathcal{P}} \cdot \boldsymbol{n} = 0$ as a result of adopting tangential surface fields for the microstress and species mass flux in $(16.24)_2$ and $(16.26)_2$, respectively. Consequently, the natural boundary conditions read

$$\left.\begin{aligned} \boldsymbol{t}_{\mathcal{S}} &= 0 \\ \xi_{\mathcal{S}} &= 0 \\ \jmath_{\mathcal{P}} \cdot \boldsymbol{n} &= 0 \end{aligned}\right\} \quad \text{on } \partial\mathcal{P}_\tau^{\text{nat}}, \tag{17.15}$$

which satisfy the requirements in (17.10) - (17.12). Notice that any tangential components of the bulk species flux $\jmath_{\mathcal{P}}$ do not contribute to the dissipation inequality in (17.12).

17.2.3 Mixed boundary conditions

In view of (17.10) - (17.12), we formulate a set of mixed (Robin) boundary conditions, which are dissipative in nature. These are given by

$$\left.\begin{aligned} \boldsymbol{t}_{\mathcal{S}} &= \tfrac{1}{L_v}\mathbf{P}_{\boldsymbol{n}}(\boldsymbol{v}_{\partial\mathcal{P}} - \boldsymbol{v}_{\mathcal{P}}) = \tfrac{1}{L_v}(\boldsymbol{v}_{\partial\mathcal{P}} - \boldsymbol{v}_{\mathcal{P}}) \\ \xi_{\mathcal{S}} &= \tfrac{1}{L_\varphi}(\mathring{\varphi}_{\partial\mathcal{P}} - \dot{\varphi}_{\mathcal{P}}) \\ \boldsymbol{\jmath}_{\mathcal{P}} \cdot \boldsymbol{n} &= -\tfrac{1}{L_\mu}(\mu_{\partial\mathcal{P}} - \mu_{\mathcal{P}}) \end{aligned}\right\} \quad \text{on } \partial\mathcal{P}_\tau^{\text{mix}}, \tag{17.16}$$

with scalars $L_v, L_\varphi, L_\mu > 0$. The expressions in (17.16) should be understood as a surface traction, surface microtraction and bulk species mass flux defined across $\partial\mathcal{P}_\tau^{\text{mix}}$, which are driven by the difference in velocity, microstructure (described by the phase field), and chemical potential, respectively, between the bulk and surface material. Here, we assume that the dependency is linear and that the parameters L_v, L_φ and L_μ act as relaxation parameters. Furthermore, notice that the rightmost expression in $(17.16)_1$ arises in view of Assumption (A.2).

In [97], a mixed type of boundary condition similar to $(17.16)_3$ was proposed for the chemical potential. The theory for mixed dynamic boundary conditions for phase-field models was further extended and presented for both the microstructure and chemical potential in [53, 54].

17.3 Static edge boundary conditions

In this Section, we complement the dynamic boundary conditions on $\partial\mathcal{P}_\tau$ (in Section 17.2) by a set of static boundary conditions on $\partial^2\mathcal{P}_\tau$. Here, static refers to the fact that the edge $\partial^2\mathcal{P}_\tau$ does not have any dynamics on its own. In particular, we present both essential and natural boundary conditions resulting from the action of a static environment on the edge $\partial^2\mathcal{P}_\tau$, i.e. the curve where the dynamic surface $\partial\mathcal{P}_\tau$ loses its smoothness. It is also possible to formulate mixed type of boundary conditions on static environments, for which the reader is referred to [55, 54].

17.3.1 Essential boundary conditions

The essential boundary conditions on static edges $\partial^2\mathcal{P}_\tau^{\text{ess}}$ read

$$\left.\begin{aligned} \boldsymbol{v}_{\partial\mathcal{P}} &= \boldsymbol{v}_{\partial^2\mathcal{P}}^{\text{env}} \\ \varphi_{\partial\mathcal{P}} &= \varphi_{\partial^2\mathcal{P}}^{\text{env}} \\ \mu_{\partial\mathcal{P}} &= \mu_{\partial^2\mathcal{P}}^{\text{env}} \end{aligned}\right\} \quad \text{on } \partial^2\mathcal{P}_\tau^{\text{ess}}, \tag{17.17}$$

where $\boldsymbol{v}_{\partial^2\mathcal{P}}^{\text{env}}$ is the action of the velocity, $\varphi_{\partial^2\mathcal{P}}^{\text{env}}$ is the assignment of the microstructure, and $\mu_{\partial^2\mathcal{P}}^{\text{env}}$ is the action of the chemical potential, all originating from a static environment acting on the edge $\partial^2\mathcal{P}_\tau^{\text{ess}}$.

17.3.2 Natural boundary conditions

On natural edges $\partial^2\mathcal{P}_\tau^{\text{nat}}$, we prescribe the following boundary conditions

$$\left.\begin{aligned} \boldsymbol{h}_{\partial\mathcal{S}} &:= \{\!\{\mathbf{H}\boldsymbol{\nu}\}\!\} = \boldsymbol{h}_{\partial\mathcal{S}}^{\text{env}} \\ \tau_{\partial\mathcal{S}} &:= \{\!\{\boldsymbol{\tau} \cdot \boldsymbol{\nu}\}\!\} = \tau_{\partial\mathcal{S}}^{\text{env}} \\ \jmath_{\partial^2\mathcal{P}} &:= -\{\!\{\boldsymbol{\jmath}_{\partial\mathcal{P}} \cdot \boldsymbol{\nu}\}\!\} = \jmath_{\partial^2\mathcal{P}}^{\text{env}} \end{aligned}\right\} \quad \text{on } \partial^2\mathcal{P}_\tau^{\text{nat}}, \tag{17.18}$$

where $\boldsymbol{h}^{\mathrm{env}}_{\partial\mathcal{S}}$ and $\tau^{\mathrm{env}}_{\partial\mathcal{S}}$ are the assigned edge traction and edge microtraction of the static environment across $\partial^2\mathcal{P}^{\mathrm{nat}}_{\tau}$. Furthermore, $J^{\mathrm{env}}_{\partial^2\mathcal{P}}$ represents the transfer of species from the static environment to $\partial^2\mathcal{P}^{\mathrm{nat}}_{\tau}$.

17.4 Lyapunov decay relation

In this Section, we are interested in understanding the behaviour of the total energy variation of the coupled bulk and surface material. Using the constitutive response functions formulated in Section 13.2, we derive the relation for the temporal change in the free-energy functional in Subsection 17.4.1. In Subsection 17.4.2, we present the temporal variation in the kinetic energy of the bulk-surface system. Then, by employing the boundary conditions formulated in Section 17.2, we arrive at the Lyapunov decay relation in Subsection 17.4.3.

17.4.1 Free-energy rate

First, we restrict our attention to the bulk and surface material's free-energy rate, and write

$$
\begin{aligned}
\overline{\mathcal{F}(\mathcal{P}_\tau,\partial\mathcal{P}_\tau)}^{\cdot} &:= \overline{\int_{\mathcal{P}_\tau} \varrho_{\mathcal{P}}\psi_{\mathcal{P}}\,\mathrm{d}v_\tau}^{\cdot} + \overline{\int_{\partial\mathcal{P}_\tau} \rho\ell_\tau\psi_{\partial\mathcal{P}}\,\mathrm{d}a_\tau}^{\cdot} \\
&= \int_{\mathcal{P}_\tau} \varrho_{\mathcal{P}}\dot{\psi}_{\mathcal{P}}\,\mathrm{d}v_\tau + \int_{\partial\mathcal{P}_\tau} \rho\ell_\tau\mathring{\psi}_{\partial\mathcal{P}}\,\mathrm{d}a_\tau \\
&= \int_{\mathcal{P}_\tau} \varrho_{\mathcal{P}}\left(\partial_{\varphi_{\mathcal{P}}}\psi_{\mathcal{P}}\dot{\varphi}_{\mathcal{P}} + \partial_{\mathrm{grad}\,\varphi_{\mathcal{P}}}\psi_{\mathcal{P}}\cdot(\mathrm{grad}\,\varphi_{\mathcal{P}})^{\cdot}\right)\mathrm{d}v_\tau \\
&\quad + \int_{\partial\mathcal{P}_\tau} \rho\ell_\tau^2\left(\partial_{\varphi_{\partial\mathcal{P}}}\psi\mathring{\varphi}_{\partial\mathcal{P}} - \psi\,\mathrm{div}_{\mathcal{S}}\boldsymbol{v}_{\partial\mathcal{P}}\right)\mathrm{d}a_\tau \\
&\quad + \int_{\partial\mathcal{P}_\tau} \rho\ell_\tau^2\partial_{\mathrm{grad}_{\mathcal{S}}\varphi_{\partial\mathcal{P}}}\psi\cdot(\mathrm{grad}_{\mathcal{S}}\varphi_{\partial\mathcal{P}})^{\circ}\,\mathrm{d}a_\tau,
\end{aligned}
\tag{17.19}
$$

where we have used the constitutive dependencies of $\psi_{\mathcal{P}}$ and $\psi_{\partial\mathcal{P}}$ formulated in (16.17) and (16.22). Next, we use the constitutive response functions for the internal microforces (16.25) and microstresses (16.24) to rewrite the above as

$$
\begin{aligned}
\overline{\mathcal{F}(\mathcal{P}_\tau, \partial\mathcal{P}_\tau)}^{\cdot} &= \int_{\mathcal{P}_\tau} \big(\varrho_{\mathcal{P}}\mu_{\mathcal{P}}\dot{\varphi}_{\mathcal{P}} - \pi\dot{\varphi}_{\mathcal{P}} + \boldsymbol{\xi}\cdot(\operatorname{grad}\varphi_{\mathcal{P}})^{\cdot}\big)\,\mathrm{d}v_\tau \\
&\quad + \int_{\partial\mathcal{P}_\tau} \big(\rho\ell_\tau\mu_{\partial\mathcal{P}}\mathring{\varphi}_{\partial\mathcal{P}} - \varpi\mathring{\varphi}_{\partial\mathcal{P}} - \rho\ell_\tau^2\psi\,\mathrm{div}_{\mathcal{S}}\boldsymbol{v}_{\partial\mathcal{P}} + \boldsymbol{\tau}\cdot(\operatorname{grad}_{\mathcal{S}}\varphi_{\partial\mathcal{P}})^{\circ}\big)\,\mathrm{d}a_\tau \\
&= \int_{\mathcal{P}_\tau} \big(\varrho_{\mathcal{P}}\mu_{\mathcal{P}}\dot{\varphi}_{\mathcal{P}} - \pi\dot{\varphi}_{\mathcal{P}} + \boldsymbol{\xi}\cdot\operatorname{grad}\dot{\varphi}_{\mathcal{P}} - (\operatorname{grad}\varphi_{\mathcal{P}}\otimes\boldsymbol{\xi}) : \operatorname{grad}\boldsymbol{v}_{\mathcal{P}}\big)\,\mathrm{d}v_\tau \\
&\quad + \int_{\partial\mathcal{P}_\tau} \big(\rho\ell_\tau\mu_{\partial\mathcal{P}}\mathring{\varphi}_{\partial\mathcal{P}} - \varpi\mathring{\varphi}_{\partial\mathcal{P}} - \rho\ell_\tau^2\psi\,\mathrm{div}_{\mathcal{S}}\boldsymbol{v}_{\partial\mathcal{P}}\big)\,\mathrm{d}a_\tau \\
&\quad + \int_{\partial\mathcal{P}_\tau} \big(\boldsymbol{\tau}\cdot\operatorname{grad}_{\mathcal{S}}\mathring{\varphi}_{\partial\mathcal{P}} - (\operatorname{grad}_{\mathcal{S}}\varphi_{\partial\mathcal{P}}\otimes\boldsymbol{\tau}) : \operatorname{grad}_{\mathcal{S}}\boldsymbol{v}_{\partial\mathcal{P}}\big)\,\mathrm{d}a_\tau \\
&= \int_{\mathcal{P}_\tau} (\varrho_{\mathcal{P}}\mu_{\mathcal{P}} - \pi - \mathrm{div}\,\boldsymbol{\xi})\,\dot{\varphi}_{\mathcal{P}}\,\mathrm{d}v_\tau - \int_{\mathcal{P}_\tau} (\operatorname{grad}\varphi_{\mathcal{P}}\otimes\boldsymbol{\xi}) : \operatorname{grad}\boldsymbol{v}_{\mathcal{P}}\,\mathrm{d}v_\tau \\
&\quad + \int_{\partial\mathcal{P}_\tau} (\rho\ell_\tau\mu_{\partial\mathcal{P}} - \varpi - \mathrm{div}_{\mathcal{S}}(\mathbf{P}_{\!n}\boldsymbol{\tau}))\,\mathring{\varphi}_{\partial\mathcal{P}}\,\mathrm{d}a_\tau - \int_{\partial\mathcal{P}_\tau} \rho\ell_\tau^2\psi\,\mathrm{div}_{\mathcal{S}}\boldsymbol{v}_{\partial\mathcal{P}}\,\mathrm{d}a_\tau \\
&\quad - \int_{\partial\mathcal{P}_\tau} (\operatorname{grad}_{\mathcal{S}}\varphi_{\partial\mathcal{P}}\otimes\boldsymbol{\tau}) : \operatorname{grad}_{\mathcal{S}}\boldsymbol{v}_{\partial\mathcal{P}}\;\mathrm{d}a_\tau \\
&\quad + \int_{\partial\mathcal{P}_\tau} \dot{\varphi}_{\mathcal{P}}\boldsymbol{\xi}\cdot\boldsymbol{n}\,\mathrm{d}a_\tau + \int_{\partial^2\mathcal{P}_\tau} \mathring{\varphi}_{\partial\mathcal{P}}\{\!\{\boldsymbol{\tau}\cdot\boldsymbol{\nu}\}\!\}\,\mathrm{d}\sigma_\tau,
\end{aligned}
\tag{17.20}
$$

where we have expanded $(\operatorname{grad}\varphi_{\mathcal{P}})^{\cdot}$ and $(\operatorname{grad}_{\mathcal{S}}\varphi_{\partial\mathcal{P}})^{\circ}$ using identities (16.13) and (16.14), respectively, and subsequently applied the divergence theorems. We now introduce the external microforces γ and ζ into relation (17.20) through the microforce balances (15.14), and use the definition of the surface and edge microtraction (15.16) to obtain

$$
\begin{aligned}
\overline{\mathcal{F}(\mathcal{P}_\tau, \partial\mathcal{P}_\tau)}^{\cdot} &= \int_{\mathcal{P}_\tau} (\varrho_{\mathcal{P}}\mu_{\mathcal{P}} + \gamma)\,\dot{\varphi}_{\mathcal{P}}\,\mathrm{d}v_\tau - \int_{\mathcal{P}_\tau} (\operatorname{grad}\varphi_{\mathcal{P}}\otimes\boldsymbol{\xi}) : \operatorname{grad}\boldsymbol{v}_{\mathcal{P}}\,\mathrm{d}v_\tau \\
&\quad + \int_{\partial\mathcal{P}_\tau} (\rho\ell_\tau\mu_{\partial\mathcal{P}} + \zeta)\,\mathring{\varphi}_{\partial\mathcal{P}}\,\mathrm{d}a_\tau - \int_{\partial\mathcal{P}_\tau} \rho\ell_\tau^2\psi\,\mathrm{div}_{\mathcal{S}}\boldsymbol{v}_{\partial\mathcal{P}}\,\mathrm{d}a_\tau \\
&\quad - \int_{\partial\mathcal{P}_\tau} (\operatorname{grad}_{\mathcal{S}}\varphi_{\partial\mathcal{P}}\otimes\boldsymbol{\tau}) : \operatorname{grad}_{\mathcal{S}}\boldsymbol{v}_{\partial\mathcal{P}}\;\mathrm{d}a_\tau - \int_{\partial\mathcal{P}_\tau} (\mathring{\varphi}_{\partial\mathcal{P}} - \dot{\varphi}_{\mathcal{P}})\,\xi_{\mathcal{S}}\,\mathrm{d}a_\tau \\
&\quad + \int_{\partial^2\mathcal{P}_\tau} \mathring{\varphi}_{\partial\mathcal{P}}\tau_{\partial\mathcal{S}}\,\mathrm{d}\sigma_\tau.
\end{aligned}
\tag{17.21}
$$

Finally, we employ the pointwise bulk and surface balances of species mass (14.36) and (14.37), and subsequently the divergence theorem and the constitutive response functions for the bulk and surface species fluxes (16.26), to arrive at

$$
\begin{aligned}
\overline{\mathcal{F}(\mathcal{P}_\tau,\partial\mathcal{P}_\tau)}^{\boldsymbol{\cdot}} = &\int_{\mathcal{P}_\tau} (\mu_{\mathcal{P}} s_{\mathcal{P}} + \gamma\dot{\varphi}_{\mathcal{P}} - \mu_{\mathcal{P}}\mathrm{div}\,\boldsymbol{\jmath}_{\mathcal{P}})\,\mathrm{d}v_\tau - \int_{\mathcal{P}_\tau} (\mathrm{grad}\,\varphi_{\mathcal{P}} \otimes \boldsymbol{\xi}) : \mathrm{grad}\,\boldsymbol{v}_{\mathcal{P}}\,\mathrm{d}v_\tau \\
&+ \int_{\partial\mathcal{P}_\tau} (\mu_{\partial\mathcal{P}} s_{\partial\mathcal{P}} + \zeta\mathring{\varphi}_{\partial\mathcal{P}} - \mu_{\partial\mathcal{P}}\mathrm{div}_{\mathcal{S}}(\mathbf{P}_n\boldsymbol{\jmath}_{\partial\mathcal{P}}))\,\mathrm{d}a_\tau - \int_{\partial\mathcal{P}_\tau} \rho\ell_\tau^2\psi\,\mathrm{div}_{\mathcal{S}}\boldsymbol{v}_{\partial\mathcal{P}}\,\mathrm{d}a_\tau \\
&- \int_{\partial\mathcal{P}_\tau} (\mathrm{grad}_{\mathcal{S}}\varphi_{\partial\mathcal{P}} \otimes \boldsymbol{\tau}) : \mathrm{grad}_{\mathcal{S}}\boldsymbol{v}_{\partial\mathcal{P}}\,\mathrm{d}a_\tau - \int_{\partial\mathcal{P}_\tau} (\mathring{\varphi}_{\partial\mathcal{P}} - \dot{\varphi}_{\mathcal{P}})\,\xi_{\mathcal{S}}\,\mathrm{d}a_\tau \\
&+ \int_{\partial\mathcal{P}_\tau} \mu_{\partial\mathcal{P}}\boldsymbol{\jmath}_{\mathcal{P}}\cdot\boldsymbol{n}\,\mathrm{d}a_\tau + \int_{\partial^2\mathcal{P}_\tau} \mathring{\varphi}_{\partial\mathcal{P}}\tau_{\partial\mathcal{S}}\,\mathrm{d}\sigma_\tau \\
= &\int_{\mathcal{P}_\tau} (\mu_{\mathcal{P}} s_{\mathcal{P}} + \gamma\dot{\varphi}_{\mathcal{P}})\,\mathrm{d}v_\tau - \int_{\mathcal{P}_\tau} \mathrm{grad}\,\mu_{\mathcal{P}}\cdot\boldsymbol{M}_{\mathcal{P}}\mathrm{grad}\,\mu_{\mathcal{P}}\,\mathrm{d}v_\tau \\
&- \int_{\mathcal{P}_\tau} (\mathrm{grad}\,\varphi_{\mathcal{P}} \otimes \boldsymbol{\xi}) : \mathrm{grad}\,\boldsymbol{v}_{\mathcal{P}}\,\mathrm{d}v_\tau \\
&+ \int_{\partial\mathcal{P}_\tau} (\mu_{\partial\mathcal{P}} s_{\partial\mathcal{P}} + \zeta\mathring{\varphi}_{\partial\mathcal{P}})\,\mathrm{d}a_\tau - \int_{\partial\mathcal{P}_\tau} \mathrm{grad}_{\mathcal{S}}\mu_{\partial\mathcal{P}}\cdot\boldsymbol{M}_{\partial\mathcal{P}}\mathrm{grad}_{\mathcal{S}}\mu_{\partial\mathcal{P}}\,\mathrm{d}a_\tau \\
&- \int_{\partial\mathcal{P}_\tau} \rho\ell_\tau^2\psi\,\mathrm{div}_{\mathcal{S}}\boldsymbol{v}_{\partial\mathcal{P}}\,\mathrm{d}a_\tau - \int_{\partial\mathcal{P}_\tau} (\mathrm{grad}_{\mathcal{S}}\varphi_{\partial\mathcal{P}} \otimes \boldsymbol{\tau}) : \mathrm{grad}_{\mathcal{S}}\boldsymbol{v}_{\partial\mathcal{P}}\,\mathrm{d}a_\tau \\
&- \int_{\partial\mathcal{P}_\tau} (\mathring{\varphi}_{\partial\mathcal{P}} - \dot{\varphi}_{\mathcal{P}})\,\xi_{\mathcal{S}}\,\mathrm{d}a_\tau - \int_{\partial\mathcal{P}_\tau} (\mu_{\mathcal{P}} - \mu_{\partial\mathcal{P}})\boldsymbol{\jmath}_{\mathcal{P}}\cdot\boldsymbol{n}\,\mathrm{d}a_\tau \\
&+ \int_{\partial^2\mathcal{P}_\tau} (\mathring{\varphi}_{\partial\mathcal{P}}\tau_{\partial\mathcal{S}} - \mu_{\partial\mathcal{P}}\{\!\{\boldsymbol{\jmath}_{\partial\mathcal{P}}\cdot\boldsymbol{\nu}\}\!\})\,\mathrm{d}\sigma_\tau.
\end{aligned} \tag{17.22}
$$

17.4.2 Kinetic-energy rate

In this Subsection, we are interested in understanding the temporal changes in the kinetic energy of the bulk and surface material. We use the pointwise force balances (15.19) and (15.20) to arrive at the following relation for the kinetic-energy rate

$$
\begin{aligned}
\overline{\mathcal{K}(\mathcal{P}_\tau,\partial\mathcal{P}_\tau)}^{\boldsymbol{\cdot}} :&= \overline{\int_{\mathcal{P}_\tau} \tfrac{1}{2}\varrho_{\mathcal{P}}|\boldsymbol{v}_{\mathcal{P}}|^2\,\mathrm{d}v_\tau}^{\boldsymbol{\cdot}} + \overline{\int_{\partial\mathcal{P}_\tau} \tfrac{1}{2}\rho\ell_\tau|\boldsymbol{v}_{\partial\mathcal{P}}|^2\,\mathrm{d}a_\tau}^{\boldsymbol{\cdot}} \\
&= \int_{\mathcal{P}_\tau} \varrho_{\mathcal{P}}\boldsymbol{v}_{\mathcal{P}}\cdot\dot{\boldsymbol{v}}_{\mathcal{P}}\,\mathrm{d}v_\tau + \int_{\partial\mathcal{P}_\tau} \rho\ell_\tau\boldsymbol{v}_{\partial\mathcal{P}}\cdot\mathring{\boldsymbol{v}}_{\partial\mathcal{P}}\,\mathrm{d}a_\tau \qquad (17.23) \\
&= \int_{\mathcal{P}_\tau} \boldsymbol{v}_{\mathcal{P}}\cdot(\boldsymbol{b}^{\mathrm{ni}} + \mathrm{div}\,\mathbf{T})\,\mathrm{d}v_\tau + \int_{\partial\mathcal{P}_\tau} \boldsymbol{v}_{\partial\mathcal{P}}\cdot(\boldsymbol{g}^{\mathrm{ni}} - \boldsymbol{t}_{\mathcal{S}} + \mathrm{div}_{\mathcal{S}}(\mathbf{HP}_n))\,\mathrm{d}a_\tau.
\end{aligned}
$$

Lastly, application of the divergence theorems, followed by substitution of the relations for the surface and edge traction (15.15), the kinetic energy rate reads

$$
\begin{aligned}
&\overline{\int_{\mathcal{P}_\tau} \tfrac{1}{2}\varrho_{\mathcal{P}}|\boldsymbol{v}_{\mathcal{P}}|^2\,\mathrm{d}v_\tau}^{\boldsymbol{\cdot}} + \overline{\int_{\partial\mathcal{P}_\tau} \tfrac{1}{2}\rho\ell_\tau|\boldsymbol{v}_{\partial\mathcal{P}}|^2\,\mathrm{d}a_\tau}^{\boldsymbol{\cdot}} \\
&\quad= \int_{\mathcal{P}_\tau} (\boldsymbol{v}_{\mathcal{P}}\cdot\boldsymbol{b}^{\mathrm{ni}} - \mathbf{T} : \mathrm{grad}\,\boldsymbol{v}_{\mathcal{P}})\,\mathrm{d}v_\tau + \int_{\partial\mathcal{P}_\tau} (\boldsymbol{v}_{\partial\mathcal{P}}\cdot\boldsymbol{g}^{\mathrm{ni}} - \mathbf{HP}_n : \mathrm{grad}_{\mathcal{S}}\boldsymbol{v}_{\partial\mathcal{P}})\,\mathrm{d}a_\tau \\
&\qquad - \int_{\partial\mathcal{P}_\tau} (\boldsymbol{v}_{\partial\mathcal{P}} - \boldsymbol{v}_{\mathcal{P}})\cdot\boldsymbol{t}_{\mathcal{S}}\,\mathrm{d}a_\tau + \int_{\partial^2\mathcal{P}_\tau} \boldsymbol{v}_{\partial\mathcal{P}}\cdot\boldsymbol{h}_{\partial\mathcal{S}}\,\mathrm{d}\sigma_\tau.
\end{aligned} \tag{17.24}
$$

Note that the above procedure is also captured by expression (16.9) in Section 16.1.

17.4.3 Lyapunov decay relation

In view of the free- and kinetic-energy rates in (17.22) and (17.24), and by the symmetry of $\mathbf{T}$ and $\mathbf{H}$ due to frame indifference (15.31), the temporal variation in total energy reads

$$\begin{aligned}\overline{\mathcal{F}(\mathcal{P}_\tau,\partial\mathcal{P}_\tau)+\mathcal{K}(\mathcal{P}_\tau,\partial\mathcal{P}_\tau)}^{\boldsymbol{\cdot}} = &\int_{\mathcal{P}_\tau}(\mu_\mathcal{P} s_\mathcal{P}+\gamma\dot{\varphi}_\mathcal{P})\,\mathrm{d}v_\tau - \int_{\mathcal{P}_\tau}\operatorname{grad}\mu_\mathcal{P}\cdot\boldsymbol{M}_\mathcal{P}\operatorname{grad}\mu_\mathcal{P}\,\mathrm{d}v_\tau\\
&-\int_{\mathcal{P}_\tau}(\mathbf{T}+\operatorname{grad}\varphi_\mathcal{P}\otimes\boldsymbol{\xi}):\mathbf{D}_\mathcal{P}\,\mathrm{d}v_\tau+\int_{\mathcal{P}_\tau}\boldsymbol{v}_\mathcal{P}\cdot\boldsymbol{b}^{\mathrm{ni}}\,\mathrm{d}v_\tau\\
&+\int_{\partial\mathcal{P}_\tau}(\mu_{\partial\mathcal{P}}s_{\partial\mathcal{P}}+\zeta\mathring{\varphi}_{\partial\mathcal{P}})\,\mathrm{d}a_\tau-\int_{\partial\mathcal{P}_\tau}\operatorname{grad}_\mathcal{S}\mu_{\partial\mathcal{P}}\cdot\boldsymbol{M}_{\partial\mathcal{P}}\operatorname{grad}_\mathcal{S}\mu_{\partial\mathcal{P}}\,\mathrm{d}a_\tau\\
&-\int_{\partial\mathcal{P}_\tau}\rho\ell_\tau^2\psi\,\operatorname{div}_\mathcal{S}\boldsymbol{v}_{\partial\mathcal{P}}\,\mathrm{d}a_\tau-\int_{\partial\mathcal{P}_\tau}(\mathbf{H}\mathbf{P}_{\!n}+\operatorname{grad}_\mathcal{S}\varphi_{\partial\mathcal{P}}\otimes\boldsymbol{\tau}):\mathbf{D}_{\partial\mathcal{P}}\,\mathrm{d}a_\tau\\
&+\int_{\partial\mathcal{P}_\tau}\boldsymbol{v}_{\partial\mathcal{P}}\cdot\boldsymbol{g}^{\mathrm{ni}}\,\mathrm{d}a_\tau-\int_{\partial\mathcal{P}_\tau}(\mathring{\varphi}_{\partial\mathcal{P}}-\dot{\varphi}_\mathcal{P})\,\xi_\mathcal{S}\,\mathrm{d}a_\tau\\
&-\int_{\partial\mathcal{P}_\tau}(\mu_\mathcal{P}-\mu_{\partial\mathcal{P}})\boldsymbol{\jmath}_\mathcal{P}\cdot\boldsymbol{n}\,\mathrm{d}a_\tau-\int_{\partial\mathcal{P}_\tau}(\boldsymbol{v}_{\partial\mathcal{P}}-\boldsymbol{v}_\mathcal{P})\cdot\boldsymbol{t}_\mathcal{S}\,\mathrm{d}a_\tau\\
&+\int_{\partial^2\mathcal{P}_\tau}(\mathring{\varphi}_{\partial\mathcal{P}}\tau_{\partial\mathcal{S}}-\mu_{\partial\mathcal{P}}\{\!\{\boldsymbol{\jmath}_{\partial\mathcal{P}}\cdot\boldsymbol{\nu}\}\!\}+\boldsymbol{v}_{\partial\mathcal{P}}\cdot\boldsymbol{h}_{\partial\mathcal{S}})\,\mathrm{d}\sigma_\tau,\end{aligned}\tag{17.25}$$

where we recall that the rates of deformation are defined as $\mathbf{D}_\mathcal{P}:=\operatorname{sym}\operatorname{grad}\boldsymbol{v}_\mathcal{P}$ and $\mathbf{D}_{\partial\mathcal{P}}:=\operatorname{sym}\operatorname{grad}_\mathcal{S}\boldsymbol{v}_{\partial\mathcal{P}}$. We now employ the constitutive response functions for the bulk and surface stresses (16.35) and the definition for $p_{\partial\mathcal{P}}^{\mathrm{therm}}$ (16.33), which specializes (17.25) to the following expression

$$\begin{aligned}\overline{\mathcal{F}(\mathcal{P}_\tau,\partial\mathcal{P}_\tau)+\mathcal{K}(\mathcal{P}_\tau,\partial\mathcal{P}_\tau)}^{\boldsymbol{\cdot}} = &\int_{\mathcal{P}_\tau}(\mu_\mathcal{P} s_\mathcal{P}+\gamma\dot{\varphi}_\mathcal{P})\,\mathrm{d}v_\tau - \int_{\mathcal{P}_\tau}\operatorname{grad}\mu_\mathcal{P}\cdot\boldsymbol{M}_\mathcal{P}\operatorname{grad}\mu_\mathcal{P}\,\mathrm{d}v_\tau\\
&-\int_{\mathcal{P}_\tau}2\bar{\mu}_\mathcal{P}|\mathbf{D}_\mathcal{P}^0|^2\,\mathrm{d}v_\tau+\int_{\mathcal{P}_\tau}\boldsymbol{v}_\mathcal{P}\cdot\boldsymbol{b}^{\mathrm{ni}}\,\mathrm{d}v_\tau\\
&+\int_{\partial\mathcal{P}_\tau}(\mu_{\partial\mathcal{P}}s_{\partial\mathcal{P}}+\zeta\mathring{\varphi}_{\partial\mathcal{P}})\,\mathrm{d}a_\tau-\int_{\partial\mathcal{P}_\tau}\operatorname{grad}_\mathcal{S}\mu_{\partial\mathcal{P}}\cdot\boldsymbol{M}_{\partial\mathcal{P}}\operatorname{grad}_\mathcal{S}\mu_{\partial\mathcal{P}}\,\mathrm{d}a_\tau\\
&-\int_{\partial\mathcal{P}_\tau}\big(2\bar{\mu}_{\partial\mathcal{P}}|\mathbf{P}_{\!n}\mathbf{D}_{\partial\mathcal{P}}^0|^2+\bar{\kappa}_{\partial\mathcal{P}}(\operatorname{div}_\mathcal{S}\boldsymbol{v}_{\partial\mathcal{P}})^2\big)\,\mathrm{d}a_\tau+\int_{\partial\mathcal{P}_\tau}\boldsymbol{v}_{\partial\mathcal{P}}\cdot\boldsymbol{g}^{\mathrm{ni}}\,\mathrm{d}a_\tau\\
&-\int_{\partial\mathcal{P}_\tau}\big((\mathring{\varphi}_{\partial\mathcal{P}}-\dot{\varphi}_\mathcal{P})\,\xi_\mathcal{S}+(\mu_\mathcal{P}-\mu_{\partial\mathcal{P}})\boldsymbol{\jmath}_\mathcal{P}\cdot\boldsymbol{n}+(\boldsymbol{v}_{\partial\mathcal{P}}-\boldsymbol{v}_\mathcal{P})\cdot\boldsymbol{t}_\mathcal{S}\big)\,\mathrm{d}a_\tau\\
&+\int_{\partial^2\mathcal{P}_\tau}(\mathring{\varphi}_{\partial\mathcal{P}}\tau_{\partial\mathcal{S}}-\mu_{\partial\mathcal{P}}\{\!\{\boldsymbol{\jmath}_{\partial\mathcal{P}}\cdot\boldsymbol{\nu}\}\!\}+\boldsymbol{v}_{\partial\mathcal{P}}\cdot\boldsymbol{h}_{\partial\mathcal{S}})\,\mathrm{d}\sigma_\tau,\end{aligned}\tag{17.26}$$

where we have used the viscous dissipation identities in (16.31), the isochoric constraint $\operatorname{tr}\mathbf{D}_\mathcal{P}=\operatorname{div}\boldsymbol{v}_\mathcal{P}=0$ in (14.14), as well as the identity $\operatorname{tr}(\mathbf{P}_{\!n}\mathbf{D}_{\partial\mathcal{P}})=\operatorname{div}_\mathcal{S}\boldsymbol{v}_{\partial\mathcal{P}}$.

In the following, we split the boundary into different parts. In particular, we consider $\partial\mathcal{P}_\tau:=\partial\mathcal{P}_\tau^{\mathrm{ess}}\cup\partial\mathcal{P}_\tau^{\mathrm{nat}}\cup\partial\mathcal{P}_\tau^{\mathrm{mix}}$, and let $\partial\mathcal{P}_\tau^{\mathrm{ess}}\cap\partial\mathcal{P}_\tau^{\mathrm{nat}}=\partial\mathcal{P}_\tau^{\mathrm{nat}}\cap\partial\mathcal{P}_\tau^{\mathrm{mix}}=\partial\mathcal{P}_\tau^{\mathrm{ess}}\cap\partial\mathcal{P}_\tau^{\mathrm{mix}}=\emptyset$. Also, let the edge be partitioned as follows $\partial^2\mathcal{P}_\tau:=\partial^2\mathcal{P}_\tau^{\mathrm{ess}}\cup\partial^2\mathcal{P}_\tau^{\mathrm{nat}}$, with $\partial^2\mathcal{P}_\tau^{\mathrm{ess}}\cap\partial^2\mathcal{P}_\tau^{\mathrm{nat}}=\emptyset$. We account for the static contributions from the environment acting on $\partial^2\mathcal{P}_\tau$ and introduce the essential and natural boundary condition formulated in Section 17.3 into the total energy variation (17.26). Furthermore, in view of the essential (17.13), natural (17.15) and mixed (17.16) dynamic boundary conditions, as well as the essential (17.17) and natural (17.18) static boundary conditions on the edge, we obtain

$$\begin{aligned}
\overline{\mathcal{F}(\mathcal{P}_\tau,\partial\mathcal{P}_\tau)+\mathcal{K}(\mathcal{P}_\tau,\partial\mathcal{P}_\tau)}^{\cdot} &= \int_{\mathcal{P}_\tau}(\mu_{\mathcal{P}}s_{\mathcal{P}}+\gamma\dot{\varphi}_{\mathcal{P}})\,\mathrm{d}v_\tau - \int_{\mathcal{P}_\tau}\mathrm{grad}\,\mu_{\mathcal{P}}\cdot\boldsymbol{M}_{\mathcal{P}}\mathrm{grad}\,\mu_{\mathcal{P}}\,\mathrm{d}v_\tau \\
&\quad - \int_{\mathcal{P}_\tau}2\bar{\mu}_{\mathcal{P}}|\mathbf{D}^0_{\mathcal{P}}|^2\,\mathrm{d}v_\tau + \int_{\mathcal{P}_\tau}\boldsymbol{v}_{\mathcal{P}}\cdot\boldsymbol{b}^{\mathrm{ni}}\,\mathrm{d}v_\tau \\
&\quad + \int_{\partial\mathcal{P}_\tau}(\mu_{\partial\mathcal{P}}s_{\partial\mathcal{P}}+\zeta\mathring{\varphi}_{\partial\mathcal{P}})\,\mathrm{d}a_\tau - \int_{\partial\mathcal{P}_\tau}\mathrm{grad}_{\mathcal{S}}\mu_{\partial\mathcal{P}}\cdot\boldsymbol{M}_{\partial\mathcal{P}}\mathrm{grad}_{\mathcal{S}}\mu_{\partial\mathcal{P}}\,\mathrm{d}a_\tau \\
&\quad - \int_{\partial\mathcal{P}_\tau}\big(2\bar{\mu}_{\partial\mathcal{P}}|\mathbf{P}_{\boldsymbol{n}}\mathbf{D}^0_{\partial\mathcal{P}}|^2+\bar{\kappa}_{\partial\mathcal{P}}(\mathrm{div}_{\mathcal{S}}\boldsymbol{v}_{\partial\mathcal{P}})^2\big)\,\mathrm{d}a_\tau + \int_{\partial\mathcal{P}_\tau}\boldsymbol{v}_{\partial\mathcal{P}}\cdot\boldsymbol{g}^{\mathrm{ni}}\,\mathrm{d}a_\tau \\
&\quad - \int_{\partial\mathcal{P}^{\mathrm{mix}}_\tau}\Big(\tfrac{1}{L_\varphi}(\mathring{\varphi}_{\partial\mathcal{P}}-\dot{\varphi}_{\mathcal{P}})^2+\tfrac{1}{L_\mu}(\mu_{\mathcal{P}}-\mu_{\partial\mathcal{P}})^2+\tfrac{1}{L_v}|\boldsymbol{v}_{\partial\mathcal{P}}-\boldsymbol{v}_{\mathcal{P}}|^2\Big)\,\mathrm{d}a_\tau \\
&\quad + \int_{\partial^2\mathcal{P}^{\mathrm{ess}}_\tau}\Big(\dot{\varphi}^{\mathrm{env}}_{\partial^2\mathcal{P}}\tau_{\partial\mathcal{S}}-\mu^{\mathrm{env}}_{\partial^2\mathcal{P}}\{\!\{\boldsymbol{\jmath}_{\partial\mathcal{P}}\cdot\boldsymbol{\nu}\}\!\}+\boldsymbol{v}^{\mathrm{env}}_{\partial^2\mathcal{P}}\cdot\boldsymbol{h}_{\partial\mathcal{S}}\Big)\,\mathrm{d}\sigma_\tau \\
&\quad + \int_{\partial^2\mathcal{P}^{\mathrm{nat}}_\tau}\Big(\mathring{\varphi}_{\partial\mathcal{P}}\tau^{\mathrm{env}}_{\partial\mathcal{S}}+\mu_{\partial\mathcal{P}}\jmath^{\mathrm{env}}_{\partial^2\mathcal{P}}+\boldsymbol{v}_{\partial\mathcal{P}}\cdot\boldsymbol{h}^{\mathrm{env}}_{\partial\mathcal{S}}\Big)\,\mathrm{d}\sigma_\tau. \qquad (17.27)
\end{aligned}$$

Thus, the *Lyapunov decay relation* is given by

$$\begin{aligned}
\overline{\mathcal{F}(\mathcal{P}_\tau,\partial\mathcal{P}_\tau)+\mathcal{K}(\mathcal{P}_\tau,\partial\mathcal{P}_\tau)}^{\cdot} &\le \int_{\mathcal{P}_\tau}(\mu_{\mathcal{P}}s_{\mathcal{P}}+\gamma\dot{\varphi}_{\mathcal{P}})\,\mathrm{d}v_\tau + \int_{\mathcal{P}_\tau}\boldsymbol{v}_{\mathcal{P}}\cdot\boldsymbol{b}^{\mathrm{ni}}\,\mathrm{d}v_\tau \\
&\quad + \int_{\partial\mathcal{P}_\tau}(\mu_{\partial\mathcal{P}}s_{\partial\mathcal{P}}+\zeta\mathring{\varphi}_{\partial\mathcal{P}})\,\mathrm{d}a_\tau + \int_{\partial\mathcal{P}_\tau}\boldsymbol{v}_{\partial\mathcal{P}}\cdot\boldsymbol{g}^{\mathrm{ni}}\,\mathrm{d}a_\tau \\
&\quad + \int_{\partial^2\mathcal{P}^{\mathrm{ess}}_\tau}\Big(\dot{\varphi}^{\mathrm{env}}_{\partial^2\mathcal{P}}\{\!\{\boldsymbol{\tau}\cdot\boldsymbol{\nu}\}\!\}-\mu^{\mathrm{env}}_{\partial^2\mathcal{P}}\{\!\{\boldsymbol{\jmath}_{\partial\mathcal{P}}\cdot\boldsymbol{\nu}\}\!\}+\boldsymbol{v}^{\mathrm{env}}_{\partial^2\mathcal{P}}\cdot\{\!\{\mathbf{H}\boldsymbol{\nu}\}\!\}\Big)\,\mathrm{d}\sigma_\tau \\
&\quad + \int_{\partial^2\mathcal{P}^{\mathrm{nat}}_\tau}\Big(\mathring{\varphi}_{\partial\mathcal{P}}\tau^{\mathrm{env}}_{\partial\mathcal{S}}+\mu_{\partial\mathcal{P}}\jmath^{\mathrm{env}}_{\partial^2\mathcal{P}}+\boldsymbol{v}_{\partial\mathcal{P}}\cdot\boldsymbol{h}^{\mathrm{env}}_{\partial\mathcal{S}}\Big)\,\mathrm{d}\sigma_\tau, \qquad (17.28)
\end{aligned}$$

where we have used the residual dissipation inequalities in (16.27). For a passive environment, we arrive at

$$\overline{\mathcal{F}(\mathcal{P}_\tau,\partial\mathcal{P}_\tau)+\mathcal{K}(\mathcal{P}_\tau,\partial\mathcal{P}_\tau)}^{\cdot} \le 0. \qquad (17.29)$$

Thus, in (17.28), we identify the following environmental contributions

- $\mu_{\mathcal{P}}s_{\mathcal{P}}$ represents the rate at which energy is transferred to $\mathcal{P}_\tau$ due to the production of species, and $\mu_{\partial\mathcal{P}}s_{\partial\mathcal{P}}$ represents the rate at which energy is transferred to $\partial\mathcal{P}_\tau$ due to species production;

- $\gamma\dot{\varphi}_{\mathcal{P}}$ represents the power expended on the microstructure of $\mathcal{P}_\tau$ by sources external to the body $\mathcal{P}_\tau$, whereas $\zeta\mathring{\varphi}_{\partial\mathcal{P}}$ denotes the power expended on the microstructure of $\partial\mathcal{P}_\tau$ by sources external to the boundary of the body $\partial\mathcal{P}_\tau$, which do not originate from $\mathcal{P}_\tau$;

- $\boldsymbol{v}_{\mathcal{P}}\cdot\boldsymbol{b}^{\mathrm{ni}}$ represents power expended in $\mathcal{P}_\tau$ by the environment, whereas $\boldsymbol{v}_{\partial\mathcal{P}}\cdot\boldsymbol{g}^{\mathrm{ni}}$ represents the power expended on $\partial\mathcal{P}_\tau$ by the environment;

- $\dot{\varphi}^{\mathrm{env}}_{\partial^2\mathcal{P}}\tau_{\partial\mathcal{S}}$ denotes the power expended by the static environment acting on the microstructure of $\partial^2\mathcal{P}^{\mathrm{ess}}_\tau$, and $\mathring{\varphi}_{\partial\mathcal{P}}\tau^{\mathrm{env}}_{\partial\mathcal{S}}$ represents the power expended across $\partial^2\mathcal{P}^{\mathrm{nat}}_\tau$ by edge microtractions from the environment exterior to both $\partial\mathcal{P}_\tau$ and $\mathcal{P}_\tau$;

- $-\mu^{\text{env}}_{\partial^2\mathcal{P}}\{\!\{\boldsymbol{\jmath}_{\partial\mathcal{P}} \cdot \boldsymbol{\nu}\}\!\}$ represents the energy exchange induced by species transport across $\partial^2\mathcal{P}^{\text{ess}}_\tau$ via an assigned environmental chemical potential, and $\mu_{\partial\mathcal{P}} \jmath^{\text{env}}_{\partial^2\mathcal{P}}$ represents the energy exchange across $\partial^2\mathcal{P}^{\text{nat}}_\tau$ induced by a tangent-normal species mass flux from the exterior of $\partial\mathcal{P}_\tau$ and $\mathcal{P}_\tau$;

- $\boldsymbol{v}^{\text{env}}_{\partial^2\mathcal{P}} \cdot \boldsymbol{h}_{\partial\mathcal{S}}$ represents the power expended by an external velocity field acting on $\partial^2\mathcal{P}^{\text{ess}}_\tau$, whereas $\boldsymbol{v}_{\partial\mathcal{P}} \cdot \boldsymbol{h}^{\text{env}}_{\partial\mathcal{S}}$ represents the power expended across $\partial^2\mathcal{P}^{\text{nat}}_\tau$ by edge tractions from the environment.

Lastly, the following terms may contribute to the total dissipation $\mathcal{D}(\mathcal{P}_\tau, \partial\mathcal{P}_\tau)$ in the bulk-surface system

- $\operatorname{grad}\mu_{\mathcal{P}} \cdot \boldsymbol{M}_{\mathcal{P}} \operatorname{grad}\mu_{\mathcal{P}}$ and $\operatorname{grad}_{\mathcal{S}}\mu_{\partial\mathcal{P}} \cdot \boldsymbol{M}_{\partial\mathcal{P}} \operatorname{grad}_{\mathcal{S}}\mu_{\partial\mathcal{P}}$ represent dissipation due to species diffusion in $\mathcal{P}_\tau$ and $\partial\mathcal{P}_\tau$, respectively;

- the term $2\bar{\mu}_{\partial\mathcal{P}}|\mathbf{P}_{\!n}\mathbf{D}^0_{\partial\mathcal{P}}|^2$ represents the viscous dissipation in $\mathcal{P}_\tau$, while $2\bar{\mu}_{\partial\mathcal{P}}|\mathbf{P}_{\!n}\mathbf{D}^0_{\partial\mathcal{P}}|^2 + \bar{\kappa}_{\partial\mathcal{P}}(\operatorname{div}_{\mathcal{S}}\boldsymbol{v}_{\partial\mathcal{P}})^2$ denotes the viscous dissipation in $\partial\mathcal{P}_\tau$;

- $\frac{1}{L_\varphi}|\mathring{\varphi}_{\partial\mathcal{P}} - \dot{\varphi}_{\mathcal{P}}|^2$ represents power expended across $\partial\mathcal{P}^{\text{mix}}_\tau$ driven by the difference in microstructure (as described by the phase field) between $\partial\mathcal{P}_\tau$ and the adjacent $\mathcal{P}_\tau$;

- $-\frac{1}{L_\mu}|\mu_{\partial\mathcal{P}} - \mu_{\mathcal{P}}|^2$ represents energy exchange across $\partial\mathcal{P}^{\text{mix}}_\tau$ due to the difference in chemical potential between $\partial\mathcal{P}_\tau$ and the adjacent $\mathcal{P}_\tau$;

- $\frac{1}{L_v}|\boldsymbol{v}_{\partial\mathcal{P}} - \boldsymbol{v}_{\mathcal{P}}|^2 = \frac{1}{L_v}|\mathbf{P}_{\!n}(\boldsymbol{v}_{\partial\mathcal{P}} - \boldsymbol{v}_{\mathcal{P}})|^2$ represents power expended across $\partial\mathcal{P}^{\text{mix}}_\tau$ driven by the difference in the tangential velocity components between $\partial\mathcal{P}_\tau$ and the adjacent $\mathcal{P}_\tau$.

Chapter 18

Concluding Remarks and Future Directions

In this Part, we developed a continuum theory for bulk-surface materials undergoing deformation and phase separation. In particular, we focussed on an immiscible binary bulk fluid enclosed by a thin film of another immiscible binary fluid. We treated this thin film as a material surface with a small, yet finite, surface thickness.

In this theory, the bulk-surface material was only allowed to undergo isochoric motions, and is thereby behaving as an incompressible body. This assumption implied no volume change for the bulk material, as well as no volume change for the surface material from a microscopic viewpoint. The isochoric constraints and pointwise mass balances that were derived reflect these implications. To account for diffusive species transport in the bulk-surface material, we supplemented the theory with pointwise balances of species mass, and recovered a contribution from the bulk in the pointwise balance of surface species mass.

The mathematical framework of this theory is based on the principle of virtual powers. To account for the deformation and phase separation, we extended the principle of virtual power presented for phase-fields with bulk-surface dynamics by Espath [53, 54]. We arrived at the field equations for the kinematical processes in the bulk and surface captured by scalar and vector quantities, as well as expressions for the surface and edge (micro)tractions. We established symmetry of both the bulk and surface stress using the frame-indifference requirement for the internal virtual power. Furthermore, the partwise balances of (micro)forces showed that the surface (micro)traction and the normal component of the bulk (micro)stress cancel across the dynamic surface, respectively. Thus, the environmental contributions, such as the external body bulk (micro)force and external surface body (micro)force, form a partwise balance with the external edge contributions, namely the edge (micro)traction. Similar results were obtained for the partwise balance of torques, where only the external fields appeared in the partwise balance due to the symmetry of the bulk and surface stress. Aside from the external contributions, a contribution from the microstresses does appear in the partwise balance of microtorques.

To ensure thermodynamical consistency, we presented a suitable set of constitutive response functions guided by the pointwise free-energy imbalances. We treated the free-energy density function of the surface material in a microscopic way, and postulated that it is linearly dependent on the surface thickness. By considering a linear dependence of stress on the rate of strain in the surface material, we recovered a Boussinesq-Scriven surface stress, which includes two surface viscosity coefficients and a thermodynamical pressure representing surface tension, in addition to a capillary stress contribution. The final set of equations governing the bulk-surface system show resemblance to a Navier-Stokes-Cahn-Hilliard equation for the bulk and surface.

Lastly, we supplemented the system with appropriate boundary conditions. Using a free-energy imbalance for the dynamic surface, we presented essential, natural and mixed conditions for the coupling between the bulk and the surface. By deriving the Lyapunov decay relation, we characterized the dissipative nature of the system and the environmental contributions acting on it.

Limitations of the current work include considerations about more restrictive choices for the constitutive response functions. As these can be highly dependent on the application, they are in this work left to future users of this continuum theory to decide upon. We wish to emphasize that extra caution might be necessary when making particular modelling choices for the dilatational viscosity $\bar{\kappa}_{\partial\mathcal{P}}$. This function is allowed to depend on the thickness of the thin layer of surface fluid, but not all relations may be consistent with the framework presented here.

Furthermore, in this Part we have demonstrated that the virtual power formalism is a useful tool to establish bulk-surface continuum theories. In future research, the presented framework could be extended to more complex bulk-surface materials, for instance to those exhibiting viscoelastic behaviour. Such a continuum theory has applications in areas studying vesicle dynamics and compartmentalized transport processes in cell biology. As a point of departure for such a framework, the results presented here and the continuum theory for pure elastic bulk-surface materials established by Gurtin & Murdoch [82] should be considered. Another non-trivial, yet useful, extension would be to include reaction dynamics at the surface and bulk. In addition, Larché-Cahn based gradient energies could be considered in such multicomponent bulk-surface systems. For bulk materials, a theoretical framework for such a reactive multicomponent system with phase transformations is presented by Clavijo *et al.* [33]. In the thermochemical theory of such a bulk-surface system, special care has to be taken with where the resulting products of a chemical reaction at the dynamic surface end up living, that is, in the bulk or in the surface material. Again, applications of such theory can be found in more complex systems, which involve *active* surfaces with their own dynamics.

Finally, it is non-trivial to solve the equations that follow from this continuum theory numerically. Numerical implementation requires parametrization of the sharp dynamic surface boundary, whose tangential velocity may not match the bulk material's tangential velocity at the dynamic boundary. Thus, numerical studies would require the use of advanced numerical techniques developed for moving boundary problems.

Chapter 19

Final Reflections

In this work we have navigated through the world of diffuse and sharp representations of interfaces to formulate fundamental theories for bulk-surface interactions.

What framework can be used to base such a bulk-surface theory upon? In Part I, we demonstrated that different perspectives can be employed to base these fundamental theories upon. Although each of the four perspectives has its own characteristics, they all capture interfacial evolution using a functional representing the state of the system and a dissipation mechanism.

Modelling interfacial movement using a geometric approach, as presented in Chapter 2, is a natural way of dealing with (closed) sharp interfaces. Shape calculus allows for the definition of geometric gradient-descent flows. However, this approach is limited in its application, as certain physics is difficult to describe within this framework, e.g. dynamics involving topological changes, such as merging or pinching of interfaces and mixture theory related effects.

Phase-field variables acting as indicators of diffuse transitions layers in the material of interest form a natural alternative to this sharp-interface description, as they are able to capture the additional physics, whilst allowing for efficient computation. Phase-field models can be derived as gradient flows (Chapter 3), as they embody processes that follow the path of steepest descent in an energy landscape. In this phase-field gradient flow perspective, mathematical insights in the wellposedness, numerical error analysis and time-discretization schemes are made accessible, yet physical interpretation and motivation for the phase-field equations remains difficult.

The variational framework presented in Chapter 4 provided such physical interpretation, as it is based on a rational approach to thermodynamics. Balance laws, in particular a mass balance law involving the phase-field variable, are key to establishing the phase-field equations.

Then, the final perspective in Chapter 5 introduced an additional balance law, that is the balance of microforces, motivated by a microkinetic interpretation of the phase field. Again, using rational arguments phase-field equations can be derived that are consistent with the second law of thermodynamics.

In Part II, we saw that bulk-surface coupling can be established in phase-field models by introduction of a regularizing function in the underlying energy functional of the system, which restricts the interaction to the diffuse interface. Using the variational framework in Chapter 4, we proposed a phase-field theory for adhesion, extendable to applications in which local surface dynamics regulate the adhesive interactions. In addition, we developed an asymptotic framework to characterize steady states of the phase-field problem, thereby connecting the diffuse-interface theory to the geometrical perspective presented in Chapter 2.

In Part III, we proposed a continuum theory for bulk-surface materials undergoing deformation and phase separation. Here, the material surface is described by a sharp interface, yet we allow for local variations in its thickness. The mathematical framework of this theory is based on a bulk-surface principle of virtual power. Based on a free-energy imbalance for the surface, we presented dynamic conditions for the coupling between the bulk and the surface.

Finally, the methods and frameworks presented in this thesis can, with or without further extension, be used for a variety of bulk-surface applications. To use these frameworks for specific applications, more detailed modeling choices are required, which should be tailored to the material of interest and may require expertise knowledge about the application of interest. In these cases, it is essential to validate the model's predictions through comparison with real-world (experimental) data. This way, using appropriate numerical techniques, the mathematical frameworks presented in this work can provide valuable insights in biological and engineering applications that involve active interfaces.

Bibliography

[1] A. Abdollahi and I. Arias, *Phase-field modeling of the coupled microstructure and fracture evolution in ferroelectric single crystals*, Acta Materialia, 59 (2011), pp. 4733–4746.

[2] ——, *Phase-Field Modeling of Fracture in Ferroelectric Materials*, Archives of Computational Methods in Engineering, 22 (2015), pp. 153–181.

[3] N. Adam, *Physics and chemistry of surfaces*, (1941).

[4] A. W. Adamson and A. P. Gast, *Physical chemistry of surfaces*, John Wiley & Sons, Inc., 6th ed., 1997.

[5] S. Aland, S. Egerer, J. Lowengrub, and A. Voigt, *Diffuse interface models of locally inextensible vesicles in a viscous fluid*, Journal of Computational Physics, 277 (2014), pp. 32–47.

[6] B. Alberts, A. Johnson, J. Wilson, J. Lewis, T. Hunt, K. Roberts, M. Raff, and P. Walter, *Molecular Biology of the Cell*, Garland Science, 2008.

[7] S. M. Allen and J. W. Cahn, *A microscopic theory for antiphase boundary motion and its application to antiphase domain coarsening*, Acta Metallurgica, 27 (1979), pp. 1085–1095.

[8] A. Alphonse, C. M. Elliott, and J. Terra, *A coupled ligand-receptor bulk-surface system on a moving domain: Well posedness, regularity, and convergence to equilibrium*, SIAM Journal on Mathematical Analysis, 50 (2018), pp. 1544–1592.

[9] S. S. Antman and J. E. Osborn, *The principle of virtual work and integral laws of motion*, Archive for Rational Mechanics and Analysis, 69 (1979), pp. 231–262.

[10] S. Badia, F. Guillén-González, and J. V. Gutiérrez-Santacreu, *Finite element approximation of nematic liquid crystal flows using a saddle-point structure*, Journal of Computational Physics, 230 (2011), pp. 1686–1706.

[11] Y. Bazilevs, K. Takizawa, and T. E. Tezduyar, *Computational Fluid-Structure Interaction*, John Wiley & Sons, Ltd, Chichester, UK, jan 2013.

[12] A. L. Bertozzi, S. Esedoglu, and A. Gillette, *Inpainting of Binary Images Using the Cahn–Hilliard Equation*, IEEE Transactions on Image Processing, 16 (2007), pp. 285–291.

[13] T. Biben, K. Kassner, and C. Misbah, *Phase-field approach to three-dimensional vesicle dynamics*, Physical Review E - Statistical, Nonlinear, and Soft Matter Physics, 72 (2005), pp. 1–15.

[14] K. BINDER AND H. L. FRISCH, *Dynamics of surface enrichment: A theory based on the kawasaki spin-exchange model in the presence of a wall*, Zeitschrift für Physik B Condensed Matter, 84 (1991), pp. 403–418.

[15] M. J. BORDEN, C. V. VERHOOSEL, M. A. SCOTT, T. J. HUGHES, AND C. M. LANDIS, *A phase-field description of dynamic brittle fracture*, Computer Methods in Applied Mechanics and Engineering, 217-220 (2012), pp. 77–95.

[16] A. BOSCHMAN, L. ESPATH, AND K. VAN DER ZEE, *A bulk-surface continuum theory for fluid flows and phase segregation with finite surface thickness*, Physica D, (2024).

[17] B. BOURDIN, G. A. FRANCFORT, AND J.-J. MARIGO, *The Variational Approach to Fracture*, Springer Netherlands, Dordrecht, 2008.

[18] M. BOUSSINESQ, *Sur l'existence d'une viscosité superficielle, dans la mince couche de transition séparant un liquide d'un autre fluide contigu*, Ann. Chim. Phys., 29 (1913), pp. 349–357.

[19] C. BRANGWYNNE, P. TOMPA, AND R. PAPPU, *Polymer physics of intracellular phase transitions*, Nature Physics, 11 (2015), pp. 899–904.

[20] L. BRONSARD AND B. STOTH, *Volume-preserving mean curvature flow as a limit of a nonlocal ginzburg-landau equation*, SIAM Journal on Mathematical Analysis, 28 (1997), pp. 769–807.

[21] G. CAGINALP, *An analysis of a phase field model of a free boundary*, Archive for Rational Mechanics and Analysis, 92 (1986), pp. 205–245.

[22] G. CAGINALP, *Stefan and Hele-Shaw type models as asymptotic limits of the phase-field equations*, Physical Review A, 39 (1989), pp. 5887–5896.

[23] G. CAGINALP AND X. CHEN, *Phase field equations in the singular limit of sharp interface problems*, in On the Evolution of Phase Boundaries, Springer New York, 1992, pp. 1–27.

[24] G. CAGINALP AND X. CHEN, *Convergence of the phase field model to its sharp interface limits*, European Journal of Applied Mathematics, 9 (1998), pp. 417–445.

[25] G. CAGINALP AND P. C. FIFE, *Dynamics of Layered Interfaces Arising from Phase Boundaries*, SIAM Journal on Applied Mathematics, 48 (1988), pp. 506–518.

[26] J. W. CAHN, *Free Energy of a Nonuniform System. II. Thermodynamic Basis*, The Journal of Chemical Physics, 30 (1959), pp. 1121–1124.

[27] J. W. CAHN AND J. E. HILLIARD, *Free Energy of a Nonuniform System. I. Interfacial Free Energy*, The Journal of Chemical Physics, 28 (1958), pp. 258–267.

[28] ——, *Free Energy of a Nonuniform System. III. Nucleation in a Two-Component Incompressible Fluid*, The Journal of Chemical Physics, 31 (1959), pp. 688–699.

[29] C. CANCÈS, T. O. GALLOUËT, AND L. MONSAINGEON, *The gradient flow structure for incompressible immiscible two-phase flows in porous media*, Comptes Rendus Mathematique, 353 (2015), pp. 985–989.

[30] D. CAPECCHI, *History of Virtual Work Laws*, Springer Milan, 2012.

[31] P. Cermelli, E. Fried, and M. Gurtin, *Transport relations for surface integrals arising in the formulation of balance laws for evolving fluid interfaces*, Journal of Fluid Mechanics, 544 (2005), pp. 339–351.

[32] X. Chen, *Global asymptotic limit of solutions of the cahn-hilliard equation*, Journal of Differential Geometry, 44 (1996).

[33] S. P. Clavijo, L. Espath, and V. M. Calo, *Extended larché–cahn framework for reactive cahn–hilliard multicomponent systems*, Continuum Mechanics and Thermodynamics, 33 (2021), pp. 2391–2410.

[34] T. H. Colding, W. P. Minicozzi, and E. K. Pedersen, *Mean curvature flow*, Bulletin of the American Mathematical Society, 52 (2015), pp. 297–333.

[35] B. D. Coleman and W. Noll, *The thermodynamics of elastic materials with heat conduction and viscosity*, Archive for Rational Mechanics and Analysis, 13 (1963), pp. 167–178.

[36] P. Colli, T. Fukao, and K. F. Lam, *On a coupled bulk–surface allen–cahn system with an affine linear transmission condition and its approximation by a robin boundary condition*, Nonlinear Analysis, 184 (2019), pp. 116–147.

[37] C. Cowan, *The Cahn-Hilliard Equation as a Gradient Flow*, PhD thesis, Simon Frase Univeristy, Burnaby, Canada, 2005.

[38] M. C. Delfour and J.-P. Zolésio, *Structure of shape derivatives for nonsmooth domains*, Journal of Functional Analysis, 104 (1992), pp. 1–33.

[39] ——, *Shapes and Geometries: Analysis, Differential Calculus and Optimization*, vol. 4 of SIAM Series on Advances in Design and Control, Society for Industrial and Applied Mathematics, first ed., 2001.

[40] M. C. Delfour and J. P. Zolésio, *Shapes and Geometries: Analysis, Differential Calculus and Optimization*, SIAM Advances in Design and Control, Society for Industrial and Applied Mathematics, second ed., 2011.

[41] J. Donea, A. Huerta, J.-P. Ponthot, and A. Rodrï¿½ï¿½guez-Ferran, *Arbitrary Lagrangian-Eulerian Methods*, in Encyclopedia of Computational Mechanics, John Wiley & Sons, Ltd, Chichester, UK, nov 2004.

[42] A. Dreher, I. S. Aranson, and K. Kruse, *Spiral actin-polymerization waves can generate amoeboidal cell crawling*, New Journal of Physics, 16 (2014).

[43] Q. Du, *Phase field calculus, curvature-dependent energies, and vesicle membranes*, Philosophical Magazine, 91 (2011), p. 165–181.

[44] Q. Du, C. Liu, R. Ryham, and X. Wang, *A phase field formulation of the willmore problem*, Nonlinearity, 18 (2005), pp. 1249–1267.

[45] F. Duda, F. Forte Neto, and E. Fried, *Modelling of surface reactions and diffusion mediated by bulk diffusion*, Philosophical Transactions of the Royal Society A, 381 (2023), p. 20220367.

[46] F. P. Duda, A. F. Sarmiento, and E. Fried, *Coupled diffusion and phase transition: Phase fields, constraints, and the cahn–hilliard equation*, Meccanica, 56 (2021), pp. 1707–1725.

[47] G. DZIUK AND C. ELLIOTT, *Eulerian finite element method for parabolic PDEs on implicit surfaces*, Interfaces and Free Boundaries, (2008), pp. 119–138.

[48] D. EDWARDS, H. BRENNER, AND D. WASAN, *Interfacial Transport Processes and Rheology*, Butterworth-Heinemann, Boston, 1991.

[49] K. R. ELDER, M. GRANT, N. PROVATAS, AND J. M. KOSTERLITZ, *Sharp interface limits of phase-field models*, Physical Review E, 64 (2001), p. 021604.

[50] C. M. ELLIOTT AND B. STINNER, *Analysis of a diffuse interface approach to an advection diffusion equation on a moving surface*, Mathematical Models and Methods in Applied Sciences, 19 (2009), pp. 787–802.

[51] H. EMMERICH, *The Diffuse Interface Approach in Materials Science: Thermodynamic Concepts and Applications of Phase-Field Models*, vol. 73 of Lecture Notes in Physics, Springer Berlin Heidelberg, Berlin, Heidelberg, 2003.

[52] L. ESPATH, *On the control volume arbitrariness in the navier–stokes equation*, Physics of Fluids, 33 (2021).

[53] L. ESPATH, *A continuum framework for phase field with bulk-surface dynamics*, Partial Differential Equations and Applications, 4 (2022).

[54] ——, *Mechanics and Geometry of Enriched Continua*, Springer International Publishing, 2023.

[55] L. ESPATH AND V. CALO, *Phase-field gradient theory*, Zeitschrift für angewandte Mathematik und Physik, 72 (2021).

[56] L. C. EVANS, H. M. SONER, AND P. E. SOUGANIDIS, *Phase transitions and generalized motion by mean curvature*, Communications on Pure and Applied Mathematics, 45 (1992), pp. 1097–1123.

[57] K. FELLNER, E. LATOS, AND B. Q. TANG, *Well-posedness and exponential equilibration of a volume-surface reaction–diffusion system with nonlinear boundary coupling*, Annales de l'Institut Henri Poincaré C, Analyse non linéaire, 35 (2018), pp. 643–673.

[58] K. FELLNER, S. ROSENBERGER, AND B. Q. TANG, *Quasi-steady-state approximation and numerical simulation for a volume-surface reaction-diffusion system*, Communications in Mathematical Sciences, 14 (2016), pp. 1553–1580.

[59] F. H. FENTON, E. M. CHERRY, A. KARMA, AND W.-J. RAPPEL, *Modeling wave propagation in realistic heart geometries using the phase-field method*, Chaos: An Interdisciplinary Journal of Nonlinear Science, 15 (2005), p. 013502.

[60] P. C. FIFE, *Models for phase separation and their mathematics*, Electronic Journal of Differential Equations, 2000 (2000), pp. 1–26.

[61] R. FOSDICK, *A generalized continuum theory with internal corner and surface contact interactions*, Continuum Mechanics and Thermodynamics, 28 (2015), pp. 275–292.

[62] R. L. FOSDICK AND E. G. VIRGA, *A variational proof of the stress theorem of cauchy*, Archive for Rational Mechanics and Analysis, 105 (1989), pp. 95–103.

[63] E. FRIED AND M. GURTIN, *Dynamic solid-solid transitions with phase characterized by an order parameter*, Physica D: Nonlinear Phenomena, 72 (1994), pp. 287–308.

[64] E. FRIED AND M. E. GURTIN, *Continuum theory of thermally induced phase transitions based on an order parameter*, Physica D: Nonlinear Phenomena, 68 (1993), pp. 326–343.

[65] ——, *Tractions, balances, and boundary conditions for nonsimple materials with application to liquid flow at small-length scales*, Archive for Rational Mechanics and Analysis, 182 (2006), pp. 513–554.

[66] ——, *Thermomechanics of the interface between a body and its environment*, Continuum Mechanics and Thermodynamics, 19 (2007), pp. 253–271.

[67] M. FRITTELLI, A. MADZVAMUSE, AND I. SGURA, *Bulk-surface virtual element method for systems of PDEs in two-space dimensions*, Numerische Mathematik, 147 (2021), pp. 305–348.

[68] X. FU, L. CUETO-FELGUEROSO, AND R. JUANES, *Viscous fingering with partially miscible fluids*, Physical Review Fluids, 2 (2017).

[69] P. GARCÍA-PEÑARRUBIA, J. J. GÁLVEZ, AND J. GÁLVEZ, *Mathematical modelling and computational study of two-dimensional and three-dimensional dynamics of receptor–ligand interactions in signalling response mechanisms*, Journal of Mathematical Biology, 69 (2013), pp. 553–582.

[70] P. GERMAIN, *La méthode des puissances virtuelles en mécanique des milieux continus, premiere partie: théorie du second gradient*, Journal de mécanique, 12 (1973), pp. 235–274.

[71] ——, *The method of virtual power in continuum mechanics. part 2: Microstructure*, SIAM Journal on Applied Mathematics, 25 (1973), pp. 556–575.

[72] ——, *The method of virtual power in the mechanics of continuous media, i: Second-gradient theory*, Mathematics and Mechanics of Complex Systems, 8 (2020), pp. 153–190. Translated by M. Epstein and R. E. Smelser.

[73] A. GIORGINI AND P. KNOPF, *Two-phase flows with bulk–surface interaction: Thermodynamically consistent navier–stokes–cahn–hilliard models with dynamic boundary conditions*, Journal of Mathematical Fluid Mechanics, 25 (2023).

[74] A. GLITZKY AND A. MIELKE, *A gradient structure for systems coupling reaction–diffusion effects in bulk and interfaces*, Zeitschrift für angewandte Mathematik und Physik, 64 (2012), pp. 29–52.

[75] H. GOMEZ, L. CUETO-FELGUEROSO, AND R. JUANES, *Three-dimensional simulation of unstable gravity-driven infiltration of water into a porous medium*, Journal of Computational Physics, 238 (2013), pp. 217–239.

[76] H. GOMEZ, T. J. HUGHES, X. NOGUEIRA, AND V. M. CALO, *Isogeometric analysis of the isothermal Navier–Stokes–Korteweg equations*, Computer Methods in Applied Mechanics and Engineering, 199 (2010), pp. 1828–1840.

[77] H. GOMEZ, A. REALI, AND G. SANGALLI, *Accurate, efficient, and (iso)geometrically flexible collocation methods for phase-field models*, Journal of Computational Physics, 262 (2014), pp. 153–171.

[78] H. GOMEZ AND K. G. VAN DER ZEE, *Computational Phase-Field Modeling*, in Encyclopedia of Computational Mechanics Second Edition, John Wiley & Sons, Ltd, Chichester, UK, 12 2017, pp. 1–35.

[79] S. GROSS, M. A. OLSHANSKII, AND A. REUSKEN, *A trace finite element method for a class of coupled bulk-interface transport problems*, ESAIM: Mathematical Modelling and Numerical Analysis, 49 (2015), pp. 1303–1330.

[80] F. GUILLÉN-GONZÁLEZ AND G. TIERRA, *On linear schemes for a Cahn–Hilliard diffuse interface model*, Journal of Computational Physics, 234 (2013), pp. 140–171.

[81] Z. GUO, F. YU, P. LIN, S. WISE, AND J. LOWENGRUB, *A diffuse domain method for two-phase flows with large density ratio in complex geometries*, Journal of Fluid Mechanics, 907 (2020).

[82] M. GURTIN AND A. MURDOCH, *A continuum theory of elastic material surfaces*, Archive for rational mechanics and analysis, 57 (1975), pp. 291–323.

[83] M. E. GURTIN, *An introduction to continuum mechanics*, Academic press, 1981.

[84] ——, *Generalized ginzburg-landau and cahn-hilliard equations based on a microforce balance*, Physica D: Nonlinear Phenomena, 92 (1996), pp. 178–192.

[85] M. E. GURTIN, *A gradient theory of single-crystal viscoplasticity that accounts for geometrically necessary dislocations*, Journal of the Mechanics and Physics of Solids, 50 (2002), pp. 5–32.

[86] M. E. GURTIN, E. FRIED, AND L. ANAND, *The Mechanics and Thermodynamics of Continua*, Cambridge University Press, Apr. 2010.

[87] J. S. HADAMARD, *Mémoire sur le problème d'analyse relatif à l'équilibre des plaques élastiques encastrées*, in Euvres de Jacques Hadamard, C.N.R.S Editions, Paris, 1968, pp. 515–641. Originally published in Mém. Sav. Étrang., 33, 1907.

[88] F. HAUSSER, W. MARTH, S. LI, J. LOWENGRUB, A. RÄTZ, AND A. VOIGT, *Thermodynamically Consistent Models for Two-Component Vesicles*, International Journal of Biomathematics and Biostatics, 2 (2013), pp. 19–48.

[89] A. HAWKINS-DAARUD, K. G. VAN DER ZEE, AND J. TINSLEY ODEN, *Numerical simulation of a thermodynamically consistent four-species tumor growth model*, International Journal for Numerical Methods in Biomedical Engineering, 28 (2012), pp. 3–24.

[90] C. HERRING, *The use of classical macroscopic concepts in surface energy problems*, in Structure and Properties of Solid Surfaces, The University of Chicago Press, Chicago, 1953, pp. 5–81.

[91] D. HILHORST, J. KAMPMANN, T. N. NGUYEN, AND K. G. V. D. ZEE, *Formal asymptotic limit of a diffuse-interface tumor-growth model*, Mathematical Models and Methods in Applied Sciences, 25 (2015), pp. 1011–1043.

[92] C. HIRT AND B. NICHOLS, *Volume of fluid (VOF) method for the dynamics of free boundaries*, Journal of Computational Physics, 39 (1981), pp. 201–225.

[93] S. HONG, E. ERGEZEN, R. LEC, AND K. A. BARBEE, *Real-time analysis of cell–surface adhesive interactions using thickness shear mode resonator*, Biomaterials, 27 (2006), pp. 5813–5820.

[94] J. N. ISRAELACHVILI, *Intermolecular and Surface Forces*, Academic Press, Elsevier, 3rd ed., 2011.

[95] A. Khalili and M. Ahmad, *A review of cell adhesion studies for biomedical and biological applications*, International Journal of Molecular Sciences, 16 (2015), pp. 18149–18184.

[96] P. Knopf and K. F. Lam, *Convergence of a robin boundary approximation for a cahn–hilliard system with dynamic boundary conditions*, Nonlinearity, 33 (2020), pp. 4191–4235.

[97] P. Knopf, K. F. Lam, C. Liu, and S. Metzger, *Phase-field dynamics with transfer of materials: The cahn–hilliard equation with reaction rate dependent dynamic boundary conditions*, ESAIM: Mathematical Modelling and Numerical Analysis, 55 (2021), pp. 229–282.

[98] J. Kockelkoren, H. Levine, and W. J. Rappel, *Computational approach for modeling intra- and extracellular dynamics*, Physical Review E - Statistical, Nonlinear, and Soft Matter Physics, 68 (2003), pp. 377021–377024.

[99] R. Krueger, *Virtual crack closure technique: History, approach, and applications*, Applied Mechanics Reviews, 57 (2004), pp. 109–143.

[100] Y.-I. Kwon and J. J. Derby, *Modeling the coupled effects of interfacial and bulk phenomena during solution crystal growth*, Journal of Crystal Growth, 230 (2001), pp. 328–335.

[101] B. Ladoux and R. Mège, *Mechanobiology of collective cell behaviours*, Nature reviews Molecular cell biology, 18 (2017), pp. 743–757.

[102] L. Landau and V. Ginzburg, *English translation: On the theory of superconductivity*, in Collected Papers of L.D. Landau, Elsevier, k teorii s ed., jan 1965, pp. 546–568.

[103] A. A. Lee, A. Münch, and E. Süli, *Sharp-interface limits of the cahn–hilliard equation with degenerate mobility*, SIAM Journal on Applied Mathematics, 76 (2016), pp. 433–456.

[104] D. Lee, J.-Y. Huh, D. Jeong, J. Shin, A. Yun, and J. Kim, *Physical, mathematical, and numerical derivations of the cahn–hilliard equation*, Computational Materials Science, 81 (2014), pp. 216–225.

[105] K. Y. Lervåg and J. Lowengrub, *Analysis of the diffuse-domain method for solving PDEs in complex geometries*, Communications in Mathematical Sciences, 13 (2015), pp. 1473–1500.

[106] V. Levich, *Physicochemical Hydrodynamics*, Prentice-Hall, Englewood Cliffs, New Jersey, 1962.

[107] H. Levine and W.-J. Rappel, *Membrane-bound Turing patterns*, Physical Review E, 72 (2005), p. 061912.

[108] B. Li and J. Lowengrub, *Geometric evolution laws for thin crystalline films: modeling and numerics*, Commun. Comput. . . . , 6 (2009), pp. 433–482.

[109] B. Q. Li, *Discontinuous Finite Elements in Fluid Dynamics and Heat Transfer*, Computational Fluid and Solid Mechanics, Springer-Verlag, London, 1 ed., 2006.

[110] P. Lidström, *On the principle of virtual power in continuum mechanics*, Mathematics and Mechanics of Solids, 17 (2011), pp. 516–540.

[111] C. LIU AND H. WU, *An energetic variational approach for the cahn–hilliard equation with dynamic boundary condition: Model derivation and mathematical analysis*, Archive for Rational Mechanics and Analysis, 233 (2019), pp. 167–247.

[112] J. S. LOWENGRUB, H. B. FRIEBOES, F. JIN, Y.-L. CHUANG, X. LI, P. MACKLIN, S. M. WISE, AND V. CRISTINI, *Nonlinear modelling of cancer: bridging the gap between cells and tumours.*, Nonlinearity, 23 (2010), pp. R1–R9.

[113] J. S. LOWENGRUB, A. RÄTZ, AND A. VOIGT, *Phase-field modeling of the dynamics of multicomponent vesicles: Spinodal decomposition, coarsening, budding, and fission*, Physical Review E - Statistical, Nonlinear, and Soft Matter Physics, 79 (2009), pp. 1–13.

[114] S. LUCKHAUS AND L. MODICA, *The gibbs-thompson relation within the gradient theory of phase transitions*, Archive for Rational Mechanics and Analysis, 107 (1989), pp. 71–83.

[115] G. MACDONALD, J. MACKENZIE, M. NOLAN, AND R. INSALL, *A computational method for the coupled solution of reaction–diffusion equations on evolving domains and manifolds: Application to a model of cell migration and chemotaxis*, Journal of Computational Physics, 309 (2016), pp. 207–226.

[116] A. MADZVAMUSE AND A. H. CHUNG, *The bulk-surface finite element method for reaction–diffusion systems on stationary volumes*, Finite Elements in Analysis and Design, 108 (2016), pp. 9–21.

[117] A. MADZVAMUSE, A. H. W. CHUNG, AND C. VENKATARAMAN, *Stability analysis and simulations of coupled bulk-surface reaction–diffusion systems*, Proceedings of the Royal Society A: Mathematical, Physical and Engineering Sciences, 471 (2015), p. 20140546.

[118] G. A. MAUGIN, *The method of virtual power in continuum mechanics: Application to coupled fields*, Acta Mechanica, 35 (1980), pp. 1–70.

[119] C. MIEHE, F. WELSCHINGER, AND M. HOFACKER, *Thermodynamically consistent phase-field models of fracture: Variational principles and multi-field FE implementations*, International Journal for Numerical Methods in Engineering, 83 (2010), pp. 1273–1311.

[120] A. MIELKE, *A gradient structure for reaction–diffusion systems and for energy-drift-diffusion systems*, Nonlinearity, 24 (2011), pp. 1329–1346.

[121] R. MINDLIN, *Second gradient of strain and surface-tension in linear elasticity*, International Journal of Solids and Structures, 1 (1965), pp. 417–438.

[122] R. D. MINDLIN AND N. ESHEL, *On first strain-gradient theories in linear elasticity*, International Journal of Solids and Structures, 4 (1968), pp. 109–124.

[123] L. MODICA, *The gradient theory of phase transitions and the minimal interface criterion*, Archive for Rational Mechanics and Analysis, 98 (1987), pp. 123–142.

[124] N. MOËS, J. DOLBOW, AND T. BELYTSCHKO, *A finite element method for crack growth without remeshing*, International Journal for Numerical Methods in Engineering, 46 (1999), pp. 131–150.

[125] A. MOURE AND H. GOMEZ, *Phase-field model of cellular migration: Three-dimensional simulations in fibrous networks*, Computer Methods in Applied Mechanics and Engineering, 320 (2017), pp. 162–197.

[126] ——, *Three-dimensional simulation of obstacle-mediated chemotaxis*, Biomechanics and Modeling in Mechanobiology, 17 (2018), pp. 1243–1268.

[127] ——, *Phase-Field Modeling of Individual and Collective Cell Migration*, Archives of Computational Methods in Engineering, (2019).

[128] W. F. NOH AND P. WOODWARD, *Slic (simple line interface calculation)*, Springer, Berlin, Heidelberg, 1976, pp. 330–340.

[129] W. NOLL, *On the material frame indifference*, research report 95-NA-022, Carnegie Mellon University, (1995).

[130] M. NONOMURA, *Study on multicellular systems using a phase field model*, PLoS ONE, 7 (2012), pp. 1–9.

[131] J. T. ODEN, A. HAWKINS, AND S. PRUGHOMME, *General Diffuse-Interface Theories and an Approach to Predictive Tumor Growth Modeling*, Mathematical Models and Methods in Applied Sciences, 20 (2010), pp. 477–517.

[132] S. OSHER AND J. A. SETHIAN, *Fronts propagating with curvature-dependent speed: Algorithms based on Hamilton-Jacobi formulations*, Journal of Computational Physics, 79 (1988), pp. 12–49.

[133] M. A. PELETIER, *Variational modelling : energies, gradient flows, and large deviations*, arXiv.org;, 1402.1990 [math-ph] (2014), p. s.n.

[134] C. S. PESKIN, *Flow patterns around heart valves: A numerical method*, Journal of Computational Physics, 10 (1972), pp. 252–271.

[135] G. D. PIERO, *On the method of virtual power in continuum mechanics*, Journal of Mechanics of Materials and Structures, 4 (2009), pp. 281–292.

[136] P. PODIO-GUIDUGLI AND M. VIANELLO, *Hypertractions and hyperstresses convey the same mechanical information*, Continuum Mechanics and Thermodynamics, 22 (2010), pp. 163–176.

[137] S. O. POULSEN AND P. W. VOORHEES, *Smoothed boundary method for diffusion-related partial differential equations in complex geometries*, International Journal of Computational Methods, 15 (2018), p. 1850014.

[138] N. PROVATAS AND K. ELDER, *Phase-Field Methods in Materials Science and Engineering*, Wiley-VCH Verlag GmbH & Co. KGaA, Weinheim, Germany, oct 2010.

[139] A. RÄTZ AND M. RÖGER, *Symmetry breaking in a bulk–surface reaction–diffusion model for signalling networks*, Nonlinearity, 27 (2014), pp. 1805–1827.

[140] A. RÄTZ AND A. VOIGT, *PDE's on surfaces—a diffuse interface approach*, Communications in Mathematical Sciences, 4 (2006), pp. 575–590.

[141] A. RÄTZ AND A. VOIGT, *A diffuse-interface approximation for surface diffusion including adatoms*, Nonlinearity, 20 (2007), pp. 177–192.

[142] S. REUTHER AND A. VOIGT, *Incompressible two-phase flows with an inextensible newtonian fluid interface*, Journal of Computational Physics, 322 (2016), pp. 850–858.

[143] W. J. RIDER AND D. B. KOTHE, *Reconstructing Volume Tracking*, Journal of Computational Physics, 141 (1998), pp. 112–152.

[144] M. RÖGER AND R. SCHÄTZLE, *On a modified conjecture of de giorgi*, Mathematische Zeitschrift, 254 (2006), pp. 675–714.

[145] L. RUBINŠTEĬN, *The Stefan Problem*, vol. 27 of Translations of Mathematical Monographs, American Mathematical Society, Providence, Rhode Island, 1971.

[146] A. V. S. ALAND, J. LOWENGRUB, *Two-phase flow in complex geometries: A diffuse domain approach*, Computer Modeling in Engineering & Sciences, 57 (2010), pp. 77–108.

[147] L. SCHMELLER AND D. PESCHKA, *Gradient flows for coupling order parameters and mechanics*, SIAM Journal on Applied Mathematics, 83 (2023), pp. 225–253.

[148] L. SCRIVEN, *Dynamics of a fluid interface equation of motion for newtonian surface fluids*, Chemical Engineering Science, 12 (1960), pp. 98–108.

[149] D. SHAO, H. LEVINE, AND W.-J. RAPPEL, *Coupling actin flow, adhesion, and morphology in a computational cell motility model*, Proceedings of the National Academy of Sciences, 109 (2012), pp. 6851–6856.

[150] D. SHAO, W.-J. RAPPEL, AND H. LEVINE, *Computational Model for Cell Morphodynamics*, Physical Review Letters, 105 (2010), p. 108104.

[151] J. SHEN, J. XU, AND J. YANG, *The scalar auxiliary variable (SAV) approach for gradient flows*, Journal of Computational Physics, 353 (2018), pp. 407–416.

[152] ——, *A New Class of Efficient and Robust Energy Stable Schemes for Gradient Flows*, SIAM Review, 61 (2019), pp. 474–506.

[153] Y. SHIN AND C. BRANGWYNNE, *Liquid phase condensation in cell physiology and disease*, Science, 357 (2017), p. eaaf4382.

[154] H. SMITH, *Pattern Formation by Lateral Inhibition in Physiological and Tumour Angiogenesis*, phd thesis, University of Nottingham, 2019.

[155] J. SOKOLOWSKI AND J.-P. ZOLESIO, *Introduction to Shape Optimization*, Springer Berlin Heidelberg, 1992.

[156] G. SOLIGO, A. ROCCON, AND A. SOLDATI, *Mass-conservation-improved phase field methods for turbulent multiphase flow simulation*, Acta Mechanica, 230 (2019), pp. 683–696.

[157] I. STEINBACH, *Phase-field models in materials science*, Modelling and Simulation in Materials Science and Engineering, 17 (2009), pp. 1–31.

[158] P. STERNBERG, *The effect of a singular perturbation on nonconvex variational problems*, Archive for Rational Mechanics and Analysis, 101 (1988), pp. 209–260.

[159] E. STORVIK, J. W. BOTH, J. M. NORDBOTTEN, AND F. A. RADU, *A cahn–hilliard–biot system and its generalized gradient flow structure*, Applied Mathematics Letters, 126 (2022), p. 107799.

[160] K. E. TEIGEN, X. LI, J. LOWENGRUB, F. WANG, AND A. VOIGT, *A diffuse-interface approach for modeling transport, diffusion and adsorption/desortpion of material quantities on a deformable interface*, Communications in Mathematical Sciences, 4 (2009), pp. 1009–2037.

[161] K. E. TEIGEN, P. SONG, J. LOWENGRUB, AND A. VOIGT, *A diffuse-interface method for two-phase flows with soluble surfactants*, Journal of Computational Physics, 230 (2011), pp. 375–393.

[162] G. TOMASSETTI, *A direct, coordinate-free approach to the mechanics of thin shells*, arXiv preprint arXiv:2305.08884, (2023).

[163] R. A. TOUPIN, *Elastic materials with couple-stresses*, Archive for Rational Mechanics and Analysis, 11 (1962), pp. 385–414.

[164] ——, *Theories of elasticity with couple-stress*, Archive for Rational Mechanics and Analysis, 17 (1964), pp. 85–112.

[165] C. TRUESDELL AND W. NOLL, *The Non-Linear Field Theories of Mechanics*, Springer Berlin Heidelberg, Berlin, Heidelberg, third ed., dec 2004.

[166] S. O. UNVERDI AND G. TRYGGVASON, *A front-tracking method for viscous, incompressible, multi-fluid flows*, Journal of Computational Physics, 100 (1992), pp. 25–37.

[167] J. D. VAN DER WAALS, *The thermodynamic theory of capillarity under the hypothesis of a continuous variation of density*, Journal of Statistical Physics, 20 (1979), pp. 200–244.

[168] K. G. VAN DER ZEE, *Goal-Adaptive Discretization of Fluid-Structure Interaction*, PhD thesis, Technische Universiteit Delft, Delft, the Netherlands, June 2009.

[169] G. VAN ZWIETEN, J. VAN ZWIETEN, C. VERHOOSEL, E. FONN, T. VAN OPSTAL, AND W. HOITINGA, *Nutils*, 2020.

[170] G. VILANOVA, I. COLOMINAS, AND H. GOMEZ, *Capillary networks in tumor angiogenesis: From discrete endothelial cells to phase-field averaged descriptions via isogeometric analysis*, International Journal for Numerical Methods in Biomedical Engineering, 29 (2013), pp. 1015–1037.

[171] ——, *A mathematical model of tumour angiogenesis: growth, regression and regrowth*, Journal of The Royal Society Interface, 14 (2017), p. 20160918.

[172] C. VILLANI, *Optimal Transport*, Springer Berlin Heidelberg, 2009.

[173] M. ŠILHAVÝ, *A direct approach to nonlinear shells with application to surface-substrate interactions*, Mathematics and Mechanics of Complex Systems, 1 (2013), pp. 211––232.

[174] X. WANG, *Asymptotic analysis of phase field formulations of bending elasticity models*, SIAM Journal on Mathematical Analysis, 39 (2008), pp. 1367–1401.

[175] S. M. WISE, J. S. LOWENGRUB, H. B. FRIEBOES, AND V. CRISTINI, *Three-dimensional multispecies nonlinear tumor growth-I. Model and numerical method*, Journal of Theoretical Biology, 253 (2008), pp. 524–543.

[176] O. WODO AND B. GANAPATHYSUBRAMANIAN, *Computationally efficient solution to the Cahn–Hilliard equation: Adaptive implicit time schemes, mesh sensitivity analysis and the 3D isoperimetric problem*, Journal of Computational Physics, 230 (2011), pp. 6037–6060.

[177] X. YANG, *Linear, first and second-order, unconditionally energy stable numerical schemes for the phase field model of homopolymer blends*, Journal of Computational Physics, 327 (2016), pp. 294–316.

[178] F. YU, Z. GUO, AND J. LOWENGRUB, *Higher-order accurate diffuse-domain methods for partial differential equations with dirichlet boundary conditions in complex, evolving geometries*, Journal of Computational Physics, 406 (2020), p. 109174.

[179] J. ZHAO, Q. WANG, AND X. YANG, *Numerical approximations for a phase field dendritic crystal growth model based on the invariant energy quadratization approach*, International Journal for Numerical Methods in Engineering, 110 (2017), pp. 279–300.

[180] F. ZIEBERT AND I. S. ARANSON, *Effects of Adhesion Dynamics and Substrate Compliance on the Shape and Motility of Crawling Cells*, PLoS ONE, 8 (2013), p. e64511.

[181] ——, *Computational approaches to substrate-based cell motility*, npj Computational Materials, 2 (2016), p. 16019.

[182] F. ZIEBERT, S. SWAMINATHAN, AND I. S. ARANSON, *Model for self-polarization and motility of keratocyte fragments*, Journal of The Royal Society Interface, 9 (2012), pp. 1084–1092.

[183] J.-P. ZOLÉSIO, *Identification de domaines par déformation*, PhD thesis, Université de Nice, Nice, France, 1979.